Karlsruher Institut für Technologie

Fakultät für Physik
Institut für Theorie der Kondensierten Materie

Elastic coupling and quantum critical fluctuations in complex magnetic structures

Zur Erlangung des akademischen Grades eines
DOKTORS DER NATURWISSENSCHAFTEN (Dr. rer. nat.)

von der KIT-Fakultät für Physik
des Karlsruher Instituts für Technologie (KIT)
angenommene

Dissertation

von
MPhys Charles R. W. Steward
aus Basingstoke

Tag der mündlichen Prüfung: 6th June 2025
Referent: Prof. Dr. Jörg Schmalian
Korreferent: Dr. Igor V. Gornyi

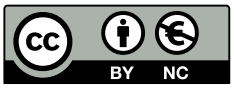

Ich erkläre hiermit, dass ich die vorliegende Arbeit selbständig verfasst, keine anderen als die angegebenen Quellen und Hilfsmittel verwendet habe und alles kenntlich gemacht wurde, dass aus Arbeiten anderer unverändert oder mit Abänderungen entnommen ist.

Karlsruhe, den

Charles Steward

List of Figures

List of Tables

Introduction

Magnetism plays an undeniable role in modern life, from storing data in computers, to anti-lock braking systems in cars, many pieces of technology being commonly used most likely rely on something magnetic. Recently emerging fields include spintronics [1, 2], in which spin polarised currents are used to send information more efficiently than charge currents, magnonics [3] in which magnons are used to send information, as well as materials with a large magnetoelectric effect, in which only a small current is needed to switch the magnetisation in a system, implying use in highly efficient memory devices [4]. Fields such as these require an understanding of the materials which host the complex magnetic structures whose attributes can be leveraged to create such devices and this is the contribution this thesis hopes to make.

When one first learns of magnetic systems, two types immediately come to mind, ferromagnets and antiferromagnets. In a ferromagnet, the individual magnetic moments align, leading to an overall magnetisation in the system which is easily detectable in an experiment, even without the presence of a magnetic field. In antiferromagnets, the magnetic moments anti-align, producing a magnetic state with no-net magnetisation. Such a state can still be detected, for example, through neutron scattering, where the magnetic moment of the neutron interacts with the magnetic ions in the lattice, giving magnetic diffraction peaks [5].

These considerations naturally lead to the question as to what else could there be? In both cases mentioned above, the formation of a magnetically ordered state is associated with the breaking of a symmetry, in a ferromagnet, order sets in below the Curie temperature and time-reversal symmetry is broken, while the translation symmetry of the system is maintained. In antiferromagnets below the Néel temperature, time-reversal symmetry is broken and translation of one lattice spacing is also broken, while the combined operation of the two remains a symmetry. This then suggests that it could be worth investigating what would happen if the operation in question were not translation but some other operation which leaves the lattice invariant. If the operation in question is, for example, a rotation, one is left with something of a relation to an antiferromagnet but with a new set of properties which are of use in the production of highly efficient electronics. We see a simple depiction of this in Fig. 1. Such a system would combine the zero net-magnetisation of an antiferromagnet with the spin-splitting exhibited by ferromagnets. This would allow for the formation of spin currents used in spintronic devices, without the danger of such devices coupling to one another through a magnetic field generated by the material [2]. This type of magnetism has been dubbed an altermagnet, it is related to the Pomeranchuk instability [6] in the spin channel for higher angular momentum, in which the Fermi surface becomes unstable with respect to deformations and can exhibit the symmetries described above. The properties of an altermagnet make their detection highly non-trivial. One would need a way to test whether a particular material, which may look like an antiferromagnet, is actually an altermagnet. The fact that the altermagnet breaks a symmetry of the overall crystal system suggests that it could couple to strain and can therefore be manipulated by applied strain. There already exists a wealth of literature dedicated to measurements of strain and strain fluctuations (phonons) [7–9] which

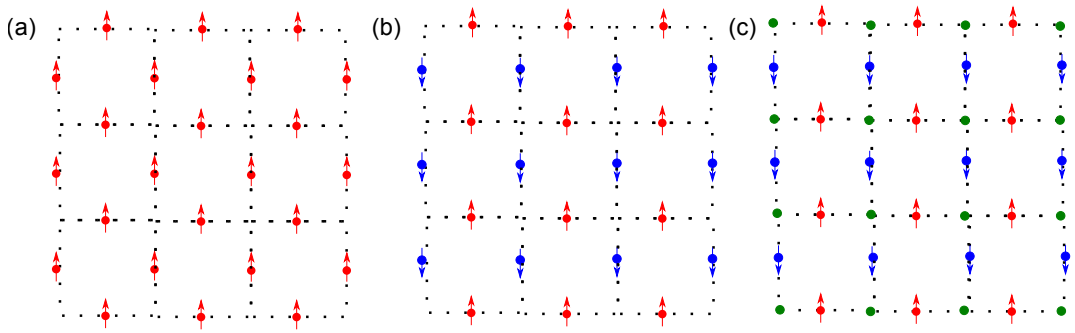

Figure 1: Magnets can be defined by the symmetries their moments form (red for spin up, blue for spin down). For example a ferromagnet (panel (a)) breaks time-reversal but keeps translation invariance, an antiferromagnet (panel (b)) breaks time reversal and translation by a lattice spacing but keeps the combination of the two constant. Another option is to break a rotational symmetry and time reversal, keeping the two as a symmetry. Here a different unit cell to that of the antiferromagnet is enforced by the non-magnetic atoms (green), leaving two magnetic atoms per unit cell. In the non-magnetic state, the blue and red atoms are identical.

implies that if such couplings exist, they would offer a route to indirectly detect altermagnetism. We consider the regime where quantum fluctuations of the order parameter are at their strongest and using group theory, we construct symmetry-allowed coupling terms between magnetism and strain and see how this is manifested physically through observable properties of the system.

This thesis is not just restricted to altermagnetism, we also discuss orbital magnetism in twisted bilayer graphene [10–13] with large magnetoelectric effect, of interest due to applications in memory devices [4]. Twisted bilayer graphene is an incommensurate system which allows for an extended elasticity theory and additional couplings not possible in commensurate crystals. We also briefly discuss the implications of our analysis for nematic order, relevant to iron-based superconductors [14–16], which, much like altermagnets, break rotational symmetry but not time-reversal.

Structure of the thesis

Chapter 1 serves as an introduction to the important concepts needed to understand the chapters which follow. It is split into four parts, the first of which outlines the theory of elasticity. Elasticity is described using a field theory which we then use to deduce the dispersion relations of the collective modes of lattice deformations, i.e. the phonons. We then discuss the formation of complex magnetic structures, what properties these structures have and under which conditions they materialise. These systems will be studied in the regime at which quantum fluctuations are strong, this happens close to the phase transition at zero temperature, i.e. the quantum critical point. We will discuss the general behaviour of systems near such a point and how it affects the finite temperature properties of a system. Once the field theories of the magnetic structures and elasticity have been established, we will use a group theoretic analysis to couple the two degrees of freedom and discuss possible experiments which can then probe this.

Chapter 2 discusses a piezomagnetic coupling, where an altermagnetic order parameter is

coupled to strain via mediation by an external magnetic field and is based on Refs. [17]&[18]. The magnetic field allows for both, tuning of the coupling strength and the position of the quantum critical point. We show that this coupling leads to the emergence of lattice softening along certain directions, in analogy with the well-studied nematic systems [16, 19]. The emergence of soft directions changes the universality class of the system, without destroying the critical point itself. We also find two regimes of behaviour above the critical point, again as is known for the nematic systems [16]. The behaviour in the higher temperature regime is that of the bare critical regime (without elastic coupling) but below a magnetic field-dependent crossover temperature, the behaviour is dominated by the effects of coupling to elasticity. We show that this elastic quantum critical regime is qualitatively different to that of a Fermi liquid through a calculation of the elastocaloric effect, a realisation that is not recognised through a calculation of the heat capacity or single particle self-energy. The qualitative change in behaviour of observables through the presence of an external magnetic field suggests that altermagnetism can be indirectly detected. The analysis of the elastocaloric effect also has implications for criticality in nematic systems.

In Chapter 3, we introduce a dynamic coupling which does not rely on an external field to materialise and is based on Ref. [20]. Elasticity can be directly coupled to the time derivative of the magnetic order parameter, an effect that is therefore at its strongest when fluctuations are strong, i.e. close to the quantum critical point. In this case we find that the magnon modes and phonon modes hybridise, the anisotropy of the magnetism is then reflected in the phonon spectrum, leading to a direction-dependent softening of the phonons. If this softening is detected, then it would allow for the detection of an altermagnetic state and for the deduction of its symmetries.

In Chapter 4 we use this dynamic coupling again, this time in an incommensurate system, based on Ref. [21]. The system in question is twisted bilayer graphene. Here anharmonic terms in the adhesion potential serve to damp the elastic modes, leading to the emergence of phasons [22]. The elastic modes transform under the same irreducible representation as the orbital ferromagnetic state which emerges when twisted bilayer graphene is partially aligned to hexagonal boron-nitride [10, 23, 24]. We see that the coupled mode which retains a predominantly magnonic character inherits this damping and the system is driven towards the quantum critical point as damping is increased.

In Chapter 5, we provide a summary of each chapter and discuss the next steps and future directions of the analysis presented here.

Contents

1 Chapter 1

Fundamentals: Quantum phase transitions of magnetic structures coupled to elasticity

We begin with an introduction to the concepts needed to understand the analysis presented in the following chapters. This thesis concerns itself with complex magnetic structures which are coupled to elasticity in the vicinity of a quantum critical point (the point at which the transition temperature between the disordered paramagnetic phase and ordered magnetic phase is suppressed to zero). The complexity for the systems in question means either possessing symmetries not found within the standard ferromagnetic or antiferromagnetic systems, or a type of magnetism possessing a purely orbital nature, with an only marginal input from the spin degrees of freedom. It is therefore crucial that we first in Section 1.1 provide an overview of elasticity in crystalline systems and show how this is underpinned by group theoretic methods also relevant to the complex magnetic systems we define in Section 1.2. These systems undergo a quantum phase transition (i.e. a phase transition at zero temperature); in Section 1.3 we study the general behaviour one could expect to find in systems where these transitions occur, including how fluctuations of the order parameter affect the finite temperature properties of a system and how it is possible to find theoretically the point at which the system orders. Having identified the elastic modes and order parameters we then show how to deduce possible couplings through a symmetry analysis of the various collective modes in Section 1.4 and how this is relevant for experimental probing of magnetic structures.

1.1 Field theories of elasticity

There naturally exists a coupling between magnetic degrees of freedom and the lattice; any change in the lattice parameter a must in turn come with a modification to the exchange interaction between the individual magnetic moments situated on the lattice [25, 26]. We will represent this interplay through a long-wavelength collective field theory. This implies that the coupling of magnetism to the lattice which hosts it is implemented through a consideration of the collective modes. The collective mode of the magnetism is of course the magnons, which we will discuss in detail in Section. 1.2, and for the elasticity, the collective modes are phonons. We begin with a general analysis of long-wavelength field theories of elasticity in crystals.

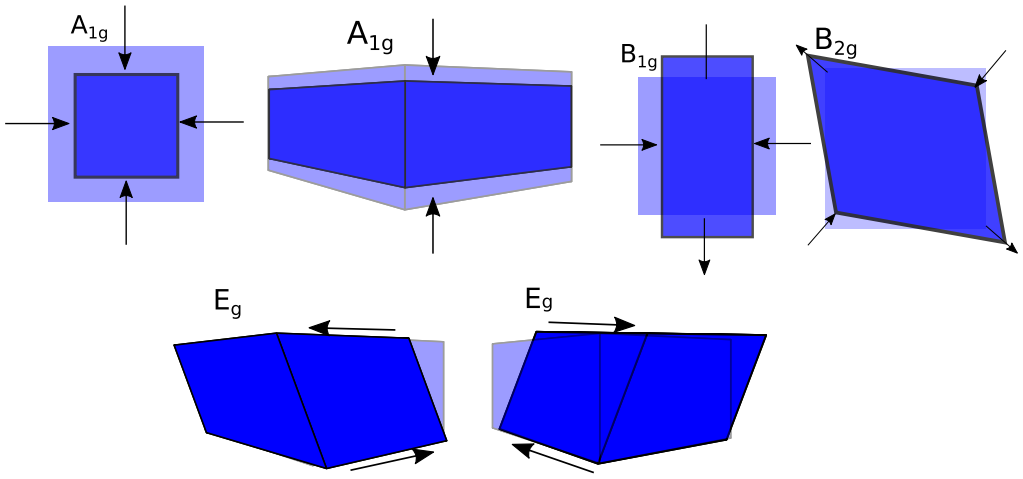

Figure 1.1: The strain of a tetragonal crystal can be represented through the irreducible representations of the crystal symmetry.

The quantity which describes the deformation of the lattice is the symmetrised strain tensor [27]

$$\varepsilon_{ij} = \frac{1}{2}\left(\partial_i u_j + \partial_j u_i\right), \tag{1.1}$$

where ∂_i is a partial derivative with respect to the coordinate x_i and u_j is a displacement of a point on the lattice from its equilibrium position in the direction x_j. If we consider a tetragonal crystal (which will be the system used in much of this thesis), we then study Table 1.1 to see which combinations of ε are symmetry allowed. Each crystal transforms according to a symmetry group which defines which transformations leave a system invariant. This point group can be decomposed into the direct sum of a set of irreducible representations of this group [28], each of which could potentially describe a way under which strain transforms. The quadratic functions column states which functions transform according to the relevant irreducible representation, from this we see that the irreducible representations of the strain are

$$\varepsilon_{A_{1g}} = \varepsilon_{xx} + \varepsilon_{yy},\ \varepsilon_{zz}, \qquad \varepsilon_{B_{1g}} = \varepsilon_{xx} - \varepsilon_{yy}, \qquad \varepsilon_{B_{2g}} = \varepsilon_{xy}, \qquad \varepsilon_{E_{1g}} = \begin{pmatrix}\varepsilon_{xz}\\ \varepsilon_{yz}\end{pmatrix}. \tag{1.2}$$

These combinations correspond to the irreducible representations which include a quadratic function. A depiction of these strain elements can be found in Fig. 1.1.

Knowledge of the allowed combinations of strain makes it possible to derive the symmetry allowed phononic excitations. The free energy density for elastic degrees of freedom is given by [19]

$$F_{\text{el}}\left[\mathbf{u}\right] = C_{ij,kl}\varepsilon_{ij}\varepsilon_{kl} = \frac{1}{2}u_i M_{ij} u_j, \tag{1.3}$$

where $C_{ij,kl}$ are the elastic constants and M_{ij} is the dynamic matrix. The point group symmetry is used to identify $C_{ij,kl}$; the symmetries are used to relate certain elements to one another, reducing the number of independent elements [27]. The free energy of a tetragonal

crystal is then (using the convention of Ref. [19], we note that this sometimes appears with a coefficient 2 of C_{44} and C_{66} [17])

$$\begin{aligned} F_{\text{el}} = &\frac{C_{11}}{2}\left(\varepsilon_{xx}^2+\varepsilon_{yy}^2\right)+\frac{C_{33}}{2}\varepsilon_{zz}^2+\frac{C_{44}}{2}\left(\varepsilon_{xz}^2+\varepsilon_{yz}^2\right) \\ &+\frac{C_{66}}{2}\varepsilon_{xy}^2+C_{12}\varepsilon_{xx}\varepsilon_{yy}+C_{13}\left(\varepsilon_{xx}+\varepsilon_{yy}\right)\varepsilon_{zz}, \end{aligned} \tag{1.4}$$

with the elastic constants given in Voigt notation. We see that certain elastic constants (for example those corresponding to terms for ε_{xx}^2 and ε_{yy}^2) are the same as a result of the symmetry a tetragonal crystal possesses in the $x-y$ plane.

The elastic degrees of freedom are described by the action

$$S_\varepsilon = \int d^3x \int dt \left[\frac{\rho}{2}\dot{\mathbf{u}}^2 + F_{\text{el}}\left[\mathbf{u}\right]\right], \tag{1.5}$$

where ρ is a mass density.

To find the dispersions of the phonon modes, we find the eigenvectors of the dynamic matrix or solve for

$$\det\left(\rho\omega^2 - M\right) = 0. \tag{1.6}$$

Which, if we simplify by assuming $C_{13} = -C_{44}$ and $C_{66} = \frac{C_{11}-C_{12}}{2}$, decoupling the in-plane and out of plane elasticity (a simplification we make here in order to be able to calculate the phonon modes analytically but will also be able to justify in other cases), gives the phonon modes

$$\begin{aligned} \rho\Omega_1(\mathbf{q}) &= \sqrt{\frac{1}{\rho}\left(C_{44}|\mathbf{q}_{2d}|^2 + C_{11}q_z^2\right)}, \\ \rho\Omega_2(\mathbf{q}) &= \sqrt{\frac{1}{\rho}\left(C_{11}|\mathbf{q}_{2d}|^2 + C_{44}q_z^2\right)}, \\ \rho\Omega_3(\mathbf{q}) &= \sqrt{\frac{1}{\rho}\left(\frac{C_{11}-C_{12}}{2}|\mathbf{q}_{2d}|^2 + C_{44}q_z^2\right)}, \end{aligned} \tag{1.7}$$

where Ω is the energy of the phonon mode and $\mathbf{q}_{2d} = \left(q_x, q_y\right)$ is the in-plane momentum. The eigenmodes of the dynamical matrix give the polarisation vectors of the modes with $\vec{\lambda}_1(\mathbf{q}) = (0,0,1)^T$, $\vec{\lambda}_2(\mathbf{q}) = \frac{1}{|\mathbf{q}_{2d}|}(q_x, q_y, 0)^T$, and $\vec{\lambda}_3(\mathbf{q}) = \frac{1}{|\mathbf{q}_{2d}|}(-q_y, q_x, 0)^T$, respectively. Once the symmetry of a crystal is known, it is trivial to deduce the dispersions of the phonons which the lattice hosts and by extension generate a field theory for the elasticity of the crystal in question.

In crystals, phonon modes are symmetry protected and as such, are not subject to damping. Alternatively, in addition to phonons there exists another candidate for the elastic collective mode. In twisted bilayer graphene, long-wavelength fluctuations are dominated by phason modes [29]. Twisted bilayer graphene is the result of stacking two graphene layers at a relative twist angle (see Fig. 1.4) [30, 31]. This somewhat complicates the elasticity of the system. Unlike in commensurate crystals where the collective modes arise as a result of vibrations of a rigid crystal, in twisted bilayer graphene, the modes correspond to the relative displacement

D_{4h}	E	$2C_4$	C_2	$2C_2'$	$2C_2''$	i	Linear functions	Quadratic functions
A_{1g}	$+1$	$+1$	$+1$	$+1$	$+1$	1	-	x^2+y^2, z^2
A_{2g}	$+1$	$+1$	$+1$	-1	-1	1	R_z	-
B_{1g}	$+1$	-1	$+1$	$+1$	-1	1	-	x^2-y^2
B_{2g}	$+1$	-1	$+1$	-1	$+1$	1	-	xy
E_g	$+2$	0	-2	0	0	2	$\left(R_x, R_y\right)$	(xz, yz)
A_{1u}	$+1$	$+1$	$+1$	$+1$	$+1$	-1	-	-
A_{2u}	$+1$	$+1$	$+1$	-1	-1	-1	z	-
B_{1u}	$+1$	-1	$+1$	$+1$	-1	-1	-	-
B_{2u}	$+1$	-1	$+1$	-1	$+1$	-1	-	-
E_u	$+2$	0	-2	0	0	-2	(x, y)	-

Table 1.1: The character table for point group D_{4h}. The x-axis coincides with the C_2' axis [28].

of the two layers. In analogy with the strain tensor, the twist angle can be written as

$$\Omega = \partial_x u_y - \partial_y u_x. \tag{1.8}$$

This describes an antisymmetric tensor $\Omega_{xy} = -\Omega_{yx}$ which is in direct contrast to the elastic tensor ε_{ij}. While we discuss this for twisted bilayer graphene, it must be noted that this is not a unique case, such a term generally enters the elasticity theory for quasiperiodic systems [32–35]. Disorder in the moiré lattice as a result of disorder in the relative orientation, and thermal fluctuations serves to damp the collective modes, leading to the formation of overdamped phason modes [22]. The fact that this elastic component transforms like a rotation around the z axis means that this transforms like A_{2g}, this is an irreducible representation not applicable in symmetric elasticity. This will be important later, with regards to constructing coupling terms. The disorder in the relative displacement is a result of the fact that the twist angle is neither static nor homogeneous, areas of lattice relaxation form, leading to an inhomogeneity over the lattice [36]. This leads to dramatically different behaviour despite the similarity of phasons to acoustic phonons. The similarity is a result of the fact that the elastic theory of TBG is inherited from the phonon modes of both individual graphene layers [22].

The focus is on the in-plane collective modes of the moiré structure. The fact that the pattern is an incommensurate superlattice implies that the low energy excitations are damped phasons, similar to those one would find in quasicrystals [22, 37, 38]. The incommensurate property of the lattice [35] breaks the translation symmetry which protected the phonons and so the phasons are instead associated with the invariance of the system under translations of the layers relative to one another [29], in which what occurs is a shift of the centre of the beat pattern [39]. For our purposes it is important to know how disorder and anharmonic vibrations of the graphene layers affect the phason dispersion as shown in Ref. [22].

We consider an inhomogeneous twist angle with variance [22]

$$\frac{\delta\bar{\theta}^2}{\bar{\theta}^2} \sim \frac{L_m^2}{\pi^2 L_c^2} \ln\left(\frac{L_c}{L_m}\right), \tag{1.9}$$

where bars represent an average over disorder, $\delta\theta \equiv \theta - \bar{\theta}$, L_m is the moiré period and L_c is

the length scale beyond which disorder causes stacking order to be lost.

The inhomogeneity of the twist angle over length scale L_c leads to a gap in the phonon dispersion. This gap introduces the energy scale [22]

$$\delta\omega \sim \omega_{\mathrm{ZB}} L_m / L_c, \tag{1.10}$$

where ω_{ZB} is the acoustic phonon frequency at the boundary of the moiré Brillouin zone. The occurrence of a gap in the spectrum is another manifestation of the fact that the phasons are not protected by a conservation law. This occurs because if the stacking order is lost on a length scale L_c, the phasons will then acquire a gap on the momentum scale $q_c = 2\pi/L_c$ and so Eq. 1.10 is derived using the long-wavelength dispersion. This is the result of static disorder causing the loss of stacking order on finite length scales [22].

It is crucial that we also consider the effects of thermal fluctuations. It is in the effects of anharmonicity on the dynamical response that the damping has its origins. Thermal fluctuations which arise from anharmonic contributions to the adhesion potential are the most relevant here. These contributions stop the linear momentum of each layer being locally conserved and contribute to the imaginary part of the phason self-energy. The relaxation rate of the relative momentum between the layers is determined by phason scattering which converts phason modes from one branch into the other. One finds two regimes: at long wavelengths, the phasons become diffusive, whereas they are propagating at short wavelengths. The propagating regime is characterised by a sharp quasiparticle peak in the susceptibility [22]. The dispersion can be seen through the spectral function in Fig. 1.2.

The damping of phason modes will then also affect the magnetic collective modes if the two are coupled. While the magnetic collective modes are initially undamped, the introduction of a coupling strength and the hybridisation of the two modes will cause some damping to be present in the hybridised mode which retains a mostly magnonic character. We therefore anticipate that the nature of the collective elastic modes will have an important effect on the magnetic collective modes in Chapter. 4.

1.2 Complex magnetic structures

Having analysed how collective modes of elasticity are deduced, the other half of the coupling terms, the magnetic structures will now be discussed.

The impact on magnetism in forming the world around us is undeniable, it is a major component in advancing technology, meaning that from modern society's formative years until the current day, magnetism plays at least some role in almost everything we do. As a result, it is difficult not to get excited about new developments in a field which could, in turn, lead to significant technological advancements. The considerations presented here represent a more fundamental theoretical analysis of novel magnetic structures, highlighting that such works are still near the embryonic stages of their development, while maintaining some view towards their applications.

In recent years, complex orders of magnetism have gained significant attention. The two forms pertinent to this thesis are the almost purely orbital magnetism, present in twisted bilayer graphene aligned with hexagonal boron-nitride [10, 23, 24] and the other, which forms the bulk of the focus of the following chapters, is altermagnetism [2, 40–56]. Altermagnetism is a purely multipolar magnetism, meaning that its net dipole moment vanishes by symmetry.

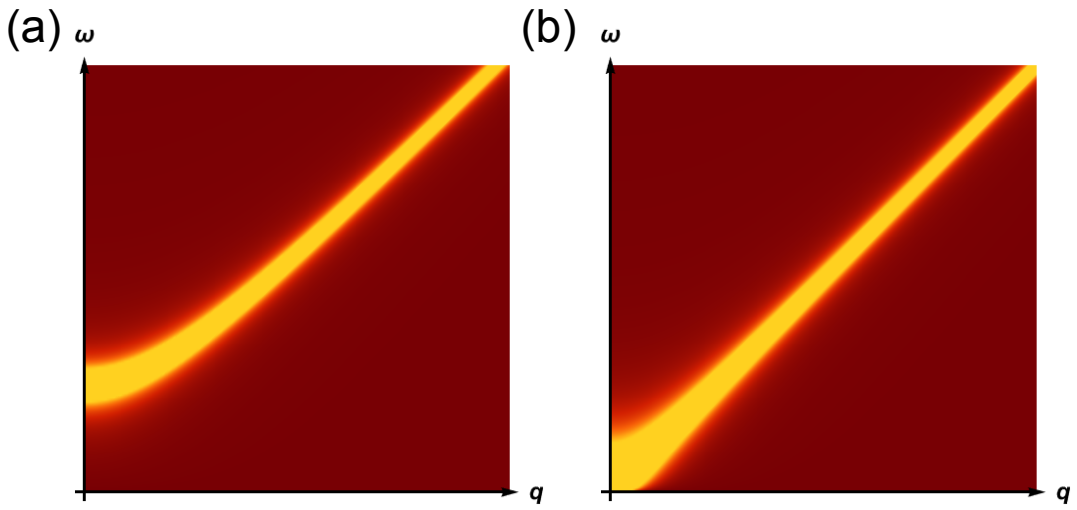

Figure 1.2: The spectral function of the phason mode acquires a damping which gives a dispersive mode at long wavelengths and propagating at short wavelengths. In the presence of static disorder the mode acquires a gap (panel (a)), in its absence, the mode is massless (panel (b)) (Figure adapted from Ref. [22].)

The order parameter then corresponds to a higher order multipole, a toroidal moment or some configuration of dipoles with a net dipole moment which vanishes by symmetry [20]. This is the family of systems with which we begin our analysis.

1.2.1 Altermagnetism

To briefly reiterate what has already been said about point groups, every crystal belongs to a particular symmetry class, determined by the shape of its unit cell and how this unit cell behaves under various transformations [28]. We will demonstrate in the following sections, how powerful a concept this is, allowing us to deduce not just how the crystal itself behaves with regards to the elastic degrees of freedom but also the types of magnetic order that a lattice is capable of hosting.

Magnetism is associated with a spontaneous breaking of symmetry. Consider a set of magnetic moments, each situated on a lattice point. In a ferromagnet, below the Curie temperature, it becomes energetically favourable for the magnetic moments to align, such that the material acquires a finite net-magnetisation and time-reversal symmetry is spontaneously broken [57]. In an antiferromagnet, the magnetic moments anti-align; this creates a system where time-reversal symmetry is broken, in addition to a lack of invariance of a translation along a lattice spacing, while keeping the combined application of the two operations a symmetry of the system. These properties define the symmetry group for the magnet. In the presence of spin-orbit coupling, the spins are pinned in certain, symmetry allowed, directions [58]. The symmetries broken by a magnetic state then match those of the crystal [17, 20, 58], this leaves a set of irreducible representations, not corresponding to ferromagnets or antiferromagnets which could still describe a magnetic system. As the magnet would not transform like a ferromagnet, it possesses a zero net dipole moment. Something which does not transform like a dipole cannot represent an object with a dipole moment. A magnet with such properties

can be defined analogously to an antiferromagnet, with the translation replaced by a point group operation. The class of magnet which breaks these symmetries has been dubbed an altermagnet [2].

Altermagnets are of great interest, not least because of the exotic symmetries that such a configuration can have. Altermagnets combine ferromagnetic properties, such as a broken Kramer's degeneracy, with properties associated with antiferromagnets where moments alternate in a compensated anti-aligned order [2]. In order to define such states, we use the symmetry of the system which hosts this state. If we consider the case that translation symmetry is not broken, then it suffices to use the point group for the crystal [28]. We again focus on a tetragonal crystal, belonging to the D_{4h} point group, to demonstrate the concept and provide a more concrete definition of an altermagnet. The full point group symmetry for a tetragonal crystal is classified in Table. 1.1. We see a set of irreducible representations which will define the symmetries of the potential altermagnetic order parameters.

If we consider the case that the altermagnet transforms according to the irreducible representation B_{1g}, the character table tells us that this is antisymmetric under a C_4 rotation, i.e. a rotation by $\frac{\pi}{2}$. Given that a magnetic state must also be antisymmetric under time-reversal, under both transformations, the point group operation and time-reversal in combination, the system is invariant. The altermagnet spontaneously breaks both symmetries as it orders. We are therefore able to define a set of possible altermagnetically ordered states just from the point group table. We need to preserve inversion symmetry, hence only the irreducible representations with the subscript g are possible candidates. If the point group operation which connects one moment to its opposite is inversion symmetry then this is not an altermagnet but an antiferromagnet [58]. A_{2g} transforms like a rotation around the z-axis and is hence a ferromagnet aligned along z and E_g is a two component order parameter which also transforms as a ferromagnet with one component aligned along x and the other along y. Our options for altermagnets in D_{4h} hence correspond to the trivial representation A_{1g} and the representations B_{1g} and B_{2g}. The rationale behind using the point group symmetry of the crystal to define the altermagnets is that even a weak spin-orbit coupling is enough to fix the magnetic moments along certain directions which then satisfy these symmetries [58]. In the absence of spin-orbit coupling, a different group-theoretic analysis is required. In some cases this is resolved with the use of so-called spin groups [2, 52]. The spin groups are, in fact, only applicable for the case where spin orbit coupling is neglected completely, whereas the definition of altermagnetism which we present here, based upon the point group of the crystal, holds for the more physical case in which spin-orbit coupling is present. The presence of spin-orbit coupling (even in the case that the effect is small) restricts the possible directions of the magnetic moments and the altermagnet must be defined by the point group symmetry of the crystal. This method also makes clear the connection between altermagnets and multipolar order as each of the irreducible representations discussed here is itself associated with a multipole [58].

To understand the magnetic structure, we consider the form of the order parameter. If the spins all align out of plane we have [17]

$$\phi_{B_{1g}} \sim \sum_{\mathbf{k}} f_{B_{1g}}(\mathbf{k}) \left\langle c^{\dagger}_{\mathbf{k}} \sigma^z c_{\mathbf{k}} \right\rangle, \tag{1.11}$$

where $c^{\dagger}$ and c are fermion creation and annihilation operators respectively, σ_z is a Pauli

matrix in spin space and $f_{B_{1g}}$ is a form factor that corresponds to a B_{1g} order parameter but actually transforms according to B_{2g} due to the product rules for irreducible representations, which we will derive in Sec. 1.4. This is simply a single component Ising order parameter. The form factor must transform in this manner because the expectation value transforms according to A_{2g}, as it corresponds to a dipole aligned along the z-axis. The product between this and the form factor gives a B_{1g} order parameter. The form factor defines how local magnetic moments are distributed within the unit cell. The inhomogeneous distribution of magnetic moments is the consequence of multiple magnetic atoms per unit cell [20]. A form factor which transforms like B_{2g} this must transform like xy in the $z = 0$ plane. In momentum space, this becomes $f_{B_{1g}}(\mathbf{k}) = \sin(k_x)\sin\left(k_y\right)$. For a B_{2g} altermagnet we use a form factor which transforms like B_{1g} and so $f_{B_{2g}}(\mathbf{k}) = \cos(k_x) - \cos\left(k_y\right)$. For A_{1g}, the form factor transforms like A_{2g}; this is satisfied by in-plane spins and a form factor which transforms like E_g. We will focus on the ordered states where the spins are aligned out of plane. These form factors modulate the expectation value in Eq. (1.11) which is a pseudovector which transforms like a magnetic dipole [59]. If the form factor transforms trivially, the object ϕ transforms like a dipole. Introducing form factors which do not transform like a dipole immediately means that, by symmetry, the net magnetisation must be zero. In Fig. 1.3 we show a density plot of the form factors which define the two choices of order parameter for out-of-plane spins. The form factors of B_{1g} and B_{2g} order parameters produce similar results, that of a quadrupolar distribution. The angular momentum of a quadrupole corresponds to angular momentum $l = 2$, such that the total angular momentum of ϕ, $j = l + 1 = 3$. $\phi_{B_{1g}/B_{2g}}$ is therefore an order parameter which describes an octupolar ordered state. In agreement with Table. 1.1, a rotation by C_4 transforms $\phi \to -\phi$ and so, in combination with time-reversal, the order parameter is invariant. The structure of an A_{1g} altermagnet is more complex, it corresponds to a hexadecapolar distribution of spins ($l = 4$) such that the order parameter corresponds to a dotriacontapole with $j = 1 + l = 5$. We therefore see that the form factor mediates the creation of a higher order multipole, as opposed to the $l = 0$ dipole which condenses when the form factor is trivial [20].

Multipolar order has gained significant attention due to its potential technological applications [1, 2, 60–62]. The magnetic structure suggests that the magnetic collective modes (altermagnons) will be chiral in nature. In antiferromagnets, chiral magnons are degenerate as a result of protection from inversion and translation symmetry [2, 63], theoretical works have shown however that in altermagnets there exists non-degenerate chiral spin waves [64]. If we consider two magnetisations $\mathbf{m}_1$ and $\mathbf{m}_2$ where one transforms into the other under a $\frac{\pi}{2}$ rotation such that the system has a C_4 symmetry, then following the principles outlined in Sec. 1.3 there exists a symmetry allowed term in the free energy

$$F_{\text{ani}} \propto k_x k_y \mathbf{m}_1^2 - k_x k_y \mathbf{m}_2^2, \tag{1.12}$$

where under C_4 rotation $xy \to -xy$ and $\mathbf{m}_1 \to \mathbf{m}_2$ such that the free energy remains invariant. Such a term gives rise to non-degenerate chiral modes in altermagnets [64]. It has been suggested [60] that this effect makes altermagnons an attractive possibility in magnonics due to magnon-generated spin currents of which one can now take advantage [2, 60]. Magnonics involves using magnons in order to transfer and process information [3]. Magnons in ferromagnets also carry spin currents but exist in the GHz range, making them unsuitable due to

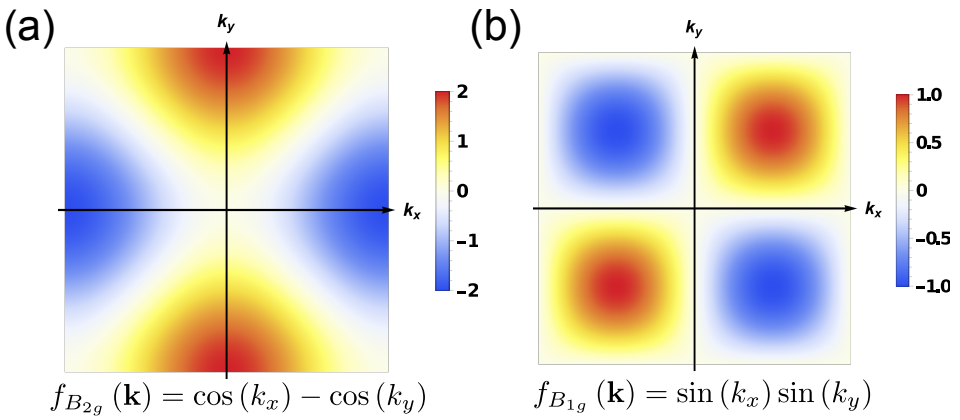

Figure 1.3: A density plot for a form factor which transforms as B_{1g} (panel (a)) corresponding to a B_{2g} altermagnet and a form factor which transforms like B_{2g} (panel (b)) corresponding to a B_{1g} altermagnet. We see that the form factors define the distribution of magnetic moments within the unit cell and define its symmetry. In this case, the state is odd under a C_4 rotation, the minus sign acquired under this rotation can then be cancelled by time-reversal and we therefore have an altermagnet.

difficulties exciting such quasiparticles [60].

An altermagnet, which breaks invariance under a C_4 rotation, possesses a d-wave symmetry, which suggests the possibility of interactions with unconventional superconductors [2]. Many effects of magnetism on superconductivity are well known; in ferromagnetic systems, magnetism suppresses spin-singlet superconductivity, allowing other pairing channels to dominate, whereas antiferromagnets can support spin singlet superconductivity, such as in iron based superconductors [65]. In an altermagnet, the symmetries lead to a set of even numbered anisotropic (due to the momentum dependent spin-polarisation) spin-polarised Fermi surfaces [66]. The number is even in order to enforce net zero magnetisation. There exist spin degenerate nodal surfaces for which spin-singlet pairing may occur as in antiferromagnets, however the spin-split momenta can support spin-triplet pairing similarly to a ferromagnet. In an altermagnet the average of the spins is zero by symmetry. Each split of the Fermi surface contains its own order parameter [2]. This raises the prospect of new physics emerging not only in systems where altermagnetism and superconductivity coexist such as the potential for anisotropic Cooper pairing [2, 65] but also in heterostructures comprised of altermagnetic materials and superconductors, examples include orientation dependent Andreev reflection [65, 67, 68] and Josephson effect [69, 70], as well as finite momentum Cooper pairing [71].

Another possible application is in the field of spintronics [2]. Much like ferromagnets, altermagnets break time-reversal symmetry and exhibit spin splitting, which implies they can be used to recreate the effects of ferromagnetic spintronic devices. In such devices the two spin channels polarise electric currents. The effects associated with this include spin-transfer torque and giant/tunnelling magnetoresistance which can be utilised to switch the magnetisations of two ferromagnetic electrodes between parallel or antiparallel. This effect is leveraged in commercial memory devices. The vanishing magnetisation in altermagnets suggests the lack of any stray field and so spintronic devices using altermagnets can be closer together without the fear of them coupling together (a danger one would have with ferromagnets), this suggests

that altermagnets could be a key component to producing small, highly efficient devices. These properties make altermagnets incredibly promising for use in spintronics [1, 61, 62].

These applications elucidate which properties make altermagnetic materials important. In general the zero net magnetisation of these systems makes actually detecting which compounds are altermagnetic non-trivial. There already exists candidate materials for altermagnetism such as RuO_2 [72, 73] and MnTe [74, 75]. This thesis will focus on theoretical studies for possible experimental detection through the interaction of altermagnetic order with strain. This would allow for candidate materials to be verified, before potentially being used in the technologies considered above.

There currently exist several promising routes, which don't necessarily rely on strain. Ordering of octupolar order means transport properties in altermagnets are also of interest. For example Hall effects [76], where by symmetry, the anomalous Hall effect is absent but there exists a finite third-order effect of the form

$$j_\alpha = \sigma^H_{\alpha\beta\gamma\delta} E_\beta E_\gamma E_\delta. \tag{1.13}$$

where j is the associated current, E is an electric field and $\sigma^H_{\alpha\beta\gamma\delta}$ is a third order Hall conductivity coefficient. Detection of such a current would allow one to probe the altermagnetic state. We will however take a different approach. Rather than investigating the transport properties of unstrained altermagnets, we will construct a model which couples them to strain and explore if this suggests new ways of probing such states, in some cases in analogy with methods already documented for nematic systems [16, 77, 78]. We will also investigate the elasto-Hall effect in Chapter. 2.

While this is discussed as a new classification of magnetism, the idea of a d-wave (or higher order multipole) magnet is not new in and of itself. We can see a discussion of similar systems in the work of Pomeranchuk [6] as far back as 1958. A Pomeranchuk instability describes an instability in a Fermi surface with respect to deformations. Such a deformation can lead to a system with the same symmetries that we are currently attributing to altermagnets. Altermagnets therefore correspond to an even parity spin-triplet instability with $l = 2$ for a d-wave altermagnet or $l = 4$ for g-wave [6, 58].

We see that altermagnets provide a potential foundation for the development of new, highly efficient technologies. Here, we have provided a robust definition for an altermagnet in the presence of spin orbit coupling. We will see that the fact that the irreducible representations of the altermagnet and strain match one another creates natural couplings to strain, some of which do not exist for an out of plane ferromagnet. This is the result of the lack of an A_{2g} strain element in commensurate crystals, however given that we also study incommensurate systems, where such a strain element does exist and the collective modes are more complex, we can also use strain to probe orbital ferromagnetism in twisted bilayer graphene, a phenomenon we discuss next.

1.2.2 Orbital ferromagnetic ordering in twisted bilayer graphene

As well as altermagnetism, we also study a complex type of ferromagnetism, originating in twisted bilayer graphene partially aligned with hexagonal boron-nitride. Such a system hosts an almost entirely orbital type of ferromagnetism [10, 23, 24]. Twisted bilayer graphene is composed of two graphene layers stacked at a relative twist angle. Such a system corresponds

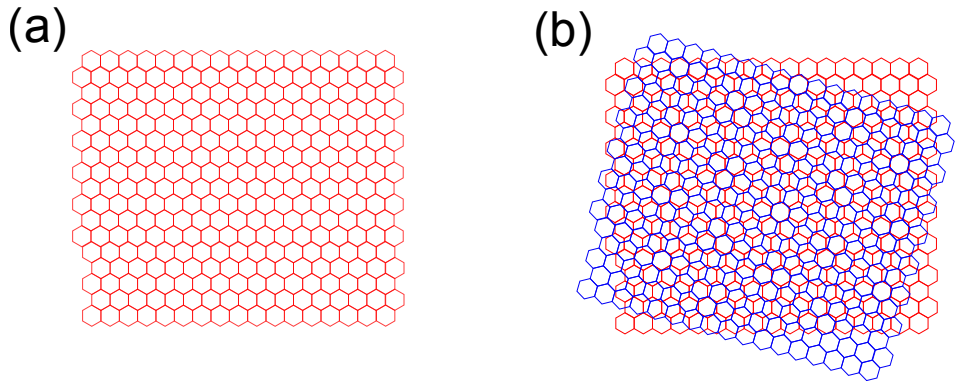

Figure 1.4: A moiré pattern is created by taking two graphene layers (a) and stacking them at a slight twist angle (b), this creates a periodic beat pattern.

to an incommensurate crystal with a broken rotational symmetry for a generic twist angle, creating a moiré superlattice. The moiré lattice is characterised by a beating pattern which arises from the fact the triangular lattices are periodic [29], we depict this in Fig. 1.4. Using the twist angle as a tunable parameter creates a way to change the properties of a system, without changing the chemical composition of the material. The two layers are coupled through an adhesion potential [22].

The tunability of the twist angle has a crucial effect on the band structure of the material. At so-called 'magic angles', two bands become almost flat [31, 79]. In these flat bands the Fermi velocity at the moiré Dirac points vanishes, this leads to the presence of electrons which possess a greatly diminished kinetic energy, such that the total energy is dominated by interactions. The fact that adjusting this twist-angle has such an effect on the band structure suggests a strong coupling between the elastic theory associated with this angle and various electronic degrees of freedom, this is something which we will leverage to our benefit in Chapter. 4. A system where interactions dominate provides fertile ground for the study of strongly correlated systems; in twisted bilayer graphene, unconventional superconductivity [80, 81] and correlated insulators [82] are both observed depending on the electron density [83]. The focus of this section will be spontaneous Ising ferromagnetism, this is observed in a system composed of twisted bilayer graphene partially aligned with hexagonal boron-nitride near 3/4 filling, which then displays a large anomalous Hall effect (AHE) [10, 11, 13, 23]. The detection of an AHE in twisted bilayer graphene prompted the search for the spontaneous time-reversal symmetry breaking state which this relies on. We will discuss in this section, the origins of the time-reversal breaking. The stray fields from ferromagnetic states have already been observed through superconducting interference devices (SQUIDs) [12] as has a large magnetic hysteresis [23, 84] and chiral edge conduction [23].

Ordinarily the spontaneous magnetic moment of a material arises as a result of both spin and orbital degrees of freedom. These orbital degrees of freedom usually account for a relatively small part of the total magnetisation, as this part is formed from loop currents at the atomic scale and is thus considered a secondary effect. However, in TBG the current loops form on the scale of the moiré length, promoting it to a primary effect [85]. To understand how a set of orbital magnetic moments can order spontaneously without spin-orbit coupling (which is low in twisted bilayer graphene [10]), we need to consider the band structure topology of

twisted bilayer graphene.

One can consider first, a more trivial example of orbital magnetism [85]. A 2D electron gas in a strong magnetic field leads to cyclotron motion and a set of Landau levels. When the Fermi level lies between two Landau levels, electrons drift perpendicular to an electric field due to a lack of scattering. As a result, the material exhibits a Hall conductivity related to topological invariants carried by the Landau levels (we will discuss this momentarily) [86]. A key element to the properties of this model, is the fact that the Landau levels are flat and so the Coulomb interactions become the dominant effect [85]. This strongly suggests that twisted bilayer graphene would be the perfect system with which to study the physics discussed here.

To understand the origin of the AHE and orbital magnetism in twisted bilayer graphene we must consider the topology of the flat bands. The presence of an AHE is dependent on a non-zero Berry curvature. The Berry curvature is defined as the phase an eigenstate acquires when parameters are changed adiabatically around a loop in parameter space [87]. If a Hamiltonian depends on a set of parameters $\mathbf{x}$ with eigenstates

$$H(\mathbf{x})\left|n(\mathbf{x})\right\rangle = \varepsilon(\mathbf{x})\left|n(\mathbf{x})\right\rangle. \tag{1.14}$$

Allowing this state to vary gives a phase

$$\left|\psi_n(t)\right\rangle = e^{i\gamma_n(t)}\exp\left[-\frac{i}{\hbar}\int_0^t dt'\varepsilon_n\left(\mathbf{x}\left(t'\right)\right)\right]\left|n\left(\mathbf{x}(t)\right)\right\rangle. \tag{1.15}$$

The first exponential is the Berry phase, which as we shall see is, in general, crucial for understanding some electronic properties of systems. We can use this to define the Berry vector potential

$$\gamma_n = \int_{\mathcal{C}} d\mathbf{x}\cdot\mathcal{A}_n(\mathbf{x}), \tag{1.16}$$

where the introduction of a vector potential suggests analogies with electrodynamics and as such, we can introduce a Berry curvature

$$\Omega^n_{\mu\nu}(\mathbf{x}) = \frac{\partial}{\partial x^\mu}\mathcal{A}^n_\nu(\mathbf{x}) - \frac{\partial}{\partial x^\nu}\mathcal{A}^n_\mu(\mathbf{x}). \tag{1.17}$$

Integrating the Berry curvature over a closed manifold gives the number of monopoles contained within the manifold, this is referred to as the Chern number [87]. The Berry curvature requires a broken time-reversal or inversion symmetry in order to be non-zero. The Berry curvature is responsible for the introduction of an anomalous velocity which gives a current perpendicular to the electric field [87]

$$\mathbf{v}_{\text{anom}} = -\frac{e}{\hbar}\mathbf{E}\times\mathbf{\Omega}_n(\mathbf{k}), \tag{1.18}$$

and a Hall conductivity

$$\sigma_{xy} = \frac{e^2}{\hbar}\int_{\text{BZ}}\frac{d^2k}{(2\pi)^2}\Omega_{k_xk_y}. \tag{1.19}$$

The Chern number n is directly related to the Hall conductance and is thus needed for a quantum Hall effect to manifest itself in the system. This leads to a boundary current, which

is associated with a non-zero orbital magnetisation. In the absence of a magnetic field, this is caused by a spontaneous orbital ordering. Systems which exhibit a quantum anomalous Hall effect are also called Chern insulators [88].

This discussion can now be focussed on the graphene itself, rather than more generic considerations. Twisted bilayer graphene has Bloch states consisting of four flavours, given by the spin and valley degrees of freedom [89]. The two valleys are mapped onto one another by time-reversal symmetry and hence a spontaneous valley polarisation (for example caused by electron correlations [29]), where each valley has a different number of charge carriers, breaks the time-reversal symmetry of the system. This then allows for a non-zero Chern number of the bands (in this case a Chern number $C = 1$ is observed [84, 90]). The mapping of one valley to another is the result of an unbroken $C_2\mathcal{T}$ symmetry, i.e. a π rotation and time-reversal. Breaking such a symmetry would then introduce a finite gap at the Dirac crossings, this can be achieved with partial alignment with hexagonal boron-nitride [11, 91–94]. If the Fermi level is situated in the gap for an odd number of Bloch state flavours, then the QAH effect materialises [89, 95] and is dependent on the, now ordered, orbital magnetic moments.

For each superlattice point, there exists a set of orbitals. The orbitals related to local magnetic moments aligned out of plane are the $p_+ = p_x + ip_y$ and $p_- = p_x - ip_y$ orbitals. A finite magnetic moment is generated by an imbalance in occupation of the two orbitals. The order parameter is then

$$\phi\left(\mathbf{r}\right) = \frac{1}{2} c^\dagger\left(\mathbf{r}\right) \sigma_z c\left(\mathbf{r}\right), \tag{1.20}$$

where σ_z acts in orbital space, such that the order parameter counts $N_{p_+} - N_{p_-}$, i.e. the difference in p_+ and p_- occupations. From what we have already established for altermagnetic systems, we see this order parameter is of a similar structure to that of an altermagnet with a trivial form factor, meaning it does indeed transform like a dipole.

The flat bands possess a large Berry curvature, which gives a giant orbital magnetoelectric effect. This manifests itself physically via a very low current needed to switch the direction of the magnetisation. As a result, like altermagnetic systems, TBG could also be useful in the field of the manufacture of highly efficient devices, in this case low power memory devices [4].

1.3 Quantum phase transitions

The magnetic structures discussed in the previous section are capable of undergoing a quantum phase transition, where the transition temperature is reduced to zero. Close to such phase transitions, quantum fluctuations are greatly enhanced and the finite-temperature properties of the system are impacted. This can be discussed in terms of a general Ising variable ϕ [57].

Many phase transitions correspond to phenomena with which we are familiar through our everyday lives, from seeing an ice cube melt in a cold drink on a summer day to boiling water in a kettle to make a cup of tea. These are all finite temperature phase transitions (or classical/thermal phase transitions) [96] governed by a system which is, in general, forced to minimise its free energy, given by [57]

$$F = E - TS, \tag{1.21}$$

where E is the internal energy of a system, T is the temperature and S is the entropy. We see then that these phase transitions are governed by the interplay between the temperature

and entropy of a system [57]. It is possible that a phase transition is associated with some broken symmetry. In the case of water freezing and turning to ice, the initially disorganised water molecules order into ice crystals, a process which breaks the rotational symmetry which was present in the water [57]. This theory of thermal phase transitions does not however describe all types of phase transition one can consider within condensed matter physics. In this subsection, we will discuss the existence and analyse the behaviour of phase transitions occurring at zero temperature and how even the existence of such a transition has a profound impact on the finite temperature properties of systems. The phase transitions occurring in water represent first order transitions, where latent heat is input during the change of phase. The processes we will be focusing on are second order transitions, where the two phases in question do not coexist [97]. Such transitions have been of great interest ever since 1869 when Andrews set about analysing the phase diagram of carbon dioxide [98]. He found that at a temperature of 31°C and a pressure of 73 atmospheres, the liquid and gaseous phases are impossible to distinguish, causing the carbon dioxide to strongly scatter light, in what is called critical opalescence [99]. A situation where two phases become indistinguishable is known as a critical point. In the years following this, other critical points were found. The most pertinent for a thesis about magnetic structures being by Pierre Curie in iron at the ferromagnetic transition [100]. In these cases, as the transition is approached, the fluctuations diverge such that the typical length and time scales on which these fluctuations decay also diverge [99]. It is this behaviour which we will not only analyse, but also leverage in order to determine the existence and position on the phase diagram of a quantum phase transition.

The phase transitions which constitute our focus belong to the family of phase transitions for which the transition temperature can be suppressed to zero. This is carried out experimentally through the tuning of an external control parameter, denoted r in Fig. 1.5. r can take the form of many tunable non-thermal parameters of the system, for example transitions can be induced through an applied pressure [101, 102] or doping strength [103, 104]. The point at which the transition temperature reaches zero is referred to as the quantum critical point (QCP) [105]. While this point occurs, by definition, at zero temperature, we will see that the existence of a QCP is responsible for a wide-ranging set of behaviours of a system, even at finite temperature.

While quantum phase transitions exist for a wide variety of states, this thesis will focus on transitions from disordered paramagnetic systems to systems which become magnetic in the ordered state. This describes, however, only a very small sample of the eclectic range of phase transitions which can occur at zero temperature. Others include the transition to a nematic state [16, 106], Mott insulating states [107, 108] and spin glasses [109, 110]. A large array of states and behaviours can be obtained via a quantum phase transition and hence their study is an enduringly important aspect of condensed matter physics; for example, it is also common for the area around a magnetic quantum critical point to host superconductivity due to strong fermion-fermion interactions [111]. As previously mentioned, these phase transitions can be associated with some kind of spontaneous symmetry breaking, in the case of magnetism, as the magnetisation becomes finite, the system spontaneously breaks time-reversal symmetry.

Before discussing the QCP itself, we summarise some of the important aspects of quantum statistical physics. The partition function of a system governed by the Hamiltonian H is [112]

$$Z(\beta) = \mathrm{Tr} e^{-\beta H}, \tag{1.22}$$

where $\beta = \frac{1}{T}$.

Given the partition function in Eq. 1.22, we notice the similarity to the time evolution operator $U = e^{-iHt}$. If we now allow the system to evolve over an imaginary time period $t = -i\beta$, they become the same expression [112]. The partition function can be calculated via a path integral, which when written in terms of a transfer matrix reveals a correspondence with the classical problem in $d+1$ dimensions, where the imaginary time dimension extends to a length β [112, 113]. We hence see that the quantum path integral at imaginary time and $d+1$ dimensional statistical mechanics bear a striking analogy. This happens due to the correlations in time which occur when one considers the quantum problem. This correspondence will be relevant to the following analysis with regards to scaling and the renormalisation group as the strength of fluctuations in a system is heavily influenced by its dimensionality.

The analogy between time evolution and thermal averaging through the introduction of imaginary time can also be constructed in terms of frequency. To this end we consider Matsubara frequencies. These are frequencies defined as $\omega_n = 2n\pi T$ for bosons and $\omega_n = \pi\left(2n+1\right)T$ for fermions, where $n \in \mathbb{Z}$. Only certain values of ω contribute and integrals over frequency become sums on the imaginary axis.

1.3.1 Landau theory

We can construct a simple theory of phase transitions, using initially the assumption that the fluctuations of some order parameter which we denote ϕ are, in any case, small. This will allow us to gain some intuition about the importance of symmetries, and the tuning parameter r. In magnetic systems, we are fortunate that there exists an obvious choice of order parameter, we will use the magnetisation of the system. The order parameters we will discuss can all be described by a single-component Ising order parameter [57]. In the disordered state $\langle\phi\rangle = 0$ and in the ordered state $\langle\phi\rangle \neq 0$, of course once the system orders, a finite magnetisation must be acquired. The effects of fluctuations are diminished in higher dimensions, above some upper critical dimension, which we will show later, they can be considered negligible. If fluctuations are small, it is possible to replace ϕ by its averaged value and carry out a mean-field analysis for the system. We can consider a Landau expansion [114], which provides a phenomenological understanding for second-order phase transitions. The free energy density becomes

$$f\left[\phi\right] = f_0 + h\phi + \frac{r}{2}\phi^2 + \frac{u}{4}\phi^4, \tag{1.23}$$

where h is a magnetic field, u governs the strength of interactions and r is a parameter which is used to tune the system through the QCP. We deduce this form from the symmetry of a magnetic order parameter. ϕ is time reversal odd and must therefore appear in even powers, such that the free energy is time-reversal even, or coupled to a conjugate field h (which is also time-reversal odd). If ϕ is a ferromagnet, h is the magnetic field aligned along the same direction as the magnetisation. It is also possible to continue the expansion and include higher order terms. If $h = 0$, calculating the minima of $f\left[\phi\right]$, we see that to obtain physical results, the interaction strength $u > 0$. For $r > 0$, the only minimum is at $\phi = 0$, implying a disordered state. For $r < 0$, there exists a finite minimum. On this basis, we see that r is a tuning parameter which tunes the system through the phase transition.

1.3.2 Critical fluctuations

The theory presented up to this point constitutes a simple mean-field analysis of phase transitions, useful to see how a system behaves in the absence of fluctuations. However, fluctuations are crucial when considering the effects of a QCP on the finite temperature properties of a system. The nature of these fluctuations depends on the regime the system finds itself in. Within the system, there exists two energy scales, one given by the temperature, $k_B T$, and the other is the characteristic frequency of long range order parameter fluctuations $\hbar\omega_c$. If the thermal scale is much larger than the quantum one (for example at high temperatures), the thermal fluctuations dominate, destroying long-range order and the system is disordered (see Fig. 1.5). If instead the quantum fluctuations dominate, at $r > r_c$ the system is effectively in a disordered ground state [105]. Directly above the QCP there exists a crossover region in which both types of fluctuation are important. This region persists at relatively high temperatures, which in turn drive the system away from criticality. If there exists order at finite-temperatures, there is a true phase transition (rather than merely a crossover regime) with thermal fluctuations the most relevant close to the phase boundary but diminishing as the temperature decreases. The QCP is then the endpoint of this phase boundary located at $T = 0$ [105]. The fact that the QCP is responsible for strong fluctuations at finite temperatures is the effect alluded to when discussing the effect of a QCP on the phase diagram.

The coupling of order parameter fluctuations to other modes is also crucial to understanding quantum critical behaviour [105]. Any complete description of the system contains, not only collective modes related to fluctuations of the order parameter, but also a potential coupling of these modes to fermions. However, provided there are no gapless fermions in the system, then near the QCP, the order-parameter fluctuations are the only low-energy excitations. In this case fermions can be integrated out of the theory without introducing divergences [105]. We integrate out degrees of freedom by rewriting Eq. 1.22 in the language of an action S. For the degrees of freedom, for example, ϕ and u this becomes

$$Z = \int D\phi Du \exp\Big\{-S\left[\phi, u\right]\Big\}. \tag{1.24}$$

Provided the degree of freedom in the partition function is Gaussian, we can use the usual identity

$$\int_{-\infty}^{\infty} dx \exp\Big\{-\Big(ax^2 + bx + c\Big)\Big\} = \sqrt{\frac{\pi}{a}} \exp\left\{\frac{b^2}{4a} - c\right\}, \tag{1.25}$$

where by integrating out the degree of freedom u, we obtain a theory in ϕ where the effects of u become included in the ϕ propagator, this is referred to as an effective theory in ϕ.

If there does exist a coupling to low-energy fermions, then it can still be possible to write a theory in terms of the order parameter only, but now non-analytic terms such as Landau damping are introduced to the effective theory. Fermions are included through a coupling term to bosons. Landau damping for a B_{1g} (see Sec. 1.4) nematic in an iron-based superconductor was calculated in Ref. [16]. In some cases however, the fermions cannot be integrated out and a theory must be composed of both degrees of freedom [105].

In the case that both bosonic and fermionic excitations must be taken into account, one finds the existence of critical bosons and fermions [115], rather than the conventional quasiparticles, near the QCP. Such particles can be the cause of phenomena such as a non-Fermi liquid (NFL)

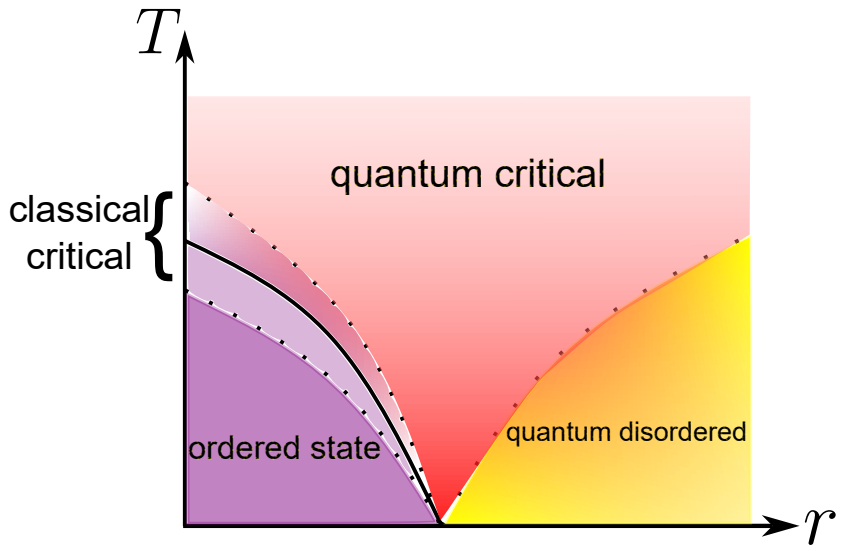

Figure 1.5: A schematic phase diagram for a quantum phase transition shows that there exists not only the ordered and disordered regimes but also a quantum critical regime, close to which quantum fluctuations are strong. This represents a crossover regime and hence dotted lines are used to separate these regions. A solid line denotes a true phase transition(Figure adapted from Ref. [105]).

regime [105]. An example of this is observed in magnetic systems [115]. If one analyses the fermionic excitations, a divergence in the effective mass m^* is observed through a divergence of the electronic specific heat coefficient and the usual Fermi liquid theory no longer applies. In studies of nematic systems [16, 116–118] it has been shown that the electron-electron interaction becomes long-ranged, electrons again become unusually massive and acquire a reduced lifetime. As a result, as well as a divergence in the specific heat coefficient, the electron self energy is altered and the Fermi-surface becomes hot. If Fermi liquid theory breaks down completely, meaning the base assumptions have been rendered invalid, as opposed to slight deviations that can still be described within a Fermi liquid framework, then the main options to model such behaviours are either new weakly interacting quasiparticles or perhaps no quasiparticles are able to form and the excitations are incoherent [119].

This gives some concrete examples of the effects of a QCP on the finite-temperature properties of a system.

1.3.3 The renormalisation group and scaling

We can use the divergence of fluctuations in second order phase transitions as a clear signifier that a change of phase has occurred. At the phase transition, order parameter fluctuations cause the correlation length, ξ to diverge. In the disordered phase, while the average of the order parameter is zero, the fluctuations are not. Close to the critical point, the spacial correlations of order parameter fluctuations become long-ranged. At this point, there exists no characteristic length scale which, in turn, leads to the emergence of scaling laws which define the universality class of the system [120]. Knowing a system's universality class allows us to make statements about entire classes of second order phase transitions, without necessarily

knowing everything about the system. In fact, different transitions belonging to the same universality class can occur in very different systems. The necessary pieces of information to deduce the scaling laws are the symmetry of the order parameter and the dimensionality of the system [105]. The lack of any characteristic length scale means that all lengths can be rescaled and parameters adjusted such that the correlation length retains its value. For example the free energy density of a ferromagnetic system scales with [99]

$$f\left(r,h,T\right)=b^{-\left(d+z\right)}f\left(rb^{1/\nu},hb^{y_h},Tb^{z}\right), \tag{1.26}$$

where r is the distance to the quantum critical point and b is the function used to rescale length in the system. The dimensionality d of the system appears in the scaling relations, as well as a dynamical exponent which defines how temperature scales ($T'=Tb^z$), due to the fact that an extensive quantity scales with the effective dimension. The correlation length exponent ν defines how the correlation length diverges. Given that the scaling parameter rescales momentum and must therefore be considered a length scale, $b^{1/\nu}r\sim 1$ defines the correlation length

$$\xi\propto r^{-\nu}. \tag{1.27}$$

To see how this scales with temperature, we use again

$$b=r^{-\nu}. \tag{1.28}$$

Then if

$$b^{z}T=r^{-z\nu}T\sim 1, \tag{1.29}$$

this suggests r scales with temperature as $r\sim T^{1/\nu z}$. The correlation length then scales as

$$\xi\sim T^{-1/z}, \tag{1.30}$$

and the correlation time as [99]

$$\tau_c\sim\xi^{z}\sim T^{-1}, \tag{1.31}$$

where τ_c is the time scale on which fluctuations decay. We therefore see that both diverge.

The scaling parameter b is arbitrary, however we will determine a set of scaling equations using $b=e^{l}$ where l is the parameter through which length scales are varied. This analysis will allow us to make statements about the transition which go beyond a mean-field theory. To do so, we will calculate a set of renormalisation group (RG) equations. The concept of RG is perhaps best known within particle physics but as we have seen, an imaginary time formulation of quantum field theory is analogous to the calculation of partition functions. It therefore comes as no surprise that RG is also well at home within the quantum field theoretic methods used in condensed matter physics (although there still exist major differences in the actual methods within the two fields due to the coarse graining approach used in condensed matter [121]). We will consider an Ising model as it is most applicable to the calculations presented in the following chapters, this should however also serve as a more general introduction to the concept of RG. From the Ising model, we can perform a Hubbard-Stratonovich transformation. This allows us to translate a theory of a set of interacting spins to a continuum

field theory [57]. A system in an insulating state near the QCP is governed by the action

$$S = \int_{\mathbf{q},\omega_n} \left(r + \mathbf{q}^2 + \frac{\omega_n^2}{c^2} \right) \phi\left(q\right) \phi\left(-q\right) + u \int_x \phi\left(x\right)^4 , \tag{1.32}$$

where ϕ represents the scalar field related to the spin degrees of freedom of the Ising model, it describes the magnons in the system, i.e the magnetic collective modes, c is the magnon velocity and $\omega_n = 2\pi n T$ denotes the Matsubara frequencies; this action is written on the imaginary axis. The integral over Matsubara frequencies is, hence, a discrete sum

$$\int_{\omega_n} f\left(\omega_n\right) \hat{=} T \sum_{n=-\infty}^{\infty} f\left(\omega_n\right) , \tag{1.33}$$

which is approximated as an integral in the limit $T \to 0$. Note the similarity to the Landau theory we deduced after expanding the free energy density in powers of the order parameter, now with gradient terms as the order parameter is not homogeneous in time and space.

Within this action for the magnetic system, there is no Landau damping term, i.e. we have not considered fermion interactions. The reason for this is that in writing down this action, we consider a Mott insulator, this is something we will also do in Chapter. 4. The consequence of this is that we only have terms related to fluctuations in space and time of the order parameter and not due to interactions on the Fermi surface as there is no Fermi surface if the Fermi level is situated in the gap. To give some physical intuition, Mott insulators can be described by a Hubbard model with a hopping term t and on-site Coulomb interaction U [122]. Provided the Coulomb interaction dominates such that U/t is large, the electrons become localised with one on each site and the material acts like an insulator. The strong electron-electron interactions which can create magnetic states can also lead to insulating states, even in cases where the band theory suggests that a material should be a conductor. When one wishes to consider conducting systems, this is not sensible and we must consider fermionic excitations, we discuss such a case in Chapter. 2.

We can now use the fact that in momentum space we are able to scale $q' = bq$ and the order parameter $\phi'\left(q'\right) = b^{-\rho}\phi\left(b^{-1}q'\right)$. By power counting, this yields $r' = b^2 r$ and $\omega_n' = b\omega_n$ (such that $z = 1$). Also by power counting we find that $u' = ub^{4-d-z}$. This sets the upper critical dimension of the system where fluctuations destroy the Landau theory, for $d < 4 - z$, the interaction strength, u, becomes a relevant variable, i.e. it grows with l. In a classical system the upper critical dimension would be set at $d = 4$, this is a manifestation of the fact that it is possible to map a quantum system onto the higher dimensional classical equivalent. One obtains the same upper critical dimension via a direct perturbation theory which diverges for $d < d_{uc}$, this divergence is caused by long wavelength fluctuations $q \to 0$. Given that fluctuations on all length scales are important, a fact we can deduce from the very concept of scaling, we integrate out long wavelength fluctuations, just leaving shell integrations for $\Lambda/b < q < \Lambda$ where $\Lambda \sim a^{-1}$ is a cutoff generated by the lattice constant, a [123].

The term ω_n^2 which now appears in a quantum treatment of the problem has its own scaling dimension, which affects the effective dimensionality of the system. Scaling for both space and time must be considered and so if for example $z = 2$, we now see the upper critical dimension is $d = 2$, meaning the fluctuations are small and a mean-field treatment can be used for a three dimensional system. Through a perturbation of the order parameter, fluctuations are

taken into account. Formally, this corresponds to a summation over Feynman diagrams [123]. Adding in terms corresponding to vertex corrections up to one-loop order to the ϕ^2 term as well as the interaction term ϕ^4, followed by the application of the aforementioned rescaling, gives the following flow equations

$$\begin{aligned}
\frac{dr}{dl} &= 2r + 3u\frac{d}{dl}\int_q^> \chi_0(q) - 3ur\frac{d}{dl}\int_q^> \chi_0(q)^2, \\
\frac{du}{dl} &= \epsilon u - 9u^2\frac{d}{dl}\int_q^> \chi_0(q)^2, \qquad (1.34) \\
\frac{dT}{dl} &= T, \qquad (1.35)
\end{aligned}$$

where we have expanded the propagator, $\chi = \frac{1}{r+q^2+\omega^2/c^2}$, for small r, $\epsilon = 4-d-z$, we use $\omega_n = 2\pi nT$ to determine how the temperature scales and the momentum integral is taken over a shell $\Lambda b^{-1} < q < \Lambda$. We can solve these equations for $d = 3$ such that $\epsilon = 0$ by expanding in small ϵ and then taking $\epsilon \to 0$ at the end. We have integrated out the long-wavelength modes which led to divergences below the upper critical dimension in the direct perturbation theory. We see that below the upper critical dimension, we need to consider the next leading order terms as u grows with l.

At the quantum critical point, due to the divergence of ξ, we expect the theory to be scale invariant and hence r and u should not change with l. A QPT can only occur at $T = 0$ and so approximating the Matsubara sums as integrals in the manner mentioned above and finding the point where r and u stop scaling, we can find the location of the critical point. To do so, we must first calculate the shell integrals. In general, scaling affords us the freedom to assume that $b \approx 1$, such that we can expand in l, this gives

$$\begin{aligned}
\frac{d}{dl}\int_q^> F(q) &= \frac{d}{dl}\int\limits_{\Lambda e^{-l}<|\boldsymbol{q}<\Lambda|} \frac{d^dq}{(2\pi)^d}\int_{-\infty}^{\infty}\frac{d\omega}{2\pi}F\left(|\boldsymbol{q}|,\omega\right) \\
&= \frac{K_d\Lambda^d}{(2\pi)^d}\int_{-\infty}^{\infty}\frac{d\omega}{2\pi}F\left(\Lambda,\omega\right),
\end{aligned}$$

where $K_d = \frac{2\pi^{d/2}}{\Gamma[d/2]}$. Including the integral over the Matsubara frequencies, we obtain for the shell integrals

$$\begin{aligned}
\frac{d}{dl}\int_q^> \chi_0(q)^n &= \frac{K_d\Lambda^d}{(2\pi)^d}\int_{-\infty}^{\infty}\frac{d\omega}{2\pi}\frac{1}{\left(\Lambda^2 + c^{-2}\omega^2\right)^n} \\
&= \frac{K_d c\Lambda^{d-2n+1}}{(2\pi)^{d+1}}\sqrt{\pi}\frac{\Gamma\left(n-\frac{1}{2}\right)}{\Gamma(n)}. \qquad (1.36)
\end{aligned}$$

It follows

$$\begin{aligned}\frac{d}{dl}\int_q^> \chi_0(q) &= \frac{K_d c\Lambda^{d-1}}{2(2\pi)^d},\\ \frac{d}{dl}\int_q^> \chi_0(q)^2 &= \frac{K_d c\Lambda^{d-3}}{4(2\pi)^d},\end{aligned} \tag{1.37}$$

and we obtain the flow equations

$$\begin{aligned}\frac{dr}{dl} &= 2r + 3u\frac{K_d c\Lambda^{d-1}}{2(2\pi)^d} - 3ur\frac{K_d c\Lambda^{d-3}}{4(2\pi)^d},\\ \frac{du}{dl} &= \epsilon u - 9u^2\frac{K_d c\Lambda^{d-3}}{4(2\pi)^d}.\end{aligned} \tag{1.38}$$

If we introduce dimensionless variables

$$\begin{aligned}g &= \frac{9K_d c}{4(2\pi)^d}\Lambda^{d-3}u,\\ m &= \frac{r}{\Lambda^2},\end{aligned}$$

the flow equations simplify to

$$\begin{aligned}\frac{dm}{dl} &= 2m + \frac{2}{3}g - \frac{1}{3}gm,\\ \frac{dg}{dl} &= \epsilon g - g^2.\end{aligned}$$

We can then deduce the fixed point by finding the values of m and g which correspond to $\frac{dm}{dl} = \frac{dg}{dl} = 0$. There is an unstable Gaussian fixed point at $m = g = 0$ and the fixed point of interest $g^* = \epsilon$ and $m^* = -\frac{\epsilon}{3}$. If we consider deviations $\delta g = g - g^*$ such that δ is small (as well as ϵ as we must be close to the upper critical dimension for such an expansion to be trusted) then we find the flow equations become

$$\frac{d}{dl}\begin{pmatrix}\delta m\\ \delta g\end{pmatrix} = \begin{pmatrix}2-\frac{1}{3}\epsilon & \frac{2}{3}+\frac{1}{9}\epsilon\\ 0 & -\epsilon\end{pmatrix}\begin{pmatrix}\delta m\\ \delta g\end{pmatrix}. \tag{1.39}$$

The equation has two eigenvalues $\lambda_1 = 2 - \frac{1}{3}\epsilon$ and $\lambda_2 = -\epsilon$. The eigenvector of the positive eigenvalue is $(1, 0)$. The eigenvector in the stable direction (i.e. belonging to the negative eigenvalue) is $\left(-\frac{1}{3} + \frac{\epsilon}{18}, 1\right)$. It points along the critical surface. Fig. 1.6 shows the flow above and below the upper critical dimension. We see that above the critical dimension, only the Gaussian fixed point is present and that it is stable. Below the upper critical dimension, we have another fixed point which corresponds to the Ising transition, we see that this critical surface points from the Gaussian fixed point to the Ising fixed point. Away from this surface m diverges. The critical surface hence defines a surface where the system flows to the fixed

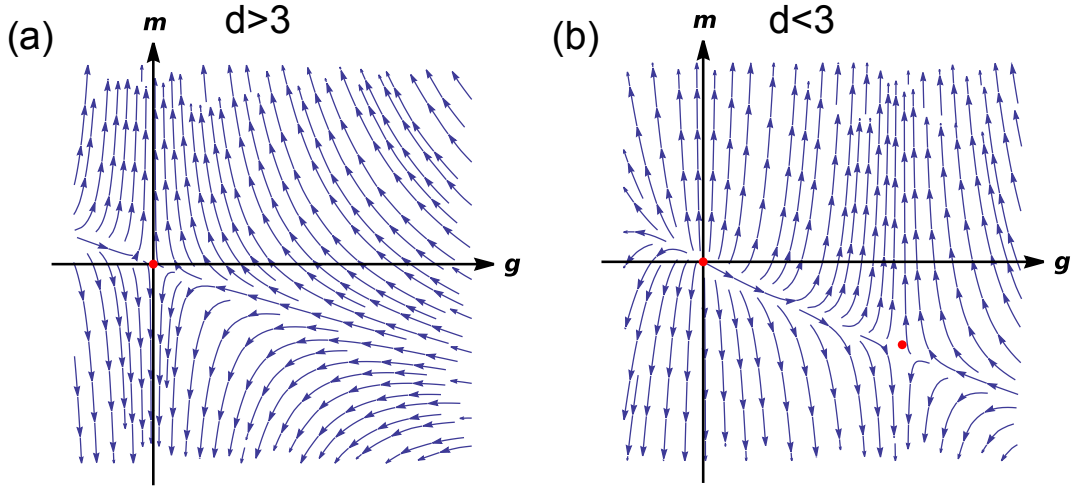

Figure 1.6: We show the flow of the RG equations above the upper critical dimension $d = 3.5$ (panel (a)), we see that the Gaussian fixed point at $(0, 0)$ is stable. Below the upper critical dimension, $d = 2.5$ (panel (b)), the Gaussian fixed point becomes unstable with the flow moving away from this point in all directions, a new fixed point emerges which is stable along the critical direction and unstable in m, i.e. we see that away from this critical direction, m diverges.

point. From this, a distance to the fixed point can be deduced and is given by [57]

$$t = m - g\left(-\frac{1}{3} - \frac{\epsilon}{18}\right). \tag{1.40}$$

The positive eigenvalue corresponds to the inverse correlation length exponent

$$\xi \propto \delta m^{-\nu}, \tag{1.41}$$

with $\lambda_1 = \nu^{-1}$. To leading order in ϵ follows:

$$\nu = \frac{1}{2} + \frac{\epsilon}{12}. \tag{1.42}$$

We therefore see that scaling and RG equations are a powerful tool for the analysis of quantum field theories and for the theoretical detection of quantum critical points. This analysis is carried out at $T = 0$, however the same flow equations are also applicable at finite temperature. A finite temperature crossover analysis $T \ll \Lambda c$ must be considered in order to deduce the boundary of finite-temperature phase transitions. We use

$$\chi_0 = \frac{1}{q^2 + \omega_n^2/c^2}. \tag{1.43}$$

Using the dimensionless variables

$$\tilde{q} = q/\Lambda, \tag{1.44}$$

$$\tilde{\omega} = \omega/\left(c\Lambda\right), \tag{1.45}$$

we rewrite the propagator as

$$\chi_0 = \frac{1}{\tilde{q}^2\Lambda^2 + \tilde{\omega}_n^2\Lambda^2}. \tag{1.46}$$

We must now set about calculating the shell integrals, we now do this specifically in three dimensions. Integrating over the momentum first, yields

$$\begin{aligned}
\frac{d}{dl}\int_q^> \chi_0^m(q) &= \frac{d}{dl}\int_{\Lambda e^{-l}<|\boldsymbol{q}|<\Lambda} \frac{d^3q}{(2\pi)^3} T\sum_{n=-\infty}^{\infty} \chi_0^m\left(|\boldsymbol{q}|,\omega_n\right) \\
&= \frac{d}{dl}\int_{\Lambda e^{-l}<|\boldsymbol{q}|<\Lambda} \frac{q^2\sin(\theta)\,dqd\theta d\phi}{(2\pi)^3} T\sum_{n=-\infty}^{\infty} \chi_0^m\left(|\boldsymbol{q}|,\omega_n\right) \\
&= 4\pi\frac{\Lambda^{4-2m}c}{(2\pi)^3}\tilde{T}\sum_{n=-\infty}^{\infty}\tilde{\chi}_0^m(1,\tilde{\omega_n}) \qquad (1.47)\\
&= 4\pi\frac{\Lambda^{4-2m}c}{(2\pi)^3}F_m(T), \qquad (1.48)
\end{aligned}$$

where the functions $F_m(T)$ are dependent on the Matsubara sums.

This leaves the flow equations

$$\begin{aligned}
\frac{dr}{dl} &= 2r + 3u4\pi\frac{\Lambda^2 c}{(2\pi)^3}F_1(T) - 3ur4\pi\frac{c}{(2\pi)^3}F_2(T), \\
\frac{du}{dl} &= \epsilon u - 9u^2 4\pi\frac{c}{(2\pi)^3}F_2(T).
\end{aligned} \tag{1.49}$$

We switch to dimensionless variables

$$g = \frac{3uc}{(2\pi)^3}, \quad m = \frac{r}{\Lambda^2}. \tag{1.50}$$

The flow equations are now

$$\begin{aligned}
\frac{dm}{dl} &= 2m + 4\pi g F_1(T) - 4\pi g m F_2(T), \\
\frac{dg}{dl} &= \epsilon g - 3g^2 4\pi F_2(T).
\end{aligned} \tag{1.51}$$

In order to solve these equations, we use the method outlined in Ref. [124]. We first take the limit $T \to 0$ in order to identify the quantum critical point. At the transition, m and g no longer scale with l and so by setting the derivatives to zero, we find to first order in ϵ

$$\left(m^*, g^*\right) = \left(-\frac{\epsilon F_1(0)}{6F_2(0)}, \frac{\epsilon}{12\pi F_2(0)}\right), \tag{1.52}$$

such that the distance from the critical point $t = m + bg$ where $b = 2\pi F_1(0)$. We can calculate

the Matsubara sum directly

$$F_1 = \tilde{T} \sum_{-\infty}^{\infty} \frac{1}{1 + (2\pi n T)^2} = \frac{1}{2} \coth\left(\frac{1}{2T}\right), \tag{1.53}$$

and so $F_1(0) = \frac{1}{2}$ such that $t = m + \pi g$. We now consider the case that T is finite but remains in a crossover regime $T \ll c\Lambda$. We can solve for g

$$g(l) = \frac{g_0}{1 + 12\pi g_0 l F_2(T)}. \tag{1.54}$$

We see that as long as g_0 is small, we can disregard thermal fluctuations as these only enter at $\mathcal{O}\left(g_0^2\right)$. We instead just take the $T = 0$ solution. For m we use the ansatz

$$m = m_0 e^{\xi(l)} h(l). \tag{1.55}$$

This solves our flow equation when

$$\begin{aligned} \xi(l) &= 2l - 4\pi \int_0^l g\left(l'\right) F_2\left(l'\right) dl', \\ h(l) &= 1 + \frac{4\pi}{m_0} \int_0^l e^{-\xi\left(l'\right)} F_1\left(l'\right) g\left(l'\right) dl', \end{aligned} \tag{1.56}$$

and so

$$m = e^{\xi} \left(m_0 + 4\pi \int_0^l e^{-\xi\left(l'\right)} F_1\left(l'\right) g\left(l'\right) dl' \right). \tag{1.57}$$

We can write

$$F_1(T) = \frac{1}{2} \coth\left(\frac{1}{2T}\right) = \frac{1}{2} + \frac{1}{e^{\frac{1}{T}} - 1}, \tag{1.58}$$

This then gives the full expression for the distance from the critical point

$$t(l) = e^{\xi} \left(m_0 + \pi g_0 + 4\pi \int_0^l e^{-2l} g_0 \frac{1}{e^{\frac{1}{T}} - 1} dl' \right). \tag{1.59}$$

If we use the transformation $x = \frac{1}{T_0} e^{-l}$ and the fact that at the critical point we can, by definition, scale infinitely such that $l \to \infty$, we then get

$$t(l) = e^{\xi} \left(m_0 + \pi g_0 + 4\pi T_0^2 g_0 \int_0^{\frac{1}{T_0}} \frac{x}{e^x - 1} dx \right), \tag{1.60}$$

and so the equation for T_c is,

$$m_0 + \pi g_0 + 4\pi T_c^2 g_0 \left(\frac{\pi^2}{6} + \frac{1}{T_c} \log\left[1 - e^{-\frac{1}{T_c}}\right] - \mathrm{Li}_2\left[e^{-\frac{1}{T_c}}\right] \right) = 0, \tag{1.61}$$

where Li_2 is the polylogarithm. This equation is not solvable analytically; we resort to nu-

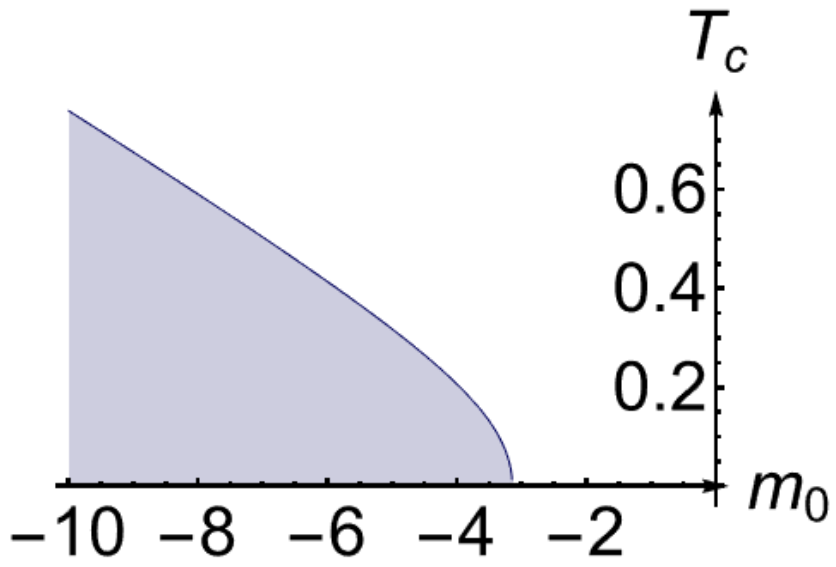

Figure 1.7: Using the RG equations, we are able to calculate at what temperature the Ising model orders (shaded region) depending on the bare dimensionless magnon mass m_0. This is plotted for $g_0 = 1$.

merical methods to obtain the transition temperature, we see the results of this in Fig. 1.7.

An RG analysis allows us to take into account the logarithmic corrections due to fluctuations which occur at the upper critical dimension. The phase transition at zero and finite temperature can be found through the application of scaling, with the understanding that there exists no preferred length scale at the phase transition. As discussed already, the exotic phenomena exhibited near the type of quantum critical point we have found in this simple model can have a profound effect on the phase diagrams for the systems which we will study in this thesis. We reiterate that the ϕ^4 theory presented here is already applicable to a wide variety of systems, including the magnetic systems we consider. In this thesis, we will use these methods to see how different parameters affect the location of the quantum critical point, given by the critical value of m.

Having established a theory of elasticity as well as the relevant magnetic structures and their fluctuations near the QCP, we can now deduce how these modes can be coupled together.

1.4 Magnetoelastic coupling

It is well known that there exist numerous systems in which the coupling of electronic degrees of freedom to the lattice, in the form of electron-phonon coupling, plays a crucial role in understanding the properties and observables of the system. Examples include superconductors, where electron-phonon coupling enables the formation of Cooper pairs [125, 126], or electron-phonon scattering, which affects the transport properties of a system [127, 128]. In this section, we will take the time, not only to show how the procedure of constructing the relevant terms in the Hamiltonian is carried out, but also some noteworthy examples in

magnetic systems which will feature in the upcoming chapters. Having carried out an analysis for the order parameters we are focusing on in the preceding sections, we will continue with the use of an Ising order parameter. It should be mentioned that this describes, not only magnetic systems but also nematic systems [16], p-wave superconductors [129] and others which undergo second order phase transitions, making it an incredibly rich and widely applicable universality class. Here we analyse the formation of hybridised modes, which we refer to as magnon-like or phonon-like polarons [130], depending on whether the mode retains more of the uncoupled magnon or phonon mode character respectively.

1.4.1 Group theory of elasticity-order parameter coupling

There is an extensive catalogue of phonon-magnon coupling terms which hybridise the relevant collective modes. One of which is the coupling between magnetic and elastic collective modes which exhibits magnetostriction [130, 131] with a coupling term

$$\mathcal{H}_c = \int d^3\mathbf{r} N_{ijkl}\varepsilon_{ij}\left(\mathbf{r}\right)\phi_k\left(\mathbf{r}\right)\phi_l\left(\mathbf{r}\right). \tag{1.62}$$

The magnetostriction response tensor N_{ijkl}, couples the strain to the staggered magnetisation. It is defined by $\varepsilon_{ij} = N_{ijkl}M_kM_l$. This, creates a hybridisation effect [130, 131], opening up a gap when the dispersions cross. In opening up a gap, it becomes possible to promote topological effects within the system, with bands acquiring finite Chern numbers [132, 133]. Magnetostriction allows for the changing, for example, of volume (N_{iijj}) when magnetic order sets in. We hence see how the microscopic theory, which describes the interplay of the exchange interaction and the value of the lattice parameter manifests itself in the language of the collective modes. Another important effect, which emerges from the interplay of lattice degrees of freedom and magnetic order, is piezomagnetism. This is defined through the tensor $\varepsilon_{ij} = \Lambda_{ijk}M_k$ [134]. In this case we see that a distortion of the lattice can create a magnetisation and conversely, that magnetic fields can lead to lattice distortions [135, 136].

In order to deduce a more complete range of effects which arise from the hybridisation of collective modes, we need to understand how the symmetry groups of such modes allow us to write down terms in the Hamiltonian or action which couple the two degrees of freedom. Most importantly, we need to know how the product of two objects, which transform according to particular irreducible representations of the point group, itself transforms. In order to be symmetry allowed, the product of these objects must transform trivially, such that the energy of the system does not depend on the angle at which it is observed, anything else would of course, make no physical sense.

We take, initially, the example of a tetragonal system D_{4h}. We reiterate that it is possible to use the set of functions in Table. 1.1 to expand the symmetrised strain ε_{ij} in a set of symmetry allowed terms [29]

$$\varepsilon_{B_{1g}} = \varepsilon_{xx} - \varepsilon_{yy}, \tag{1.63}$$

$$\varepsilon_{B_{2g}} = \varepsilon_{xy}, \tag{1.64}$$

$$\varepsilon_{A_{1g}} = \varepsilon_{xx} + \varepsilon_{yy},\ \varepsilon_{zz}, \tag{1.65}$$

$$\varepsilon_{E_g} = \begin{pmatrix} \varepsilon_{yz} \\ -\varepsilon_{xz} \end{pmatrix}. \tag{1.66}$$

The realisation that the strain elements transform according the irreducible representations of the point group, in much the same way the possible altermagnetically ordered states in the presence of spin-orbit coupling do, means that we can start to deduce coupling terms. The conditions for a term to be symmetry allowed are that it is even under time-reversal and that the term transforms according to the trivial irreducible representation A_{1g}. We need to know the product rules for the irreducible representations; in order to do this we follow the method presented in Ref. [137]. We consider a multiple component Ising parameter with components $\{\phi_a\}$, which we initially couple with strain components $\{\varepsilon_a\}$ (we will also have to couple magnetic field components but once we know how to find the product of two objects, one just repeats the process for the third). The components transform according to the group symmetries $g \in G$ according to the representations ρ. In order to couple the objects, we need to know how the composite object $\{\phi_a \varepsilon_b\}$ transforms. We define the unitary group representations according to the Hilbert space symmetry operators, $U(g)$ (which are a unitary group representation)

$$U^{-1}(g)\,\phi_a U(g) = \sum_{b=1}^{\dim\phi} \rho^{\phi}_{ab}(g)\,\phi_b, \tag{1.67}$$

$$U^{-1}(g)\,\varepsilon_a U(g) = \sum_{b=1}^{\dim\varepsilon} \rho^{\varepsilon}_{ab}(g)\,\varepsilon_b, \tag{1.68}$$

such that the composite object transforms according to

$$U^{-1}(g)\,\phi_a\varepsilon_b U(g) = \sum_{b=1}^{\dim\phi} \rho^{\phi}_{ac}\rho^{\varepsilon}_{bd}(g)\,\phi_b\varepsilon_d, \tag{1.69}$$

or according to the direct product $\rho^{\phi}(g) \otimes \rho^{\varepsilon}(g)$ of the two representations. We change basis such that the direct product is block diagonal for all g, where these matrices on the diagonal are denoted $\rho^{\lambda_i}(g)$, where λ denotes the irreducible representation and is hence the direct product of irreducible representations. The basis change is then given by a matrix M such that

$$M^{-1}\rho^{\phi}(g) \otimes \rho^{\varepsilon}(g)\,M = \begin{pmatrix} \rho^{\lambda_1}(g) & 0 & 0 & \dots \\ 0 & \rho^{\lambda_2}(g) & 0 & \\ 0 & 0 & \rho^{\lambda_3}(g) & \\ \vdots & & & \ddots \end{pmatrix} \equiv \rho^{\lambda_1}(g) \oplus \rho^{\lambda_2}(g) \oplus \rho^{\lambda_3}(g) \oplus \dots \tag{1.70}$$

We do this by first diagonalising the individual matrices i.e. the various matrices arising from $\rho^{\phi}(g) \otimes \rho^{\varepsilon}(g)$.

To find the product of the irreducible representations, we first find the individual matrices $\rho^{\lambda_i}(g)$. For the one-dimensional irreducible representations, we can just read this off the character table, for example, looking at Table. 1.1, we see that $\rho^{A_{2g}}(C_{4z}) = 1$. We then find the corresponding sets of λ which satisfy

$$\rho^{\lambda_1}(g) \times \rho^{\lambda_2}(g) = \rho^{\lambda_3}(g), \tag{1.71}$$

$\otimes$	A_{1g}	A_{2g}	B_{1g}	B_{2g}
A_{1g}	A_{1g}	A_{2g}	B_{1g}	B_{2g}
A_{2g}	A_{2g}	A_{1g}	B_{2g}	B_{1g}
B_{1g}	B_{1g}	B_{2g}	A_{1g}	A_{2g}
B_{2g}	B_{2g}	B_{1g}	A_{2g}	A_{1g}

Table 1.2: The product table for the one-dimensional irreducible representations of D_{4h}.

to find the product table given in Table. 1.2. It is simple to deduce which products are symmetry allowed for 1D representations. The product of an irreducible representation with itself gives the trivial representation and is therefore symmetry allowed.

We must also consider how to carry out the equivalent procedure for higher dimensional irreducible representations, for example the product of a one and two-dimensional irreducible representation. In this case we use a single component Ising parameter ϕ and a strain which transforms according to E_g, which is a two-dimensional irreducible representation. We will consider how the product looks for different one dimensional irreducible representations of ϕ. Constructing a vector from the Kronecker product

$$v = (\phi\varepsilon_1, \phi\varepsilon_2), \tag{1.72}$$

where ε_1 and ε_2 refer to the E_g components of strain given in Eq. (1.66).

We transform this vector for each choice of ϕ.

The product of the two, should still transform like E_g. We deduce this from the fact that the multiplication of a one and two-dimensional irreducible representation has to yield a two-dimensional irreducible representation, of which E_g is the only option within D_{4h}. We must find a unitary matrix M such that

$$M^{-1}\rho^{\lambda}(g) \otimes \rho^{E}(g) M = \rho^{E}(g). \tag{1.73}$$

As already mentioned, we identify the ρ for the one-dimensional representations from the character table. For the E_g representation the generators are

$$\rho^{E_g}(C_{4z}) = \begin{pmatrix} 0 & -1 \\ 1 & 0 \end{pmatrix}, \qquad \rho^{E_g}(C_{2x}) = \begin{pmatrix} 1 & 0 \\ 0 & -1 \end{pmatrix}, \qquad \rho^{E_g}(C_{2d}) = \begin{pmatrix} 0 & 1 \\ 1 & 0 \end{pmatrix}, \tag{1.74}$$

which represent a $\frac{\pi}{2}$ rotation around the z and half rotation around x and $d = x + y + z$ axes respectively. This is deduced purely from the consideration of which matrices represent the correct rotations in coordinate space.

We then use the matrix, M to rotate the vector, v, to find

$$A_{1g} \otimes E_g = \begin{pmatrix} \varepsilon_1\phi \\ \varepsilon_2\phi \end{pmatrix}, \tag{1.75}$$

$$A_{2g} \otimes E_g = \begin{pmatrix} -\varepsilon_2\phi \\ \varepsilon_1\phi \end{pmatrix}, \tag{1.76}$$

$$B_{1g} \otimes E_g = \begin{pmatrix} \varepsilon_1\phi \\ -\varepsilon_2\phi \end{pmatrix}, \tag{1.77}$$

$$B_{2g} \otimes E_g = \begin{pmatrix} \varepsilon_2\phi \\ \varepsilon_1\phi \end{pmatrix}. \tag{1.78}$$

In doing so, we ensure that the matrices corresponding to group elements such as rotations are identical for each case. The products above all therefore correspond to E_g for the various choices of ϕ.

The last case we need to consider for D_{4h} is that of two two-dimensional irreducible representations corresponding to (ϕ_1, ϕ_2) and $(\varepsilon_1, \varepsilon_2)$ multiplied together. The product can be written as

$$E_g \otimes E_g = A_{1g} \oplus A_{2g} \oplus B_{1g} \oplus B_{2g}. \tag{1.79}$$

We deduce this from the great orthogonality theorem [28] which states that this sum is unique. Using the generators of the group we can find the characters for the character table from the trace

$$\chi_\rho(g) = \mathrm{Tr}\Big\{\rho(g)\Big\}. \tag{1.80}$$

The trace is of course invariant under a change of basis. Using

$$\chi_{\rho_1 \oplus \rho_2} = \chi_{\rho_1} + \chi_{\rho_2}, \tag{1.81}$$

and

$$\chi_{\rho_1 \otimes \rho_2} = \chi_{\rho_1} \times \chi_{\rho_2}, \tag{1.82}$$

we deduce Eq. 1.79 from Table. 1.1. We see that from the set of objects given by $(\phi_1, \phi_2) \otimes (\varepsilon_1, \varepsilon_2)$, we have to deduce which combinations transform like each one-dimensional representation. The change of basis matrix M in this case is the matrix which simultaneously diagonalises $\rho^E(C_{4z}) \otimes \rho^E(C_{4z})$, $\rho^E(C_{2x}) \otimes \rho^E(C_{2x})$ and $\rho^E(C_{2d}) \otimes \rho^E(C_{2d})$. In general this is found using the eigenvalues and eigenvectors of the generators and then comparing the eigenvalues to the character table to discern which column of M corresponds to each one-dimensional irreducible representation (We show this in full in Appendix. A.1). This yields the result

$$A_{1g} = \varepsilon_1\phi_1 + \varepsilon_2\phi_2, \tag{1.83}$$

$$A_{2g} = \varepsilon_2\phi_1 - \phi_2\varepsilon_1, \tag{1.84}$$

$$B_{1g} = \phi_1\varepsilon_1 - \phi_2\varepsilon_2, \tag{1.85}$$

$$B_{2g} = \phi_1\varepsilon_2 + \phi_2\varepsilon_1, \tag{1.86}$$

where, to be specific about the basis we use for these calculations

$$\begin{pmatrix} H_x \\ H_y \end{pmatrix} \in E_g, \qquad H_z \in A_{2g}, \tag{1.87}$$

$$\varepsilon_{x^2-y^2} \in B_{1g}, \qquad \varepsilon_{xy} \in B_{2g}, \qquad \begin{pmatrix} \varepsilon_{yz} \\ -\varepsilon_{xz} \end{pmatrix} \in E_g. \tag{1.88}$$

These rules effectively provide a recipe for deducing coupling terms in the action. It also elucidates how the altermagnetic terms are constructed. Using a magnetic dipole which, as we see above, transforms with A_{2g} and then constructing a form factor to mediate this dipole throughout the unit cell, the form factor is chosen such that the product of the irreducible representations of the dipole and form factor, according to the rules above, corresponds to an altermagnet with the desired symmetry.

To briefly summarise, the general method for finding the correct products consists of constructing a vector, v, from the Kronecker product of ϕ and ε, we then find the change of basis matrix using the eigenvectors of the product representations of the generators. This allows us to find the desired M such that

$$M^{-1}\rho^{\lambda_1}(g) \otimes \rho^{\lambda_2}(g) M = \bigoplus_i \rho^{\lambda_i}(g), \tag{1.89}$$

where the subscript i runs over the λ which correspond to the direct sum deduced from the character tables [28]. This matrix can be used to rotate v such that $M^{-1}v$ yields the combinations of ϕ_a and ε_a which correspond to the representations in the direct sum. In Appendix. A.1, we show this method in more detail for the product of two E_g irreducible representations in D_{4h}, which can be extended to irreducible representations of even higher order and crystals belonging to other point groups. We also include full product tables for the tetragonal group D_{4h} (Tab. A.1), hexagonal group D_{6h} (Tab. A.2) and cubic group O_h (Tab. A.3) as a reference for deriving symmetry allowed coupling terms.

We can apply these rules to already studied systems. Consider the case of nematoelastic coupling [16]

$$S_{\text{coupling}} = \lambda \int d^3\mathbf{r}dt\phi(\mathbf{r},t)\,\varepsilon_{\Gamma^+}(\mathbf{r},t), \tag{1.90}$$

where Γ denotes the irreducible representation that the object transforms under and the superscript $+$ is used to denote a time-reversal even object. For a nematic system such a coupling is symmetry allowed, provided that ϕ also transforms according to Γ^+. This coupling has been thoroughly studied [16, 19]. In such systems we see a softening of the elastic constants [19], leading to a structural phase transition, as well as an elastic quantum critical region where the heat capacity remains Fermi liquid-like around the QCP, in distinction to the bare quantum critical behaviour one derives from an electron only theory where the heat capacity becomes non-Fermi liquid-like [16]. This coupling, while symmetry allowed for nematics, must be adjusted for magnetic degrees of freedom. If ϕ now denotes a magnetic order parameter, it is odd with respect to time-reversal. Some other parameter must be introduced to correct this, for example a magnetic field. Instead consider the coupling term

$$S = \lambda H \int d^3\mathbf{r}dt\phi(\mathbf{r},t)\,\varepsilon_{\Gamma^+}(\mathbf{r},t). \tag{1.91}$$

The introduction of the magnetic field H, ensures that the term is time-reversal even. Both ϕ and H are time-reversal odd, such that their product is even. The condition for this term to be symmetry allowed is then

$$\Gamma_{\phi}^{-} \in \Gamma_{H}^{-} \otimes \Gamma_{\varepsilon}^{+}. \tag{1.92}$$

If this condition is met, then the term transforms trivially or at the very least, contains a symmetry allowed element. We can briefly consult Table. 1.2 and see that this condition holds because the product of an irreducible representation with itself gives an element which transforms according to the trivial representation. If ϕ is a ferromagnet aligned along z and $\mathbf{H} = H\hat{e}_z$ such that both terms transform according to A_{2g} then the coupling is

$$S = \lambda H_z \int d^3\mathbf{r}dt\phi\left(\mathbf{r},t\right)\left(\varepsilon_{xx}\left(\mathbf{r},t\right)+\varepsilon_{yy}\left(\mathbf{r},t\right)\right), \tag{1.93}$$

yielding the well-known piezomagnetic coupling term where ferromagnetism is coupled to a change in volume, mediated by an external magnetic field [138]. In the case that both the strain and magnetic field transform like E_g, we must then find the correct combination of components which matches the irreducible representation under which ϕ transforms. We can use Eq. 1.85 to demonstrate this. If ϕ transforms under B_{1g} and the strain components and magnetic field components are $\begin{pmatrix}\varepsilon_{yz}\\-\varepsilon_{xz}\end{pmatrix}$ and $\begin{pmatrix}H_x\\H_y\end{pmatrix}$ respectively, the combination which transforms under B_{1g} is then $H_x\varepsilon_{yz}+H_y\varepsilon_{xz}$ such that the coupling term is

$$S = \lambda \int_{r,t}\left(H_x\varepsilon_{yz}+H_y\varepsilon_{xz}\right)\phi_{B_{1g}}. \tag{1.94}$$

This corresponds to the piezomagnetic term for an altermagnet which transforms under B_{1g} in a magnetic field aligned in the $x-y$ plane. The above analysis therefore allows for the construction of terms which couple to symmetry breaking strain. The enhanced set of symmetries which altermagnets possess leads to new types of coupling to the lattice, which were not possible with the usual ferromagnetic and antiferromagnetic order parameters. While altermagnetic states are, due to their symmetry enforced net-zero magnetisation, difficult to detect, the coupling to the lattice provides a potential path to indirectly observing the symmetry breaking these systems are expected to display, thus identifying which materials are actually altermagnetic and which are merely antiferromagnets. A symmetry breaking strain allows for the formation of a net magnetisation, which a magnetic field is then able to couple to. We will analyse the effects of piezomagnetism in Chapter 2. Another option to account for the fact that ϕ is now time-reversal odd is to couple to dynamics

$$S_{\text{coupling}} = \lambda \int d^3\mathbf{r}dt\partial_t\phi\left(\mathbf{r},t\right)\varepsilon_{\Gamma^+}\left(\mathbf{r},t\right), \tag{1.95}$$

where the condition for this to be symmetry allowed is

$$\Gamma_{\phi} = \Gamma_{\varepsilon}. \tag{1.96}$$

In this case strain then couples to fluctuations of the order parameter, which as we discussed in Sec. 1.3 become strong close to the QCP. The time derivative accounts for the fact that ϕ is time-reversal odd. We will analyse this coupling in Chapter 3 and Chapter 4. We also

see here that the fact that in TBG there is an element of strain which transforms according to A_{2g} now allows for a coupling to the ferromagnetism aligned along z which would not be possible in a commensurate lattice; a result of the fact that ferromagnetism also transforms according to A_{2g} when aligned along z in TBG.

The coupling of Eq. 3.10 can also be obtained alternatively by following the approach of Refs. [139, 140] (also used in Ref. [20]), which shows that a consideration of infinitesimal strain is completely consistent with the group theory approach. If we consider a fermionic field operator $c(\boldsymbol{x})$ that is a spinor in spin and orbital space, performing a deformation of the lattice with non-symmetrized strain $\widetilde{\varepsilon}_{\alpha\beta} = \partial_\alpha u_\beta$, corresponds to the coordinate transformation

$$\boldsymbol{x'} = \hat{\Gamma}(t)^T \boldsymbol{x}, \tag{1.97}$$

where

$$\hat{\Gamma}(t) = e^{\widetilde{\varepsilon}}. \tag{1.98}$$

We consider an arbitrary strain field such that $\hat{\Lambda}(t)$ is an arbitrary matrix with a positive determinant. The fermionic field transforms as [139]

$$c_{\widetilde{\varepsilon}}(\boldsymbol{x}) = \sqrt{\det \Gamma}\, c\left(\Gamma^T \boldsymbol{x}\right). \tag{1.99}$$

If the change is small, then $\widetilde{\varepsilon} \to \widetilde{\varepsilon} + \delta\widetilde{\varepsilon}$

$$\frac{\partial}{\partial \widetilde{\varepsilon}_{\alpha\beta}} c_{\widetilde{\varepsilon}}(\boldsymbol{x}) = \frac{\delta_{\alpha\beta}}{2} c_{\widetilde{\varepsilon}}(\boldsymbol{x}) + x'_\alpha \frac{\partial}{\partial x'_\beta} c_{\widetilde{\varepsilon}}(\boldsymbol{x}). \tag{1.100}$$

Setting $\widetilde{\varepsilon} = 0$ allows for the study of an infinitesimal change, such that $\boldsymbol{x}' = \boldsymbol{x}$. The infinitesimal transformation is then:

$$c_{\widetilde{\varepsilon}}(\boldsymbol{x}) = \left[1 - i \sum_{\alpha\beta} \widetilde{\varepsilon}_{\alpha\beta} \mathcal{L}_{\alpha\beta}\right] c(\boldsymbol{x}), \tag{1.101}$$

where

$$\mathcal{L}_{\alpha\beta} = \frac{i\delta_{\alpha\beta}}{2} + i x_\alpha \frac{\partial}{\partial x_\beta} = -\frac{1}{2}\left(x_\alpha p_\beta + p_\beta x_\alpha\right). \tag{1.102}$$

We then denote the generator denoting to rotations in internal space as $\mathcal{S}_{\alpha\beta}$ and consider the total angular momentum $\mathcal{J}_{\alpha\beta} = \mathcal{L}_{\alpha\beta} + \mathcal{S}_{\alpha\beta}$. Specific examples, can be found in Refs. [139, 140]. $\mathcal{J}_{\alpha\beta}$ is even under parity, odd under time reversal and its symmetric part transforms like a symmetric second rank tensor, i.e. just like a multipolar order parameter. The field operator $c_{\widetilde{\epsilon}}(\boldsymbol{r})$ of the strained system is therefore related to the unstrained case via:

$$c_{\widetilde{\varepsilon}}(\boldsymbol{x}) = e^{-i\mathrm{Tr}\left(\widetilde{\varepsilon}^T \mathcal{J}\right)} c(\boldsymbol{x}) = U(t)\, c(\boldsymbol{x}), \tag{1.103}$$

with strain generators $\mathcal{J}_{\alpha\beta} = -\frac{1}{2}\left(x_\alpha p_\beta + p_\beta x_\alpha\right) + \frac{i}{8}\left[\sigma_\alpha, \sigma_\beta\right]$. $\boldsymbol{x}$ and $\boldsymbol{p} = -i\nabla$ are the position and momentum operators and the Pauli matrices σ_α act in orbital space.

$U(t)$ represents a time-dependent transformation such that

$$S_{\mathrm{c}} = -i \int d\tau d^3\boldsymbol{x} c^\dagger(\boldsymbol{x}) U(t) \frac{d}{dt}\left(U(t)^{-1}\right) c(\boldsymbol{x}). \tag{1.104}$$

The coupling term that emerges from the relation between the strained and unstrained system is hence [139, 140] $S_{\mathrm{c}} = \int d\tau d^3\boldsymbol{x} \sum_{\alpha\beta} \widetilde{\varepsilon}_{\alpha\beta} \frac{d}{d\tau} c^\dagger \mathcal{J}_{\alpha\beta} c$. Such that it couples strain to the time derivative of a fermionic bilinear that transforms like a multipolar magnetic order parameter. The coupling to dynamics that we deduced from symmetry can therefore also be derived from the generators of infinitesimal strain.

1.4.2 Experimental probing of order coupled to elasticity

The fact that there exists a natural coupling between electronic degrees of freedom and strain has led to a great number of possible experiments for probing states [78, 141]. One of which that is of particular importance to Chapter. 2 is the elastocaloric effect. This is defined as the adiabatic change in temperature with respect to a changing strain [78, 141]. Given that strain is one of the options available to us as a parameter which allows for a system to be tuned through the QCP [142], it is clear that this represents a crucial method for probing ordering. The elastocaloric effect is measured by applying an AC strain to a material, the adiabatic temperature change of the sample is then measured as the strain is applied and then released [141]. Experiments of this type have many uses in terms of probing order, for example in the determination of phase diagrams of unconventional superconductors [142] or carrying out the experiment in different symmetry channels to reveal something about the symmetry of the order parameter. In nematic systems it has been used to rule out certain types of nematic ordering [77]. The fact that this experiment is so prevalent in its use with regards to nematic systems already suggests an importance to the altermagnetic, this is a direct result of the similarities in the symmetries of the relevant order parameters.

We can utilise a simple calculation based on a Landau expansion in order to give some intuition as to how the elastocaloric effect probes order in the classical regime [78] (the quantum equivalent will be shown in Chapter 2). The change in temperature with respect to strain (also called by the elastocaloric coefficient η) is given by

$$\eta = \left.\frac{dT}{d\epsilon}\right|_S = -\frac{\partial S/\partial\epsilon}{\partial S/\partial T}, \tag{1.105}$$

where S is entropy and ϵ is in this case a strain which forms a symmetry allowed coupling to some altermagnetic order parameter ϕ (i.e. it breaks a symmetry). We know from basic thermodynamics that

$$\frac{\partial S}{\partial T} = \frac{C_\epsilon}{T}, \tag{1.106}$$

where C_ϵ is the specific heat at constant strain. We know that

$$\frac{dS}{d\epsilon} = -\frac{d^2F}{dTd\epsilon}, \tag{1.107}$$

where F is the free energy. Writing down a Landau expansion for the free energy of the

coupled degrees of freedom, as outlined in Section. 1.3 gives

$$F = \frac{1}{2}\chi^{-1}(T)\,\phi^2 + \frac{C_0}{2}\epsilon^2 + \lambda H\phi\epsilon, \tag{1.108}$$

where $\chi(T)$ is the altermagnetic susceptibility and diverges as the system orders, C_0 is the elastic constant (or combination of elastic constants) associated with the strain ϵ and H is a magnetic field which facilitates a piezomagnetic coupling between magnetism and strain. The product of ϵ and ϕ must, once again, contain the same irreducible representation as the magnetic field for such an expansion to be symmetry allowed. Note that we ignore any terms above second order, this is reasonable provided we are close to the transition such that ϕ is small. We can then minimise the free energy with respect to ϕ, this is the equivalent of integrating out the electronic degrees of freedom, doing so renormalises the elastic constant

$$C = C_0 - \lambda^2 H^2 \chi(T). \tag{1.109}$$

Taking the necessary derivatives of the free energy yields an expression for the elastocaloric change in temperature

$$\eta = -\lambda^2 H^2 \frac{T}{C_\epsilon}\frac{d\chi}{dT}\epsilon. \tag{1.110}$$

We see immediately from this expression why this is a useful method to probe ordering; at a second order transition, χ diverges and this will be reflected in the elastocaloric change in temperature. This shows clearly that elastocaloric measurements provide a method to probe the critical fluctuations present close to a second order phase transition [78].

Another measure of the onset of order in systems which couple to elasticity can be seen from Eq. 1.109, in particular for specific values of T, H, λ, the elastic constant becomes soft, which then leads to a structural distortion, this lattice softening is also detectable through experiment in the case of nematics [143] and therefore, with a strong enough coupling, should also be relevant in altermagnetic systems.

Other methods for probing order involve the measurement of phonons. Phonons can be measured for example through pump-probe measurements [144], in which phonons are first excited by an initial pumping laser, followed by a less powerful probe laser. The probe laser then provides data on quantities such as the reflectivity, Raman scattering, induced absorption etc. Theoretical calculations yield how phonons are affected by hybridisation, which would then allow for one to indirectly detect magnetic collective modes by measuring phonon spectra, this will be a focus of Chapter. 3.

This analysis provides evidence for how powerful the concept of symmetry is in considerations of order parameter-strain coupling, even beyond magnetism and that the new and considerably more varied symmetries of an altermagnet and of the elastic degrees of freedom in TBG create opportunities to study exotic phenomena through the effects of magnetism on strain.

Chapter 2

2 Critical fluctuations in altermagnets

Above an altermagnetic and nematic critical point, fluctuations drive a divergence in the heat capacity and elastocaloric change in temperature which is no longer consistent with Fermi liquid theory. Nematic order parameters are able to couple directly to symmetry breaking strain; in such cases, the divergence in the heat capacity is suppressed, leading to the appearance of Fermi liquid behaviour of heat capacity and single-fermion lifetime at leading order [16]. This creates a region of elastic quantum criticality (QC) above the critical point and below a crossover temperature to the bare quantum critical regime. The symmetries of an altermagnet allow for a coupling with similar structure, a piezomagnetic coupling to symmetry breaking strain. This creates a coupling between altermagnetism and strain with effects which are then tuned by the strength of an external magnetic field. The two regions which exist close to the critical point can then be tuned by the magnetic field, allowing for the bare QC regime to be expanded all the way down to the QCP, creating a region of non-Fermi liquid behaviour which is not accessible in nematic systems. In Ref. [17] (which most of this chapter either adapts or quotes from) an analysis is presented of this elastic QC regime showing that it is not a true Fermi liquid. Coupling to strain leads to gapless modes along specific directions in momentum space. Observables such as the heat capacity and single particle self-energy are not sensitive to these gapless modes, the contributions thereof are subleading (leading to FL behaviour). In order to detect what we call singular Fermi liquid behaviour, an analysis of the collective modes of the fermions must be carried out. One can measure the temperature change with respect to a varying a.c. strain, known as the elastocaloric coefficient. An analysis of this quantity shows that while the effect becomes less singular in the elastic quantum critical regime, it is sensitive to these modes and retains divergences, thus proving that this state is not a Fermi liquid. This chapter will focus on altermagnetic systems, however the results also hold for nematic systems [17].

2.1 Introduction

Nematic and altermagnetic order parameters can, in many cases, break the same rotational symmetries. This allows for similar couplings to strain in both systems. We briefly recount what is known about nematic systems in the interest of contextualising the altermagnetic equivalent. In nematic systems it has been shown that critical fluctuations can drive non-Fermi liquid behaviour [15, 116, 117, 145–151]. This is manifested physically in two dimensional

systems as anomalous powerlaw dependencies in the single-particle lifetime and the electronic specific heat, and as marginal Fermi-liquid behaviour in three dimensions [152]. Nematic states break rotational symmetry and leave translation invariance unaffected [57], this allows for a coupling to acoustic phonons of the same symmetry; this coupling takes the form

$$H_{\mathrm{nem-latt}} = \lambda \int d^3\boldsymbol{x} \epsilon_{\Gamma_\phi^+}(\boldsymbol{x})\, \phi(\boldsymbol{x}), \tag{2.1}$$

where λ is the nematoelastic coupling strength, Γ_ϕ^+ is the irreducible representation of the nematic order parameter $\phi(\boldsymbol{x})$, where the superscript indicates that it is even under time-reversal. $\epsilon_{\Gamma_\phi^+}$ is the strain field that transforms under Γ_ϕ^+. An analysis of this coupling was carried out in Ref. [19] in which it was shown that coupling to strain leads to a softening of the shear modulus at the nematic transition [153–155]. The renormalised elastic constants, related to the symmetry channel of strain which the nematic order parameter couples to, is given by [19, 153]

$$C_{\mathrm{ren}}^{-1} = C^{-1} + \frac{\lambda^2}{C^2}\chi_{\mathrm{nem}}, \tag{2.2}$$

where C is the bare elastic constant, the value of which is approached at high temperatures where the nematic susceptibility, χ_{nem}, is small. The nematic susceptibility diverges at the second order transition, leading to a renormalised elastic constant which vanishes. Ref. [19] showed that when nematic fluctuations cause the lattice to soften, long-range strain forces act back onto the nematic modes, leading to a crossover to mean-field behaviour [156, 157].

Another analysis of these systems is given in Ref. [16], in which it was shown that in addition to the non-Fermi liquid behaviour around the QCP, there exists a region of quantum critical behaviour strongly altered by the elastic degrees of freedom, which we hereafter refer to as the elastic quantum critical region. In this region, the leading order behaviour of the heat capacity and single-particle lifetime is Fermi liquid-like. At higher temperatures there exists the bare quantum critical regime where these observables exhibit non-Fermi liquid behaviour at leading order. In the absence of this coupling, the bare quantum critical region persists down to the quantum critical point and the Sommerfeld coefficient $\gamma(T) = c(T)/T$, with specific heat $c(T)$, diverges like $\gamma \sim \log\Big(T_0/T\Big)$, like in a marginal Fermi liquid [152] with temperature scale

$$T_0 = \frac{1}{3\pi\alpha}\left(\frac{\Lambda}{k_F}\right)^3 E_F, \tag{2.3}$$

determined by the Fermi energy E_{F}, the bosonic cut off Λ, the Fermi wave vector k_F, and the dimensionless coupling constant α of electrons to nematic collective modes.

Ref. [16] showed that the existence of a coupling between the nematic modes and the lattice changes the universality class of the QCP and the Sommerfeld coefficient saturates below the temperature

$$T_* \sim \frac{\lambda^3}{C^{3/2}J^3}T_0, \tag{2.4}$$

where J is an energy scale which characterises the total band width of the nematic collective mode. C is the bare elastic constant of Eq. 2.2 that governs the symmetry channel of the nematic order parameter. Hence, the expected divergence $\gamma \sim \log\Big(T_0/T\Big)$ is suppressed and

replaced by $\gamma \sim \log\left(T_0/T_*\right)$. Similar behaviour also occurs for the single-particle self-energy. This behaviour originates from a sound velocity which now vanishes along isolated lines in momentum space, giving rise to non-analytic, long-range order parameter interactions which suppress both classical and quantum fluctuations. At the QCP, the heat capacity and single particle lifetimes are indistinguishable from a Fermi liquid, provided one only considers the leading order low T contribution and therefore as far as the fermions are concerned, this region is a Fermi liquid. It is therefore interesting to see whether there exists an observable which does distinguish between the elastic QC and a Fermi liquid at leading order. Fermi liquid theory describes fermionic quasiparticles alongside their collective modes. To reiterate, in Ref. [16] coupling to strain re-establishes well-defined fermionic quasiparticles. One might therefore conclude that a nematic QCP and, as we will soon see, by analogy, an altermagnetic QCP in an external field is governed entirely by Fermi liquid physics, with the remaining QCP-associated soft modes contributing only subleading corrections. However, our analysis reveals that the situation is more nuanced: the elastocaloric effect exhibits behaviour that deviates from standard Fermi liquid predictions. Importantly, this deviation does not stem from an independent anomaly in the systems elastic properties. We will show that this result can alternatively be derived from the fermionic contribution to the entropy. Taking a strain derivative, as is done in the elastocaloric effect, amplifies what would otherwise appear as a subleading correction. This motivates the characterisation of such a state as a singular Fermi liquid. While this analysis of the QC regime is applicable to nematic systems, we will focus here on its applicability to altermagnetic systems.

A proper analysis of the elastic QC regime therefore lies in an analysis of the fermionic collective modes, carried out by considering the elastocaloric effect [17]. This effect is outlined in Sec. 1.4 and allows for the performing of high accuracy measurements [158]. The measurements are of the adiabatic temperature change with respect to an applied strain, i.e.

$$\eta(T) = \left.\frac{dT}{d\epsilon_0}\right|_S , \tag{2.5}$$

where ϵ_0 denotes strain which transforms trivially under point group operations. An analysis of $\eta\left(T\right)$ shows that it behaves differently to that of a Fermi liquid in the elastic QC regime, suggesting that even at the lowest temperatures, this is not a Fermi liquid state with regards to the collective modes of the fermions (although it is less singular in this temperature range) [17]. In Table. 2.1, we see the temperature dependence of the heat capacity and elastocaloric effect in both the elastic and bare QC regimes.

	$c\left(T\right)$	$\eta\left(T\right)$
Fermi liquid	$\propto T$	$\propto T$
bare quantum critical	$\propto T \log T$	$\propto T^{1/3}/\log T$
elastic quantum critical	$\propto T$	$\propto T \log T$

Table 2.1: Heat capacity $c(T)$ and elastocaloric effect $\eta(T)$ as function of temperature in the Fermi liquid, the bare quantum critical (for $d = 3$ and without coupling to the lattice), and the elastic quantum critical regimes. From the perspective of the heat capacity (and the single particle life time) the elastic QC below T^* is indistinguishable from the Fermi liquid, while the elastocaloric effect is able to discriminate between the two regimes (Table reprinted from Ref. [17]).

The coupling between nematic order and strain given in Eq. (2.1) takes a very similar form to that of a piezomagnetic coupling in an altermagnetic system. Like nematics, altermagnets also break a symmetry which can be a rotation; the distinction between the two systems comes from the fact that altermagnets break time reversal symmetry and hence another time-reversal odd parameter must be introduced to any coupling term. In order to achieve a piezomagnetic effect, the parameter chosen is the magnetic field and the piezomagnetic [134, 135] coupling is given by

$$H_{\mathrm{am-latt}} = \sum_i \sum_\alpha \lambda^a_{\alpha,i} H_\alpha \int d^3\boldsymbol{x} \epsilon_{\Gamma_i^+}(\boldsymbol{x})\, \phi^a(\boldsymbol{x})\,. \tag{2.6}$$

It is symmetry-allowed, provided that $\Gamma^-_\phi \in \Gamma^-_{H_\alpha} \otimes \Gamma^+_{\epsilon_i}$, i.e. the product representation of the α-th component of the magnetic field $\Gamma^-_{H_\alpha}$ and strain $\Gamma^+_{\epsilon_i}$ must contain the order parameter representation Γ^-_ϕ. It is this coupling which we will analyse here, with mention of the analogy with the nematic case [16, 17]. We see that the two couplings are of a very similar form, with the introduction of a magnetic field in the altermagnetic case which can now be used to tune the coupling strength. Given that the crossover temperature between the bare and elastic QC regimes is dependent on the coupling strength [16], this suggests that the two regions can be tuned by an applied magnetic field. In Fig. 2.1, we show a schematic representation of the piezomagnetic coupling. Initially the unstrained altermagnet has a net-zero magnetisation within the unit cell; once a strain is applied, the symmetries which previously forbade the formation of a magnetisation are broken. The induced magnetisation in strained altermagnets is given by [20, 58, 159–161]

$$M_\mu = \Lambda_{\mu\gamma\delta}\epsilon_{\gamma\delta}, \tag{2.7}$$

where $\Lambda_{\mu\gamma\delta}$ is the piezomagnetic tensor and M_μ is the component of the magnetisation density aligned along the μ direction. A magnetic field can then couple to the induced magnetisation.

In this chapter we will show that a piezomagnetic coupling between an altermagnetic order parameter and the lattice leads to the formation of a direction selective criticality and the emergence of gapless bosons along these directions. For reference, we will give a list of the possible piezomagnetic couplings and coupling to fermions for a tetragonal system in this chapter and for hexagnonal, cubic and orthorhombic systems in Appendix. B. We will use the coupling to fermions to show that the magnons acquire a Landau damping term which, unlike for nematic systems [16] is not dependent on the direction of momentum $\mathbf{q}$. We will show how gapless bosons give two regimes of behaviour, the aforementioned elastic and bare QC regimes and through calculations of the electron self-energy and heat capacity, that these regions are tunable via an applied field. This will allow for an experimentally accessible region of NFL behaviour above the critical point which is not accessible in the nematic systems studied in Ref. [16]. We see this summarised in the schematic diagram in Fig. 2.2. An analysis of the elastocaloric effect will prove that the elastic QC is not a Fermi liquid, or more accurately the collective modes do not display Fermi liquid behaviour at leading order in low temperatures, a result of which is actually relevant for both nematic and altermagnetic systems. We will show that this is consistent with an analysis of the generalised scaling behaviour near the elastic QC regime. This scaling behaviour is outlined in Ref. [162]. We will also show that the piezomagnetic coupling has an analogy with the Hall effect in strained altermagnets insofar as the strains which induce a finite magnetisation can also induce a finite Berry curvature and hence, nonzero Hall current.

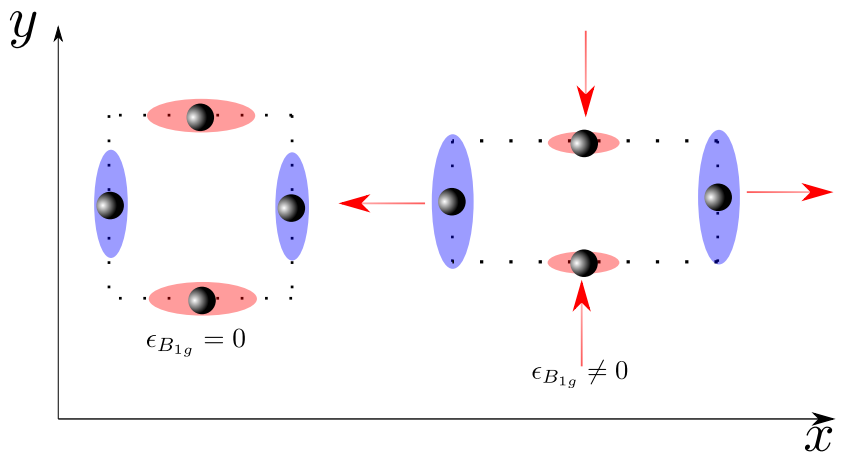

Figure 2.1: The physical origin of the coupling considered here is simple to visualise. An altermagnet which transforms according to the irreducible representation B_{2g} has the order parameter $\phi_{B_{2g}} \sim \sum_{\mathbf{k}} f_{B_{2g}}(\mathbf{k}) \left\langle c^{\dagger}_{\mathbf{k}} \sigma^z c_{\mathbf{k}} \right\rangle$. Spins aligned along the z direction are distributed in the unit cell according to the irreducible representation B_{1g}, such that the object transforms like B_{2g}. There exists no net magnetisation and the magnetic field cannot couple. Breaking this symmetry by applying a B_{1g} strain allows for the formation of a ferromagnetic moment and allows for a coupling to an external magnetic field. (Figure reprinted from Ref. [17])

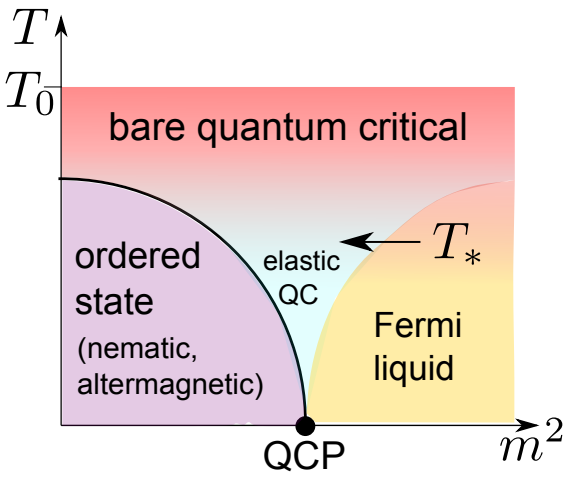

Figure 2.2: Phase diagram near a nematic or altermagnetic quantum critical point (QCP). The phase is tuned by the non-thermal parameter m^2. The coupling to elastic degrees of freedom gives rise to a change in the universality class of the QCP [16] from the bare quantum critical to the elastic quantum critical regime at the crossover temperature T_*. In an altermagnetic system, T_* can be tuned by applying an external magnetic field, where $T_*(H = 0) = 0$. (Figure reprinted from Ref. [17])

2.2 Piezomagnetic coupling in altermagnets

The piezomagnetic coupling of Eq. (2.6) is underpinned by the group theory outlined in Sec. 1.4, which is then used to deduce which components of $\lambda^a_{\alpha,i}$ are nonzero and how many are independent. We consider an altermagnet with an order parameter denoted ϕ^a, this order parameter corresponds to multipolar magnetism meaning that, as discussed in Sec. 1.2, it breaks time-reversal symmetry, keeps translation unchanged and does not transform like a magnetic dipole. The latter ensures that the net-moment in the unit cell is zero by symmetry. a labels the components of the order parameter, an index that we drop if we consider single-component systems. For a g-dimensional representation, $a = 1 \cdots g$ labels the components.

The symmetry-allowed coupling of ϕ^a to lattice fluctuations will be crucial for our subsequent analysis. In order to provide a concrete set of interaction terms, we performed a group theory analysis (Appendix. B) for several important point groups. These couplings allow for the probing of an altermagnetic order parameter through measurements in the change of magnetisation with respect to the strain

$$\sum_a \lambda^a_{\alpha,i}\phi^a = \partial M_\alpha / \partial \epsilon_{\Gamma^+_i}. \tag{2.8}$$

Choosing the appropriate field direction and strain symmetry then allows to determine the otherwise rather hidden altermagnetic order parameter. The symmetry allowed piezomagnetic couplings for a tetragonal system are listed in Table 2.2. In addition we summarize the couplings for systems with hexagonal (Table B.2), cubic (Table B.3), and orthorhombic (Table B.1) symmetries in the Appendix B.1. In these tables we also list the symmetry-allowed coupling of ϕ^a to fermionic modes of a single band system. The latter was discussed in the context of protected nodal lines of the Zeeman splitting [58]. These couplings will be crucial when we analyse the dynamics near altermagnetic quantum critical points due to the Landau damping which arises as a result.

The list of possible couplings reveals several aspects which are worth noting: the piezomagnetic coupling can also be constructed for ferromagnetic systems. These are indicated in grey in the tables. Secondly, in some cases, such as tetragonal crystals, piezomagnetic couplings can be used to uniquely identify the symmetry of an altermagnetic state, this is however, not the case for other symmetries, such as cubic and hexagonal systems. Finally, there also exist altermagnetic states that cannot be detected through first order piezomagnetic couplings. The state identified in the systems discussed here is the order parameter that transforms under A^-_{1g} in cubic crystals, see table B.3. This state is a combination of a spin dipole and a charge hexadecapole that forms a dotriacontapolar state. It can still be identified if one simultaneously applies strain of T^+_{2g} and E^+_g symmetries and analyses piezomagnetic effects that are nonlinear in the strain fields, however the fact that this is a higher order effect suggests that it is much smaller in comparison with the other couplings listed.

2.3 Classical fluctuations

While the focus of this chapter is on quantum critical fluctuations, an analysis of the classical fluctuations of a piezomagnetically coupled altermagnet reveals important characteristics, including of the structural phase transition discussed in nematics [16, 19] and how fluctuations

D_{4h} $(4/mmm)$ point group		
AM irrep	coupling to fermions	piezomagnetic coupling
A_{1g}^-	$g\phi k_z\Big(k_y\sigma_x - k_x\sigma_y\Big)$	$\lambda\phi\left(\epsilon_{yz}H_x - \epsilon_{xz}H_y\right)$
B_{1g}^-	$g\phi k_z\Big(k_y\sigma_x + k_x\sigma_y\Big)$	$\lambda\phi\left(\epsilon_{yz}H_x + \epsilon_{xz}H_y\right)$
	$g'\phi k_x k_y\sigma_z$	$\lambda'\phi\epsilon_{xy}H_z$
B_{2g}^-	$g\phi k_z\Big(k_x\sigma_x - k_y\sigma_y\Big)$	$\lambda\phi\left(\epsilon_{xz}H_x - \epsilon_{yz}H_y\right)$
	$g'\phi\left(k_x^2 - k_y^2\right)\sigma_z$	$\lambda'\phi\epsilon_{x^2-y^2}H_z$
FM irrep		
A_{2g}^-	$g\phi\sigma_z$	$\lambda\phi\epsilon_{A_{1g}}H_z$
		$\lambda'\phi\left(\epsilon_{zx}H_x + \epsilon_{yz}H_y\right)$
E_g^-	$g\left(\phi_1\sigma_x + \phi_2\sigma_y\right)$	$\lambda\epsilon_{A_{1g}}\left(\phi_1 H_x + \phi_2 H_y\right)$
		$\lambda'\epsilon_{x^2-y^2}\left(\phi_1 H_x - \phi_2 H_y\right)$
		$\lambda''\epsilon_{xy}\left(\phi_1 H_y + \phi_2 H_x\right)$
		$\lambda'''\left(\phi_1\epsilon_{xz} + \phi_2\epsilon_{yz}\right)H_z$

Table 2.2: The coupling of altermagnetic (AM) and ferromagnetic (FM) order parameters ϕ to fermions and to simultaneous magnetic and strain fields (piezomagnetism) for the tetragonal point group D_{4h} $(4/mmm)$. Ferromagnetic ϕ have been listed (in grey) for the sake of completeness. The first column indicates the irreducible representation (irrep) according to which ϕ transforms. g and λ are coupling constants, k_α is the momentum, σ_α are Pauli matrices, $\epsilon_{\alpha\beta}$ is the strain tensor, and H_α is the magnetic field. The possibility of having $g' \neq g$ and $\lambda' \neq \lambda$ is a result of the fact that there exists magnetic anisotropy in the system. $\epsilon_{A_{1g}}$ are the strain components which transform trivially. The coupling to lattice fermions is deduced by replacing k_α with $\sin k_\alpha$. The results of this and other tables agree with Ref. [58] where they overlap. (Table reprinted from Ref. [17])

are suppressed by the resulting soft modes. These realisations will also be important for the quantum analysis which follows.

2.3.1 Field-induced lattice softening

We see that the coupling Eq. (2.6) allows for analogies to be constructed with respect to nematic systems, by absorbing the magnetic field into the coupling constant

$$\lambda_H = \lambda_{\alpha,i} H_\alpha, \tag{2.9}$$

the system essentially behaves as a nematic system, yet with different symmetries of the strain field, as dictated by Table 2.2 and Tables B.1-B.3. One can then follow the analysis of Ref. [153] to investigate how this coupling affects the elastic degrees of freedom. If we assume the lattice is stable at zero field, the order parameter, ϕ, is the dominant order parameter that is responsible for the transition and drives the critical behaviour, while ϵ is field induced and secondary, meaning it will not order on its own. In this case we can write for the classical many-body action of the problem

$$S_{tot}\left[\phi, \epsilon\right] = S\left[\phi\right] + \int d^d x \left(\frac{C_0}{2}\epsilon^2 - \lambda_H \phi\epsilon - h_\phi \phi - \sigma\epsilon \right). \tag{2.10}$$

Here $S\left[\phi\right]$ is some non-linear action which describes a system near a critical point. The explicit form of $S\left[\phi\right]$ is not crucial for what follows. Since ϵ is the secondary order parameter, it is reasonable to ignore higher order couplings or terms that are non-local in space or time, i.e. we assume that the bare action of the secondary order parameter is Gaussian. We include two external fields h_ϕ and σ that couple to the altermagnetic order parameter and strain respectively. h_ϕ does not, of course, correspond to an actual magnetic field as it must transform under the same representation as ϕ, which as discussed, does not transform like a dipole. At first glance, it seems that such a field is not easily realisable in the laboratory, however, in the presence of a magnetic field, stress essentially plays the role of this conjugated field. This gives rise to a close relation between the altermagnetic susceptibility

$$\chi_{\text{am}} = -\left.\frac{\partial^2 F}{\partial h_\phi^2}\right|_{h_\phi \to 0, \sigma = 0}, \tag{2.11}$$

and the elastic constant

$$C^{-1} = -\left.\frac{\partial^2 F}{\partial \sigma^2}\right|_{h_\phi = 0, \sigma \to 0}. \tag{2.12}$$

For $\lambda_H = 0$, it holds that C equals the bare elastic constant C_0.

For the Free energy

$$dF = -\left\langle \epsilon \right\rangle d\sigma - \left\langle \phi \right\rangle dh_\phi, \tag{2.13}$$

with Hooke's Law

$$C_0 \left\langle \epsilon \right\rangle = \sigma + \sigma_{\text{int}}, \tag{2.14}$$

where the internal stress is given by

$$\sigma_{\text{int}} = \lambda_H \langle \phi \rangle . \tag{2.15}$$

This gives the equation of state

$$\begin{aligned} \langle \epsilon \rangle &= -\frac{\partial F}{\partial \sigma} = \frac{\sigma}{C_0} + \frac{\lambda_H}{C_0} \langle \phi \rangle \\ &= \frac{\sigma}{C_0} - \frac{\lambda_H}{C_0} \frac{\partial F}{\partial h_\phi}. \end{aligned} \tag{2.16}$$

For the two order parameters we expect two coupled equations of state. One of which requires an actual solution of the critical behaviour due to $S[\phi]$ which is therefore is hard to determine, the other is given above and establishes a simple relationship between $\langle \varepsilon \rangle$, stress and the primary order parameter $\langle \phi \rangle$. For $\sigma = 0$ both order parameters are proportional to each other, in agreement with

$$M_\alpha = -\frac{1}{V} \left. \frac{\partial F}{\partial H_\alpha} \right|_{H \to 0} = \sum_{i,a} \lambda^a_{\alpha,i} \epsilon_{\Gamma_i^+} \phi^a. \tag{2.17}$$

From the equation of state we find

$$\frac{\partial \langle \epsilon \rangle}{\partial \sigma} = \frac{1}{C_0} - \frac{\lambda_H}{C_0} \frac{\partial^2 F}{\partial h_\phi \partial \sigma}, \tag{2.18}$$

$$\frac{\partial \langle \epsilon \rangle}{\partial h_\phi} = -\frac{\lambda_H}{C_0} \frac{\partial^2 F}{\partial h_\phi^2}. \tag{2.19}$$

The relationship between the derivative with respect to σ and h_ϕ allows us to derive a relation between the two order parameter susceptibilities:

$$\frac{\partial \langle \epsilon \rangle}{\partial \sigma} = \frac{1}{C_0} - \frac{\lambda_H^2}{C_0^2} \frac{\partial^2 F}{\partial h_\phi^2}. \tag{2.20}$$

It follows

$$C^{-1} = C_0^{-1} + \frac{\lambda_H^2}{C_0^2} \chi_{\text{am}}. \tag{2.21}$$

This is an exact relation. The divergence of the altermagnetic susceptibility at a second order phase transition gives rise to a field induced lattice softening. If we are now specific about the symmetry of the altermagnetic order parameter, we can consider a B_{2g} altermagnet with coupling

$$S_c = \lambda H_z \int_{\mathbf{x}} \left(\epsilon_{xx} - \epsilon_{yy} \right) \phi_{B_{2g}} \tag{2.22}$$

where λ is the coupling strength and H_z is an external magnetic field, aligned along the z direction. This coupling term holds as the magnetic field aligned along z transforms under A_{2g}. The product of the order parameter, magnetic field and strain therefore transforms according to A_{1g}. The elastic constant related to the B_{1g} strain element is $\frac{1}{2}(C_{11} - C_{12})$ and this is the combination of elastic constants which vanishes at the transition. This combination

of elastic constants vanishes at the phase transition in a B_{1g} nematic system [16, 19]. The irreducible representation of the order parameter differs as a nematic order parameter can be coupled directly to strain without another parameter to mediate this coupling.

This would in theory allow for a measurement of the altermagnetic susceptibility, however in many currently known altermagnetic materials, the small energy scales of the field compared to the ordering temperature make this difficult to observe [163]. Following Ref. [19], we can still use an RG calculation to show the regime where this softening occurs and understand how this softening affects fluctuations.

2.3.2 Critical behaviour

We mentioned in the introduction that in nematic systems, when nematic fluctuations cause the lattice to soften, the long-range strain forces drive the nematic modes to a mean-field regime. This analysis was carried out in Ref. [19] and we can perform a very similar analysis for the altermagnet. Following the method of Ref. [19] and integrating out the strain field gives a ϕ^4 theory with a modified propagator

$$S = \int_{\mathbf{q}} \chi_0 \left(\mathbf{q}\right) \phi_{\mathbf{q}} \phi_{-\mathbf{q}} + \frac{u}{4} \int_{\mathbf{x}} \phi_{\mathbf{x}}^4, \tag{2.23}$$

with a propagator that softens along specific directions:

$$\chi_0 \left(\boldsymbol{q}\right)^{-1} = r + q^2 + h_1 \Lambda^2 \frac{\left(q_x^2 - q_y^2\right)^2}{q^4} + h_2 \Lambda^2 \frac{q_\perp^2}{q^2}, \tag{2.24}$$

where $h_i \Lambda^2 = -\frac{\lambda^2 H_z^2}{\left(C_{11} - C_{12}\right)^2} \mu_i$ where Λ is the momentum cutoff and (see Ref. [19] Appendix. A)

$$\mu_1 = \frac{1}{8} \left(c_{11} + c_{66} - \frac{\left(c_{11} - c_{66}\right)^2}{c_{12} - c_{66}} \right), \qquad \mu_2 = c_{44}. \tag{2.25}$$

This creates a soft direction along $q_x = \pm q_y$, while all other directions, denoted by $q_\perp$ are hard. There are two approaches one can take to number the hard and soft directions. The method used in Ref. [19] suggests using $m = d - 2$ soft directions. This yield an upper critical dimension of 2. The approach we will take here is to consider a d dimensional system where m directions are soft and $d - m$ directions are hard. Both approaches are equivalent in $d = 3$, however using $m = 1$ is correct in both two and three dimensions. We will see from the scaling analysis in Sec. 2.5 that hard dimensions are counted twice, whereas soft directions scale as usual. This gives an effective dimension of $d_{\text{eff}} = 2\left(d - m\right) + m$ where $d_{\text{eff}} = 5$ when $d = 3$ and $m = 1$. We therefore see that the presence of hard and soft directions suppresses fluctuations through a higher effective dimension. This also yields an upper critical dimension of $d_{\text{uc}} = 2.5$ [162] and therefore in two dimensional systems an epsilon expansion can be applied.

We can perform a one-loop RG for this model, which yields the usual flow equations [57]

$$\begin{aligned}\frac{dr}{dl} &= 2r + 3u\frac{d}{dl}\int_{\boldsymbol{q}}^{>}\chi_0\left(\boldsymbol{q}\right) - 3ur\frac{d}{dl}\int_{\boldsymbol{q}}^{>}\chi_0\left(\boldsymbol{q}\right)\chi_0\left(\boldsymbol{q}\right),\\ \frac{du}{dl} &= \left(4-D\right)u - 9u^2\frac{d}{dl}\int_{\boldsymbol{q}}^{>}\chi_0\left(\boldsymbol{q}\right)\chi_0\left(\boldsymbol{q}\right),\end{aligned} \tag{2.26}$$

where $\int_{\boldsymbol{q}}^{>}\cdots$ stands for integrating out the shell $\Lambda/b < q^2 < \Lambda$ with $b = e^l$ and the integrals are taken at $r = 0$. The flow equations for $h_{1,2}$ are given as

$$h_{1,2}\left(l\right) = h_{1,2}e^{2l}, \tag{2.27}$$

which follows from power counting. Given the non-analytic character of the terms that are proportional to the h_i no shell integration will be able to give higher order corrections. Hence, these are the exact flow equations for $h_{1,2}$ [19]. One then needs to perform the shell integrations which yields

$$\begin{aligned}\int_{\boldsymbol{q}}^{>}\chi_0\left(\boldsymbol{q}\right) &= l\Lambda^{d-2}A_d\left(h_1,h_2\right),\\ \int_{\boldsymbol{q}}^{>}\chi_0\left(\boldsymbol{q}\right)\chi_0\left(\boldsymbol{q}\right) &= l\Lambda^{d-4}B_d\left(h_1,h_2\right).\end{aligned} \tag{2.28}$$

where [19]

$$\begin{aligned}A_d\left(h_1,h_2\right) &= \frac{K_{d-2}}{\left(2\pi\right)^{d-1}}\int_0^1 dy\frac{y^{d-3}}{\sqrt{\left(1+h_2y^2\right)\left(1+h_2y^2+h_1\left(1-y^2\right)^2\right)}},\\ B_d\left(h_1,h_2\right) &= \frac{\pi K_{d-2}}{\left(2\pi\right)^{d}}\int_0^1 dy\frac{y^{d-3}\left(2+2h_2y^2+h_1\left(1-y^2\right)^2\right)}{\left(\left(1+h_2y^2\right)\left(1+h_2y^2+h_1\left(1-y^2\right)^2\right)\right)^{3/2}},\end{aligned} \tag{2.29}$$

where we introduced $y = q_\perp/\Lambda$ and $K_d = \frac{2\pi^{d/2}}{\Gamma[d/2]}$. Again following Ref. [19], the renormalised h_i will always eventually become large and so for $h_i \gg 1$ it holds

$$\begin{aligned}A_d\left(h_1,h_2\right) &= \frac{a_d}{\sqrt{h_1h_2^{d-2}}},\\ B_d\left(h_1,h_2\right) &= \frac{b_d}{\sqrt{h_1h_2^{d-2}}},\end{aligned} \tag{2.30}$$

where $a_d = \Gamma\left(\frac{3-d}{2}\right)/\left(2^{d-1}\pi^{\frac{d+1}{2}}\right)$ and $b_d = \frac{3-d}{2}a_d$.

This yields the flow equations

$$\begin{aligned}\frac{dr}{dl} &= 2r + 3\Lambda^{d-2}\frac{a_d u}{\sqrt{h_1 h_2^{d-2}}} - 3r\Lambda^{d-4}\frac{b_d u}{\sqrt{h_1 h_2^{d-2}}},\\ \frac{du}{dl} &= (4-d)\,u - 9\Lambda^{d-4}\frac{b_d u^2}{\sqrt{h_1 h_2^{d-2}}}.\end{aligned} \tag{2.31}$$

Introducing the dimensionless coupling constant $\tilde{u}$ and mass $\tilde{r}$

$$\tilde{u} = 9\Lambda^{D-4} b_D \frac{u}{\sqrt{h_1 h_2^{D-2}}}, \qquad \tilde{r} = \frac{3b_D}{a_D}\frac{r}{\Lambda^2}. \tag{2.32}$$

The flow equations become

$$\begin{aligned}\frac{d\tilde{r}}{dl} &= 2\tilde{r} + \tilde{u} - \frac{1}{3}\tilde{r}\tilde{u},\\ \frac{d\tilde{u}}{dl} &= 2\left(\frac{5}{2} - d\right)\tilde{u} - \tilde{u}^2.\end{aligned} \tag{2.33}$$

As expected the upper critical dimension is $d_{\mathrm{uc}} = 2.5$, this is in contrast to Ref. [19] due to the different choice for counting hard and soft modes. We can also calculate the correlation length exponent from this. From the analysis in Sec. 1.3, the pertinent fixed point is $\tilde{u}^* = \epsilon$, $\tilde{r}^* = -\frac{\epsilon}{2}$. We then look at deviations from this fixed point with $\tilde{r} = \delta\tilde{r} + \tilde{r}^*$ and $\tilde{u} = \delta\tilde{u} + \tilde{u}^*$, which gives

$$\frac{d}{dl}\begin{pmatrix}\delta\tilde{r}\\ \delta\tilde{u}\end{pmatrix} = \begin{pmatrix}2\left(1-\frac{\epsilon}{6}\right) & 1+\frac{\epsilon}{6}\\ 0 & -\epsilon\end{pmatrix}\begin{pmatrix}\delta\tilde{r}\\ \delta\tilde{u}\end{pmatrix}. \tag{2.34}$$

The positive eigenvector is then $2 - \frac{\epsilon}{3}$, which gives $\nu = \frac{1}{2} + \frac{\epsilon}{12}$. If $d = 2$, then $\epsilon = 1$ and we have

$$\nu = \frac{7}{12}. \tag{2.35}$$

In Ref. [19] it is noted that this analysis breaks down at a length scale, l^* where $h_i\left(l^*\right) \approx 1$. Considering this point allows one to determine where the mean-field behaviour is valid [19]. In this case

$$\frac{h_2\left(l^*\right)}{h_1\left(l^*\right)} = \frac{h_2\left(0\right)}{h_1\left(0\right)} \approx h_2\left(l^*\right). \tag{2.36}$$

This holds as $h_1\left(l^*\right) \approx 1$ and both h_i scale in the same way. Consider the correlation length exponent ν, we're interested in the mean-field behaviour so we take $D \approx 2.5$ such that $\nu = \frac{1}{2}$. If we take the mean-field exponent and then consider how r scales, we have

$$r\left(l^\star\right) \sim r\left(0\right) e^{2l^*} \approx \frac{r\left(0\right)}{h_1\left(0\right)}. \tag{2.37}$$

We can then relate this to ξ using the critical exponent, i.e. if r scales with e^{2l} then ξ scales

with e^{-l}

$$\xi\left(l^*\right) = \xi\left(0\right) e^{-l^*} = \xi\left(0\right)\sqrt{h_1\left(0\right)}. \tag{2.38}$$

We then know that the analysis breaks down at the point where $\xi\left(l^*\right) < a$, i.e. the correlation length is smaller than the lattice spacing. Using the value of $h_1\left(0\right)$

$$h_1\left(0\right) = -\frac{\lambda_H^2}{\left(C_0\right)^2\Lambda^2}\mu_1, \tag{2.39}$$

where we already know from the analysis of the elasticity in Ref. [19] that c_0 and μ_1 are combinations of elastic constants. So we now have that the mean-field behaviour is valid in the regime

$$\xi\left(0\right) > \frac{a\Lambda C_0}{\lambda_H\sqrt{\mu_1}} \approx \sqrt{\frac{C_0}{\lambda_H^2}}, \tag{2.40}$$

where we used $\Lambda a \approx 1$ and that $\mu_i \sim C_0$, the experimental data which justifies this for nematic systems can be found in Ref. [164], for altermagnetic systems we use the data from Ref. [165]. Using the mean-field exponents we find $\xi^2 = \chi_{\mathrm{am}}$ such that we now have the condition for the mean-field regime in terms of the altermagnetic susceptibility

$$\chi_{\mathrm{am}} > \frac{C_0}{\lambda_H^2}. \tag{2.41}$$

Looking at how the elastic constants are renormalised by the piezomagnetic coupling, we immediately notice that when the mean-field condition is met, $\frac{\lambda_H^2}{C_0}\chi_{\mathrm{am}} > 1$ and we get a large renormalisation of the elastic constants. The elastic constants hence soften in the same region as the region where the behaviour can be described by a mean-field theory.

This calculation shows that, just like for nematic systems [16, 19, 162], when altermagnetic fluctuations cause the lattice to soften, the long range strain forces, act back on the altermagnetic mode and cause a crossover to mean-field behaviour. Coupling to strain also introduces an effective spacial dimension and changes the universality class of the system. Unlike for nematic systems, this only holds for the case that a magnetic field is applied.

2.4 Criticality at an altermagnetic QCP

We can use the coupling rules given in Table 2.2 to construct a coupling term for a B_{2g} altermagnet in an arbitrary magnetic field. This is the symmetry of the order parameter which we will consider in the following analysis, however it is a relatively simple endeavour to carry out the same analysis for other order parameter symmetries. If we consider an arbitrary magnetic field, the allowed coupling is

$$S = \int_x \phi\left(x\right)\left(\lambda_z H_z\left(\epsilon_{xx}\left(x\right) - \epsilon_{yy}\left(x\right)\right) + \lambda_\perp\left(\epsilon_{xz}H_x - \epsilon_{yz}H_y\right)\right), \tag{2.42}$$

where λ_z is the coupling to B_{1g} strain, mediated by the magnetic field in the z direction and $\lambda_\perp$, the coupling to E_{1g} strain, mediated by the in-plane magnetic field. One crucial element to the following analysis is that while the magnetic field modifies the properties of the QCP,

it does not destroy it entirely. This is in contrast to the case where a ferromagnet has a field applied along the easy direction. If we just consider a magnetic field along the z direction, the coupling term reduces to Eq. (2.22). It is this coupling term which will use in the analysis which follows for the remainder of this chapter. This is equivalent to the nematic coupling term with a B_{1g} nematic order parameter, although we now have a coupling that is linear in the applied field, allowing us to tune the coupling strength with an external parameter.

2.4.1 Direction selective criticality

We will now consider one-loop corrections to the bosons and fermions from the coupling to elasticity and electrons at the Fermi surface following the analysis of Ref. [16]. We consider the following action

$$S = S_c + S_\phi + S_\epsilon + S_{\epsilon-\phi} + S_{c-\phi}, \tag{2.43}$$

which consists of the part that describes free fermions with band dispersion $\xi(\mathbf{k})$:

$$S_c = -\sum_{\sigma=\uparrow,\downarrow} \int_k c^\dagger_\sigma(k)(i\omega - \xi(\mathbf{k}))c_\sigma(k), \tag{2.44}$$

with $\int_k \cdots = T\sum_\omega \int \frac{d^3k}{(2\pi)^3} \cdots$ and $k = (\omega, \mathbf{k})$ combining frequency and momenta. Aside from the Landau damping, that we discuss below, our results will not depend on the details of the dispersion $\xi(\mathbf{k})$. We consider a spherical Fermi surface in the main text, however our results are unchanged if we consider a cylindrical Fermi surface; this is a direct consequence of the fact that we will see the critical lines of soft phonons are in the $x-y$ plane, where the symmetries of the two Fermi surfaces are identical. (The results are qualitatively different for a magnetic field along x as this creates a soft mode along the z direction, we consider this case in Appendix. B.2) Hence, for now we use $\xi(\mathbf{k}) = \frac{|\mathbf{k}|^2}{2m} - \mu$. The altermagnet is described by a single component Ising order parameter with the corresponding action

$$S_\phi = \frac{1}{2}\int_q \phi(q)\Big(m^2 + \omega^2 + v_\phi^2|\mathbf{q}|^2\Big)\phi(-q), \tag{2.45}$$

where v_ϕ, which has dimension of a velocity, determines the spatial stiffness of altermagnetic fluctuations and m^2 now denotes the distance to the critical point. We do not include non-linear interactions $\sim \phi^4$ of the Ising degree of freedom as it is an irrelevant correction at the QCP. The elastic degrees of freedom are given in Sec. 1.1 but we reiterate the analysis here for the sake of completeness. The elastic degrees of freedom are determined by

$$S_\epsilon = \int_x \left[\frac{\rho}{2}\sum_{i=x,y,z}(\partial_\tau u_i)^2 + F_{\rm el}[\{u_i\}]\right], \tag{2.46}$$

where ρ is the mass density, $\int_x \cdots = \int d\tau \int d^3x \cdots$, and the elastic energy [19]

$$\begin{aligned} F_{\rm el}[u_i] = &\frac{C_{11}}{2}(\epsilon_{xx}^2 + \epsilon_{yy}^2) + \frac{C_{33}}{2}\epsilon_{zz}^2 + \frac{C_{44}}{2}(\epsilon_{xz}^2 + \epsilon_{yz}^2) \\ &+ \frac{C_{66}}{2}\epsilon_{xy}^2 + C_{12}\epsilon_{xx}\epsilon_{yy} + C_{13}(\epsilon_{xx} + \epsilon_{yy})\epsilon_{zz}, \end{aligned} \tag{2.47}$$

is determined by the usual elastic constants C_{ij}, given in Voigt notation and with strain field $\epsilon_{ij} = \frac{1}{2}\left(\partial_i u_j + \partial_j u_i\right)$ expressed in terms of the displacement u_i. This term determines the dispersion relations and polarisation vectors for the elastic modes. For example, with the assumptions $C_{13} = -C_{44}$, $C_{66} = \frac{C_{11}-C_{12}}{2}$ [20], we obtain the elastic modes $\Omega_i(\mathbf{q})$:

$$\begin{aligned}\rho\Omega_1^2(\mathbf{q}) &= C_{44}|\mathbf{q}_{2d}|^2 + C_{11}q_z^2,\\ \rho\Omega_2^2(\mathbf{q}) &= C_{11}|\mathbf{q}_{2d}|^2 + C_{44}q_z^2,\\ \rho\Omega_3^2(\mathbf{q}) &= \frac{C_{11}-C_{12}}{2}|\mathbf{q}_{2d}|^2 + C_{44}q_z^2,\end{aligned} \tag{2.48}$$

where the polarization vectors of the elastic modes are $\vec{\lambda}_1(\mathbf{q}) = (0,0,1)^T$, $\vec{\lambda}_2(\mathbf{q}) = \frac{1}{|\mathbf{q}_{2d}|}(q_x, q_y, 0)^T$, and $\vec{\lambda}_3(\mathbf{q}) = \frac{1}{|\mathbf{q}_{2d}|}(-q_y, q_x, 0)^T$, respectively, with $\mathbf{q}_{2d} = \Big(q_x, q_y\Big)$. Due to the assumptions made for the elastic constants, the elastic mode $\Omega_3(\mathbf{q})$ of Eq. (2.48) leads to a soft plane at $q_z = 0$ when $C_{11,\mathrm{ren}} \approx C_{12,\mathrm{ren}}$. This is a fine-tuned result. In the generic case, only the lines with $q_x = \pm q_y$, $q_z = 0$ form the softening manifold [16, 19] for the D_{4h} symmetry group. Despite this, calculating the phonon modes for a generic choice of elastic constants gives the same qualitative results, this is due to the form factor $\vec{\lambda}_3(\mathbf{q})$, involved in the renormalized mass of the boson, which lifts the degeneracy to the lines $q_x = \pm q_y$, $q_z = 0$.

The action is Gaussian in the elastic modes and we can therefore integrate out the phonons using the method outlined in Sec. 1.3. For a generic magnetic field this introduces the direction-dependent correction to the order parameter action:

$$\begin{aligned}\Delta S_{\epsilon-\phi}^{(\mathrm{am})} = -\frac{1}{8}\int_q \phi(q)\phi(-q)\Bigg[&\frac{\lambda_\perp^2(H_x q_x - H_y q_y)^2}{\rho\Omega_1^2(\mathbf{q})}\\ &+ \frac{1}{|\mathbf{q}_{2d}|^2}\frac{\Big(\lambda_z H_z(q_x^2 - q_y^2) - \lambda_\perp q_z(H_x q_x - H_y q_y)\Big)^2}{\rho\Omega_2^2(\mathbf{q})}\\ &+ \frac{1}{|\mathbf{q}_{2d}|^2}\frac{\Big(2\lambda_z H_z q_x q_y - \lambda_\perp(H_y q_x + H_x q_y)q_z\Big)^2}{\rho\Omega_3^2(\mathbf{q})}\Bigg].\end{aligned} \tag{2.49}$$

Choosing $\mathbf{H} = H\hat{z}$, the mass is renormalized and becomes

$$m^2(\mathbf{q}, H_z) = m^2 - \frac{(\lambda H_z)^2}{4\rho}\frac{1}{|\mathbf{q}_{2d}|^2}\Big(\frac{(q_x^2 - q_y^2)^2}{\Omega_2^2(q)} + \frac{4q_x^2 q_y^2}{\Omega_3^2(q)}\Big). \tag{2.50}$$

In analogy with the nematic case [16], $m(\mathbf{q}, H_z)^2$ has minimum value

$$m_{\min}^2(H_z) = m^2 - m_{*H}^2, \tag{2.51}$$

where $m_{*H}^2 = \frac{\lambda^2 H_z^2}{2\left(C_{11}-C_{12}\right)}$, along the two lines $q_x = \pm q_y$. It is along these lines where the boson mass drops to zero and the system becomes critical. Coupling to the lattice hence leads to the emergence of a direction selective criticality. The hard and soft directions are depicted in Fig. 2.3. We see that by varying the magnetic field strength, the position of the critical

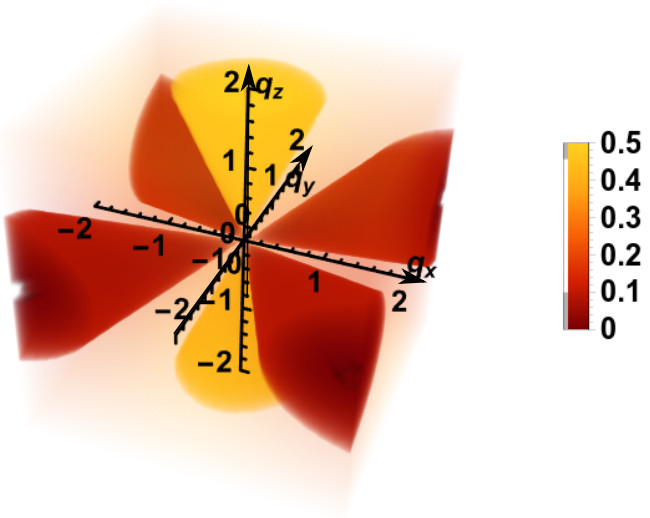

Figure 2.3: A density plot of $\frac{m^2\left(\mathbf{q},H_z\right)-m^2_{\min}}{\lambda^2 H_z^2}$ shows two directions where the bosons become critical (i.e. the soft directions discussed in the main text), where $q_x = \pm q_y$ in the $q_z = 0$ plane. This is plotted for $C_{11} = 1$, $C_{12} = 0$ and $C_{44} = 1$. (Figure adapted from Ref. [17])

point is also moved but never destroyed. This means that a transition can be field-induced (see Fig. 2.7). The renormalized critical mass ($m_{\min} = 0$) can be approximated near the high symmetry directions

$$m^2(\mathbf{q},\mathbf{H}) \approx \begin{cases} m^2_{*H}\frac{q_2^2+q_z^2}{q_1^2}, & |q_1| \gg |q_2|, |q_z|, \\ m^2_{*H}\frac{q_1^2+q_z^2}{q_2^2}, & |q_2| \gg |q_1|, |q_z|, \\ m^2_{*H}, & |q_z| \gg |q_1|, |q_2|, \end{cases} \tag{2.52}$$

where $q_1 = \frac{q_x+q_y}{\sqrt{2}}$, $q_2 = \frac{q_x-q_y}{\sqrt{2}}$. Here we set the coefficients to be 1 for simplicity. Note that we use the notation m^2_{*H} to show the field dependence at criticality. We will see that this relation implies a magnetic field dependent crossover temperature T^* proportional to H_z^3.

The soft directions obtained from this consideration of quantum fluctuations correspond to the soft directions that emerge from the lattice softening calculation with the same choice of irreducible representation B_{2g} in Sec. 2.3.1. Once the choice of order parameter and magnetic field orientation makes it clear that the coupling is to B_{1g} strain, the corresponding elastic constant $C_{11} - C_{12}$ becomes soft and the sound velocity vanishes along $q_x = \pm q_y$ [19].

2.4.2 Landau damping

As well as the coupling to elasticity, the boson is also renormalised as a result of coupling to fermions. In nematics, whether this coupling leads to the addition of a Landau damping term in the boson propagator is dependent on the Fermi surface geometry, the choice of an

isotropic dispersion over, for example, a tight binding model is therefore not unreasonable as it would not affect the results [16]. The coupling of electrons to the order parameter is given by

$$S_{c-\phi}^{(\mathrm{am})} = \int_{k,q} \phi(q) c_\alpha^\dagger(k+q/2)\Big[g_1 h_z(k)\sigma_{\alpha\beta}^z + g_2\Big(h_x(k)\sigma_{\alpha\beta}^x + h_y(k)\sigma_{\alpha\beta}^y\Big)\Big] c_\beta(k-q/2), \quad (2.53)$$

where it follows with the help of Table 2.2 that

$$\begin{aligned} \mathbf{h}(k) &= (h_x(k), h_y(k), h_z(k)) \\ &= (-\sin k_x \sin k_z, \sin k_y \sin k_z, \cos k_x - \cos k_y). \end{aligned} \quad (2.54)$$

The spin Pauli matrices are a consequence of the broken time-reversal symmetry, leading to an extended form factor when compared to the equivalent calculation for a nematic system [16].

The one-loop correction to the order-parameter propagator due to the fermion-boson coupling is given by

$$\Delta S_\phi^c = \frac{1}{2}\int_q \phi(q)\phi(-q)\Big[g_1^2 D_z(q) + g_2^2\Big(D_x(q) + D_y(q)\Big)\Big], \quad (2.55)$$

where $tr[\sigma^i\sigma^j] = 2\delta^{ij}$ was used, while

$$\begin{aligned} D_i(q) &= 2\int_k h_i^2(\mathbf{k}) G(k-q/2) G(k+q/2) \\ &= -2i\int \frac{d^3k}{(2\pi)^3} h_i^2(\mathbf{k}) \frac{\theta(\xi_{\mathbf{k}-\mathbf{q}/2}) - \theta(\xi_{\mathbf{k}+\mathbf{q}/2})}{\Omega + i(\xi_{\mathbf{k}-\mathbf{q}/2} - \xi_{\mathbf{k}+\mathbf{q}/2})}, \end{aligned} \quad (2.56)$$

where, $i = x, y, z$ and $q = (\Omega, \mathbf{q})$.

With the assumption of a spherical Fermi surface ($\xi_{\mathbf{k}} = \frac{|\mathbf{k}|^2}{2m} - \mu$) and a low temperature approximation, we find

$$D_i(q) \approx \frac{2i}{v_\mathrm{F}} \int \frac{d^3k}{(2\pi)^3} h_i^2(k)\delta(k-k_\mathrm{F}) \frac{v_\mathrm{F}\mathbf{q}\cdot\hat{k}}{\Omega - i v_\mathrm{F}\mathbf{q}\cdot\hat{k}}, \quad (2.57)$$

where v_F, k_F and $\hat{k}$ are the Fermi velocity, wave vector and the normalized radial vector respectively. To determine the fermion-induced dynamics, we introduce the quantity $\Delta D_i(q)$, given by

$$\begin{aligned} \Delta D_i(q) &\equiv D_i(\Omega, \mathbf{q}) - D_i(0, \mathbf{q}) \\ &= \frac{2}{v_\mathrm{F}} \int \frac{d^3k}{(2\pi)^3} h_i(\mathbf{k})\delta(k-k_\mathrm{F}) \frac{1}{1 - i v_\mathrm{F}\mathbf{q}\cdot\hat{k}/\Omega}. \end{aligned} \quad (2.58)$$

The term $D_i(0, \mathbf{q})$ modifies m^2 and gives a $|q|^2$ term, related to the bare kinetic term of the

boson. Converting to spherical coordinates, we can obtain the following results:

$$\Delta S_\phi^c \approx \int_q \frac{1}{2}\phi(q)\frac{k_{\mathrm{F}}^2(k_{\mathrm{F}}a)^4}{4\pi^3 v_{\mathrm{F}}}\Bigg[g_1^2\eta_x(\theta_q,\phi_q,\alpha) + g_2^2\Big(\eta_y(\theta_q,\phi_q,\alpha)+\eta_z(\theta_q,\phi_q,\alpha)\Big)\Bigg]\phi(-q), \tag{2.59}$$

where θ_q, ϕ_q are the polar and the azimuthal angles of the momentum $\mathbf{q}$, respectively, while $\alpha = \frac{|\Omega|}{v_{\mathrm{F}}|\mathbf{q}|}$. The functions η_x, η_y and η_z are given by

$$\eta_x = \int \frac{d\theta d\phi \sin^5\theta\cos^2(2\phi)}{1+\alpha^{-2}[\cos\theta\cos\theta_q+\cos\Big(\phi-\phi_q\Big)\sin\theta\sin\theta_q]^2}, \tag{2.60}$$

$$\eta_y = \int \frac{d\theta d\phi \sin^3\theta\cos^2\theta\cos^2\phi}{1+\alpha^{-2}[\cos\theta\cos\theta_q+\cos\Big(\phi-\phi_q\Big)\sin\theta\sin\theta_q]^2}, \tag{2.61}$$

$$\eta_z = \int \frac{d\theta d\phi \sin^3\theta\cos^2\theta\sin^2\phi}{1+\alpha^{-2}[\cos\theta\cos\theta_q+\cos\Big(\phi-\phi_q\Big)\sin\theta\sin\theta_q]}, \tag{2.62}$$

where we have suppressed the θ_q, ϕ_q and α dependence of the η's and the integrals are taken over the unit sphere.

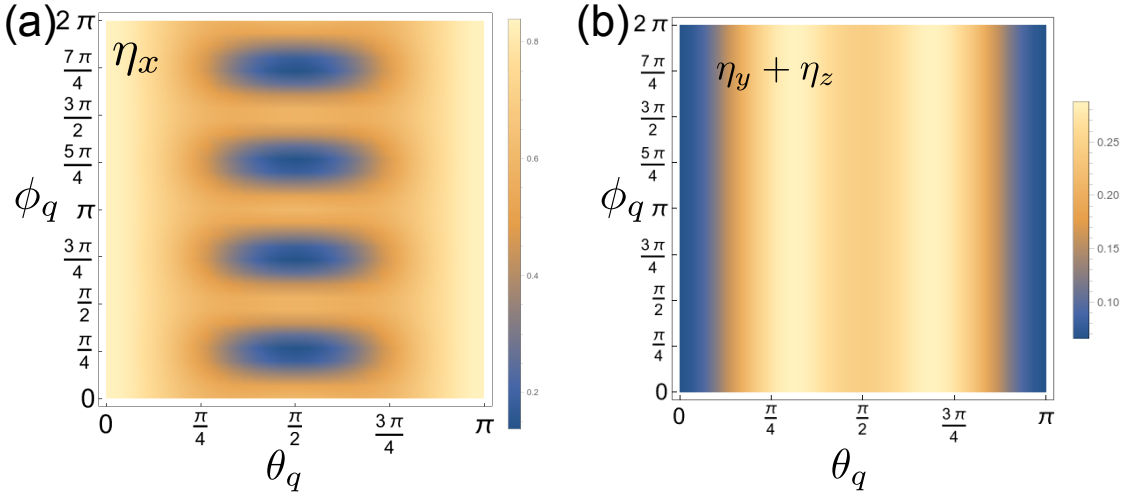

Figure 2.4: Panel (a) shows that η_x a term linear in Ω everywhere, apart from at $\theta_q = 0$ and $\phi_q = (2n+1)/4\pi$, where $n = 0, 1, 2, 3$ where the damping is approximately quadratic in Ω. A density plot of $\eta_y + \eta_z$ shows a term linear in Ω when $\theta_q = 0, \pi$. This suggests that when the two are summed, the main contribution comes from the linear Ω term at low energies everywhere on the Fermi surface. This is plotted at $\alpha = 0.1$. (Figure reprinted from Ref. [17])

It suffices to carry out a numerical analysis. We find that there always exists a damping term regardless of the Fermi surface geometry, which we show in Fig. 2.4; this is in direct contrast with the nematic case. This is a result of the introduction of Pauli matrices in the

form factor which give extra terms when compared with the form factor for a nematic order parameter [16]. We approximate this damping term in the low energy limit as

$$\Delta S_\phi^c \approx \frac{\xi^2}{2} \int \frac{d^4q}{(2\pi)^4} \phi(q) \frac{|\Omega|}{v_{\mathrm{F}}|\mathbf{q}|} \phi(-q), \tag{2.63}$$

where $\xi = \sqrt{6\pi\alpha} v_\phi k_F$ and α is a dimensionless coupling constant

$$\alpha = \frac{g^2}{12\pi^2 v_F v_\phi^2}. \tag{2.64}$$

for the coupling strength to fermions.

The energy scale ξ sets the strength of the Landau damping. The result of this is the order-parameter action

$$S_\phi = \frac{1}{2} \int_q \phi(q) \chi(q)^{-1} \phi(-q), \tag{2.65}$$

with susceptibility

$$\chi\left(\mathbf{q}, \omega\right) = \left(m^2(\mathbf{q}, H_z) + \omega^2 + v_\phi^2 |\mathbf{q}|^2 + \xi^2 \frac{|\omega|}{v_{\mathrm{F}} q} \right)^{-1}. \tag{2.66}$$

This result is dependent on the shape of the Fermi surface as Landau damping is generated by the creation of particle-hole pairs, where the soft directions characterising the critical regions are parallel to the Fermi surface, hence this theory would not be applicable for a system with nested Fermi surfaces or van Hove points.

2.4.3 Fermionic self-energy

A calculation of the fermion self-energy allows one to deduce a crossover from the bare to elastic QC regime, an analysis at $T = 0$ and no magnetic field also allows one to deduce the characteristic energy scale T_0, below which, quantum critical behaviour sets in. The self-energy is given by

$$\Sigma\left(\mathbf{k}, \omega_n\right) \propto g^2 h_{\mathbf{k}}^2 \int_{\mathbf{q},\omega'} G_{\mathbf{k}+\mathbf{q}}\left(\omega + \omega'\right) \chi_{\mathbf{q}}\left(\omega'\right), \tag{2.67}$$

where $G_{\mathbf{k}}\left(\omega\right)$ is the electron propagator, $\chi_q\left(\omega\right)$ is the boson propagator, $h_{\mathbf{k}}$ is a form factor discussed in the Landau damping section and $k \gg q$ such that we can ignore the q dependence

of the form factor and move this outside of the integral. The self-energy is then given by

$$\Sigma_{\mathbf{k}_F} \approx g^2 h^2_{\mathbf{k}_F} \int_{-\infty}^{\infty} \int \frac{d^3q}{(2\pi)^3} \frac{d\omega'}{2\pi} \frac{1}{v_\phi^2 q^2 + \xi^2 \frac{\omega-\omega'}{v_F q}} \frac{1}{i\omega' - v_f q_\perp} \tag{2.68}$$

$$\approx g^2 h^2_{\mathbf{k}_F} \int_{-\infty}^{\infty} \frac{d\omega'}{2\pi} \int \frac{d^2q_\parallel}{(2\pi)^2} \frac{1}{v_\phi^2 q_\parallel^2 + \xi^2 \frac{\omega-\omega'}{v_F q_\parallel}} \int \frac{dq_\perp}{2\pi} \frac{1}{i\omega' - v_f q_\perp} \tag{2.69}$$

$$= -i \frac{g^2 h^2_{\mathbf{k_F}}}{4 v_F v_\phi^2} \int \frac{d\omega'}{2\pi} \mathrm{sign}\left(\omega'\right) \int_0^\Lambda \frac{q_\parallel^2 dq_\parallel}{q_\parallel^3 + \xi^2 \frac{|\omega-\omega'|}{v_\phi^2 v_F}} \tag{2.70}$$

$$\approx -i\omega \frac{g^2 h^2_{\mathbf{k}_F}}{12\pi^2 v_F v_\phi^2} \log\left(\frac{\Lambda^3 v_\phi^2 v_F}{\xi^2 |\omega|}\right). \tag{2.71}$$

If the imaginary part of the self energy on the real axis is

$$\mathrm{Im}\Sigma\left(\omega\right) = -\frac{\pi}{2}\alpha |\omega| \, \theta\left(T_0 - |\omega|\right), \tag{2.72}$$

with the dimensionless coupling α, this then implies that on the imaginary axis

$$\Sigma\left(\omega\right) = -\alpha \left(\omega \log\left(\frac{T_0}{|\omega|}\right) - i\frac{\pi}{2}|\omega|\right), \tag{2.73}$$

and so

$$\Sigma\left(i\omega\right) = -\int_{-\infty}^{\infty} \frac{d\epsilon}{\pi} \frac{\mathrm{Im}\Sigma\left(\epsilon\right)}{i\omega - \epsilon} = -i\omega\alpha \log\left(\frac{T_0}{|\omega|}\right). \tag{2.74}$$

We can compare this with Eq. (2.71) to obtain the energy scale

$$T_0 = \frac{\Lambda^3 v_\phi^2 v_F}{\xi^2}, \tag{2.75}$$

at which the system crosses over to the bare QC regime.

We can now consider how the magnetic field affects the contributions to the self energy from the relevant areas of momentum space. Far away from the critical directions $q_z \gg q_1, q_2$, the direction dependence of the mass can be ignored and $m\left(\mathbf{q}, H_z\right) \approx m$. An analysis of the boson propagator then gives a temperature above which the mass is negligible. If we use Eq. 2.66 then if $m^2 \sim v_\phi^2 q^2$, then rearranging this for q and substituting this into the Landau damping term, assuming that $\omega \sim T$, we see the terms are comparable at

$$T_* = m^3 v_f / \xi^2 v_\phi. \tag{2.76}$$

Using the known equations for ξ and T_0 gives the expression

$$T_* = \frac{m_{*H}^3}{v_\phi^3 \Lambda^3} T_0. \tag{2.77}$$

We now see the emergence of a crossover scale $T_* \propto H_z^3$ (from the magnetic field dependence $m_{*H} \propto H_z$) below which the mass term must be taken into account. The two regimes can therefore be tuned with the magnetic field. We always assume $T_0 \gg T_*$, i.e. the elastic couplings are not of a strength at which behaviour is affected up to the Fermi energy. Above this temperature m can be neglected and the self-energy acquires a non-Fermi liquid form [16, 117, 118] $\Sigma\left(i\omega_n\right) \propto |\omega|^{2/3}$ in 2D and $\Sigma\left(i\omega_n\right) \propto \omega_n \log|\omega_n|$ in 3D. Below this temperature the corrections are Fermi liquid type.

At low energies we need to take the contributions from the gapless bosons into account. We would expect hot spots in the regions where the critical directions are parallel to the Fermi surface. We follow the method presented in Ref. [16]. Ignoring prefactors in order to determine the frequency dependence of the self-energy, we expand the propagator close to the critical direction

$$\chi\left(q \approx q_2\right) = q_2^2 + m_{*H}^2 \frac{q_1^2 + q_z^2}{q_2^2} + \frac{|\nu_n|}{q_2}. \tag{2.78}$$

This allows us to write the self-energy as

$$S\left(i\omega_n\right) = \int_{\mathbf{q},\nu_n} \frac{q_2^2}{q_2^4 + m_{*H}^2\left(q_1^2 + q_z^2\right) + |\nu_n|\, q_2} \frac{1}{i\omega_n + i\nu_n - q_1\cos\theta_{k_\mathrm{F}} - q_2\sin\theta_{k_\mathrm{F}}} + \left(\theta_{k_\mathrm{F}} \to \theta_{k_\mathrm{F}} + \pi/2\right), \tag{2.79}$$

where $\cos\left(\theta_{k_\mathrm{F}}\right) = \hat{n}_{k_\mathrm{F}} \cdot \hat{q}_1$ and $\hat{n}_{k_\mathrm{F}}$ is the normal to the Fermi surface. The two critical directions are perpendicular to one another such that for q_2 to be parallel to the Fermi surface $\theta_{k_\mathrm{F}} \approx 0$. Introducing $\xi = q_1\cos\theta_{k_\mathrm{F}} + q_2\sin\theta_{k_\mathrm{F}}$ and $\eta = -q_1\sin\theta_{k_\mathrm{F}} + q_2\cos\theta_{k_\mathrm{F}}$ such that $q_2 = \eta\cos\left(\theta_{k_\mathrm{F}}\right) + \xi\sin\left(\theta_{k_\mathrm{F}}\right)$ and $q_1 = \xi\cos\left(\theta_{k_\mathrm{F}}\right) - \eta\sin\left(\theta_{k_\mathrm{F}}\right)$.

The leading order contribution comes from the fermion pole, we integrate over ξ just considering this pole

$$\int_{-\Lambda}^{\Lambda} d\xi \frac{1}{i\omega_n + i\nu_n - \xi} = \log\left(\frac{i\omega_n + i\nu_n - \Lambda}{i\omega_n + i\nu_n + \Lambda}\right) \approx -i\mathrm{Sgn}\left(\omega_n + \nu_n\right)\pi. \tag{2.80}$$

This also restricts the integral over ν, given that the integral is even in ν. After integrating over q_z and ignoring the ξ dependence having only considered the fermion pole

$$S\left(i\omega_n\right) = \frac{-i\mathrm{Sgn}\left(\omega_n\right)}{m_{*H}} \int_0^{|\omega_n|} d\nu_n \int_0^1 d\eta \left[\frac{\eta^2\cos\left(\theta_{k_\mathrm{F}}\right)^2}{\sqrt{\eta^4\cos\left(\theta_{k_\mathrm{F}}\right)^4 + m_{*H}^2\eta^2\sin\left(\theta_{k_\mathrm{F}}\right)^2 + \nu_n\eta\cos\left(\theta_{k_\mathrm{F}}\right)}}\right], \tag{2.81}$$

where the integral over η is given a cutoff of 1. The leading frequency dependence is determined by $\nu_n = 0$ and so

$$S\left(i\omega_n\right) = \frac{-i\omega_n}{m_{*H}} f\left(\theta_{k_\mathrm{F}}\right), \tag{2.82}$$

where

$$f\left(\theta_{k_{\mathrm{F}}}\right)=\int_0^1 d\eta\left[\frac{\eta^2\cos\left(\theta_{k_{\mathrm{F}}}\right)^2}{\sqrt{\eta^4\cos\left(\theta_{k_{\mathrm{F}}}\right)^4+r_{0,H}\eta^2\sin\left(\theta_{k_{\mathrm{F}}}\right)^2}}\right], \tag{2.83}$$

such that this contribution is FL-like. We can then also find the contribution from the subleading term to obtain $\mathrm{Im}\Sigma$. To find this, we expand in ν_n and assume $\theta_{k_{\mathrm{F}}}$ is small as we expect hotspots around $\hat{n}_{k_{\mathrm{F}}}=\hat{q}_1$.

$$S\left(i\omega_n\right)_{\mathrm{subleading}}=\frac{i\mathrm{Sgn}\left(\omega_n\right)}{m_{*H}}\int_0^{|\omega_n|}d\nu_n\nu_n\int_{\nu^{1/3}}^1 d\eta\frac{1}{\left(\eta^2+m_{*H}^2\theta_{k_{\mathrm{F}}}^2\right)^{3/2}}, \tag{2.84}$$

which yields

$$S_{\mathrm{subleading}}=\frac{i\mathrm{Sgn}\left(\omega_n\right)|\omega_n|^{4/3}}{m_{*H}},\qquad \theta_{k_{\mathrm{F}}}\ll\frac{|\omega_n|^{1/3}}{m_{*H}}. \tag{2.85}$$

which is a subleading non-Fermi liquid like correction to the self-energy. Whether these hotspots survive is now dependent on the form factor. Along the critical directions the form factor is zero and hence these hotspots are rendered cold. In this case the main contribution comes far from the critical directions and yields the crossover T_* for the elastic to bare QC crossover. The identification of such a crossover which is dependent on the field allows for the deduction of a phase diagram using the pertinant parameters. We show this in Fig. 2.5. These results are equivalent to those of a nematic system, as reported in Ref. [16], but with a now field dependent crossover temperature.

2.4.4 Specific heat

Much like the calculation of the electron self-energy, an analysis of the heat capacity also allows one to determine different regimes of behaviour above the QCP and the crossover temperature T^* between the two (This is also carried out for nematic systems in Ref. [16]). The free energy of the system is given by

$$\begin{aligned}F&=\frac{T}{2}\sum_{\omega}\int\frac{d^3q}{(2\pi)^3}\log\chi^{-1}(\omega,\mathbf{q})\\&=-\int\frac{d^3q}{(2\pi)^3}\int_0^\infty\frac{d\omega}{2\pi}\coth\frac{\beta\omega}{2}\tan^{-1}\frac{\frac{\xi^2\omega}{|\mathbf{q}|v_{\mathrm{F}}}}{v_\phi^2|\mathbf{q}|^2+m^2(\mathbf{q},H_z)},\end{aligned} \tag{2.86}$$

where the Matsubara frequency summation is evaluated via a contour integral. The Sommerfeld coefficient $\gamma(T)=-\frac{\partial F^2}{\partial^2 T}$ is then given by

$$\gamma=\gamma_0 g\left(\bar{T},\bar{\Lambda},H_z\right), \tag{2.87}$$

where

$$\gamma_0=\frac{3}{\pi}\alpha\rho_F \tag{2.88}$$

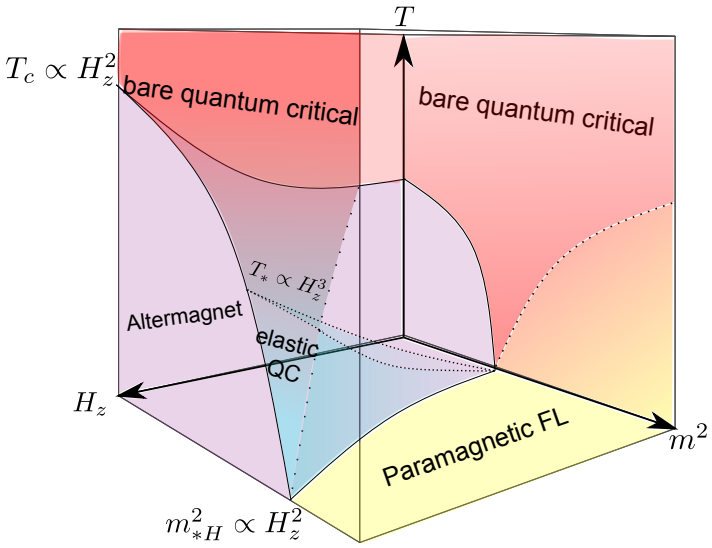

Figure 2.5: The full phase diagram for an altermagnet in a magnetic field shows initially at zero field an altermagnetically ordered regime and a disordered paramagnetic FL phase, the phase boundaries of which meet at a QCP, around this point is a region of NFL behaviour. Turning on the magnetic field increases the area of the ordered regime and introduces a new region of quantum critical elasticity around the QCP, distinct from the Fermi liquid paramagnetic phase. Phase changes are marked with solid lines and crossover behaviour with dotted lines. (Figure reprinted from Ref. [17])

and

$$g\left(\bar{T},\bar{\Lambda},H_z\right)=\int d^3\bar{q}\int_0^\infty dx\frac{x}{e^x-1}\frac{|\bar{\mathbf{q}}|^3\left(|\bar{\mathbf{q}}|^2+\bar{m}^2(\bar{\mathbf{q}},H_z)\right)^3}{\left[|\bar{\mathbf{q}}|^2\left(|\bar{\mathbf{q}}|^2+\bar{m}^2(\bar{\mathbf{q}},H_z)\right)^2+x^2\bar{T}^2\right]^2}, \tag{2.89}$$

where $\rho_F=\frac{k_F^2}{2\pi^2 v_F}$ is the density of states at the Fermi surface and we used the following dimensionless variables

$$\bar{m}\left(\boldsymbol{q},H_z\right)=\frac{m\left(\boldsymbol{q},H_z\right)}{m_{*H}},\ \bar{\boldsymbol{q}}=\frac{v_\phi \boldsymbol{q}}{m_{*H}^2},\ \bar{T}=\frac{T}{T_*}, \tag{2.90}$$

as well as $\bar{\Lambda}=\left(T_0/T_*\right)^{1/3}$ and the crossover temperature scale Eq. 2.77, which we also deduced from the calculation of the fermion self-energy.

The third power of the coefficient is due to the dynamical scaling exponent of the problem being $z=3$. We will see that this temperature scale sets the crossover from a Fermi liquid type heat capacity to the onset of non-Fermi liquid behaviour for the heat capacity as well.

In the case that there is no magnetic field present, there is no direction dependent criticality

and $\bar{m}\left(\boldsymbol{q},0\right)=1$. The calculation of the Sommerfeld coefficient is then

$$\gamma(T,0)=\gamma_0\int d^3\bar{q}\int_0^\infty dx\frac{x}{e^x-1}\frac{|\bar{\mathbf{q}}|^3\Big(|\bar{\mathbf{q}}|^2+1\Big)^3}{\Big[|\bar{\mathbf{q}}|^2\Big(|\bar{\mathbf{q}}|^2+1\Big)^2+x^2\bar{T}^2\Big]^2}. \tag{2.91}$$

In this case we find non-Fermi liquid behaviour which is robust all the way down to the QCP with

$$\gamma\left(T\right)=\frac{2\pi^3}{9}\gamma_0\log\left(\frac{T_0}{T}\right). \tag{2.92}$$

The introduction of an external magnetic field means the calculation requires a more subtle approach. The mass term becomes direction dependent with three important regions given in Eq. 2.52. If we consider first the region *(iii)* where the boson modes are gapped, we can analyse Eq. 2.89 for $\bar{T}\gg 1$ and $\bar{T}\ll 1$. Far above the crossover temperature, the logarithmic divergence remains as it is not affected by the magnetoelastic coupling, however below T_* the Sommerfeld coefficient simplifies to

$$\gamma\approx\gamma_0\frac{\pi^2}{6}\int_0^{\bar{\Lambda}}d^3\bar{q}\frac{1}{\bar{q}\left(\bar{m}^2\left(\bar{q}\right)+\bar{q}^2\right)}. \tag{2.93}$$

The mass only depends on the orientation of the momentum, $\hat{q}=\frac{\mathbf{q}}{|\mathbf{q}|}$ and so this simplifies to

$$\gamma\approx\gamma_0\frac{2\pi^2}{3}\int\frac{d\hat{q}}{4\pi}\log\frac{\bar{\Lambda}}{\bar{m}\left(\hat{q}\right)}. \tag{2.94}$$

This shows that the logarithmic divergence is now cut off by the crossover temperature T^* such that

$$\gamma^{(iii)}(T)\approx\frac{2\pi^3}{9}\gamma_0\begin{cases}\log\frac{T_0}{T_*}, & T\ll T_*\\ \log\frac{T_0}{T}, & T\gg T_*\,.\end{cases} \tag{2.95}$$

The temperature crossover is again the temperature at which the boson mass becomes negligible. Although this analysis is restricted to the momentum space corresponding to *(iii)* in Eq. (2.52), we extend the integration over all momenta and so the numerical coefficient is overestimated.

The other two regions are equivalent by symmetry and so we need only consider one of these. These regions are governed by the soft lines which only occur when an external field is present. To proceed we use spherical coordinates

$$\bar{q}_1=\bar{q}\cos\theta,\ \bar{q}_2=\bar{q}\sin\theta\cos\phi,\ \bar{q}_z=\bar{q}\sin\theta\sin\phi, \tag{2.96}$$

and set the largest momentum as $\bar{q}\cos\theta$. We enforce this through the choice $0<\theta<\theta_0\ll 1$

such that $|\bar{q}_1| \gg |\bar{q}_2|, |\bar{q}_z|$. The contribution is then

$$g^{(i)}(\bar{T}, \bar{\Lambda}, H_z) \approx 4\pi \int_0^{\bar{\Lambda}} d\bar{q} \int_0^{\theta_0} d\theta \int_0^{\infty} dx \frac{x}{e^x - 1} \frac{\bar{q}^5 \theta (\theta^2 + |\bar{q}|^2)^3}{\left[|\bar{q}|^2 (\theta^2 + |\bar{q}|^2)^2 + x^2 \bar{T}^2 \right]^2}. \tag{2.97}$$

We should first analyse this expression at $T = 0$, in this case $\gamma^{(i)}(0,0) \approx \frac{\pi^2}{9} \theta_0^2 \log\left(\frac{T_0}{T_* \theta_0^3}\right)$ such that it is finite. At finite temperatures a numerical calculation shows that the contribution has the same T dependence as for the previous case and combining them leads to the two regimes of behaviour at $T \gg T_*$ and $T \ll T_*$

$$\gamma(T) \approx \frac{2\pi^3}{9} \begin{cases} \log \frac{T_0}{T_*}, & T \ll T_*, \\ \log \frac{T_0}{T}, & T \gg T_*. \end{cases} \tag{2.98}$$

Below the crossover temperature T_*, the specific heat is Fermi liquid-like with no divergence, while above T_* the system is in the bare QC regime where it exhibits marginal Fermi liquid behaviour, as reported for nematic systems in Ref. [16]. In agreement with the calculation of the fermion self-energy, T_* is now field dependent.

2.4.5 Elastocaloric effect

Having calculated the impact of the magnetoelastic coupling on the phase diagram of an altermagnet, it appears that, taking into account only the effect at lowest order at low temperatures, coupling to the lattice introduces an area of Fermi liquid behaviour around the QCP, however an explicit calculation of the elastocaloric effect shows that it is sensitive to a deviation in Fermi liquid behaviour in the elastic QC regime all the way down to the QCP. We can write the elastocaloric change in temperature in terms of the Sommerfeld coefficient calculated in the previous section:

$$\eta = -\frac{1}{\gamma} \frac{\partial S}{\partial \epsilon}. \tag{2.99}$$

The free energy remains governed by Eq. 2.86 but now the mass $m(\mathbf{q}, H_z) \to m(\mathbf{q}, H_z, \epsilon)$, where ϵ is the strain element which transforms trivially under point group operations. Calculating the necessary derivatives, we find

$$-\frac{\partial S}{\partial \epsilon} = -\frac{\partial F^2}{\partial \epsilon \partial T} \equiv -\gamma_0 \Gamma_{*,0} T f(\bar{T}, \bar{\Lambda}, H_z), \tag{2.100}$$

where

$$\Gamma_{*,0} = -\frac{\Lambda^3}{32\pi^4 m_*^2} \frac{1}{\gamma_0 T_0} \frac{\partial m^2}{\partial \epsilon} \tag{2.101}$$

and

$$f(\bar{T}, \bar{\Lambda}, H_z) = \int d^3\bar{q} \int_0^{\infty} dx \frac{|\bar{\boldsymbol{q}}| \, x^2 \mathrm{csch}^2\left(\frac{x}{2}\right)}{\left(x\bar{T}\right)^2 + \bar{\boldsymbol{q}}^2 \left(\bar{m}^2(\boldsymbol{q}, H_z) + \bar{\boldsymbol{q}}^2\right)^2}. \tag{2.102}$$

Let's again consider the high temperature limit where the mass can be neglected, the integral then simplifies to

$$f(\bar{T},\bar{\Lambda},H_z)\approx 32\pi^4 b\bar{T}^{-2/3},\qquad \bar{T}\gg 1 \tag{2.103}$$

where $b=\frac{2\Gamma\left(\frac{4}{3}\right)\zeta\left(\frac{4}{3}\right)}{3^{5/2}\pi^2}$. This result is consistent with that reported in Ref. [166].

Considering the low temperature behaviour of the elastocaloric effect, if this were to be Fermi liquid-like, the $\bar{T}$ dependence in the numerator of Eq. (2.102) can be neglected. Carrying out the integral of the momentum magnitude leaves the angular integral $\int d\hat{q}\frac{1}{m^2\left(\hat{q}\right)}$. This integral diverges logarithmically due to the contributions from the soft directions. This suggests that the behaviour in this regime is not Fermi liquid-like and we must investigate the momentum space occupied by the gapless modes. Using the same spherical coordinates as before, we obtain

$$\begin{aligned} f^{(i)}(\bar{T},\bar{\Lambda},H_z) &= f^{(ii)}(\bar{T},\bar{\Lambda},H_z)\\ &\approx 4\pi\int_0^{\overline{\Lambda}} dq\int_0^{\theta_0} d\theta\int_0^{\infty} dx\frac{\theta q^3 x^2\mathrm{csch}^2\left(\frac{x}{2}\right)}{\left(x\bar{T}\right)^2+q^2\left(\theta^2+q^2\right)^2}. \end{aligned} \tag{2.104}$$

The analysis of the integral in the low-T limit is straightforward and yields

$$f^{(i)}(\bar{T},\bar{\Lambda},H_z)\approx\frac{8\pi^3}{9}\log\frac{\theta_0^3}{\bar{T}},\qquad \bar{T}\ll 1. \tag{2.105}$$

To obtain this result we divided the integral into regions $0\leq\bar{q}\leq 1$, and $1\leq\bar{q}\leq\infty$. The first region diverges as $T\to 0$, giving the dominant contribution, while the other yields a constant $\frac{4\pi^3}{3}\log\left(1+\theta_0^2\right)$. Hence, the origin of the low-T logarithmic divergence are the gapless low energy excitations along the remaining soft lines in momentum space. At high-T the second integral dominates and is the cause of behaviour in agreement with the bare critical point, while the first integral over the interval $0\leq\bar{q}\leq 1$ decays faster as T_*/T. Combining all the findings yields the result of Eq. (2.106). Notice, the two expressions don't match at $T\approx T_*$, a consequence of the fact that in the crossover regime, terms that are subleading at low and high-T must be included.

As a result,

$$\frac{\partial S}{\partial\epsilon_0}\approx -16\pi^3\gamma_0\Gamma_{*,0}T_*\begin{cases}\frac{1}{9}\frac{T}{T_*}\log\frac{T_*}{T}, & T\ll T_*,\\ 2\pi b\left(\frac{T}{T_*}\right)^{1/3}, & T\gg T_*,\end{cases} \tag{2.106}$$

where, as before, the temperature scale T_0 for the bare and T_* for the elastic QCP are given in Eqs. (2.3) and (2.77), respectively. At high-T we recover the bare QCP behavior, while the new result is the logarithmic dependence at low T, due to soft lines in momentum space.

Using the results of Eq. (2.98) for the Sommerfeld coefficient and the above results, we

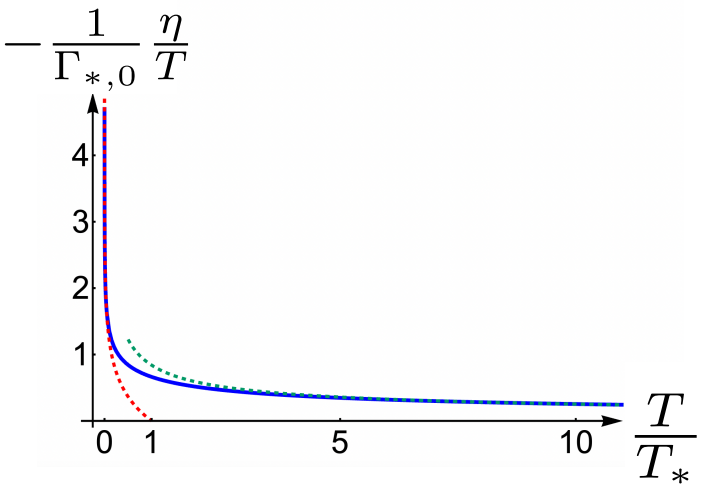

Figure 2.6: The Grüneisen parameter, η/T, as a function T/T_* at the elastic quantum critical point. This is obtained from a numerical analysis of Eq. (2.102). At low temperature ($T \ll T_*$), the Grüneisen parameter shows $\log T$ behaviour which is indicated by the red dashed lines and $T^{-2/3}/\log(T_0/T)$ behaviour in the high temperature regime ($T \gg T_*$), indicated by the green dashed line. A broad crossover regime which occurs due to higher order terms than those calculated in the text is clearly visible. (Figure reprinted from Ref. [17])

deduce the elastocaloric coefficient:

$$\eta \approx -72\Gamma_{*,0}T_* \begin{cases} \frac{1}{9}\frac{(T/T_*)\log\frac{T_*}{T}}{\log\frac{T_0}{T_*}}, & T \ll T_*, \\ 2\pi b\frac{(T/T_*)^{1/3}}{\log\frac{T_0}{T}}, & T \gg T_*. \end{cases} \tag{2.107}$$

This is the behaviour listed in Tab. 2.1. Fig. 2.6 shows a broad crossover regime where subleading corrections are the cause for the two elastocaloric terms not being the same at the crossover temperature. Most importantly, in agreement with our analytic analysis, the low temperature behaviour of η does not follow the Fermi liquid theory, even if the coupling to strain is taken into consideration. In Sec. 2.5 we discuss that this distinct behaviour is due to the fact that critical contributions to the heat capacity are subleading, while they are the dominant one for the elastocaloric effect.

As a result, the elastocaloric change in temperature is a good measure for the existence of a direction selective gapless mode of the boson due to magnetoelastic coupling. The difference in the elastocaloric effect when above or below T_* suggests that such an experiment would allow one to deduce whether the system is in the elastic QC or bare QC regime.

The free energy expression of Eq. (2.86) is the contribution due to the bosonic altermagnetic excitations where the propagator $\chi(\omega, \boldsymbol{q})$ is modified by the coupling to fermions and strain. We could alternatively write this in terms of the coupling constant integration [167]

$$F = F_0 - \int_0^1 \frac{d\lambda}{\lambda} T \sum_\omega \int \frac{d^3q}{(2\pi)^3} \Pi(\omega, \boldsymbol{q}) \chi(\omega, \boldsymbol{q}), \tag{2.108}$$

where F_0 is the free energy at $g = 0$ and $\Pi(\omega, \boldsymbol{q})$ the bosonic self energy that is responsible for the Landau damping in $\chi(\omega, \boldsymbol{q})$. As usual we replaced the coupling constant g by λg and consider the solutions for different λ. The resulting heat capacity expressions of Eqs. (2.92) and (2.88), with and without the coupling to strain, respectively are identical to those of a purely fermionic system with self energy $\Sigma(\omega, \boldsymbol{k})$ and Green's function $G(\omega, \boldsymbol{k})$. This is to be expected as the same free energy can alternatively be written as [167]

$$F = F_0 + 2\int_0^1 \frac{d\lambda}{\lambda} T \sum_\omega \int \frac{d^3k}{(2\pi)^3} \Sigma(\omega, \boldsymbol{k}) G(\omega, \boldsymbol{k}) . \tag{2.109}$$

This reflects the fact that the corrections to the free energy due to electron-boson interaction cannot be allocated to only one of the two coupled degrees of freedom. Hence, as the degrees of freedom are coupled, the same anomaly that is responsible for the non-Fermi liquid behavior of the elastocaloric effect is equally present in the electronic self energy. While the underlying non-analytic corrections are sub-leading for the self energy itself, they become dominant if one considers strain derivatives that are important for the elastocaloric effect.

2.4.6 Field tuning of elastic criticality

In an altermagnetic system, the coupling strength is tuned via an external magnetic field. This tunability suggests a method to approach the elastic QCP from the Fermi liquid regime, characterized by a finite m value, by increasing the magnetic field, see Fig. 2.7. Changes to the Sommerfeld coefficient and elastocaloric effects due to variations in the magnetic field therefore offer an interesting route to identify the elastic QCP.

To calculate the γ and η for a general value of magnetic field strength, we use the following approximated renormalised mass obtained from Eq. (2.50):

$$\frac{m(\mathbf{q}, \mathbf{H})^2}{m_{*H}^2} \approx \begin{cases} 1 - \frac{H^2}{H_{\rm cr}^2} + \frac{H^2}{H_{\rm cr}^2} \frac{q_2^2+q_z^2}{q_1^2}, & |q_1| \gg |q_2|, |q_z| \\ 1 - \frac{H^2}{H_{\rm cr}^2} + \frac{H^2}{H_{\rm cr}^2} \frac{q_1^2+q_z^2}{q_2^2}, & |q_2| \gg |q_1|, |q_z| \\ 1, & |q_z| \gg |q_1|, |q_2|, \end{cases} , \tag{2.110}$$

where $H_{\rm cr} = \sqrt{\frac{2(C_{11}-C_{12})m_{*H}^2}{\lambda^2}}$. When $H = 0$, it reduces to m_* in every momentum space which corresponds to a Fermi liquid regime, alternatively it reduces to Eq. (2.52) when $H = H_{\rm cr}$.

2.4.6.1 Specific heat

At zero magnetic field, the system possesses a bare QC point, close to this point, in the paramagnetic Fermi liquid regime (see Fig. 2.2), the Sommerfeld coefficient shows the following behaviour [16],

$$\gamma(T) \approx \frac{2\pi^3}{9}\gamma_0 \begin{cases} \log \frac{T_0}{T_{\rm FL}}, & T \ll T_{\rm FL}, \\ \log \frac{T_0}{T}, & T \gg T_{\rm FL}, \end{cases} \tag{2.111}$$

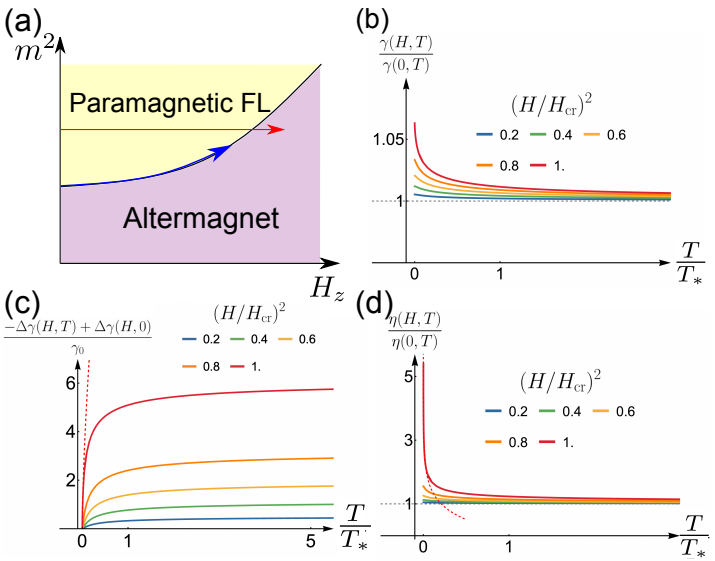

Figure 2.7: The phase diagram in the $T = 0$ plane (a) clearly shows that an increased magnetic field creates an enhanced altermagnetic regime, allowing for a tunable QCP. It is experimentally feasible to measure the heat capacity along two lines, along the critical line (blue), or by using a magnetic field to tune through the critical point (red). The second option is the easiest to carry out in an experiment as it only involves tuning one parameter. As the magnetic field reaches its critical value, H_{cr}, the Sommerfeld coefficient (panel (b)) is not sensitive to the gapless modes and thus remains Fermi liquid like, while the presence of the gapless modes can be detected through measurements of $\Delta\gamma$ (panel (c)) where the dotted line shows the $T^{2/3}$ behaviour exhibited in the low temperature regime. The clearest indication of a critical point however comes from elastocaloric measurements (panel (d)) which diverge logarithmically (dotted line) in the low temperature regime due to a sensitivity to the gapless modes not present in calculations of the heat capacity. (Figure reprinted from Ref. [17])

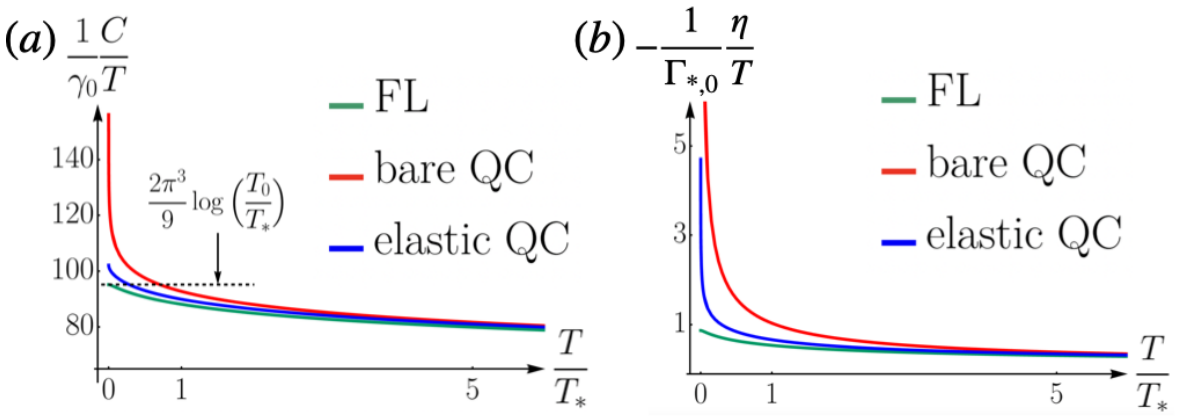

Figure 2.8: The behaviour of an altermagnetic system changes depending on the temperature regime. The heat capacity (panel (a)), diverges in the bare QC regime above T_*, below this temperature, the heat capacity behaves like a Fermi liquid and hence the lines overlap. The elastocaloric effect (panel (b)) is able to distinguish between these two regimes, as gapless bosons which form along critical lines when the system is coupled to elasticity lead to a divergence in both the elastic QC and bare QC regimes, although the bare QC regime is more singular. (Figure reprinted from Ref. [17])

where the temperature $T_{\mathrm{FL}}(m)$ is the bare quantum critical crossover temperature between the paramagnetic Fermi liquid phase at low temperature and the non-Fermi liquid phase at high temperature as shown in Fig. 2.2 and Fig. 2.5. This temperature is given by

$$T_{\mathrm{FL}}(m) = \left(\frac{m}{\nu_\phi \Lambda}\right)^3 T_0. \tag{2.112}$$

We see that the heat capacity shows the same T dependence in the paramagnetic and elastic QC regimes, and so no distinction is made between the two. We see this in Fig. 2.8 and also depicted with several different magnetic field strengths in Fig. 2.7(b).

As the heat capacity is not sensitive to the effect of the gapless excitations induced by the magnetoelastic effect, we consider $\Delta\gamma(T,H)$, given by

$$\Delta\gamma(T,H) \equiv \gamma(T,H) - \gamma(T,0), \tag{2.113}$$

for a fixed m.

In $\Delta\gamma(T,H)$, given that gapless bosons only exist when the magnetic field is switched on, the contributions from the phase space where $m(\mathbf{q}) \approx m$ and the bosons are gapped, will be cancelled. This leaves only the phase space of the reduced boson mass. To demonstrate this, we consider $\Delta\gamma(T,H)$ at the elastic quantum criticality ($m\left(\mathbf{q}\right)\Big|_{\mathrm{min}} = 0$). This contribution is

$$\Delta\gamma(T,H_{\mathrm{cr}}) \approx \frac{4\pi}{3}\gamma_0\left(c_0 - c_1\left(\frac{T}{T_*}\right)^{2/3}\right),\ T \ll T_*, \tag{2.114}$$

where c_0 and c_1 are constants independent of the momentum cutoff, magnetic field, temper-

ature and m.

The $T^{2/3}$ dependent contribution is a product of gapless boson mode. This has also been discussed in Ref. [16]. The presence of gapless modes is only possible with an external magnetic field and so performing an experiment with and without an external field, provides the potential to extract the $T^{2/3}$ dependence of the heat capacity originating from the gapless mode.

Fig. 2.7(c) shows $\Delta\gamma(T,H) - \Delta\gamma(0,H)$ for various magnetic fields. In the low temperature limit, the dashed red line shows the $T^{2/3}$ behaviour exhibited by a system with an external field which approaches H_{cr}.

2.4.6.2 Elastocaloric change

In the Fermi liquid regime, it is possible to tune the bare mass m^2 of the altermagnetic boson using a strain which transforms according to the A_{1g} irreducible representation. For D_{4h}, the corresponding strains are $\epsilon_{xx}+\epsilon_{yy}$ and ϵ_{zz}, such that $m^2(\epsilon) \sim c_{xx-yy}(\epsilon_{xx}+\epsilon_{yy}) + c_{zz}\epsilon_{zz}$. According to Ref. [166], the elastocaloric change near the bare quantum critical point with the finite m^2 of an altermagnet is given by:

$$\eta(\epsilon, T, H=0) \approx -72\Gamma_{\mathrm{FL},0}T_{\mathrm{FL}} \begin{cases} \frac{1}{9}\frac{\left(T/T_{\mathrm{FL}}\right)}{\log\frac{T_0}{T_{\mathrm{FL}}}}, & T \ll T_{\mathrm{FL}}, \\ 2\pi b\frac{\left(T/T_{\mathrm{FL}}\right)^{1/3}}{\log\frac{T_0}{T}}, & T \gg T_{\mathrm{FL}}, \end{cases} \tag{2.115}$$

where $\Gamma_{\mathrm{FL},0} = -\frac{\Lambda^3}{32\pi^4 m^2}\frac{\partial m^2}{\partial\epsilon}\frac{1}{\gamma_0 T_0}$ and T_{FL} is given by Eq. (2.112) which is now strain dependent through $m^2(\epsilon)$. Note that $\Gamma_{\mathrm{FL},0}$ and T_{FL} are identical to $\Gamma_{*,0}$ and T_* respectively, at the point where the bare mass $m = m_{*,H}$. We see that the behaviour of the elastocaloric effect in the Fermi liquid regime is qualitatively different to the results from the elastic QC regime.

As the magnetic field approaches its critical value, $\frac{\eta(H)}{\eta(H=0)}$, where H is the magnetic field, exhibits $\log T$ enhancement meaning that the ratio diverges as the system approaches the location of the elastic QCP in the low-temperature regime, as shown in Fig. 2.7(d).

2.4.7 Crossover temperature

Using the microscopic parameters of the system, we can estimate the regime where the field-induced altermagnetic coupling to the lattice becomes measurable. In order to estimate the magnitude of the the piezomagnetic coupling, we must first determine the dimensionless ratio $\lambda\mu_B B/\left(C^{1/2}J\right)$ where C is the bare elastic constant and $J = v_\phi\Lambda$ corresponds to the energy scale which characterises the bandwidth of the altermagnon mode as well as determining the ratio T_*/T_0. We rewrite the magnetoelastic coupling with $\lambda = \zeta/\sqrt{JV_0}$ where ζ is the dimensionless strength and V_0 is the volume of the unit cell. If $\Lambda \sim k_F$ and the dimensionless coupling constant $\alpha \sim 1$, this implies that T_0 is a significant fraction of E_F. We assume at least $T_*/T_0 \sim 10^{-3}$ gives an experimentally observable crossover regime. At an experimentally viable magnetic field $B = 10\,\mathrm{T}$ and using $C = 100\,\mathrm{MPa}$, $J/k_{\mathrm{B}} = 100\,\mathrm{K}$, and $V_0 = a^3$ with $a = 5\times10^{-10}\,\mathrm{m}$, one gets $\zeta \sim 10^2$. This would represent a value significantly larger than those measured in insulating altermagnets, such as MnTe [163], where $\zeta \sim 0.1$. However, one would expect piezomagnetic effects in metallic systems to be significantly larger. There

exist cases of giant piezomagnetism which have indeed been discussed in Ref. [159]. If one considers a soft material (such that C is low) with a large g-factor it becomes possible to reach values $T_*/T_0 \sim 10^{-3}$ with $\zeta \sim 1 \sim 5$. Hence, while the task of observing elastic quantum criticality in altermagnets provides a more staunch challenge than that posed by nematic systems, where such regimes are certainly accessible (in iron-based superconductors such as $\mathrm{Ba}\left(\mathrm{Fe}_{1-x}\mathrm{Co}_x\right)_2\mathrm{As}_2$ a conservative estimate for the crossover temperature gives a value of at least 10K [16]), there is some optimism that these regimes are in fact within reach.

2.5 Scaling of the elastocaloric effect

The scaling theory of quantum critical elasticity has already been formulated in Ref. [162]. This theory is based upon the critical contribution to the free energy density that obeys

$$f_{\mathrm{cr}}\left(r,T\right) = b^{-\left(d_{\mathrm{eff}}+z\right)} f_{\mathrm{cr}}\left(b^{1/\nu}r, b^z T\right), \tag{2.116}$$

with correlation length exponent ν, dynamic scaling exponent z and effective dimension d_{eff}, while r is a dimensionless measure of the distance to the QCP, such that $r \propto m^2 - m_*^2$. At criticality soft lines emerge when the external field is switched on and the effective phonon spectrum behaves as

$$\omega\left(\boldsymbol{q}\right)^2 \sim c^2 \boldsymbol{q}_\perp^2 + a q_{\mathrm{soft}}^4, \tag{2.117}$$

where we again make the choice that the system has m soft dimensions and $d-m$ hard directions, such that it is valid in both two and three dimensions. Then, to deal with this spectrum we can make the substitution $\mathbf{q}_\perp^2 \to \mathbf{q}_\perp^{'4}$. As discussed in Refs. [162, 168] such a spectrum amounts to an effective dimension $d_{\mathrm{eff}} = 2\left(d-m\right)+m$. For $d=3$ the effective dimension is therefore $d_{\mathrm{eff}} = 5$. In addition, Landau damping at a field-tuned altermagnetic QCP gives the dynamic exponent $z=3$, while the correlation-length exponent takes the mean-field value $\nu = \frac{1}{2}$. If we make the choice $b = T^{-1/z}$ for the scaling factor in Eq. (2.116) we obtain for the critical contribution $s_{\mathrm{cr}} = -T\partial f_{\mathrm{cr}}/\partial T$ to the entropy density

$$s_{\mathrm{cr}}\left(r,T\right) = T^{\frac{d_{\mathrm{eff}}}{z}}\Phi\left(rT^{-\frac{1}{\nu z}}\right), \tag{2.118}$$

with scaling function $\Phi\left(x\right)$. We can calculate for the temperature and strain derivatives at criticality and using $r \propto \epsilon_0$ for symmetry-preserving strain:

$$\begin{aligned}\frac{\partial s_{\mathrm{cr}}}{\partial T} &= u_T T^{\frac{d_{\mathrm{eff}}-z}{z}},\\ \frac{\partial s_{\mathrm{cr}}}{\partial \epsilon_0} &= u_\epsilon T^{\frac{d_{\mathrm{eff}}-\nu^{-1}}{z}}.\end{aligned} \tag{2.119}$$

u_T and u_ϵ are constant coefficients. We can now add these critical contributions to the Fermi liquid background terms we obtained by dividing the elastocaloric effect by T, i.e. the

appropriate dimensionless quantity that scales like the Grüneisen parameter:

$$\begin{aligned} \eta/T &= -\frac{\frac{\partial s_{\mathrm{FL}}}{\partial \epsilon_0}+\frac{\partial s_{\mathrm{cr}}}{\partial \epsilon_0}}{T\frac{\partial s_{\mathrm{FL}}}{\partial T}+T\frac{\partial s_{\mathrm{cr}}}{\partial T}} \\ &= -\frac{\Gamma_{\mathrm{FL}}\gamma_{\mathrm{FL}}-u_\epsilon T^{\frac{d_{\mathrm{eff}}-\nu^{-1}-z}{z}}}{\gamma_{\mathrm{FL}}+u_T T^{\frac{d_{\mathrm{eff}}-z}{z}}}, \end{aligned} \tag{2.120}$$

where Γ_{FL} is the constant Grüneisen parameter of a Fermi liquid. Let us first analyse the denominator, i.e. c/T, for $d_{\mathrm{eff}}=5$, $\nu=1/2$, and $z=3$. It follows $c/T=\gamma_{\mathrm{FL}}+u_T T^{2/3}\approx\gamma_{\mathrm{FL}}$, i.e. for the heat capacity the critical contribution is sub-leading. This is consistent with the explicit calculation of the heat capacity where we found that at leading order, the heat capacity maintained a Fermi-liquid type form in the elastic QC regime. The situation is different for the numerator, where the exponent $\frac{d_{\mathrm{eff}}-\nu^{-1}-z}{z}\to 0$, which should be interpreted as logarithmic behaviour. Hence, for the numerator, i.e. for the thermal expansion of the system, the critical contribution is the dominant one, such that

$$\eta/T\propto\log T, \tag{2.121}$$

which is again, fully consistent with our explicit analysis. Hence, elastic quantum criticality gives only sub-leading effects to the heat capacity but is the dominant contribution to the elastocaloric effect, leading to a divergence from the Fermi liquid behaviour one might have expected having calculated the other observables. The scaling argument is rather general and holds for both altermagnetic systems in an exterior magnetic field and nematic systems [17].

The physical implication of this result lies in the fact that changes in strain or stress alter the excitation spectrum more dramatically than variations in temperature. This is reflected in the larger scaling dimension associated with a strain derivative in comparison to that of a temperature variation. Consequently, quantities such as the elastocaloric effect, thermal expansion, and the Grüneisen parameter exhibit a more singular response than that of the heat capacity or the single-particle excitation spectrum.

Given the scaling analysis, one can also consider a one-loop RG as we carried out for classical systems, however once strain coupling is included, the effective spatial dimension of 5 and dynamical exponent of 3 make a small ϵ impossible.

2.6 Anomalous Hall effect in strained altermagnets

The fact that strain induces a net magnetisation suggests that it would be fruitful to investigate the potential presence of an anomalous Hall effect. We do so in Ref. [18], which this subsection quotes from. Transport properties of strained altermagnets are of interest as they could give rise to observable quantities which not only identify a state as altermagnetic but also allow for the identification of the irreducible representation according to which the order parameter transforms. In general, as we will discuss in what follows, the Berry curvature in an altermagnet averages to zero over the unit cell and hence there is no anomalous Hall effect. However, Ref. [76] identified a third order in electric field Hall effect given by

$$j_\alpha^{(3)}=\sigma^{(a)}_{\alpha\beta\gamma\delta}E_\beta E_\delta E_\gamma, \tag{2.122}$$

where the superscript (a) denotes that it is the antisymmetric part of the conductivity with respect to the first two indices. While this would potentially suffice to probe altermagnetic states, it does raise the question as to whether there exists a transport property to first order in the field. This would represent a quantity which is more practical to measure. One can instead consider the elastoconductivity $\nu_{\alpha\beta\gamma\delta}$, defined as

$$j_\alpha = \sigma_{\alpha\beta} E_\beta + \nu_{\alpha\beta\gamma\delta} E_\beta \epsilon_{\gamma\delta}. \tag{2.123}$$

In this case elasticity allows for the slight alteration of crystalline symmetries which then constrains the allowed states of electronic order [169, 170]. Analyses of this type have been used to investigate semiconductors [171], identify the role of nematic fluctuations in iron based superconductors [172] and exotic properties of states exhibiting charge density waves [173–175]. An analysis of elastotransport reveals that under strain, it is possible to generate a finite anomalous Hall current which is first order in the electric field.

Given that the Hall conductivity vanishes when no strain is applied, the current arising from the elasto-Hall conductivity response is

$$j_\alpha = \nu^{(a)}_{\alpha\beta\gamma\delta} E_\beta \epsilon_{\gamma\delta}, \tag{2.124}$$

where the components $\nu^{(a)}_{\alpha\beta\gamma\delta}$ are those of $\nu_{\alpha\beta\gamma\delta}$ that are antisymmetric in the first two indices.

The Onsager relations for the conductivity suggest

$$\nu_{\alpha\beta\gamma\delta} = -\nu_{\beta\alpha\gamma\delta}. \tag{2.125}$$

This then contributes to $\nu^{(a)}_{\alpha\beta\gamma\delta}$. The symmetry of the strain tensor then gives

$$\nu_{\alpha\beta\gamma\delta} = \nu_{\alpha\beta\delta\gamma}. \tag{2.126}$$

In altermagnets, we know that a piezomagnetic effect is generated by a symmetry breaking strain which induces a finite net magnetisation by breaking the symmetry which would otherwise forbid the formation of one. This leads to an interesting analogy with the anomalous Hall effect in altermagnets, which becomes clear when discussing the Berry curvature of such materials. The basic principles by which one obtains an anomalous Hall effect are discussed in Sec. 1.2, albeit in this case with regards to twisted bilayer graphene; the theory linking the quantities however, remains unchanged.

Here we expand on the information presented in Sec. 1.2. The Berry curvature can be written as a three-component vector $\boldsymbol{\Omega}(\boldsymbol{k}) = \left(\Omega_{yz}(\boldsymbol{k}), \Omega_{zx}(\boldsymbol{k}), \Omega_{xy}(\boldsymbol{k})\right)$. $\boldsymbol{\Omega}(\boldsymbol{k})$ transforms like an axial vector under time reversal $\mathcal{T}$ and parity $\mathcal{P}$

$$\begin{aligned} \boldsymbol{\Omega}(\boldsymbol{k}) &\xrightarrow{\mathcal{T}} -\boldsymbol{\Omega}(-\boldsymbol{k}), \\ \boldsymbol{\Omega}(\boldsymbol{k}) &\xrightarrow{\mathcal{P}} \boldsymbol{\Omega}(-\boldsymbol{k}). \end{aligned} \tag{2.127}$$

It then becomes clear that if a system has time-reversal and inversion symmetry, the Berry curvature is zero. Exceptions to this arise at Dirac points which act as monopole sources of Berry curvature. These monopoles manifest with opposite sign for opposite momenta, such that if one averages the Berry curvature over the momenta and occupied bands, it is zero

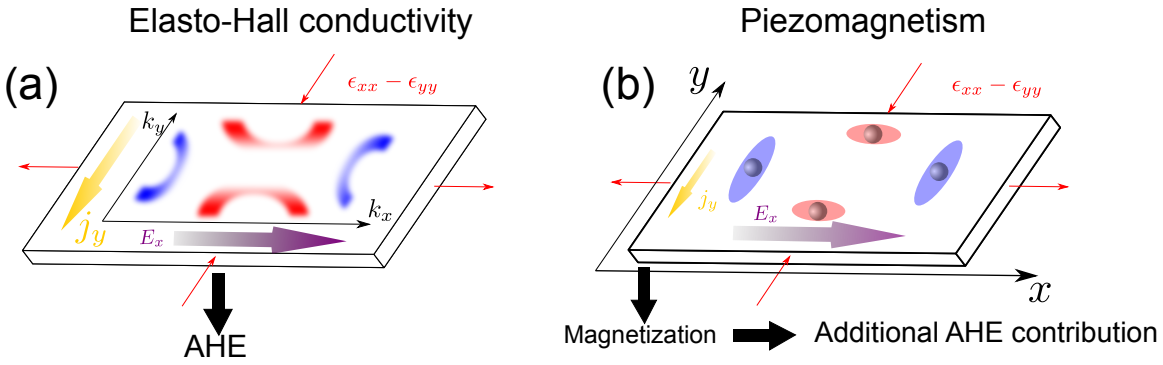

Figure 2.9: Illustration of the anomalous Hall conductivity in a strained B_{2g} altermagnet. There exists two contributions to this quantity in strained altermagnets, one is associated with the elasto-Hall conductivity response function (panel (a)) and the other from the piezomagnetic effect outlined in this chapter (panel (b)). In both cases the symmetry of the altermagnet enforces the response functions to be zero. The Berry curvature (panel (a)) has a quadrupolar form (blue for positive and red for negative values) which averages to zero over the unit cell until a symmetry breaking $\epsilon_{B_{1g}}$ strain allows for the formation of a finite Berry curvature monopole. This manifests itself physically as the formation of an AHE. The other (typically smaller) contribution comes from the finite magnetic dipole which forms under symmetry breaking strain. The spin density is deformed (blue for spin up and red for spin down), creating a finite magnetisation. The current j_y, shown in both panels, is to leading order linear in the electrical field, E_x and the strain $\epsilon_{xx} - \epsilon_{yy}$, giving rise to non-zero elasto-Hall conductivity elements $\nu^{(a)}_{xyxx} - \nu^{(a)}_{xyyy} \neq 0$, with $\nu^{(a)}_{\alpha\beta\gamma\delta}$ of Eq. (2.123) and piezomagnetic tensor components $\Lambda_{zxx} - \Lambda_{zyy} \neq 0$, given by Eq. (2.7). (Figure reprinted from Ref. [18], Copyright American Physical Society (2025))

and there is still no finite Hall conductance. We see that in order to produce a finite Hall conductivity, the symmetry of the Berry curvature relating momenta of opposite sign to one another must be changed.

If we know the irreducible representation of the order parameter, it is then possible to deduce the distribution of the Berry curvature this ordering gives rise to. By definition of a pure altermagnet (one with no ferromagnetic component) [58], there always exists a point group symmetry which, in combination with time reversal, leaves the state unchanged. This usually corresponds to a rotation, under which the Berry curvature transforms with

$$\Omega_\mu(R\mathbf{k}) = -\overline{R}_{\mu\nu}\mathbf{\Omega}_\nu(-\mathbf{k}), \tag{2.128}$$

where $\overline{R}$ and R are the representations of rotations $\mathcal{R}$ for axial and and polar vectors respectively, such that $\overline{R} = R\det(R)$. The minus sign in the prefactor is a result of the magnetic state being odd under the given rotation, such that it cancels time-reversal symmetry. The system has inversion symmetry and hence the Berry curvature is even under $\mathbf{k} \to -\mathbf{k}$. The symmetry operation of the Berry curvature can therefore be summarised as

$$\Omega_\mu(R\mathbf{k}) = \Big(D_\Omega(\mathcal{R})\Big)_{\mu\nu}\Omega_\nu(\mathbf{k}), \tag{2.129}$$

where $D_\Omega(\mathcal{R}) = D_{\Gamma_\phi^-}(\mathcal{R})\overline{R}$ where $D_{\Gamma_\phi^-}(\mathcal{R})$ is the representation of the order parameter. This implies that $D_\Omega(\mathcal{R})$ corresponds to $\Gamma_\phi^- \otimes \Gamma_{\overline{R}}$. If ϕ transforms according to B_{2g}, the transformation which cancels time reversal symmetry is therefore a C_4 rotation in the $x-y$ plane. A rotation of this type transforms like A_{2g} and the Berry curvature then transforms according to B_{1g}. The strain which breaks this symmetry would then produce a finite Berry curvature monopole. The irreducible representation of the Berry curvature being the product of the order parameter and a rotation follows the same set of rules as the piezomagnetic coupling, given that rotations and magnetic fields belong to the same irreducible representations. There exist two contributions to the Berry curvature, one comes from the interband matrix element of the strain induced perturbation and the other from the net magnetisation induced by the piezomagnetic effect. The AHE contribution which originates from the finite magnetisation is typically the smaller one. The fact that an AHE is induced from a strain-induced net magnetisation makes the link to piezomagnetism even clearer. We depict both contributions in Fig. 2.9.

The symmetry analysis up to this point assumes that the order parameter has a single component, however to linear order in the order parameter, we can use the piezomagnetic coupling to deduce the non-zero elements of $\nu_{\alpha\beta\gamma\delta}$ for multi-dimensional irreducible representations. If the strain $\epsilon_{\gamma\delta}$ induces a magnetisation M_μ, then the elements are non-zero for the combination of indices for which the Levi-Civita tensor $\varepsilon_{\alpha\beta\mu} \neq 0$. If we consider the order parameter which transforms under E_{2g} in D_{6h}, the piezomagnetic coupling induces magnetisations according to

$$\begin{aligned} M_x &= \lambda\left(\epsilon_{yz}\phi_1 - \epsilon_{xz}\phi_2\right), \\ M_y &= \lambda\left(\epsilon_{xz}\phi_1 + \epsilon_{yz}\phi_2\right), \\ M_z &= \lambda'\left(2\epsilon_{xy}\phi_1 - \epsilon_{x^2-y^2}\phi_2\right). \end{aligned} \tag{2.130}$$

If $\phi_1 \neq 0$, a magnetisation along y is induced when $\epsilon_{xz} \neq 0$. This implies $\nu_{zxxz} \neq 0$. If ϵ_{yz} is applied with the same magnitude then $\nu_{zxxz} = \nu_{yzyz}$. The order parameter can also order according to $(\phi_1, \phi_2) = (1, b)$. In this case we obtain the relations

$$\begin{aligned} \nu_{yzyz} = \nu_{zxxz} = -b\nu_{yzxz} = b\nu_{zxyz}, \\ b\nu_{xyyy} = -b\nu_{xyxx} = 2\nu_{xyxy}, \end{aligned} \tag{2.131}$$

where the first line is due to induced magnetic fields which are in-plane and the second from M_z.

We can repeat this analysis for the two-component order parameter which transforms like E_g^- in O_h, we obtain:

$$\sqrt{3}\nu_{yzyz} = -\sqrt{3}\nu_{zxxz} = -b\nu_{yzyz} = -b\nu_{zxxz} = 2b\nu_{xyxy}. \tag{2.132}$$

Finally for the three-component order parameter that transforms like T_{2g} in O_h, which we parametrise as $(\phi_1, \phi_2, \phi_3) = (1, b, c)$, we find:

$$\begin{aligned} \nu_{zxxy} = -\nu_{xyxz} = -b\nu_{yzxy} = b\nu_{xyyz} = c\nu_{yzxz} = -c\nu_{zxyz}, \\ \nu_{yzyy} = -\nu_{yzzz} = b\nu_{zxzz} = -b\nu_{zxxx} = c\nu_{xyxx} = -c\nu_{xyyy}. \end{aligned} \tag{2.133}$$

These expressions are in agreement with Table. 2.3. We see that more entries exist in Table. 2.3 than can be derived from the piezomagnetic coupling. The reason for this is terms which are higher order in the order parameter. In order to deduce the full set of non-zero terms and their relations, we use the Jahn symbols [176], based on the fact that any tensor can be expressed in terms of a polar vector, V. To clarify the notation $[\dots]$ denotes symmetric and $\{\dots\}$ denotes antisymmetric indices, such that a tensor with Jan symbol $\left[V^2\right]V$ satisfies $A_{\alpha\beta\gamma} = A_{\beta\alpha\gamma}$, whereas a tensor described by $\left\{V^2\right\}V$ behaves like $A_{\alpha\beta\gamma} = -A_{\beta\alpha\gamma}$. The other elements we will need are the rank-0 tensors $e = \pm 1$ and $a = \pm 1$ which change sign under inversion and time-reversal respectively. Given that the anti-symmetric part of the conductivity (i.e. the part which describes the Hall conductivity) must transform like $a\left\{V^2\right\}$ (with a present to ensure Onsager reciprocity) then given that the elasticity tensor is symmetric, the elasto-Hall conductivity has the Jahn symbol $a\left\{V^2\right\}\left[V^2\right]$. We can compare this to the Jahn symbol of the piezomagnetic tensor. Magnetisation transforms as a time-reversal odd axial vector aeV, including the strain gives the Jahn symbol $aeV\left[V^2\right]$. Given that the cross product of two polar vectors transforms as an axial vector, $\left\{V^2\right\}$ has the same decomposition into irreducible representations as eV, the irreducible representations of the two tensors match. A similar relationship was also noted in Ref. [177]. Using the ISOTROPY software [178] to identify the magnetic point group and the Bilbao Crystallographic server [179, 180] to obtain the symmetry allowed tensor components for a tensor with the corresponding Jahn symbol for the relevant point groups, we were able to find the full allowed components of the elasto-Hall conductivity tensor as noted in Table. 2.3. It should also be noted that these results agree (where they overlap) with the first-principle study of anomalous Hall, spin Hall and valley Hall effects in Nb_2SeTeO presented in Ref. [181].

	AM irrep.	MPG	elasto-Hall conductivity
orthorh., D_{2h} (mmm)	A_{1g}^-	mmm (8.1.24)	ν_{yzyz}, ν_{zxxz}, ν_{xyxy}
trigon. D_{3d} $(\bar{3}m)$	A_{1g}^-	$\bar{3}m$ (20.1.71)	$\nu_{xzxx} = \nu_{zxyy} = \nu_{zyxy}$, $\nu_{xzxz} = \nu_{yzyz}$
tetrag., D_{4h} $(4/mmm)$	A_{1g}^-	$4/mmm$ (15.1.53)	$\nu_{yzyz} = -\nu_{zxxz}$
	B_{1g}^-	$4'/mm'm$ (15.4.56)	$\nu_{yzyz} = \nu_{zxxz}$, ν_{xyxy}
	B_{2g}^-	$4'/mm'm$ (15.4.56)	$\nu_{yzxz} = -\nu_{zxyz}$, $\nu_{xyxx} = -\nu_{xyyy}$
hexag., D_{6h} $(6/mmm)$	A_{1g}^-	$6/mmm$ (27.1.100)	$\nu_{yzyz} = -\nu_{zxxz}$
	B_{1g}^-	$6'/m'mm'$ (27.5.104)	$\nu_{yzxy} = \nu_{zxxx} = -\nu_{zxyy}$
	B_{2g}^-	$6'/m'mm'$ (27.5.104)	$\nu_{zxxy} = \nu_{yzyy} = -\nu_{yzxx}$
	E_{2g}^-	$(1,0)$ mmm (8.1.24)	ν_{yzyz}, ν_{zxxz}, ν_{xyxy}
		$(1, \frac{1}{\sqrt{3}})$ $m'm'm$ (8.4.27)	ν_{xyxx}, ν_{xyyy}, ν_{xyzz}, ν_{xzyz}, ν_{yzxz}
		$(1,b)$ $2/m$ (5.1.12)	ν_{xzxx}, ν_{xzyy}, ν_{xzzz}, ν_{xyyz}, ν_{yzyz}, ν_{xzxz}, ν_{xyxy}, ν_{yzxy}
cubic, O_h $(m\bar{3}m)$	A_{1g}^-	$m\bar{3}m$ (29.1.109)	-
	A_{2g}^-	$m\bar{3}m'$ (32.4.121)	$\nu_{yzyz} = \nu_{zxxz} = \nu_{xyxy}$
	E_g^-	$(1,0)$ $4/mmm$ (15.1.53)	$\nu_{yzyz} = -\nu_{zxxz}$
		$(1, \frac{1}{\sqrt{3}})$ $4'/mm'm$ (15.4.56)	$\nu_{yzyz} = \nu_{zxxz}$, ν_{xyxy}
		$(1,b)$ mmm (8.1.24)	ν_{yzyz}, ν_{zxxz}, ν_{xyxy}
	T_{2g}^-	$(1,0,0)$ $4'/mm'm$ (15.4.56)	$\nu_{yzxz} = -\nu_{zxyz}$, $\nu_{xyxx} = -\nu_{xyyy}$
		$(1,1,0)$ $m'm'm$ (8.4.27)	ν_{yzxx}, ν_{yzyy}, ν_{yzzz}, ν_{xyxz}, ν_{xzxy}
		$(1,1,1)\bar{3}m$ (20.1.71)	$\nu_{xzxy} = \nu_{zyyy} = \nu_{yzxx}$, $\nu_{xzxz} = \nu_{yzyz}$
		$(1,b,0)$ $2'/m'$ (5.5.16)	ν_{xyxx}, ν_{yzxx}, ν_{xyyy}, ν_{yzyy} ν_{xyzz}, ν_{yzzz}, ν_{xzyz}, ν_{xyxz}, ν_{yzxz}, ν_{xzxy}
		$(1,1,c)$ $2/m$ (5.1.12)	ν_{xzxx}, ν_{xzyy}, ν_{xzzz}, ν_{xyyz}, ν_{yzyz}, ν_{xzxz}, ν_{xyxy}, ν_{yzxy}
		$(1,b,c)$ -1 (2.1.3)	all elements $\nu_{\alpha\beta\gamma\delta}$ are nonzero where $\alpha \neq \beta$

Table 2.3: Non-vanishing elements of the elasto-Hall conductivity tensor $\nu^{(a)}_{\alpha\beta\gamma\delta}$ defined in Eq. (2.124) for all pure altermagnetic order parameters (i.e., those with no symmetry allowed net magnetic moment in the presence of SOC) in point groups of the orthorhombic (D_{2h}), trigonal (D_{3d}), tetragonal (D_{4h}), hexagonal (D_{6h}), and cubic (O_h), crystal classes. The third column denotes the magnetic point group (MPG) that results from the condensation of the order parameter listed in the second column. The symmetry relations given in Eqs. (2.125) and (2.126) imply additional elements that occur from the permutation of the first two or the last two indices. For multi-component order parameters, the allowed tensor elements depend on the relative magnitude of the components, parametrised as $(1,b)$ or $(1,b,c)$, respectively. Among the point groups analysed, only an altermagnetic order parameter that transforms under A_{1g}^- of the cubic group O_h does not display any non-zero elements of the elasto-Hall conductivity tensor. (Table reprinted from Ref. [18], Copyright American Physical Society (2025))

2.7 Summary

Elastic fluctuations play a crucial role in the alteration of behaviour near a quantum critical point. Altermagnetic systems which break rotational symmetries couple to the lattice in the presence of an external field. Such a coupling alters the universality class of the critical point and leads to a shift in the critical point, which can be tuned by the magnetic field. The coupled acoustic phonons suppress critical order parameter fluctuations, an effect originating in the direction selective criticality, where at the altermagnetic transition the sound velocity vanishes along isolated lines in momentum space.

The main findings shown here are that the piezomagnetic coupling of an altermagnet mirrors that of a nematic order parameter coupled to the lattice, producing similar results to those reported in Ref. [16]. When an external field is switched on, the piezomagnetic coupling causes the formation of an elastic QC regime below a crossover temperature $T_* \propto H_z^3$, such that it is now tunable with an applied magnetic field. This means that altermagnetic systems allow for the study of a non-Fermi liquid region which is not accessible in nematic systems. We have shown that the elastic quantum criticality is characterised by a behaviour which deviates from the Fermi-liquid expectation at leading order in calculations of the elastocaloric effect [17]. This is contrasted by observables such as the heat capacity and single-particle self-energy, which exhibit Fermi liquid behaviour at leading order, in agreement with the results reported for nematics in Ref. [16]. This suggests that while the fermionic quasiparticles are well-defined, there exists non-analytic properties in the collective modes which are promoted to a primary effect upon taking a strain derivative, a result which is not only applicable to altermagnetic systems but more generally to nematic systems. The elastocaloric effect hence offers a promising tool for the analysis of elastic quantum criticality in altermagnets (and nematics). The fact that the temperature scale is field-dependent for altermagnets offers a tunability which could be leveraged in experimental setups to identify gapless modes and hence altermagnetic states.

This crossover temperature scale T_* is not currently well-established. It is dependent on the strength of the piezomagnetic coupling, as well as the magnetic field energy. The small energy scales of magnetic fields suggest that experimentally accessible crossover scales are more likely to occur in systems with low overall altermagnetic order energies than in itinerant systems, even though the piezomagnetic coupling tends to be higher in such systems. The analysis of altermagnetic materials is still in its infancy and so the hope is that this theory encourages the search for systems with strong piezomagnetic couplings, large magnetic g-factors, and moderate magnetic interaction scales.

The piezomagnetic coupling also plays an important role in the formation of a finite Hall current in altermagnets. Ordinarily a purely octupolar magnetic order produces a Berry phase with a quadrupolar distribution, hence averaging to zero over the unit cell. Straining the system with a symmetry breaking strain then allows for the formation of a finite Berry curvature monopole and a finite Hall conductivity [18]. This follows the same principle as the formation of a finite magnetisation arising from a symmetry allowed piezomagnetic coupling. Detection of Hall currents could then also allow for the classification of altermagnetic systems.

Overall these results show that there exist intriguing manifestations of potential couplings between electronic and lattice degrees of freedom which could form the basis of future experimental work in order to identify and probe altermagnetic states.

While these results were obtained for a coupling to B_{1g} strain, they are valid generally for

any nematic or altermagnetic order parameter which couples to symmetry breaking strain. In all cases, a momentum dependent coupling emerges, leading to a direction-dependent mass characterised by minima along certain q directions. Different irreducible representations have different form factors, which lead to a different set of directions along which the system becomes critical but specific directions will not affect the behaviour of the elastocaloric effect. In cubic systems we note that A_{1g} does not have a corresponding piezomagnetic response. For systems with a higher-dimensional irreducible representation, a cubic term emerges in the field theory (for altermagnetic systems this is field dependent), inducing a weak first-order transition and our theory no longer applies [157].

Chapter 3

3 Dynamic magnetoelastic coupling in altermagnetic materials

In Chapter. 2 we discussed the effects of a piezomagnetic coupling between strain and altermagnetism on the quantum critical behaviour. There exists however, other symmetry allowed couplings between altermagnetism and strain, we can also analyse the effects of a coupling of strain to the dynamics of the order parameter. In this case we discuss the effects of such a coupling on the collective modes of the system as well as on the phase diagram. In contrast to the piezomagnetic coupling, a coupling to dynamics is present even in the absence of a magnetic field. If we consider a system close to the quantum critical point, such that the dynamics of the order parameter are at their most relevant, we can investigate the effect of quantum fluctuations on the elastic degrees of freedom, mediated by this coupling. Strain can be decomposed into the main phonon modes of the system, coupling these to an altermagnon causes the modes to hybridise, forming magnon and phonon-like polarons. The degrees of freedom then behave in a way analogous to that of two coupled oscillators which form squeezed states where the fluctuations of one degree of freedom suppress the other. We hence see that quantum fluctuations corresponding to the magnon-like polaron are enhanced and phonon-like polarons are suppressed, we will then show how this hybridisation affects the phase diagram for the system in both two and three dimensions and how an anisotropy in this effect presents a way to detect altermagnetic states through probing the phonon spectrum. This section is adapted and in some cases directly quotes from Ref. [20].

3.1 Introduction

Having already discussed altermagnets in great detail in Chapter. 1 and Chapter. 2 we now consider the dynamics of the order parameter corresponding to the magnetisation. We show that there exists a subset of altermagnets (and some ferromagnets) which exhibit a non-trivial coupling between strain and altermagnetism.

We reiterate some of the key points of magnetoelastic coupling before formulating this new type of coupling in order to highlight the most important points of difference. In ferromagnets and antiferromagnets, i.e. dipolar magnetic materials, straining the material changes the lattice parameter and hence the exchange interaction between spins. One of the consequences of this is a hybridisation of the magnon and phonon modes in the ordered state; these

hybridised modes are called magnon-polarons [130]. Multipolar materials however, allow for different types of coupling between magnetisation and strain due to the exotic symmetries which define the altermagnet [44, 134, 182–184]. The formation of magnon-polarons is often associated with the magnetostriction response tensor N_{ijkl}, defined as $\varepsilon_{ij} = N_{ijkl}M_kM_l$ and discussed in Sec. 1.4. We have also already discussed how altermagnets exhibit a non-zero piezomagnetic response, where the piezomagnetic response tensor Λ_{ijk}, is defined by $\varepsilon_{ij} = \Lambda_{ijk}M_k$ [134]. This can create a situation analogous to nematic order coupling to a lattice [15, 185, 186] where a lattice distortion can induce a non-zero magnetisation which possibly breaks a symmetry of the system [135, 136]. The fundamental difference is that altermagnetism is time-reversal odd and nematicity is time-reversal even, for this reason we previously used a magnetic field to complete the analogy between nematicity and altermagnetism. This also suggests an alternative way to couple the altermagnetism and strain is to introduce introduce a time derivative. If ϕ is time-reversal odd, then $\partial_t\phi$ must be time-reversal even and a coupling to strain is symmetry allowed, provided the strain and order parameter both transform according to the same irreducible representation of the point group Γ. We can then write down the coupling

$$\mathcal{H}_{\mathrm{c}}^{\mathrm{dyn}} = \frac{\lambda_0}{2}c^2 \int d^3\boldsymbol{x}\varepsilon_{\Gamma^+}(\boldsymbol{x})\pi(\boldsymbol{x}). \tag{3.1}$$

where π is the conjugate momentum to ϕ introduced by coupling to the time derivative $\partial_t\phi$. The effect of this coupling is reminiscent of the Hall viscosity response [140, 187–190]. We will expand on this analogy in the following section.

This is in stark contrast to the standard static coupling (magnetostriction) [130, 131]

$$\mathcal{H}_{\mathrm{c}}^{\mathrm{mag-el}} = \int d^3\boldsymbol{x}N_{ijkl}\varepsilon_{ij}(\boldsymbol{x})\phi_k(\boldsymbol{x})\phi_l(\boldsymbol{x}), \tag{3.2}$$

where N_{ijkl} is the magnetoelastic tensor introduced above and ϕ_i are the components of the (staggered) magnetisation. Like the coupling we propose in Eq. (3.1), this also hybridises the phonon and magnon modes [130, 131] but the effect of magnetostriction is most relevant if the phonon and magnon branches cross. It can then open a gap and potentially promote nontrivial topological effects [132, 133]. The coupling we propose in Eq. (3.1) is relevant whether or not the bands cross and the effects of this will be discussed in detail in this chapter. We will see that the impact of the coupling is actually strongest in the case that the branches do not cross.

In this chapter we will study how dynamic coupling of the altermagnetism and strain affects the modes in the disordered phase close to the quantum critical point i.e. just before long range order sets in. We show that a mixing of the two degrees of freedom would allow for the detection of altermagnetic states by probing the phonon spectrum. We will see that this is analogous to two-mode squeezing [191, 192] of elastic and magnetic modes.

We also investigate how this coupling affects the transition from the paramagnetic to the altermagnetic phase. The results of this are shown in Fig. 3.1. We consider both thermal and quantum fluctuations. By tuning parameters, we find that a quantum critical point [97, 105, 193, 194] exists, defined as the point where the transition temperature is suppressed to zero and altermagnetic fluctuations affect the ground state, even in the absence of long-range order. The dynamic coupling has distinct effects on the two types of fluctuation. Quantum

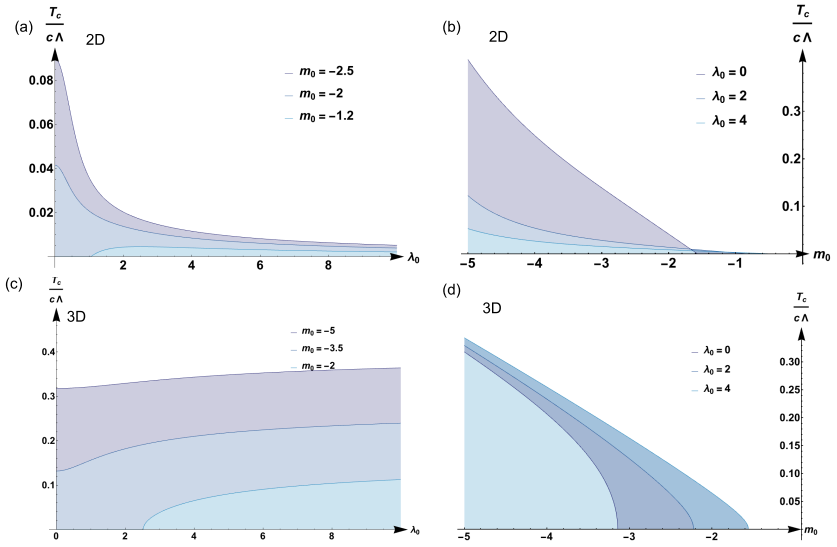

Figure 3.1: (a) Altermagnetic transition temperature T_c in a 2D system as a function of the dynamic strain coupling constant λ_0 for different values of the bare altermagnon mass $m_0 = r_0/\Lambda^2$. Note that $m_0 < 0$ ($m_0 > 0$) defines the ordered (disordered) state without the coupling to the lattice and the ϕ^4 mode coupling. The dynamic coupling to phonons suppresses order at finite temperature, but enhances or even induces order at zero temperature. (b) Altermagnetic T_c in a 2D system as a function of m_0 for different values of λ_0. (c) and (d) show the same information as panels (a) and (b) respectively but for a 3D system. These plots refer to the regime $c > v_{L,T}$; the opposite regime is shown in Fig. 3.8. (Figure reprinted from Ref. [20], Copyright American Physical Society (2023))

fluctuations are suppressed, leading to an enhanced ordered regime at $T = 0$ in both 2D and 3D, while thermal fluctuations are enhanced. In 2D this is enough to suppress the transition temperature, whereas in 3D the quantum fluctuations are still the dominant effect and the transition temperature increases slightly with increased coupling strength.

The structure of this chapter is as follows, In Sec. 3.2 we are specific about the altermagnetic order parameter and motivate the dynamic coupling to strain. In Sec. 3.3 we show that this coupling causes the modes to hybridise and we plot the modes using the effective propagator for the magnetic collective modes. From this we find that that the effects of coupling are anisotropic, before reinforcing this by plotting the spectral functions for the hybridised modes. In Sec. 3.4 we plot the phase diagram for the paramagnetic to altermagnetic phase transition, to demonstrate how coupling to strain affects the phase boundary. We finish this section with a short summary and discussion of how this analysis is also relevant for certain ferromagnetic systems in Sec. 3.5.

3.2 Dynamic magnetoelastic coupling for multipolar order

In order to motivate the proposed coupling of strain to the dynamics of the altermagnetic magnetisation order parameter, we must consider a more detailed description of multipolar moments in altermagnets than that previously discussed in Chapter. 1. We consider a general

order parameter ϕ which transforms according to some irreducible representation that we denote Γ^- where the superscript "$-$" denotes that the object is odd under time-reversal, as one would expect from a magnetic order parameter. A standard ferromagnetic order parameter must transform like a magnetic dipole under point group operations, we denote this as $\Gamma^-_{J_\alpha}$. If $\Gamma^- = \Gamma_{J_\alpha}$ then the order parameter is that of a usual ferromagnet

$$\phi^\alpha(\mathbf{x}) \sim \sum_{ab} c_a^\dagger(\mathbf{x})\, J^\alpha_{ab} c_b(\mathbf{x}), \tag{3.3}$$

where J^α is an angular momentum operator with indices a and b, which are the spin and orbital indices for the system. The simplest case that one can consider is that which has J^α as one of the Pauli matrices but in general one would also expect an orbital moment. Other representations which are also odd under time reversal but transform differently to $\Gamma^-_{J_\alpha}$ form higher order order multipoles with the form [195]

$$\phi(\boldsymbol{x}) \sim \sum_{ab} \int d^3\boldsymbol{x}' f\left(\boldsymbol{x}'\right) c_a^\dagger\left(\boldsymbol{x} + \frac{\boldsymbol{x}'}{2}\right) J^\mu_{ab} c_b\left(\boldsymbol{x} - \frac{\boldsymbol{x}'}{2}\right), \tag{3.4}$$

where $f\left(\boldsymbol{x}'\right)$ is the previously discussed form factor which defines the spin and orbital moment density within the unit cell. We see from this general expression that we recover the ferromagnetic case by setting $f(\mathbf{x}) = \delta(\mathbf{x})$. The same is also true for form factors which transform trivially under point group operations. Introducing a form factor which transforms nontrivially means Eq. 3.4 now corresponds to higher-order multipoles [59]. If the form factor transforms according to a d-wave, g-wave or i-wave form factor then the order parameter corresponds to that of an altermagnet [2, 196]. The distribution of spin and orbital moment densities is a consequence of multiple atoms within a single unit cell; this holds even in the case that only one electronic band crosses the Fermi surface. This section will focus on altermagnetic order parameters, a calculation dealing with a ferromagnetic system will be given in Chapter. 4.

Having now motivated different types of coupling between order parameters and strain, we will focus on the dynamics of the order parameter which allows for a coupling beyond the standard static couplings usually considered [130, 131]. We will see that this coupling is direct and hence does not require a magnetic field in order to mediate the interaction. We must consider now the actual dynamics of $\phi(\mathbf{x})$, if the dynamics are fairly general then the order parameter has a conjugate momentum $\pi(\mathbf{x})$. We will be carrying out our calculation in the quantum regime and so this implies the canonical commutation relation $\left[\phi(\boldsymbol{x}), \pi(\boldsymbol{x}')\right] = i\hbar\delta(\boldsymbol{x} - \boldsymbol{x}')$. One can also consider the dynamics in the classical regime in which the dynamics follow from the corresponding Poisson brackets. As has already been well established, the order parameter is odd under time-reversal, this implies that the conjugate momentum is even under time-reversal. If there exists a strain which transforms according to Γ^+, i.e. the same way as the order parameter, with the distinction of being time-reversal even, then it is possible to construct a symmetry allowed coupling. We express this as an action, in which the conjugate momentum is eliminated and the time derivative of the order parameter assumes its position

$$\mathcal{S}_{\mathrm{c}}^{\mathrm{dyn}} = \frac{\lambda_0}{2} \int_0^\beta d\tau \int d^3\boldsymbol{x} \varepsilon_{\Gamma^+}(\boldsymbol{x}, \tau) \partial_\tau \phi(\boldsymbol{x}, \tau), \tag{3.5}$$

where λ_0 is a dimensionless coupling constant, $\beta = 1/T$ is the inverse temperature and τ is imaginary time. Given that the coupling is dimensionless, we can assume that a natural value for this in strongly coupled systems is $\lambda_0 \approx 1$.

Dynamic coupling of the type Eq. (3.5) is in direct contrast with static couplings, such as piezomagnetic coupling, as it does not affect static field configurations. Instead we see a strong mixing of the dynamics of lattice and magnetic degrees of freedom, which holds even in the absence of a magnetic field. Given that the dynamics of the lattice (phonons) are observable, this creates the possibility to observe fluctuations of the mulitpolar order parameter through Raman [197–201] or neutron scattering [202–206]. This holds even in the disordered state, due to the presence of fluctuations close to the QCP. The coupling in Eq. (3.5) was derived in Sec. 1.4.

This coupling mediates an interaction between fluctuations in an altermagnetic order parameter, which then induce a non-dissipative stress in direct analogy with the Hall viscosity [190, 207, 208], the antisymmetric terms in the viscosity tensor $\eta_{ijkl} = -\eta_{klij}$. We can see this explicitly from Eq. (3.5). Consider the relationship between stress and strain [27]

$$\sigma_{ij} = C_{ijkl}\varepsilon_{kl} - \eta_{ijkl}\partial_t\varepsilon_{kl} \tag{3.6}$$

with elastic constants C_{ijkl} and viscosity tensor η_{ijkl}. The second term takes into account stresses at finite speed which are dissipative and produce heat. If we consider the rate of entropy production in a fluid (just considering the terms related to stress, as terms between heat flux and stress are independent) [207]

$$\frac{dS_\varepsilon}{dt} = \int \frac{1}{T}\left(\eta_{ijkl}\partial_t\varepsilon_{ij}\partial_t\varepsilon_{kl}\right) dV \tag{3.7}$$

we see that only the terms which are symmetric in the viscosity i.e. $\eta_{ijkl} = \eta_{klij}$, contribute to entropy production; the other terms are then non-dissipative. These terms, due to the Onsager reciprocal relations, are zero unless time-reversal symmetry is broken [190]. One way to break time-reversal symmetry is with an external magnetic field, this allows the antisymmetric components to be nonzero. The following example we discuss in detail is relevant to the D_{4h} point group. In this case we have the Hall viscosity

$$\eta^H = \eta_{xyxx}\left(B_z\right) = \eta_{xxxy}\left(-B_z\right) \tag{3.8}$$

such that as well as being antisymmetric, it is also odd under time-reversal. The Hall viscosity contribution to the action which yields the equation of motion Eq. (3.6) is then

$$\mathcal{S}_{\text{Hall}} = -\frac{1}{2}\eta^H \int d\tau d^3\boldsymbol{x}\left[\left(\epsilon_{xx} - \epsilon_{yy}\right) 2\partial_\tau\epsilon_{xy} - \left(\varepsilon_{xy} + \varepsilon_{yx}\right)\left(\partial_\tau\varepsilon_{xx} - \partial_\tau\varepsilon_{yy}\right)\right]. \tag{3.9}$$

If we consider Eq.(3.5) with $\Gamma^+ = B_{1g}$, we can compare the coupling term with the first term in the equation above, in which we now see that altermagnetic fluctuations $\partial_t\phi$ play the role of $\eta^H\left(B_z\right)\partial_\tau\varepsilon_{xy}$. The fluctuating field from the altermagnetic order parameter suffices to induce a non-dissipative stress analogous to the Hall viscosity response, even in the absence of an external magnetic field.

Up until this point we have kept the discussion of the specific order parameter very general with the intention of showing how fundamental this coupling is, however to proceed we must

now decide on a specific altermagetic order parameter. We will initially focus on layered but three-dimensional systems. If we consider a tetragonal system, it transforms under the point group D_{4h} [169]. Given that our chosen magnetic order preserves lattice translations, it suffices to use the irreducible representations of the point group to describe the altermagnet [58]. As discussed in Chapter. 1, we have three choices of irreducible representation, we will proceed with an order parameter which transforms according to B_{1g} as was just used for the Hall viscosity. Modifying the calculation for another choice of symmetry is relatively straightforward. All of the states of altermagnetic order in D_{4h} can be described as a single component Ising order parameter, ϕ [209]. This is also the order parameter which has been proposed for MnF_2 [44, 196]. The coupling to strain is then

$$H_{\mathrm{c}}^{\mathrm{dyn}} = \frac{\lambda_0}{2} c^2 \int d^3\boldsymbol{x} \varepsilon_{B_{1g}}(\boldsymbol{x}) \pi(\boldsymbol{x}), \tag{3.10}$$

where $\varepsilon_{B_{1g}}(\boldsymbol{x}) = \varepsilon_{xx}(\boldsymbol{x}) - \varepsilon_{yy}(\boldsymbol{x})$.

3.3 The effects of coupling on the collective modes

Given that the coupling Eq. (3.5) focuses on the dynamics of the order parameter, naturally we prefer to look at the regime where quantum fluctuations are strong. Quantum fluctuations are at their strongest in the quantum critical regime. This is also the regime in which multipolar order can be described using a long-wavelength collective field theory. We will next introduce the theory of collective excitations for the case of $\lambda_0 = 0$, meaning the case where there is no coupling to strain. Following this we will then use $\lambda_0 \neq 0$ in order to analyse the problem using a renormalised Gaussian approach. We can justify this given that the upper critical dimension, $d_{\mathrm{uc}} = 3$. We then look beyond the Gaussian theory to include critical fluctuations and the logarithmic corrections these generate, with a one-loop RG approach.

3.3.1 Effective field theory for coupled collective modes

Initially we will summarise the collective field theory for multipolar order in the absence of coupling to the lattice. We consider an insulating system in the regime near the QCP, once again, this is the region where the order parameter dynamics are at their most important. This is described by an Ising order parameter with the action

$$\mathcal{S}_\phi = \frac{1}{2} \int_x \phi(x) \left(r_0 - c^{-2} \partial_\tau^2 - \nabla^2 \right) \phi(x) + u \int_x \phi(x)^4. \tag{3.11}$$

We use $x = (\mathbf{x}, \tau)$ to combine imaginary time and spatial coordinates and $\int_x \cdots = \int d^3\mathbf{x} d\tau \ldots$, r_0 is a parameter which tunes the system through the quantum critical point, it is the mass term for the altermagnons. c is the velocity of the altermagnons, it is of the order of the typical magnetic interaction J times the lattice constant. The coefficient u of the interaction term penalises large amplitude fluctuations and bounds the action.

For the case that the order parameter has two components, it is worth noting that the action looks slightly different, considering the E_g^- state of O_h (see also Ref. [58]), the action is then

$$\begin{aligned} S_\phi &= \frac{1}{2}\sum_{i=1,2}\int_x \phi_i(x)\left(r_0 - c^{-2}\partial_\tau^2 - \nabla^2\right)\phi_i(x) + u\int_x \left(\phi_1(x)^2+\phi_2(x)^2\right)^2 \\ &+ v\int_x \left(\phi_1(x)^2+\phi_2(x)^2\right)^3 + w\int_x \phi_1(x)^2\left(\phi_1(x)^2 - 3\phi_2(x)^2\right)^2. \end{aligned} \tag{3.12}$$

This corresponds to the six-state clock model. It has a six-fold degenerate ground state. Minimising the last term gives the relative amplitude between ϕ_1 and ϕ_2. In the rest of this section we will focus on the case of an Ising-like altermagnetic order parameter.

If we consider long wavelengths, we can use the longitudinal and transverse phonon modes to express the elastic action [19]

$$\mathcal{S}_\varepsilon = -\frac{1}{2}\sum_{\nu=L,T}\int_x u_\nu(x)\left(\partial_\tau^2 + v_\nu^2\nabla^2\right)u_\nu(x). \tag{3.13}$$

Here $\nu = L$ and T correspond to longitudinal and transverse phonons with displacement u_L and u_T and velocity v_L and v_T, respectively. The velocities depend upon the elastic constants of the system and, for the tetragonal crystal under consideration, on the polar angle θ of the momentum.

$$\begin{aligned} v_T^2 &= \frac{1}{4}(c_{11} - c_{12} + 2c_{44} \\ &+ (-c_{11} + c_{12} + 2c_{44})\cos(2\theta)), \\ v_L^2 &= \frac{1}{2}(c_{11} + c_{44} + (-c_{11} + c_{44})\cos(2\theta)), \end{aligned} \tag{3.14}$$

where we set $c_{13} = -c_{44}$ and $c_{66} = \frac{c_{11}-c_{12}}{2}$. For stability we require that $v_L > v_T$. Our choice of elastic constants decouples the other transverse mode present in a three-dimensional system, such that we only consider the in-plane modes crucial to the point group operations relevant to a B_{1g} order parameter. We therefore only consider the transverse mode which is predominantly polarised in-plane.

We can use the definition of the symmetrised elastic tensor, $\varepsilon_{ij} = \left(\partial_i u_j + \partial_j u_i\right)$ to rewrite the coupling in terms of the transverse and longitudinal modes. We can then Fourier transform to frequency and Matsubara frequency space to find

$$\mathcal{S}_{\mathrm{c}}^{\mathrm{dyn}} = \lambda_0\int_q \frac{\omega_n}{|\boldsymbol{q}|}\phi(q)\left[\left(q_x^2 - q_y^2\right)u_L(-q) - 2q_xq_yu_T(-q)\right]. \tag{3.15}$$

Here $\omega_n = 2\pi nT$ are Matsubara frequencies and $q = (\boldsymbol{q}, \omega_n)$. Once the coupling is written in this form, it becomes immediately clear that the coupling is anisotropic. Looking at the high symmetry directions, at $\mathbf{q} = (q_x, 0)$ or $\mathbf{q} = \left(0, q_y\right)$, we see that the transverse phonon completely decouples and only the longitudinal phonon continues to mix with the magnetic collective mode. Along the other high symmetry directions $\mathbf{q} = (q_x, \pm q_x)$, the longitudinal phonon completely decouples and only the transverse phonon mixes. An anisotropic coupling to elastic degrees of freedom signals further evidence of a method to detect altermagnetic states. Studying the phonon spectrum of a phonon of well-defined symmetry along different

directions should allow for identification of some trace of the magnon mode which vanishes along specific high symmetry directions. Doing so not only identifies that an altermagnetic collective mode is present but also allows for the classification of its symmetry.

3.3.2 Spectral functions and hybridised collective modes

In three dimensions and at zero temperature, the quartic interaction u in Eq. (3.11) is marginally irrelevant. As a result of this, one expects to find logarithmic divergencies which can be accounted for using a renormalisation group approach. We anticipate the result of this analysis and first consider an effective Gaussian theory with r_0 replaced by the renormalised mass r to account for the effects of the dynamic coupling on the elastic and altermagnetic modes. We consider a mean-field theory where

$$\phi^4 \to \phi^2 \left\langle \phi^2 \right\rangle \tag{3.16}$$

At $T = 0$ this renormalises the mass term such that

$$r = r_0 + u \int_{q,\omega_n} \chi\left(\mathbf{q}, \omega_n\right) \tag{3.17}$$

where we identify $\left\langle \phi^2 \right\rangle$ with the effective propagator χ for the altermagnons. At the quantum critical point $r = 0$ and the altermagnons are massless.

Carrying out this mean-field calculation allows us to to analyse the spectral properties by integrating out two degrees of freedom and calculating the propagator for the one remaining, without having to worry about the interaction term as it is now included in the renormalisation of r.

We initially calculate the altermagnetic propagator; in the absence of the dynamic coupling, we see that the collective modes are gapped altermagnons in the disordered phase (i.e. alter-paramagnons), with velocity c. Integrating out the two phonon modes and performing the analytic continuation to the real axis ($i\omega_n \to \omega + i0^+$), gives the Gaussian renormalised altermagnon propagator

$$\chi(\boldsymbol{q}, \omega) = \frac{1}{r + \boldsymbol{q}^2 - \frac{\omega^2}{c^2}\Delta(\boldsymbol{q}, \omega)}, \tag{3.18}$$

where

$$\Delta(\boldsymbol{q}, \omega) = 1 - \frac{c^2\lambda_0^2}{\boldsymbol{q}^2}\left(\frac{\left(q_x^2 - q_y^2\right)^2}{\omega^2 - v_L^2\boldsymbol{q}^2} + \frac{4q_x^2q_y^2}{\omega^2 - v_T^2\boldsymbol{q}^2}\right). \tag{3.19}$$

For the case $c > v_{L,T}$, the poles of the propagator are given in Fig. 3.2. In this we considered $q_z = 0$ such that $\theta = \frac{\pi}{2}$. This is the regime where electronic energy scales are larger than the lattice ones, this is the most common regime and the one we focus on, however for completeness the other is also discussed below.

We see that despite Fig. 3.2 being a plot of the poles of specifically the altermagnetic propagator, the modes which initially (i.e. at zero coupling) corresponding to phonons also appear. This is a direct result of the hybridisation of the modes which is promoted by the dynamic coupling. The modes are no longer independent once coupling is introduced but

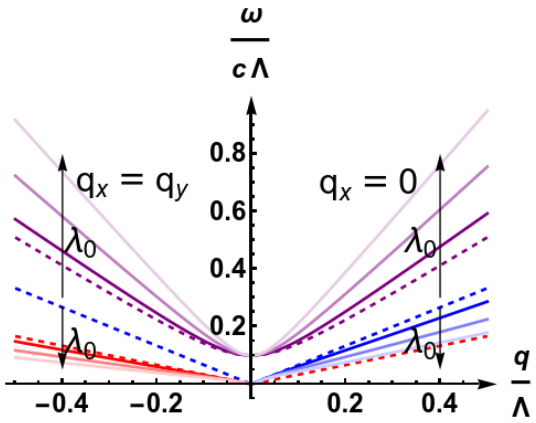

Figure 3.2: Altermagnon-like (purple), longitudinal phonon-like (blue), and transverse phonon-like (red) dispersions for momentum directions along high-symmetry lines in the $q_z = 0$ planes, plotted for different values of the coupling strength λ_0. The dispersions of the phonon-like and altermagnon-like modes are strongly influenced by the coupling. The dashed lines show the "pure" modes without coupling. The modes mix to a dynamic altermagnon-polaron at large coupling values, leading to a softening of the phonon-like modes for given directions and a hardening of the altermagnon-like mode. The modes are shown for $\lambda_0 = 0, 0.5, 1, 1.5$ with the shades getting progressively lighter with increased coupling constants. We set here $c/v_L = 3/2$ and $c/v_T = 3$. The altermagnon gap is given by $\sqrt{\frac{r}{\Lambda^2}} = 0.1$; Λ is a cutoff, as explained in the main text. (Figure reprinted from Ref. [20], Copyright American Physical Society (2023))

instead form new collective modes which, inspired by the nomenclature used in Ref. [130], we call paramagnon-polarons. We can now see from Fig. 3.2 how this hybridisation affects the modes. We see that the altermagnon-like mode is hardened with dynamic coupling, whereas the phonon-like modes are softened. We see again, as expected, that the effect of coupling is clearly anisotropic; only one phonon is softened along each high symmetry direction. At $q_x = 0$, plotted on the positive x-axis, we see that only the longitudinal phonon softens, whereas at $q_x = q_y$, only the transverse phonon softens. Away from the critical point, the altermagnon-like mode acquires a gap but at $r = 0$, three gapless modes emerge.

As previously mentioned, this result is valid for the case $c > v_{L,T}$. We can also plot the modes in the other regime, $c < v_{L,T}$, where we now find a level repulsion, as well as a greatly diminished softening of the phonon-like mode. We illustrate this regime in Fig. 3.3. This regime is applicable in systems with very low c, such that the magnetic interaction J is very small. While such a case is less common, we will make reference to both regimes, while focusing on the more common regime $c > v_{L,T}$.

Once we have obtained all three propagators χ, we are then able to calculate the spectral function for each by computing $\mathrm{Im}\chi$ in each case. We have for the transverse phonon propagator:

$$\chi_T(\boldsymbol{q}, \omega) = \frac{1}{\Delta_T(\boldsymbol{q}, \omega) - \zeta_T(\boldsymbol{q}, \omega)\,\omega^2 + v_T^2 \boldsymbol{q}^2}, \tag{3.20}$$

where χ_T is the propagator for the transverse phonon with renormalized coefficient

$$\zeta_T(\boldsymbol{q}, \omega) = 1 + \frac{\lambda_0^2}{\boldsymbol{q}^2} \frac{q_x^2 q_y^2}{r + \boldsymbol{q}^2 - \frac{\omega^2}{c^2}}, \tag{3.21}$$

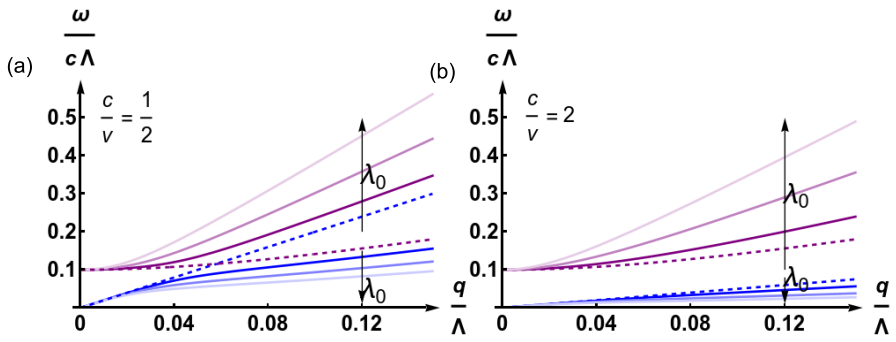

Figure 3.3: Dispersions of the altermagnon-like (purple) and longitudinal phonon-like (blue) mode for coupling constant values $\lambda = 0, 1, 2, 3$ along the $q_x = 0$ direction. The dashed lines show the uncoupled modes and the solid lines show the hybridized modes. Panel (a) refers to the case $c/v_L = \frac{1}{2}$, whereas panel (b) refers to $c/v_L = 2$. In panel (a), there is a level repulsion, whereas in panel (b), we see the modes softening. In both panels, the altermagnon gap is given by $\sqrt{\frac{r}{\Lambda^2}} = 0.1$. (Figure reprinted from Ref. [20], Copyright American Physical Society (2023))

of the dynamic term, while $\Delta_T(\boldsymbol{q}, \omega)$ corresponds to coupling of the two phonons away from both high symmetry directions

$$\Delta_T(\boldsymbol{q}, \omega) = \frac{\left(\frac{4\lambda_0^2 \omega^2 q_x q_y \left(q_x^2 - q_y^2\right)}{\boldsymbol{q}^2 \left(r + \boldsymbol{q}^2 - \frac{\omega^2}{c^2}\right)}\right)^2}{-\zeta_L(\boldsymbol{q}, \omega)\, \omega^2 + v_L^2 \boldsymbol{q}^2}, \tag{3.22}$$

with

$$\zeta_L(\boldsymbol{q}, \omega) = 1 + \frac{\lambda_0^2}{\boldsymbol{q}^2} \frac{\left(q_x^2 - q_y^2\right)^2}{r + \boldsymbol{q}^2 - \frac{\omega^2}{c^2}}. \tag{3.23}$$

For the longitudinal phonon propagator we have

$$\chi_L(\boldsymbol{q}, \omega) = \frac{1}{\Delta_L(\boldsymbol{q}, \omega) - \zeta_L(\boldsymbol{q}, \omega)\, \omega^2 + v_L^2 \boldsymbol{q}^2}, \tag{3.24}$$

where

$$\Delta_L(\boldsymbol{q}, \omega) = \frac{\left(\frac{4\lambda_0^2 \omega^2 q_x q_y \left(q_x^2 - q_y^2\right)}{\boldsymbol{q}^2 \left(r + \boldsymbol{q}^2 - \frac{\omega^2}{c^2}\right)}\right)^2}{-\zeta_T(\boldsymbol{q}, \omega)\, \omega^2 + v_T^2 \boldsymbol{q}^2}. \tag{3.25}$$

In real systems, the modes will have finite lifetimes which arise from damping or other processes; in order to model this, we add a small imaginary part to the frequency on the real axis. Fig. 3.4 shows a density plot of the spectral functions. This very much reinforces what we learned from Fig. 3.2, although perhaps now it is even clearer. For $q_x = \pm q_y$ the longitudinal phonon-like mode decouples and so for this spectral function there is no trace of the gapped altermagnon-like mode along this direction, however if we then look along $q_x = 0$, there is clearly a signal belonging to the altermagnon mode. Alternatively, looking at the

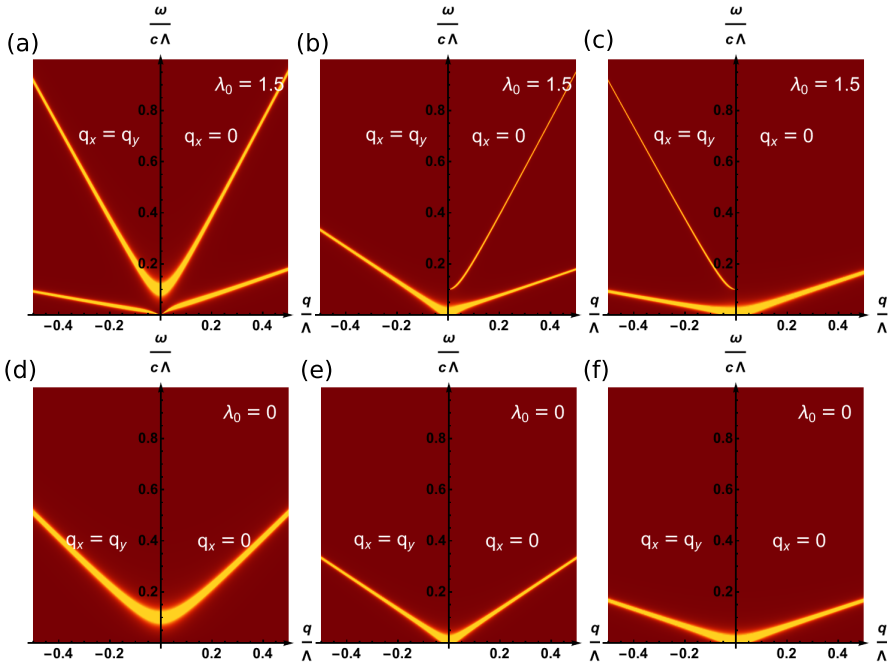

Figure 3.4: The spectral function for altermagnon (left panels), longitudinal phonon (middle panels) and transverse phonon (right panels) propagators as function of frequency ω and momentum $\mathbf{q}$ along two high-symmetry lines at the $q_z = 0$ plane. Panels (a-c) refer to a non-zero coupling constant value $\lambda_0 = 1.5$, whereas panels (d-f) correspond to $\lambda_0 = 0$. When coupled (a-c), the modes hybridize and it is possible to detect the altermagnon by measuring the phonon spectrum, except along the special directions for which the phonon mode decouples from the altermagnon. This mixing is most prominent close to the critical point where the $\mathbf{q} = \mathbf{0}$ altermagnon excitation energy is small. We have set here $c/v_L = \frac{3}{2}$ and $c/v_T = 3$. The altermagnon gap is given by $\sqrt{\frac{r}{\Lambda^2}} = 0.1$. (Figure reprinted from Ref. [20], Copyright American Physical Society (2023))

transverse phonon-like mode along $q_x = 0$, this mode decouples and there is no trace from the altermagnon-like mode, however along $q_x = q_y$ we see a gapped mode appear which is clearly the altermagnon-like mode. We can also see the same information repeated in the altermagnon propagator, along $q_x = 0$ a signal from the longitudinal phonon-like mode is present with no signal from the transverse phonon-like mode. Along $q_x = q_y$ we see the opposite, a signal from the transverse phonon mode with no signal from the longitudinal mode. In this case the individual phonon modes are identifiable from the condition $v_L > v_T$. In both cases we see a softening from the phonon-like mode which couples. We can see from these results that although measuring altermagnons represents a difficult task, measuring just the phonon spectrum is enough to access a signal from the altermagnon-like mode. This is true even at finite momentum and away from the quantum critical point. By measuring along high symmetry directions, this even suffices to determine the symmetry of the altermagnetic order parameter present in the system.

We illustrate this point even further by producing a density plot of the spectral weight for each branch of the altermagnon propagator determined by

$$\chi(\boldsymbol{q}, \omega) = \sum_i \frac{c^2 A_i(\boldsymbol{q})}{\omega^2 - E_i(\boldsymbol{q})^2}, \tag{3.26}$$

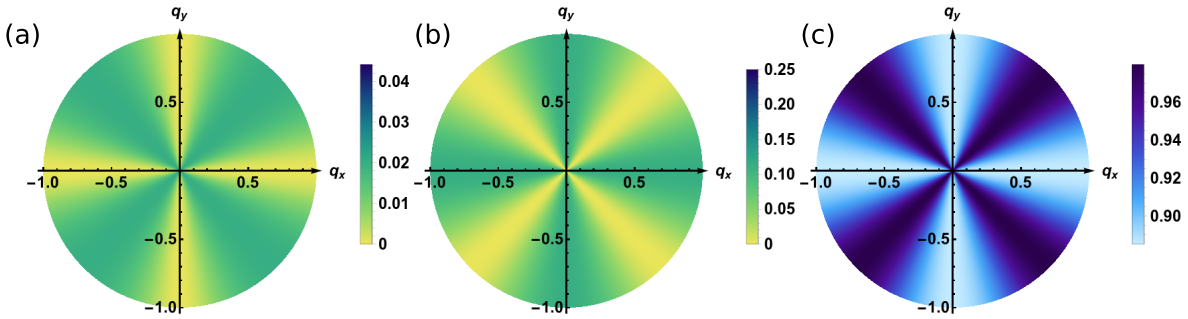

Figure 3.5: Anisotropic momentum dependence of the spectral weights of the transverse phonon-like (a), longitudinal phonon-like (b), and altermagnon-like (c) branches of the altermagnetic propagator for a non-zero coupling $\lambda_0 = 0.5$. The phonon-like modes decouple from the altermagnon-like one along high symmetry directions. These figures are plotted for $r = 0$, $c/v_L = \frac{3}{2}$ and $c/v_T = 3$. (Figure reprinted from Ref. [20], Copyright American Physical Society (2023))

where A_i is the weight of the branch and $E(\boldsymbol{q})$ is the energy of the mode. We see that the weight of the transverse phononlike branch drops to zero at $q_x = 0$ or $q_y = 0$. The weight of the longitudinal phonon propagator drops to zero at $q_x = \pm q_y$, while the weight of the altermagnon branch becomes four-fold anisotropic (although of course it never drops to zero).

Fig. 3.3 shows that if one of the phonon velocities is higher than the altermagnon velocity, we see a crossing of the two modes with a level repulsion introduced by the coupling, provided that one is not situated directly at the quantum critical point for the altermagnet. In the directions along which the phonons decouple ($q_x = \pm q_y$ for the longitudinal phonons and $q_{x,y} = 0$ for the transverse phonons), this gap disappears. This causes nodal lines of the gap to form. If we consider two modes

$$E_{\pm}^2 = \frac{1}{2}\left(\Delta^2 + \zeta_k k^2 \pm \sqrt{\left(\Delta^2 + \zeta_{\mathbf{k}} k^2\right)^2 - 4\eta^2 k^2\left(\Delta^2 + k^2\right)}\right), \tag{3.27}$$

with $\mathbf{k} = c\mathbf{q}$, $\Delta = c\sqrt{r}$, $\eta = \frac{v_L}{c}$ and $\eta_k = 1 + \eta^2 + \lambda_k^2$ where the coupling is k-dependent

$$\lambda_k = \lambda_0^2 \left(\frac{k_x^2 - k_y^2}{k^2}\right)^2. \tag{3.28}$$

We find a crossing point at

$$|\mathbf{k}| = k_0 = \frac{\Delta}{\sqrt{\eta^2 - 1}}. \tag{3.29}$$

We consider the energy splitting along the diagonal

$$\Omega(\mathbf{k}) = E_+(\mathbf{k}) - E_-(\mathbf{k}). \tag{3.30}$$

Along the diagonal such that $\lambda_k = 0$ we have

$$\Omega(\mathbf{k}) = \sqrt{\Delta^2 + k^2} - \eta k, \tag{3.31}$$

is approximately

$$\Omega\left(k, \varphi = \frac{\pi}{4}\right) \approx \frac{1-\eta^2}{\eta}\left(k - k_0\right). \tag{3.32}$$

We can also expand at this point along the ϕ direction and find that

$$\Omega\left(k_0, \varphi\right) \approx k_0\lambda_0\left|\cos 2\varphi\right| \approx 2k_0\lambda_0\left|\varphi - \frac{\pi}{4}\right|, \tag{3.33}$$

and so the magnitude of the in-plane component of the momentum at this nodal line is $\left|\boldsymbol{q}_{\parallel}\right| \sim \frac{r^{1/2}}{\sqrt{v_{L,T}^2/c^2-1}}$. Expanding the dispersion near these crossing points reveals a linear dispersion similar to the one of a Weyl system with vanishing gap. These lines are protected by the crystalline symmetry of the system, but may nevertheless have implications for surface states of the combined spectrum.

3.3.3 Coupled oscillator analogy of magnetoelastic coupling

The heart of this entire discussion is, of course, the coupling of the canonical momentum of one degree of freedom to the coordinate of another. Considering Gaussian theories, this immediately suggests an analogy to the case of two coupled oscillators, where the momentum of one is coupled to the displacement of another

$$H = \sum_{i=1,2}\left(\frac{p_i^2}{2m_i} + \frac{m_i\omega_i^2}{2}x_i^2\right) + \frac{\lambda}{2}p_1x_2, \tag{3.34}$$

where using the column $\psi = (x_1, x_2, p_1, p_2)$, the Hamiltonian becomes

$$H = \frac{1}{2}\psi^T\mathcal{H}\psi, \tag{3.35}$$

where

$$\mathcal{H} = \begin{pmatrix} m_1\omega_1^2 & 0 & 0 & 0 \\ 0 & m_2\omega_2^2 & \frac{\lambda}{2} & 0 \\ 0 & \frac{\lambda}{2} & \frac{1}{m_2} & 0 \\ 0 & 0 & 0 & \frac{1}{m_2} \end{pmatrix}. \tag{3.36}$$

We find, following the approach of Ref. [191] and Ref. [192] that this matrix diagonalises under the canonical (i.e. preserves commutation relations between ψ_i and ψ_j) symplectic transformation $\psi = \mathcal{S}\psi'$, such that $H = \frac{1}{2}\psi'^T\mathcal{S}^T\mathcal{H}\mathcal{S}\psi'$, where $\mathcal{S}^T\mathcal{H}\mathcal{S}$ is diagonal. $\mathcal{H}$ then diagonalises as

$$\mathcal{S}^T\mathcal{H}\mathcal{S} = \begin{pmatrix} \Omega_1^2 & 0 & 0 & 0 \\ 0 & \Omega_2^2 & 0 & 0 \\ 0 & 0 & 1 & 0 \\ 0 & 0 & 0 & 1 \end{pmatrix}, \tag{3.37}$$

where if $m_1 = m_2 = 1$

$$\Omega_{1,2}^2 = \frac{1}{2}\left(\omega_1^2 + \omega_2^2 \pm \sqrt{\left(\omega_1^2 - \omega_2^2\right)^2 + \lambda^2\omega_1^2}\right), \tag{3.38}$$

which yields $H = \frac{1}{2}\sum_\lambda \left(p_\lambda^2 + \Omega_\lambda^2 x_\lambda^2\right)$.

The symplectic transformation $(x_1, x_2, p_1, p_2) \to \mathcal{S}^{-1}(x_1, x_2, p_1, p_2)$ can also be phrased as a unitary transformation of the operators, such as $x_i \to U x_i U^{-1}$ where [191]

$$U = e^{i\left(ap_1p_2 + bx_1x_2\right)}. \tag{3.39}$$

Applied to the vacuum, such an operator creates two-modes squeezed states made by the two coupled oscillators. We hence see that the fluctuations of one degree of freedom suppress the other. This is in direct analogy with the hardening and softening of modes observed thus far.

3.3.4 Possible detection of modes in the ordered phase

Our analysis up to this point has focused on the disordered regime, however to make a connection with potential experiments, we must conduct an investigation which is valid in the ordered regime. It is already known how the correlation length of an Ising variable depends on the temperature [210]

$$r(T) = A\left(T - T_c\right)^{2\nu}, \quad T > T_c \tag{3.40}$$

$$= A'\left(T_c - T\right)^{2\nu}, \quad T < T_c \tag{3.41}$$

where in three dimensions $\nu = \frac{1}{2}$ and $A/A' = 4.75$ [210]. The now temperature dependent r can then be inserted into the polaron spectra which have already been calculated. In Fig. 3.6 we depict the temperature dependence of the transverse phonon-like polaron at fixed momentum; we see that this then leads to a change in the spectrum with respect to temperature and that the effect of a rising temperature now depends on whether the system is in the ordered or disordered state.

If we consider the case that phonons are excited through photon absorption and then relax back to their ground state, we can use the temperature profile

$$T(t) = T_{\text{eq}} + \Delta T e^{-t/\tau}, \tag{3.42}$$

where T_{eq} is the temperature in equilibrium, ΔT is the jump in temperature following the photoexcitation process and τ is the relaxation time as the temperature drops back to its equilibrium value. We then clearly see the temperature dependence of the phonon spectrum and how this relates to a relaxation time. An experiment to measure such an effect would only find results such as those displayed in Fig. 3.6 in the case that the phonons and altermagnon have hybridised. This is a result of the fact that $r(T)$ only appears in the uncoupled magnon mode. If the measurement is taken along a direction in which the two modes decouple, this effect would disappear as $r(T)$ would not be carried over from the magnon to the phonon mode. This then provides a method for detecting altermagnetic transitions and through angle

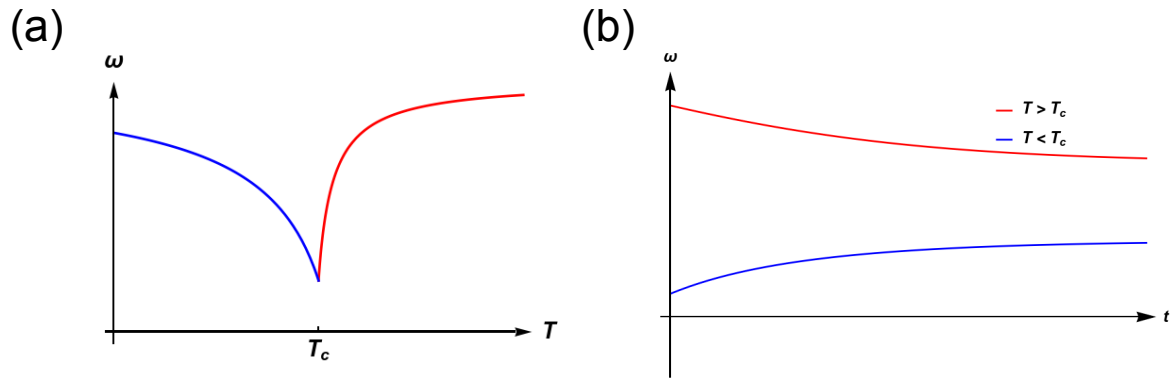

Figure 3.6: Using a temperature dependent r, we can see how the phonon-like polaron energy changes according to temperature (panel (a)). We can also consider the case in which the phonons are excited and the temperature then decays, we then clearly see how the phase transition affects the temperature trend that one would expect to measure (panel (b)).

dependent measurements, the symmetry of the altermagnet.

3.4 Effect of dynamic coupling to strain on the paramagnetic-altermagnetic phase boundary

Having already established that under dynamic coupling of altermagnetic and elastic degrees of freedom, the phonon and altermagnon modes are hybridised, leading to an anisotropic softening of the phonon modes and a hardening of the altermagnon mode, we now discuss how this effect manifests itself in the phase diagram. To determine the phase diagram, we carry out a one-loop renormalisation group (RG) calculation for the quartic coefficient u and mass term r. We first demonstrated this method using the standard ϕ^4 model (i.e. for the altermagnetic degrees of freedom in the absence of coupling) [57] in Sec. 1.3. By virtue of the fact that we can consider our order parameter as nothing more than a single component Ising order parameter, the analysis is similar with a modified propagator. We start from the coupled action. Perturbing the order parameter around the result of the Landau theory we find a set of flow equations for r and u

$$\begin{aligned}
\frac{dr}{dl} &= 2r + 3u\frac{d}{dl}\int_q^> \chi_0(q) - 3ur\frac{d}{dl}\int_q^> \chi_0(q)^2, \\
\frac{du}{dl} &= \epsilon u - 9u^2\frac{d}{dl}\int_q^> \chi_0(q)^2, \qquad (3.43) \\
\frac{dT}{dl} &= T. \qquad (3.44)
\end{aligned}$$

where $\epsilon = 3 - d$ and we use T to denote the running temperature, whereas the physical temperature corresponds to $T(l = 0)$. The altermagnon propagator (Eq. (3.18)) is expanded in r such that $\chi_0 = \chi|_{r=0}$. We integrated out the long wavelength modes leaving us with a set of shell integrals over $\Lambda e^{-l} < |\boldsymbol{q}| < \Lambda$, for some momentum cutoff Λ, with l a parameter used

to vary length-scales. We have employed no cutoff for the Matsubara frequencies, our results will not depend on this. In Chapter. 4, we will show that there are cases where one must also apply a cutoff for the Matsubara frequencies, for example when the elastic collective modes are damped. The sum does not converge due to a damping term linear in ω and a cutoff is required; here we encounter no such difficulty.

Before solving the RG equations, analysing the propagator for the altermagnon-like polaron already hints towards how the phase boundary will be altered by the coupling. The effective action is

$$S = \frac{1}{2}\int_q \phi\left(q\right)\chi^{-1}(q)\phi\left(-q\right) + u\int \phi\left(x\right)^4, \tag{3.45}$$

where χ is given is given in Eq. (3.18). By integrating out the phonons, we are able to consider a theory in just ϕ but with the effects from the phonons now included in a renormalisation of the propagator. Considering first $\omega \gg v_{T,L}\left|\boldsymbol{q}\right|$

$$\Delta(\boldsymbol{q},\omega) \approx 1 - c^2\lambda_0^2\frac{\boldsymbol{q}^2}{\omega^2}. \tag{3.46}$$

We see that the coupling renormalises the coefficient of q^2 in the altermagnetic propagator. Given that q^2 is proportional to the inverse squared correlation length, suppressing this term then suggests that spatial fluctuations are enhanced. This enhancement is of course mediated by the coupling λ_0. On the other hand, when $\omega \ll v_{L,T}\left|\boldsymbol{q}\right|$ we find

$$\Delta(\boldsymbol{q},\omega) \approx 1 + \frac{c^2\lambda_0^2}{v_T^2}, \qquad q_x = q_y, \tag{3.47}$$

$$\Delta(\boldsymbol{q},\omega) \approx 1 + \frac{c^2\lambda_0^2}{v_L^2}, \qquad q_x = 0. \tag{3.48}$$

In this regime, it is the altermagnon velocity c that is renormalized by the coupling, which suppresses quantum fluctuations. This also mirrors the already observed hardening and softening of the magnon and phonon-like spectra respectively. We now expect, given the role fluctuations play in the phase diagram, to see this behaviour represented in the RG calculation.

We aim to create a phase diagram for finite temperatures, to do so we implement the crossover method [124] already outlined for the generic ϕ^4 theory in Sec. 1.3. The key point of contrast between the two cases is that now our propagator is anisotropic and so we have angular variables to integrate over in order to average over these effects. The shell equations then become

$$\frac{d}{dl}\int_q^> \chi_0^m\left(q\right) = \frac{d}{dl}\int_{\Lambda e^{-l}<\left|\boldsymbol{q}\right|<\Lambda}\frac{d^3q}{\left(2\pi\right)^3}T\sum_{n=-\infty}^{\infty}\chi_0^m\left(q\right) \tag{3.49}$$

$$= \frac{\Lambda^3}{\left(2\pi\right)^3}T\sum_{n=-\infty}^{\infty}\int_0^{2\pi}\int_0^{\pi}d\theta d\phi\sin\left(\theta\right)\chi_0^m\left(\Lambda\right), \tag{3.50}$$

where we suppress the dependency of χ_0 on ω_n, ϕ and θ. The flow equations at one-loop level

are then

$$\begin{aligned}\frac{dm}{dl} &= 2m + g\Lambda c F_1(T) - gmc^3\Lambda^3 F_2(T),\\ \frac{dg}{dl} &= \epsilon g - 3g^2\Lambda^3 c^3 F_2(T),\\ \frac{dT}{dl} &= T,\end{aligned} \tag{3.51}$$

where $\epsilon = 3 - d$ and we defined the dimensionless quantities

$$m = \frac{r}{\Lambda^2}, \quad g = \frac{3uc\Lambda^{d-3}}{(2\pi)^d}, \tag{3.52}$$

and

$$F_m(T) = T\sum_{n=-\infty}^{\infty}\int_0^{2\pi}\int_0^{\pi} d\theta d\phi \sin(\theta)\,\chi_0^m\left(\Lambda, \omega_n, \theta, \phi\right). \tag{3.53}$$

A quantum critical point occurs when the transition temperature T_c is suppressed to zero, hence we can solve the flow equations in the limit $T \to 0$. Calculating the point at which m and g stop scaling gives the unstable Gaussian fixed point $(0,0)$ and the relevant fixed point

$$\left(m^*, g^*\right) = \left(-\frac{1}{6}\epsilon\frac{F_1(0)}{F_2(0)\,c^2\Lambda^2}, \frac{\epsilon}{3\Lambda^3 c^3 F_2(0)}\right), \tag{3.54}$$

to first order in ϵ. This implies $m_0^c = -bg_0$ where

$$b = \frac{c\Lambda}{2}F_1(0). \tag{3.55}$$

This allows us to define a distance, t, from the critical point [211]

$$t = m + \frac{c\Lambda}{2}F_1(0)\,g. \tag{3.56}$$

We plot the phase diagram in both two and three dimensions in Fig. 3.7 for $c > v$ and for $c < v$ in two dimensions in Fig. 3.8, the parametrisations of the phonon frequencies, for the case $c > v_{L,T}$, that we use throughout this section are given by

$$\begin{aligned}\frac{v_T(\theta)}{c} &= \frac{1}{6}\sqrt{\frac{9}{2} + \frac{7}{2}\cos 2\theta},\\ \frac{v_L(\theta)}{c} &= \frac{1}{3}\sqrt{\frac{3}{2} + \frac{1}{2}\cos 2\theta}.\end{aligned} \tag{3.57}$$

As for the case $c < v_{L,T}$, we considered the following parametrization:

$$\begin{aligned}\frac{v_T(\theta)}{c} &= \frac{1}{6}\sqrt{450 + 350\cos 2\theta},\\ \frac{v_L(\theta)}{c} &= \frac{1}{3}\sqrt{150 + 50\cos 2\theta}.\end{aligned} \tag{3.58}$$

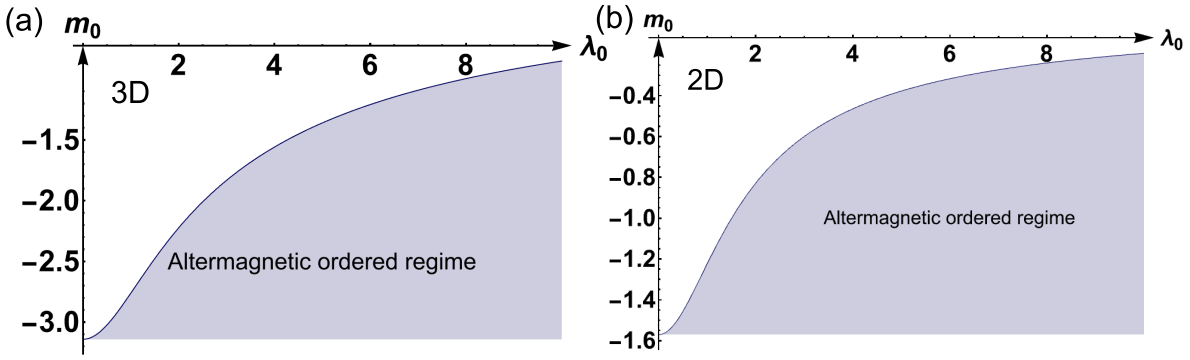

Figure 3.7: Ground-state (i.e. $T = 0$) phase diagram of altermagnetic order as a function of the control parameter $m_0 = r_0/\Lambda^2$ and the coupling constant λ_0 with $c > v_{L,T}$, Eq. (3.57) for the cases (a) 2D and (b) 3D. We see that at zero temperature, the formation of a dynamic altermagnon-polaron expands the ordered state (shaded region), since the altermagnetic transition occurs for higher values of m_0. (Figure reprinted from Ref. [20], Copyright American Physical Society (2023))

We see that in all cases at $T = 0$ the ordered regime is increased upon increasing the dynamic coupling λ_0. The coupling reinforcing long range altermagnetic order is entirely consistent with the results obtained above. We found from an analysis of the propagator that the renormalisation of c suppresses quantum fluctuations and hence a smaller $|m_0|$ is necessary to transition from the disordered paramagnetic state to the altermagnetically ordered state.

We can also solve the flow equations for the case that T is small but still finite, in this case we can employ a crossover calculation, with the method outlined in Ref. [124]. This crossover regime is relevant when $g_0 = g(l = 0) \ll 1$ and $T \ll c\Lambda$. In this regime, to first-order in g_0, it is sufficient to simply use the $T = 0$ solution for $g\left(l\right)$ [124]

$$g\left(l\right) = \frac{g_0}{1 + 3c^3\Lambda^3 F_2\left(0\right) g_0 l}. \tag{3.59}$$

As in the generic case, thermal fluctuations only enter at $\mathcal{O}\left(g_0^2\right)$. To solve for m we consider the ansatz

$$m = m_0 e^{\xi\left(l\right)} h\left(l\right). \tag{3.60}$$

This ansatz solves our flow equations when

$$\begin{aligned} \xi\left(l\right) &= 2l - \Lambda^3 c^3 \int_0^l g\left(l'\right) F_2\left(l'\right) dl', \\ h\left(l\right) &= 1 + \frac{\Lambda c}{m_0} \int_0^l e^{-\xi\left(l'\right)} F_1\left(l'\right) g\left(l'\right) dl'. \end{aligned} \tag{3.61}$$

Substituting these expressions into the flow equation for m and integrating by parts, we can find a transcendental equation for T_c to first order in g_0. At the critical point we can, by

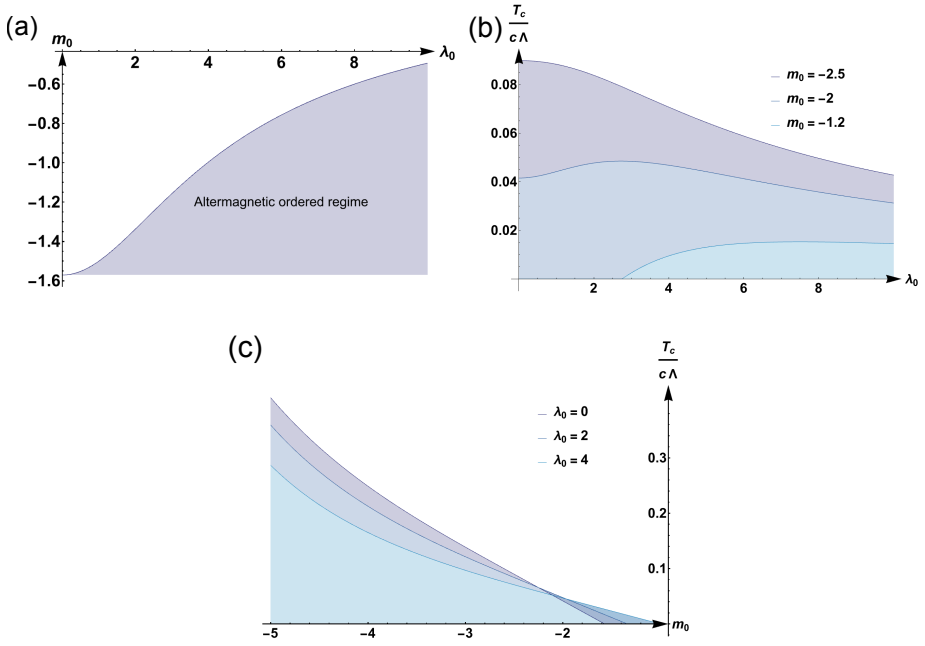

Figure 3.8: (a) Ground state phase diagram for a 2D system. (b) Altermagnetic transition temperature T_c as a function of the dynamic strain coupling constant λ_0 for different values of the bare altermagnon mass $m_0 = r_0/\Lambda^2$. (c) Altermagnetic T_c as a function of m_0 for different values of λ_0. These plots correspond to the case of a 2D system with $c < v_{L,T}$, Eq. (3.58). Compared with Fig.3.1, which refers to the case $c > v_{L,T}$, the dynamic coupling to phonons has a weakened impact in the thermal regime, but still a significant impact in the quantum regime. The former is the result of a lack of softened phonons, whereas the latter is a consequence of the hardened altermagnon. (Figure reprinted from Ref. [20], Copyright American Physical Society (2023))

definition, scale infinitely and so $l \to \infty$. This gives the expression for T_c

$$m_0^c + \frac{\Lambda c g_0}{2}\int_0^{2\pi}\int_0^{\pi} d\theta d\phi \sin(\theta)\sum_{i=1}^{3}\frac{A_i}{2E_i} + g_0\Lambda c T_c^2\int_0^{\pi}\int_0^{2\pi} d\phi d\theta \sin(\theta)\sum_{i=1}^{3}A_i\left(\frac{\pi^2}{6E_i^3} + \frac{1}{E_i^2 T_c}\log\left(1-e^{-\frac{E_i}{T_c}}\right) - \frac{1}{E_i^3}\mathrm{Li}_2\left(e^{-\frac{E_i}{T_c}}\right)\right) = 0, \tag{3.62}$$

where E_i is the energy for each mode and A_i the corresponding weight for the three branches.

This is the calculation in three dimensions, however we can also carry out the calculation in two dimensions. To do so we use an epsilon expansion with $\epsilon = 3 - d = 1$ (we also use such an expansion in Chapter. 4 and so a more detailed explanation can be found there). This calculation is very similar to the three dimensional case taken at $\theta = \frac{\pi}{2}$ and the only angular integration being over ϕ. The motivation for doing this calculation in two dimensions in addition to three is the existence of two dimensional altermagnetic candidates [196] such as the quasi-2D oxide insulator V_2Se_2O [159] and semimetal Cr_2O [212].

The equation for T_c is not solvable analytically, we therefore result to numerical methods.

We plot the phase diagrams for $c > v_{L,T}$ (using Eq. (3.57)) in both two and three dimensions in Fig. 3.1. We see that in two dimensions, in general, increasing the coupling to phonons suppresses the transition temperature. This is consistent with the above results, including in Fig. 3.2, where we see the coupling increases the population of soft phonons, which in turn suppresses order in the system through thermal fluctuations. At $T = 0$, this is not the dominant effect as no phonon modes are occupied at zero temperature. In this case, the suppressed quantum fluctuations are the dominant effect and order is reinforced in all cases considered here. We can compare Fig. 3.7 and Fig. 3.1 to see that for a given value of λ_0, unless the value of m_0 puts the system in the ordered regime at $T = 0$, the transition does not occur. Increasing λ_0 increases the magnitude of m_0^c and at the point $m_0 < m_0^c(\lambda_0)$, a transition can occur; this heavily implies that while the coupling does suppress order at finite temperatures, it also induces transitions. After this point the initial rise in the transition temperature is most likely due to being in the regime where the dominant effect is the quantum one. In three dimensions, the behaviour at $T = 0$ remains qualitatively identical but at finite temperature the results differ. Increasing the coupling leads to a slight increase in the transition temperature as thermal fluctuations are less relevant, leaving quantum fluctuations as the dominant effect. One could expect there to be a high enough temperature such that we cross over into a regime where the thermal fluctuations are again relevant, however the transition temperature begins to plateau. The reason for this is that once the system is at a high enough temperature it reaches the classical regime, this is equivalent to taking the zeroth Matsubara frequency. The coupling to phonons is proportional to the Matsubara frequency and so in this regime there is no coupling to phonons, leaving little to no effect on T_c. These results are all for the case $c > v_{L,T}$, we consider the other regime in Fig. 3.8. In this case we see that the suppression of the transition temperature is somewhat diminished, this is a result of the very minor phonon softening shown in Fig. 3.3. We only considered this in two dimensions as this is where the thermal fluctuations are interesting and the level repulsion shows these fluctuations to be the major point of contrast with the $c > v_{L,T}$ case.

3.5 Conclusion and discussion

In summary, we showed that it is possible, just through symmetry considerations, to construct a term in the action which constitutes a dynamic coupling between strain and fluctuations of a magnetic multipolar order parameter. These results are applicable for the case of altermagnetic systems in which the magnetisation order parameter can be described as having d-wave, g-wave, and i-wave symmetries. These are order parameters which, by symmetry, have a net zero dipole moment and are therefore purely multipolar states of order. We chose to focus on a B_{1g} order parameter within a system described by a D_{4h} point group (relevant for instance for the altermagnet candidate MnF_2) but this does not suggest that these results are not applicable more generally, we have also commented on crystals in the O_h point group. We show that a dynamic coupling allows the possibility to probe altermagnons directly through the phonon spectrum. This significantly reduces the difficulty that one would otherwise face in measuring these states with a zero net-magnetisation through the magnetic spectrum.

This coupling corresponds to an internal, fluctuation-induced non-dissipative response. This induces a stress σ_{ij} induced by a time-varying strain in the presence of the collective mode. This is analogous to the case where a strain occurs due to a finite Hall viscosity. The coupling

induces the creation of altermagnon-polarons, the phonon and magnetic collective modes hybridise, softening the former and hardening the latter. This has a significant effect on the strength of fluctuations and, by extension, the phase boundary between the disordered paramagnetic phase and the altermagnetically ordered phase. In two and three dimensions at $T = 0$, the suppression of quantum fluctuations reinforces order and increases the altermagnetic regime. In three dimensions at finite temperatures, the effect is the same, order is reinforced and the transition temperature, T_c rises. The reason for this is that thermal fluctuations are not the dominant force deciding when the system transitions. In two dimensions, thermal fluctuations are stronger and we see that increasing the coupling leads to a high occupation of soft phonons which suppress order. This effect diminishes for the case $v_{L,T} > c$. The results in two dimensions are not only relevant for certain quasi-2D systems but also for highly anisotropic three dimensional systems.

This chapter focused on altermagnets, however there is no reason for the coupling discussed here not to be applicable to ferromagnetic systems, in very much the same way as the piezomagnetic coupling considered in Chapter. 2. The condition for dynamic coupling is that the magnetisation order parameter and at least one of the strain components transform according to the same irreducible representation of the point group, with the magnetic degree of freedom being odd under time-reversal and the strain degree of freedom being even. In tetragonal (D_{4h}) and hexagonal (D_{6h}) systems, the in-plane moments (E_g and E_{1g} respectively) can couple to the out of plane shear strain doublet $\left(\varepsilon_{xz}, \varepsilon_{yz}\right)$ as this transforms according to the corresponding in-plane magnetic degrees of freedom. Additionally, in D_{2h} each component of the magnetisation transforms as one of the one-dimensional irreducible representations B_{ig}^{-} with $i = 1, 2, 3$ with the shear strains ε_{xy}, ε_{xz}, and ε_{yz} transforming the same way. This also holds for the orthorhombic point groups D_2 and C_{2v}. The effects discussed in this chapter hence hold for any orthorhombic ferromagnet. A promising family of materials to search for this effect are the ferromagnetic Mott insulating perovskites $A\mathrm{TiO}_3$, with appropriate rare-earth A [213]. We will next consider one of the ferromagnetic cases, although not one mentioned in this section. We will investigate the effect of dynamic coupling on an almost purely orbital ferromagnet in twisted bilayer graphene which couples to a damped collective mode.

Chapter 4

4 Orbital ferromagnetism-twist phason coupling in TBG

In twisted bilayer graphene the two layers combine to form a moiré pattern, an incommensurate superlattice. This creates an additional degree of freedom in the elastic theory, in addition to those degrees of freedom contained in commensurate lattices. This degree of freedom is a fluctuation of the relative twist angle between the two graphene layers, the collective mode of which is a damped phason due to no associated conservation law. In TBG the twist angle has a profound effect on the electronic structure of the material, leading to flat bands at the so-called magic angle [31]. When this occurs, the flat bands imply that the energy of electrons is dominated by interactions, making this an important material for the study of strongly correlated systems. Strong correlations can lead to the emergence of an orbital ferromagnetic state, which through a group theoretic analysis can be shown to couple to the twist-angle fluctuations, in analogy with the coupling of altermagnetic fluctuations and a symmetry breaking strain. One would expect that given the nature of the effect of the twist angle on electronic structure, that the twist degrees of freedom strongly couple to ferromagnetism. Here we show that, as for a 2D altermagnet, a dynamic magnetoelastic coupling suppresses the ordered regime at finite temperatures and reinforces it at zero temperature. One must however, also consider the phason damping, which we show suppresses order in both regimes. This section is based on and in some cases directly quotes from Ref. [21].

4.1 Introduction

To briefly reiterate elements discussed in Sec. 1.2, at a relative twist angle of $\theta \approx 1.05°$, flat bands emerge [31, 79], giving the electrons an infinite effective mass and hence highly localised orbitals. The kinetic energy of these states is reduced to such a degree that electron-electron interactions dominate over the kinetic energy. This leads to the emergence of a catalogue of strongly correlated effects [10] (see Sec. 1.2), including the focus of this chapter, orbital ferromagnetism.

Partially aligning twisted bilayer graphene with hexagonal boron-nitride at 3/4 reveals an anomalous Hall effect [10, 23, 24], detected experimentally through a large magnetic hysteresis [23, 84] and chiral edge conduction [23]. This anomalous Hall effect is reliant on a spontaneous time-reversal symmetry breaking as a result of ordering of the orbital magnetic

moments, which form due to an imbalance of the p_+ and p_- orbital occupation numbers of states localised on the superlattice points. This AHE hence acts as a clear indicator of time-reversal symmetry breaking, which when coupled with a low spin-orbit coupling [10] and the nontrivial topology of the flat bands, suggests that this symmetry breaking is due to orbital ordering [85]. This ferromagnetic ordering has itself been observed using SQUID's to measure stray fields [12].

It has been shown that only a small current is necessary in order for the magnetisation to switch direction, this is due to a large magnetoelectric effect which suggests that much like altermagnets, these systems could be used in the construction of low-power memory devices [4].

While we have so far only discussed the effect of the magic-angle on the electronic bands, this twist angle will neither be static, nor homogeneous in an experimental situation where slight variations in the precise value are commonplace. It is therefore to be expected that dynamic fluctuations of this twist angle are a low-energy degree of freedom which impact the moiré structure [29, 214, 215]. These are phason modes which correspond to acoustic branches of the incommensurate lattice and dominate lattice vibrations on the scale of the moiré period. If one were to ignore the structural relaxation of the lattice these modes are directly related to the relative displacement of the two layers [29]. If the displacement field describing the relative motion of carbon atoms in the two layers is denoted $\mathbf{u}(\mathbf{r}, \tau)$ then if we consider an antisymmetric counterpart to the elasticity tensor in commensurate systems

$$\Omega_{\alpha\beta} = \frac{1}{2}\left(\partial_\alpha u_\beta - \partial_\beta u_\alpha\right), \tag{4.1}$$

$\Omega \equiv \Omega_{xy}$ describes the rotation of the two layers with respect to one another. The source of finite stiffness for Ω is the adhesion potential between the two layers. These collective modes are clearly unrelated to any conservation laws of the system and are therefore subjected to damping introduced via anharmonic terms in the adhesion potential [22].

It is clear from the nature of the impact that the twist angle has on the system that one should expect a strong coupling to electronic excitations. A crucial aspect of this for our purposes is the two component spinor structure in orbital space which characterises either a positive or negative chirality. We will show in this chapter that a dynamic coupling between the two degrees of freedom is symmetry, allowed such that twist fluctuations induce fluctuations in orbital Ising-type ferromagnetism. We will also show that the damping present in the phason modes then causes damping in the magnetic collective modes, which in turn affects the phase boundary between the ferromagnetically ordered and paramagnetic disordered states.

4.2 Field theory of dynamic magnetoelastic coupling

We construct an order parameter along the same lines as was carried out in the altermagnet chapters, i.e.

$$\phi(\mathbf{r}) = \frac{1}{2} c^\dagger \sigma_z c(\mathbf{r}), \tag{4.2}$$

where the Pauli matrix now acts in orbital space. This order parameter calculates the difference in occupation number of the $p_+ = p_x + ip_y$ and $p_- = p_x - ip_y$ orbitals. When an imbalance occurs, this is manifested physically through a finite magnetic moment. Note that

this is now clearly a magnetic dipole, due to a lack of form factor transforming under a non-trivial irreducible representation.

Given the orbital structure we consider here, the order parameter is a ferromagnet with the dipole moment aligned along the z-axis, it therefore transforms according to the A_2 irreducible representation in D_6 [29]. We know that the ferromagnet aligned along z must also transform like a rotation around the z-axis, it is therefore plain to see that we can construct a coupling term for fluctuations of the orbital ferromagnetism and the twist angle, with the same structure as for an altermagnetic order parameter coupled to symmetry breaking strain of the same irreducible representation

$$H_{\text{orb-latt}} = \frac{\lambda_0}{2} c^2 \int d\mathbf{r} d\tau \Omega\left(\mathbf{r}, \tau\right) \pi\left(\mathbf{r}, \tau\right), \tag{4.3}$$

where, as before, c is the velocity of the magnon associated with the orbital magnetism, τ is imaginary time, λ_0 is a dimensionless coupling constant and π is the conjugate momentum to the order parameter, such that $\left[\phi\left(\mathbf{r}\right), \pi\left(\mathbf{r}'\right)\right] = i\hbar\delta\left(\mathbf{r} - \mathbf{r}'\right)$. Expressed in the language of an action, this becomes

$$S_{\text{orb-latt}} = \frac{\lambda_0}{2} \int d\mathbf{r} d\tau \Omega\left(\mathbf{r}, \tau\right) \partial_\tau \phi\left(\mathbf{r}, \tau\right). \tag{4.4}$$

If we convert the equation for the twist fluctuations to momentum space, we can then see that it is related to transverse displacements via

$$\Omega\left(\mathbf{q}\right) = \frac{1}{2} \left|\mathbf{q}\right| u_T\left(\mathbf{q}\right). \tag{4.5}$$

With this, the coupling is then

$$S_{\text{orb-latt}} = \lambda\left(\mathbf{q}\right) \int_q u_T\left(\mathbf{q}\right) \phi\left(-\mathbf{q}\right), \tag{4.6}$$

with the coupling, which is now non-local in both space and time

$$\lambda\left(\mathbf{q}, \omega_n\right) = \frac{\lambda_0}{2} \omega_n \left|\mathbf{q}\right|. \tag{4.7}$$

For the sake of brevity, we have used the notation $q = \left(\mathbf{q}, \omega_n\right)$.

Due to the strong electron-electron correlations in magic-angle TBG, it has been reported that the system undergoes a transition to a Mott insulating state (see Sec. 1.3) at 3/4 filling, i.e. under the same conditions needed for the QAHE to materialise [216]. Analysing a model which represents an insulating state, close to the critical point, yields the regime where the dynamics of the order parameter are most important, with the action

$$S_\phi = \frac{1}{2} \int d\mathbf{r} d\tau \left(r_0 - \nabla^2 - c^{-2}\partial_\tau^2\right) \phi\left(\mathbf{r}\right)^2 + u \int d\mathbf{r} d\tau \phi\left(\mathbf{r}\right)^4, \tag{4.8}$$

i.e. the Ising-type action for insulating systems.

The twist fluctuations can be split in two parts, the aforementioned phason modes and

spatially homogeneous twists

$$\widetilde{\varepsilon}_{\alpha\beta}\left(\boldsymbol{r},\tau\right)=\varepsilon_{\alpha\beta}^{0}\left(\tau\right)+\epsilon_{\alpha\beta}\Omega^{0}\left(\tau\right)+\int_{\mathbf{q}}iq_{\alpha}u_{\beta}\left(\boldsymbol{r},\tau\right)e^{i\boldsymbol{q}\cdot\boldsymbol{r}}, \tag{4.9}$$

where $\tilde{\varepsilon}_{\alpha\beta}=\partial_{\alpha}u_{\beta}$, i.e. the non-symmetrised strain, $\varepsilon_{\alpha\beta}^{0}$ is the homogeneous symmetrised strain and $\epsilon_{\alpha\beta}$ is the Levi-Civita tensor. We can then discuss the role of uniform displacement fields $u_{\beta}^{(0)}\left(\boldsymbol{r},\tau\right)=\left(\varepsilon_{\beta\gamma}^{0}-\Omega^{0}\epsilon_{\beta\gamma}\right)x_{\gamma}$, where x_{γ} denotes spacial coordinates. We can insert this into the lattice kinetic energy $S_{\text{kin}}^{(0)}=\int d^{2}rd\tau\sum_{\beta}\left(\frac{\partial u_{\beta}^{(0)}\left(\boldsymbol{r},\tau\right)}{\partial\tau}\right)^{2}$. The homogeneous twist contribution for a region of size L is given by

$$S_{\text{kin}}^{(0)}\sim\frac{\pi}{2}L^{4}\int d\tau\left(\frac{\partial\Omega^{0}\left(\tau\right)}{\partial\tau}\right)^{2}. \tag{4.10}$$

We then see that for a macroscopic, clean system, this term is penalised by the L^4 coefficient and the dynamics of the $\mathbf{q}=\mathbf{0}$ component are suppressed, i.e. $\Omega^{0}\left(\omega_{n}\right)\propto\delta_{n,0}$. Given that the coupling $\lambda\left(q\right)\propto\omega_{n}$, it is clear that homogeneous twists do not impact the orbital moment dynamics. We would expect these terms to be relevant in finite systems, for example in the presence of disorder.

For a generic twist angle, the lattice is incommensurate, leading to the emergence of phason modes which in the limit of small lattice relaxation can be rationalised as a twist fluctuation [22]. The incommensurate nature of the lattice allows a term in the action

$$S_{\Omega}=\frac{K}{2}\int_{\mathbf{r},\omega_{n}}\Omega\left(\mathbf{r},\omega_{n}\right)\Omega\left(\mathbf{r},-\omega_{n}\right), \tag{4.11}$$

which would otherwise vanish by rotation symmetry. Here K is a finite rotational stiffness which follows as a consequence of the adhesion potential between the two layers [29]. For the field theory related to symmetrised strain, we consider the usual action [217], with the addition of a damping term

$$S_{\text{latt}}^{(\text{sym})}\left[\boldsymbol{u}\right]=\frac{1}{2}\int_{\boldsymbol{r},\omega}\left(-\omega^{2}\left|\boldsymbol{u}\left(\boldsymbol{r},\omega\right)\right|^{2}-i\gamma_{0}\omega\left|\boldsymbol{u}\left(\boldsymbol{r},\omega\right)\right|^{2}+C_{ijkl}\varepsilon_{ij}\left(\boldsymbol{r},\omega\right)\varepsilon_{kl}\left(\boldsymbol{r},-\omega\right)\right), \tag{4.12}$$

where $\varepsilon_{ij}=\frac{1}{2}\left(\partial_{i}u_{j}+\partial_{j}u_{i}\right)$ with

$$C_{ijkl}\varepsilon_{ij}\varepsilon_{kl}=C_{11}\left(\varepsilon_{xx}^{2}+\varepsilon_{yy}^{2}\right)+2C_{12}\varepsilon_{xx}\varepsilon_{yy}+2\left(C_{11}-C_{12}\right)\varepsilon_{xy}^{2}, \tag{4.13}$$

where we have suppressed the space and Matsubara frequency dependency. $S_{\text{latt}}^{(\text{sym})}$ is hence characterised by two distinct elastic constants. We can convert this to the imaginary axis via a Kramers-Kronig transformation

$$f\left(i\omega\right)=-\int_{-\infty}^{\infty}\frac{d\epsilon}{\pi}\frac{\text{Im}\left(f\left(\epsilon\right)\right)}{-\epsilon+i\omega}. \tag{4.14}$$

When carried out on the action above, this yields

$$S_{\text{latt}}^{(\text{sym})}[\boldsymbol{u}] = \frac{1}{2}\int_{\boldsymbol{r},\omega_n}\left(\omega_n^2\left|\boldsymbol{u}\left(\boldsymbol{r},\omega_n\right)\right|^2 + \gamma\left|\omega_n\right|\left|\boldsymbol{u}\left(\boldsymbol{r},\omega_n\right)\right|^2 + C_{ijkl}\varepsilon_{ij}\left(\boldsymbol{r},\omega_n\right)\varepsilon_{kl}\left(\boldsymbol{r},-\omega_n\right)\right), \tag{4.15}$$

Following a transformation to momentum space, the combined lattice action arising from symmetric and antisymmetric elasticity is then

$$S_{\text{latt}} = \frac{1}{2}\int_q\left(\left(\omega_n^2 + \gamma_0\left|\omega_n\right|\right)\boldsymbol{u}_q\cdot\boldsymbol{u}_{-q} + \boldsymbol{u}_q\cdot\hat{D}\left(\mathbf{q}\right)\cdot\boldsymbol{u}_{-q}\right), \tag{4.16}$$

on the imaginary axis, with dynamic matrix

$$\hat{D}\left(\mathbf{q}\right) = \begin{pmatrix} C_{11}q_x^2 + \tilde{C}q_y^2 & \delta C q_x q_y \\ \delta C q_x q_y & C_{11}q_y^2 + \tilde{C}q_x^2 \end{pmatrix}. \tag{4.17}$$

Here we used $\tilde{C} = \frac{1}{2}\left(C_{11} - C_{12} + \frac{1}{2}K\right)$ and $\delta C = \frac{1}{2}\left(C_{11} + C_{12} - \frac{1}{2}K\right)$. The resulting eigenmodes are longitudinal with $\boldsymbol{e}_{L\boldsymbol{q}} = \hat{\boldsymbol{q}}$ and transverse, $\boldsymbol{e}_{T\boldsymbol{q}} = \hat{\boldsymbol{z}}\times\hat{\boldsymbol{q}}$, with frequencies $\omega_{\mathbf{q},\mu} = v_\mu q$, where $\mu = L,T$, $v_L = \sqrt{C_{11}}$ and $v_T = \sqrt{\frac{C_{11}-C_{12}+\frac{1}{2}K}{2}}$. One of the implications of the twist fluctuation's finite rotational stiffness is the fact that the transverse velocity can become larger than the longitudinal velocity: $v_T > v_L$. Expanding the displacement in terms of the longitudinal and transverse modes, $\boldsymbol{u}_{\mathbf{q}} = -i\sum_{\mu=L,T}\mathbf{e}_{\mathbf{q}\mu}u_{\mathbf{q}\mu}$, it follows

$$S_{\text{latt}} = \frac{1}{2}\sum_{\mu=L,T}\int_q\left(\omega_n^2 + \gamma\left|\omega_n\right| + v_\mu^2 q^2\right)u_{\mathbf{q}\mu}u_{-\mathbf{q}\mu}. \tag{4.18}$$

We see that the longitudinal phonons decouple and can be integrated out.

The relevant field theory for coupled phason-orbital magnon modes is therefore

$$\begin{aligned} S\left[\phi,u_T\right] &= \frac{1}{2}\int_q\left(r_0 + \boldsymbol{q}^2 + c^{-2}\omega_n^2\right)\phi\left(q\right)\phi\left(-q\right) \\ &+ u\int_x\phi\left(x\right)^4 + \int_q\frac{\lambda_0}{2}\omega_n\left|\boldsymbol{q}\right|u_T\left(q\right)\phi\left(-q\right) \\ &+ \frac{1}{2}\int_q\left(\omega_n^2 + \gamma\left|\omega_n\right| + v_T^2\boldsymbol{q}^2\right)u_T\left(q\right)u_T\left(-q\right). \end{aligned} \tag{4.19}$$

By integrating out the transverse phonons we obtain the effective theory:

$$S_{\text{orb}} = \frac{1}{2}\int_q\chi(q)^{-1}\phi\left(q\right)\phi\left(-q\right) + u\int_x\phi\left(x\right)^4, \tag{4.20}$$

with

$$\chi(q) = \frac{1}{r_0 + \boldsymbol{q}^2 + \Delta\left(\mathbf{q},\omega_n\right)\frac{\omega_n^2}{c^2}}, \tag{4.21}$$

where

$$\Delta\left(\mathbf{q},\omega_n\right)=\left(1+\frac{\frac{1}{4}\lambda_0^2c^2\boldsymbol{q}^2}{\omega_n^2+\gamma\left|\omega_n\right|+v_T^2\boldsymbol{q}^2}\right). \tag{4.22}$$

4.3 Spectra of coupled modes

Analysing the propagator provides some intuition for the effects of magnetoelastic coupling and phason damping. Considering first the limit $\gamma \ll \omega_n$ reveals effectively the same results as for the altermagnet coupled dynamically to strain [20] and so we only review them briefly. If we consider the almost-static, low frequency limit of Eq. 4.21, where $\omega_n \ll v_T\left|\boldsymbol{q}\right|$, we have the usual ϕ^4 model, yet with a renormalized strength of quantum fluctuations

$$c^{-2}\to c^{-2}\left(1+\frac{1}{4}\lambda_0^2\frac{c^2}{v_T^2}\right). \tag{4.23}$$

This reduces c and thus suppresses quantum fluctuations. On the other hand, for frequencies $\omega_n \gg v_T\left|\boldsymbol{q}\right|$, we find that

$$\boldsymbol{q}^2\to\boldsymbol{q}^2\left(1+\frac{1}{4}\lambda_0^2\right). \tag{4.24}$$

Such that spacial fluctuations are renormalised, giving rise to an enhanced correlation length. The new parameter in this system is, of course, the damping. To gain some insight into how damping effects fluctuations, we consider a mean-field theory which renormalises r and gives the condition for a phase transition (i.e. at $r=0$):

$$r_0^c=-u\int_0^{\Lambda_\omega}\int_0^{\Lambda}q\chi\left(q,\omega_n\right)dqd\omega_n, \tag{4.25}$$

where we have now introduced a cutoff for the frequency Λ_ω, in addition to the momentum cutoff Λ. This is necessary due to the fact that the term linear in ω_n stops the Matsubara sum from converging. We can extract the effect of damping on the integrand with a density plot of $q\chi\left(\gamma\right)-q\chi\left(0\right)$. We see from Fig.4.1 that higher damping produces a larger integrand and hence a much larger absolute value of r_0 is needed to transition, this implies that quantum fluctuations are strengthened by damping.

Having renormalised $r_0\to r$ due to higher order interactions, we can analytically continue the propagator to the real axis with $i\omega_n\to\omega+i0^+$

$$\chi(q)=\frac{1}{r+\boldsymbol{q}^2-\Delta\left(\mathbf{q},\omega\right)\frac{\omega^2}{c^2}}, \tag{4.26}$$

with

$$\Delta\left(\mathbf{q},\omega\right)=\left(1+\frac{\frac{1}{4}\lambda_0^2c^2\boldsymbol{q}^2}{-\omega^2-i\gamma_0\omega+v_T^2\boldsymbol{q}^2}\right). \tag{4.27}$$

We can plot the spectral function of the effective magnon propagator, we do so in Fig. 4.2. If we first consider the case that the modes are undamped, the phason-like polaron is softened and the magnon-like polaron is hardened. We anticipated this following our analysis of

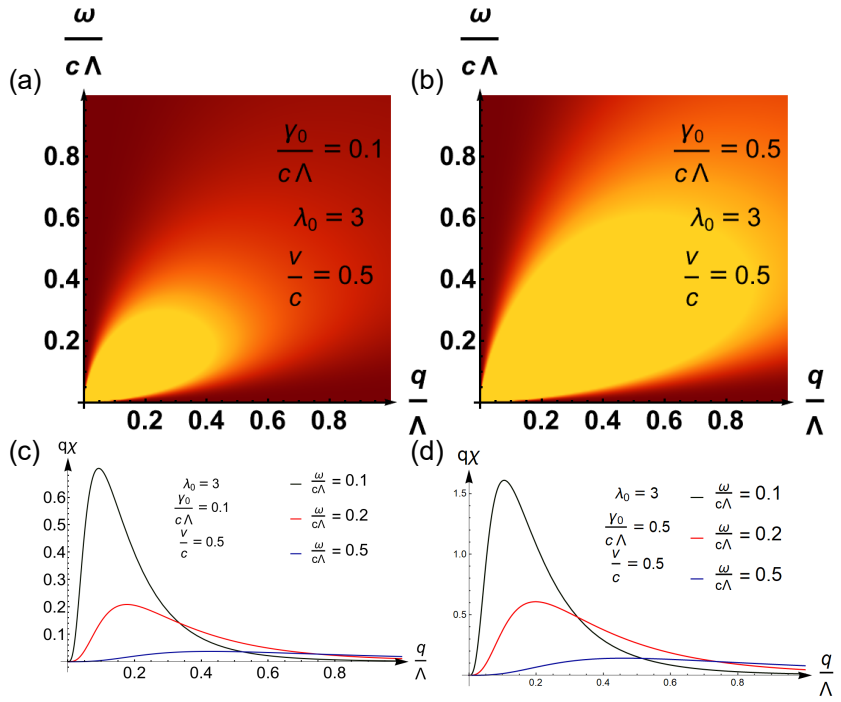

Figure 4.1: The density plot of $q\chi\left(\gamma\right) - q\chi\left(0\right)$ shows that for lower values of damping (panel (a)), the integrand is smaller when compared to higher values (panel (b)), this becomes even clearer when plotting along lines of constant ω. The integrand is again much smaller for lower damping (panel(c)) than for higher damping (panel (d)). (Figure from Ref. [21])

altermagnetic systems [20]. If we now include the damping, we see that due to a non-zero imaginary element in the propagator, the definite modes are lost. Due to finite coupling, despite the fact that the damping is in the phason part, both modes are now damped.

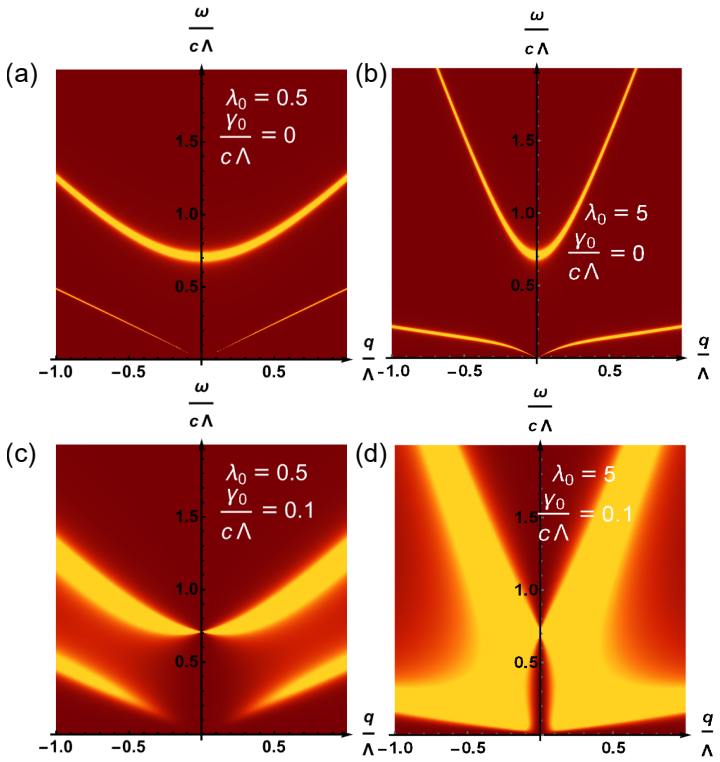

Figure 4.2: We plot the spectral functions at $\gamma_0 = 0$ and $\lambda = 0.5$(a) and $\gamma_0 = 0$ and $\lambda = 5$ (b). The phonon-like polaron is softened while the magnon-like polaron is hardened by coupling λ_0. Introducing a finite damping γ_0 leads to the loss of well defined modes and the spectrum spreads over a finite width (c) and (d). These are plotted at $\frac{v}{c} = \frac{1}{2}$ and $\frac{r}{\Lambda^2} = 0.5$. (Figure from Ref. [21])

In order to get a clearer picture of the spectra when damping is present, we plot a cut of the spectral function against frequency along constant q. We clearly see that while the coupled modes are both affected by the damping, the effect is naturally more prevalent for the phason-like polaron.

4.4 Ferromagnetic phase boundary in coupled systems

Much like the analysis for the altermagnets, we can carry out an analysis of the phase boundary between the ordered ferromagnet phase and the disordered paramagnetic phase. The one-loop RG equations are the same as previously (albeit with a new propagator), we restate them here

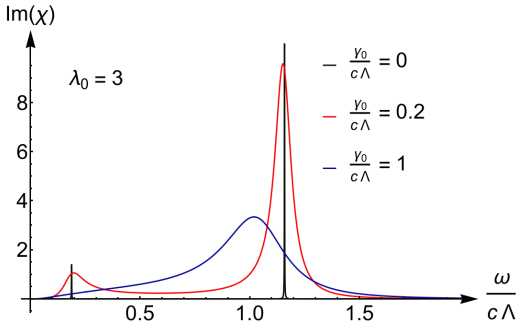

Figure 4.3: A 2D cut along $\frac{q}{\Lambda} = \frac{1}{2}$ of the spectral function at $\lambda_0 = 3$ for different values of damping. We also use $\frac{r}{\Lambda^2} = \frac{1}{2}$ and $\frac{v}{c} = \frac{1}{2}$. We see that the well defined modes become spread over a finite width due to damping. (Figure from Ref. [21])

for convenience

$$\begin{aligned}\frac{dr}{dl} &= 2r + 3u\frac{d}{dl}\int_q^> \chi_0(q) - 3ur\frac{d}{dl}\int_q^> \chi_0(q)^2, \\ \frac{du}{dl} &= \epsilon u - 9u^2\frac{d}{dl}\int_q^> \chi_0(q)^2, \\ \frac{dT}{dl} &= T,\end{aligned} \tag{4.28}$$

Here, $\epsilon = 3 - d$, l determines the running upper cut off scale $\Lambda(l) = \Lambda e^{-l}$ and $\Lambda_\omega(l) = \Lambda_\omega e^{zl}$, where we choose $z = 1$ and $\int_q^> \cdots$ stands for the integral over the shell in momentum and frequency space. Power counting would initially suggest that damping would allow for the choice $z = 2$, while this would put the system at the upper critical dimension, it also renormalises c such that it diverges with l and the problem becomes static.

While the method here is almost the same as for the altermagnetic case, we must adjust the method used to calculate the shell integrals, due to the fact that the integral is also a shell in frequency space. We use a tilde to denote variables written in dimensionless units $\tilde{q} = \frac{q}{\Lambda}$, $\tilde{\omega} = \frac{\omega}{\Lambda c}$, $\tilde{T} = \frac{T}{\Lambda c}$, $\tilde{\gamma} = \frac{\gamma}{c\Lambda}$ and $\tilde{v} = \frac{v}{c}$. In terms of these variables, the propagator $\tilde{\chi}_0 = \chi_0\Lambda^2$. For the Matsubara sums we use

$$T\sum_{n=-\infty}^{\infty} A(i\omega_n) = \int_0^{\Lambda_n} \frac{d\omega}{\pi}\frac{d\omega}{\pi}\coth\left(\omega/(2T)\right)\mathrm{Im}A\left(\omega + i0^+\right), \tag{4.29}$$

and the fact that to leading order in l

$$\int_{\Lambda_\omega}^{\Lambda_\omega b^z} d\omega A(\omega) = z\Lambda_\omega A\left(\Lambda_\omega\right) l + \mathcal{O}\left(l^2\right), \tag{4.30}$$

such that the leading order in l of the shell integrals is

$$F_m(l) = \left(\int_0^{\tilde{\Lambda}_\omega} d\tilde{\omega}\coth\left(\frac{\tilde{\omega}}{2\tilde{T}}\right)\mathrm{Im}\tilde{\chi_0}^m(1,\tilde{\omega}) + \tilde{\Lambda}_\omega\coth\left(\frac{1}{2\tilde{T}}\right)\int_0^1 d\tilde{q}\tilde{q}^{d-1}\mathrm{Im}\tilde{\chi}_0^m\left(\tilde{q},\tilde{\Lambda}_\omega\right)\right). \tag{4.31}$$

We then use the dimensionless variables

$$\begin{aligned} m &= \frac{r}{\Lambda^2}, \\ g &= \frac{3K_d c\Lambda^{d-3}}{\pi} u, \end{aligned} \tag{4.32}$$

such that the flow equations are now

$$\begin{aligned} \frac{dm}{dl} &= 2m + gF_1\left(\tilde{T}, \tilde{\gamma}\right) - gmF_2\left(\tilde{T}, \tilde{\gamma}\right), \\ \frac{dg}{dl} &= \epsilon g - 3g^2 F_2\left(\tilde{T}, \tilde{\gamma}\right). \end{aligned} \tag{4.33}$$

Taking the limit $T \to 0$ and solving the flow equations yields an expression for the distance to the critical point

$$t = m + \frac{1}{2} F_1\left(0, \gamma\right) g. \tag{4.34}$$

The phase diagram the above expression yields is displayed in Fig. 4.4. The results show, as expected from our analysis of the propagator, that quantum fluctuations are diminished through coupling to phasons, leading to a lower $|m_0|$ needed to transition. In contrast, damping enhances quantum fluctuations, leading to a reduced-size ordered regime.

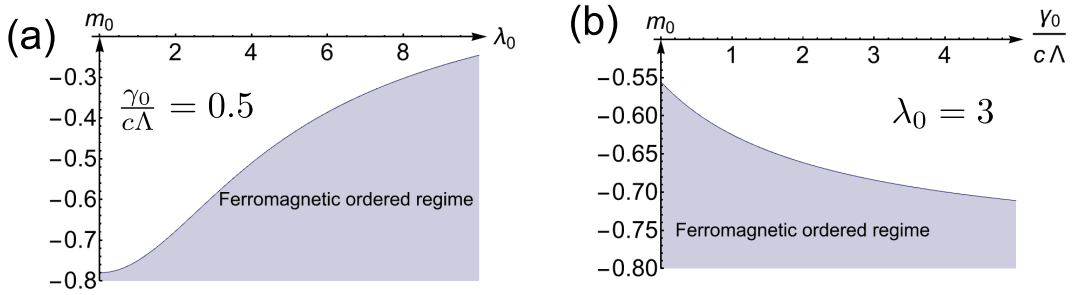

Figure 4.4: At the QCP, increasing λ_0 leads to a larger ordered regime due to the suppression of quantum fluctuations. Increasing the damping γ_0 causes a decrease in the ordered regime as expected from Fig. 4.1. Here, $\frac{v}{c} = \frac{1}{2}$. (Figure from Ref. [21])

Carrying out the calculation in the crossover regime as before (Ref. [124]) yields the transcendental equation for T_c

$$\begin{aligned} &\left(t_0 + \int_0^{\frac{1}{T_0}} g_0 \left(\int_0^{\tilde{\Lambda}_\omega} d\tilde{\omega} \frac{2xT_c}{e^{\tilde{\omega}x} - 1} \mathrm{Im}\tilde{\chi}_0\left(1, \tilde{\omega}\right) \right.\right. \\ &+ \frac{T_c^2}{2} \mathrm{Im}\tilde{\chi}_0{}'\left(1, \tilde{\omega}\right) + \tilde{\Lambda}_\omega \int_0^1 d\tilde{q} \frac{2xT_c}{e^x - 1} \tilde{q}^{d-1} \mathrm{Im}\chi_0\left(\tilde{q}, 1\right) \\ &\left.\left. + \frac{T_c^2}{2} \tilde{q}^{d-1} \mathrm{Im}\chi_0'\left(\tilde{q}, 1\right) \right) \right) dx = 0. \end{aligned} \tag{4.35}$$

Solving this equation numerically yields the phase diagram shown in Fig.4.5. It is not possible

to have a transition until we reach a value of λ_0 and γ_0 such that our chosen value of $m_0 \leq m_0^c(\lambda_0, \gamma_0)$. This suggests that coupling can induce a ferromagnetic transition, we can also see that the coupling leads to a reduction in the transition temperature, this is due to the enhanced thermal fluctuations. At $T = 0$ there are no phonons and so the dominant effect is the suppression of quantum fluctuations and hence an enhanced ordered regime emerges, consistent with the results of a 2D altermagnet [20]. The damping γ_0 suppresses order and increasing this drives the system towards the QCP. This is consistent with the $T = 0$ case in which order is also suppressed.

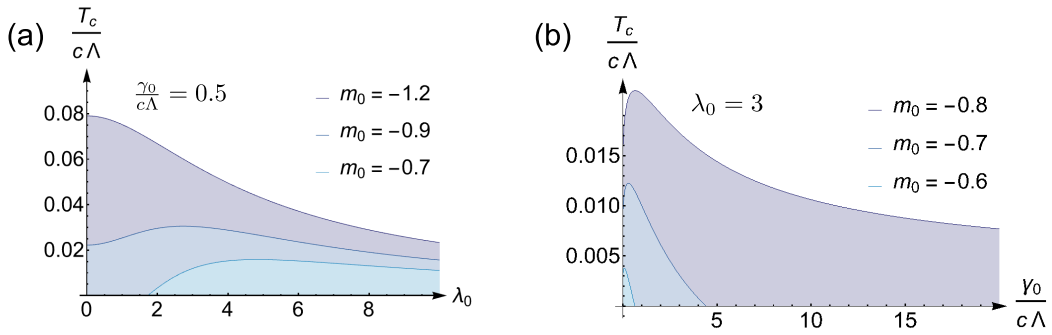

Figure 4.5: Magnetoelastic coupling (panel (a)) is able to induce a transition to the ferromagnetic state, however at higher temperatures, the dominant effect is a high occupation of soft phasons and the transition temperature is reduced. Increased damping (panel (b)) is able to drive the system to the QCP for lower values of m_0 and the transition temperature is still diminished for all values of m_0. Both phase diagrams are plotted for $\frac{v}{c} = \frac{1}{2}$. (Figure from Ref. [21])

4.5 Conclusion and discussion

Here we have analysed interactions between damped phason modes, which emerge as a result of the relative motion of the upper and lower layers in TBG, and orbital ferromagnetism. The fact that both degrees of freedom transform according to the same irreducible representation implies a symmetry allowed coupling in which orbital magnetism induces fluctuations of the twist angle.

Orbital magnetism with a huge magnetoelectric effect implies uses for low energy memory devices [4], it is therefore important to understand how these interactions affect the magnons which act as the collective modes of orbital magnetism.

We already know from Chapter. 3 that a dynamic magnetoelastic coupling in two dimensions lowers the transition temperature, such that this ferromagnetic state becomes more difficult to reach, the additional degree of freedom which one must include in such an incommensurate system is a damping to the phason modes. This arises as the collective modes have no associated conservation law. As a result of coupling, the magnon modes inherit this damping and the sharp spectral peak which would ordinarily categorise the magnons is lost.

The introduction of damping also has a profound effect on the phase diagram, not only is the transition temperature reduced for increased levels of damping, but it also increases quantum fluctuations, such that even in the quantum critical regime $T = 0$, the ordered regime is significantly diminished. A consequence of this is, in opposition to the results for

the coupling, increasing damping is not able to induce the ferromagnetic transition but rather drives the system towards the QCP. This damping is therefore detrimental to the use of twisted bilayer graphene in commercial memory devices and so a method to reduce disorder would be beneficial.

Chapter 5
5 Summary and outlook

5.1 Summary

The nature of magnetic moments situated on a lattice suggests there must be some coupling to strain, as the modification of the lattice constant must also come with a modification to the exchange interaction. In this thesis we have shown that there exists many such couplings which manifest themselves in ways both interesting from a phenomenological perspective but which also allow for the probing and tuning of such states, leveraging the attributes of complex magnetic structures. Understanding these properties is crucial to their potential use in devices.

In Chapter. 2, we showed that there exists a piezomagnetic coupling to symmetry breaking strain, which can be used to identify the symmetries of an altermagnetic order parameter by straining a system and measuring the induced magnetisation. This coupling also has a profound effect on the phase diagram of altermagnets. The critical point is shifted in such a way that a magnetic field can be used to induce a transition. An elastic QC regime also emerges above the critical point in which the logarithmic NFL behaviour of the heat capacity saturates at a crossover temperature, giving a leading order FL behaviour of the heat capacity. A calculation of the elastocaloric effect showed that this region is however, not a true Fermi liquid, this effect is sensitive to gapless modes which emerge along particular directions which, while producing a less singular result than that exhibited in the bare QC regime, is still not a Fermi liquid. This crossover temperature can be tuned with a magnetic field, meaning that, provided the system has a high enough piezomagnetic coupling, the effects of altermagnetism are evident through observable quantities of the system. The field-dependent coupling also allows for a region of NFL behaviour which is not accessible in nematic systems.

In Chapter 3, we analysed a symmetry allowed coupling of strain to the dynamics of an altermagnetic order parameter, provided that the product of the two degrees of freedom contains the trivial irreducible representation. This creates a coupling, anisotropic in momentum space, which should be visible through observations of the phonon spectra. The phonon-like polarons are softened by this coupling, however these phonon modes decouple in certain areas of momentum space. Measurements of the phonon spectra could then also allow for the identification of the presence and symmetry of altermagnetic states. This coupling effects the phase diagram, reinforcing order in the ground state, it can induce an altermagnetic transition, in 3D it also raises the transition temperature, however in 2D, phonon softening increases

thermal fluctuations to such a degree that the transition temperature is lowered.

In Chapter. 4, we applied this same dynamic magnetoelastic coupling to the case that the magnetic order parameter is a purely orbital ferromagnetic state of a moiré superlattice. In this case the character of the elastic modes is very different. The modes are associated with the relative displacement of two graphene layers and are therefore not associated with a conservation law. This leads to damped modes [22]; this damping is then inherited by the magnon modes. This changes the phase diagram by increasing quantum fluctuations of the order parameter, such that the area of the ground state ordered phase is diminished and the system can be driven towards the QCP for systems which transition at finite temperature at zero damping.

5.2 Outlook

While this thesis has sought to lay theoretical foundations for the understanding of magnetoelastic coupling on the ordered magnetic phases of twisted bilayer graphene and altermagnetism, there remains much work to be done with regards to experimental verification.

Experimental techniques such as the elastocaloric effect, which has already proven its worth in the field of nematics, being used to rule out order parameter symmetries and identify phase transitions [77], could also be used to identify the behaviour which we discuss in Chapter 2 for altermagnetic systems. Provided the piezomagnetic coupling is high enough, it should also be possible to observe the structural transition which takes place due to the elastic constant softening at the transition.

Measurements of phonon spectra in altermagnetic candidates could identify the anisotropic softening behaviour, we would expect following the calculation presented in Chapter. 3. Measuring phonon spectra in different regions of momentum space and plotting their dispersions would hopefully reveal an anisotropic sound velocity which could be attributed to hybridisation with altermagnon modes.

If one could find a way to tune the damping of phason modes, perhaps through adjustments to disorder in the system, then it would also be possible to plot and potentially confirm the phase diagram of Chapter 4, where we would see the transition temperature driven to zero.

The future does however, not only stand on the side of experiment. It would be interesting to see if similar calculations to those carried out in Chapter 4 could also be applied to other twisted heterostructures.

In all cases we have also only considered single-component order parameters, however it also stands to reason that we can investigate coupled modes with two or three component order parameters where the field theories and the RG calculations are more complex.

It would also be interesting to study further the theoretical aspects related to the elastocaloric effect, for example, we considered the elastocaloric effect in the classical regime with an applied symmetry breaking strain, but what of the quantum regime? This was not considered in this thesis but would also likely yield interesting insights into what one should expect from experiment and elucidate the mechanisms behind results already obtained, for example for the large doping dependence of the elastocaloric effect presented in Ref. [78].

The theory of Chapter 3 could also be expanded to include a much larger list of order parameters, in order to produce a more complete understanding of how phonon spectra should be influenced by coupling. This would expand the number of candidate materials this theory

could be applied to and aid in the identification of altermagnetic materials.

Hopefully following the identification of altermagnetic materials, we will begin to see the production of commercial devices which consume significantly less power than the current generation. This could surely be seen as a resounding success for the field which I hope this thesis has made a small contribution towards.

A Appendix A
Additional material for Chapter 1

A.1 Product rules for important point groups

We can create a set of product rules for the irreducible representations, which in turn allows us to deduce the piezomagnetic couplings for crystals transforming according to various point groups. In this section, we will outline the method used to calculate the product for E_g in D_{4h} as the product of 2D irreducible representations was not covered in detail in the main text. This method can then be extended for representations of even higher dimension through an analogous method.

We first need the representations of the generators of the group for E_g. These can be derived by considering the effect of the following rotations on an object which transforms with E_g and gives

$$\rho^{E_g}\left(C_{4z}\right) = \begin{pmatrix} 0 & -1 \\ 1 & 0 \end{pmatrix},\ \rho^{E_g}\left(C_{2x}\right) = \begin{pmatrix} 1 & 0 \\ 0 & -1 \end{pmatrix},\ \rho^{E_g}\left(C_{2d}\right) = \begin{pmatrix} 0 & 1 \\ 1 & 0 \end{pmatrix}, \tag{A.1}$$

where d denotes a rotation around the diagonal axis $x = y$ in the $z = 0$ plane. The outline for the method was already discussed, we just show here how we find the change of basis matrix M which simultaneously diagonalises $\rho^E\left(C_{4z}\right) \otimes \rho^E\left(C_{4z}\right)$, $\rho^E\left(C_{2x}\right) \otimes \rho^E\left(C_{2x}\right)$ and $\rho^E\left(C_{2d}\right) \otimes \rho^E\left(C_{2d}\right)$.

The eigenvalues and eigenvectors of $\rho^E\left(C_{4z}\right) \otimes \rho^E\left(C_{4z}\right)$ are

$$-1 : (-1,0,0,1)\,,\ -1 : (0,1,1,0)\,,\ 1 : (1,0,0,1)\,,\ 1 : (0,-1,1,0)\,. \tag{A.2}$$

Likewise for $\rho^E\left(C_{2x}\right) \otimes \rho^E\left(C_{2x}\right)$

$$-1 : (0,0,1,0)\,,\ -1 : (0,1,0,0)\,,\ 1 : (0,0,0,1)\,,\ 1 : (1,0,0,0)\,, \tag{A.3}$$

and finally, for $\rho^E\left(C_{2d}\right) \otimes \rho^E\left(C_{2d}\right)$

$$-1 : (-1,0,0,1)\,,\ -1 : (0,-1,1,0)\,,\ 1 : (1,0,0,1)\,,\ 1 : (0,1,1,0)\,. \tag{A.4}$$

We then look for matching eigenvectors (where superpositions of eigenvectors with degenerate eigenvalues can be taken, which we must do for the C_{2x} product). Doing so and using the eigenvalue to match the character table of the irreducible representations under the rotations

given, gives the corresponding vectors

$$v_{A_{1g}} = \begin{pmatrix} 1 \\ 0 \\ 0 \\ 1 \end{pmatrix},\ v_{A_{2g}} = \begin{pmatrix} 0 \\ -1 \\ 1 \\ 0 \end{pmatrix},\ v_{B_{1g}} = \begin{pmatrix} -1 \\ 0 \\ 0 \\ 1 \end{pmatrix},\ v_{B_{2g}} = \begin{pmatrix} 0 \\ 1 \\ 1 \\ 0 \end{pmatrix}. \tag{A.5}$$

These vectors then form the columns of the change of basis matrix M. We then see for example allowing $v_{B_{1g}}$ to act on the object $(\phi_1\varepsilon_1, \phi_1\varepsilon_2, \phi_2\varepsilon_1, \phi_2\varepsilon_1)$ gives the object $\phi_1\varepsilon_1 - \phi_2\varepsilon_2$ as the combination of objects from the product of two objects transforming according to E_g which transforms like B_{1g}. This method of using the eigenvectors of the product representations of the generators of the group can be expanded to higher dimensional irreducible representations to calculate a full set of product rules (tables A.1-A.3) which are then used to calculate the coupling terms in table 2.2 and tables B.1-B.3.

$\otimes$	$A_1\,(B)$	$A_2\,(B)$	$B_1\,(B)$	$B_2\,(B)$	$E\left(B_1\vert B_2\right)$
$A_1\,(\phi)$	$A_1\,(\phi B)$	$A_2\,(\phi B)$	$B_1\,(\phi B)$	$B_2\,(\phi B)$	$E\left(\phi B_1\vert\phi B_2\right)$
$A_2\,(\phi)$		$A_1\,(\phi B)$	$B_2\,(\phi B)$	$B_1\,(\phi B)$	$E\left(\phi B_2\vert - \phi B_1\right)$
$B_1\,(\phi)$			$A_1\,(\phi B)$	$A_2\,(\phi B)$	$E\left(\phi B_1\vert - \phi B_2\right)$
$B_2\,(\phi)$				$A_1\,(\phi B)$	$E\left(\phi B_2\vert\phi B_1\right)$
$E\left(\phi_1\vert\phi_2\right)$					$A_1\,(\phi_1 B_1 + \phi_2 B_2)$ $A_2\,(\phi_1 B_2 - \phi_2 B_1)$ $B_1\,(\phi_1 B_1 - \phi_2 B_2)$ $B_2\,(\phi_1 B_2 + \phi_2 B_1)$

Table A.1: All possible products of the irreducible representations of D_4 and D_2

$\otimes$	$A_1\,(B)$	$A_2\,(B)$	$B_1\,(B)$	$B_2\,(B)$	$E_1\left(B_1\vert B_2\right)$	$E_2\left(B_1\vert B_2\right)$
$A_1\,(\phi)$	$A_1\,(\phi B)$	$A_2\,(\phi B)$	$B_1\,(\phi B)$	$B_2\,(\phi B)$	$E_1\left(\phi B_1\vert\phi B_2\right)$	$E_2\left(\phi B_1\vert\phi B_2\right)$
$A_2\,(\phi)$		$A_1\,(\phi B)$	$B_2\,(\phi B)$	$B_1\,(\phi B)$	$E_1\left(\phi B_2\vert - \phi B_1\right)$	$E_2\left(\phi B_2\vert - \phi B_1\right)$
$B_1\,(\phi)$			$A_1\,(\phi B)$	$A_2\,(\phi B)$	$E_2\left(\phi B_1\vert - \phi B_2\right)$	$E_1\left(\phi B_1\vert - \phi B_2\right)$
$B_2\,(\phi)$				$A_1\,(\phi B)$	$E_2\left(\phi B_2\vert\phi B_1\right)$	$E_1\left(\phi B_2\vert\phi B_1\right)$
$E_1\left(\phi_1\vert\phi_2\right)$					$A_1\,(\phi_1 B_1 + \phi_2 B_2)$ $A_2\,(\phi_1 B_2 - \phi_2 B_1)$ $E_2\begin{pmatrix}\phi_1 B_1 - \phi_2 B_2 \\ \phi_1 B_2 + \phi_2 B_1\end{pmatrix}$	$B_1\,(\phi_1 B_1 - \phi_2 B_2)$ $B_2\,(\phi_1 B_2 + \phi_2 B_2)$ $E_1\begin{pmatrix}\phi_1 B_1 + \phi_2 B_2 \\ \phi_1 B_2 - \phi_2 B_1\end{pmatrix}$
$E_2\left(\phi_1\vert\phi_2\right)$						$A_1\,(\phi_1 B_1 + \phi_2 B_2)$ $A_2\,(\phi_1 B_2 - \phi_2 B_1)$ $E_2\begin{pmatrix}\phi_1 B_1 - \phi_2 B_2 \\ -\phi_1 B_2 - \phi_2 B_1\end{pmatrix}$

Table A.2: All possible products of the irreducible representations of D_6

$\otimes$	$A_1\,(B)$	$A_2\,(B)$	$E\left(B_1\vert B_2\right)$	$T_1\left(B_1\vert B_2\vert B_3\right)$	$T_2\left(B_1\vert B_2\vert B_3\right)$
$A_1\,(\phi)$	$A_1\,(\phi B)$	$A_2\,(\phi B)$	$E\left(\phi B_1\vert\phi B_2\right)$	$T_1\left(\phi B_1\vert\phi B_2\vert\phi B_3\right)$	$T_2\left(\phi B_1\vert\phi B_2\vert\phi B_3\right)$
$A_2\,(\phi)$		$A_1\,(\phi B)$	$E\left(\phi B_2\vert-\phi B_1\right)$	$T_2\left(\phi B_1\vert\phi B_2\vert\phi B_3\right)$	$T_1\left(\phi B_1\vert\phi B_2\vert\phi B_3\right)$
$E\left(\phi_1\vert\phi_2\right)$			$A_1\,(\phi_1 B_1+\phi_2 B_2)$ $A_2\,(\phi_1 B_2-\phi_2 B_1)$ $E\begin{pmatrix}\phi_1 B_1-\phi_2 B_2\\-\phi_1 B_2-\phi_2 B_1\end{pmatrix}$	$T_1\begin{pmatrix}\left(\phi_1+\sqrt{3}\phi_2\right)B_1\\\left(\phi_1-\sqrt{3}\phi_2\right)B_2\\-2\phi_1 B_3\end{pmatrix}$ $T_2\begin{pmatrix}\left(\sqrt{3}\phi_1-\phi_2\right)B_1\\-\left(\sqrt{3}\phi_1+\phi_2\right)B_2\\2\phi_2 B_3\end{pmatrix}$	$T_1\begin{pmatrix}\left(\sqrt{3}\phi_1-\phi_2\right)B_1\\-\left(\sqrt{3}\phi_1+\phi_2\right)B_2\\2\phi_2 B_3\end{pmatrix}$ $T_2\begin{pmatrix}\left(\phi_1+\sqrt{3}\phi_2\right)B_1\\\left(\sqrt{3}\phi_1-\sqrt{3}\phi_2\right)B_2\\-2\phi_1 B_3\end{pmatrix}$
$T_1\left(\phi_1\vert\phi_2\vert\phi_3\right)$				$A_1\,(\phi_1 B_1+\phi_2 B_2+\phi_3 B_3)$ $E\begin{pmatrix}\phi_1 B_1+\phi_2 B_2-2\phi_3 B_3\\\sqrt{3}\,(\phi_1 B_1-\phi_2 B_2)\end{pmatrix}$ $T_1\begin{pmatrix}\phi_2 B_3-\phi_3 B_2\\\phi_3 B_1-\phi_1 B_3\\\phi_1 B_2-\phi_2 B_1\end{pmatrix}$ $T_2\begin{pmatrix}\phi_2 B_3+\phi_3 B_2\\\phi_3 B_1+\phi_1 B_3\\\phi_1 B_2+\phi_2 B_1\end{pmatrix}$	$A_1\,(\phi_1 B_1+\phi_2 B_2+\phi_3 B_3)$ $E\begin{pmatrix}-\sqrt{3}\,(\phi_1 B_1-\phi_2 B_2)\\\phi_1 B_1+\phi_2 B_2-2\phi_3 B_3\end{pmatrix}$ $T_1\begin{pmatrix}\phi_2 B_3+\phi_3 B_2\\\phi_3 B_1+\phi_1 B_3\\\phi_1 B_2+\phi_2 B_1\end{pmatrix}$ $T_1\begin{pmatrix}\phi_2 B_3-\phi_3 B_2\\\phi_3 B_1-\phi_1 B_3\\\phi_1 B_2-\phi_2 B_1\end{pmatrix}$
$T_2\left(\phi_1\vert\phi_2\vert\phi_3\right)$					$A_1\,(\phi_1 B_1+\phi_2 B_2+\phi_3 B_3)$ $E\begin{pmatrix}\phi_1 B_1+\phi_2 B_2-2\phi_3 B_3\\\sqrt{3}\,(\phi_1 B_1-\phi_2 B_2)\end{pmatrix}$ $T_1\begin{pmatrix}\phi_2 B_3-\phi_3 B_2\\\phi_3 B_1-\phi_1 B_3\\\phi_1 B_2-\phi_2 B_1\end{pmatrix}$ $T_2\begin{pmatrix}\phi_2 B_3+\phi_3 B_2\\\phi_3 B_1+\phi_1 B_3\\\phi_1 B_2+\phi_2 B_1\end{pmatrix}$

Table A.3: All possible products of the irreducible representations of O_h

B Appendix B
Additional material for Chapter 2

B.1 Irreducible representation products to create coupling terms

We use the product rules given in Appendix. A.1 to construct piezomagnetic couplings of the type $\lambda_{i,jk,a}H_i\varepsilon_{jk}\phi_a$, where we deduce which coupling coefficients are zero and which ones are related to one another. We also calculate the coupling to fermions. In this case the coupling takes the form $g_{i,jk,a}H_i\sigma_k k_i k_j \phi_a$ where σ are Pauli matrices. These couplings are calculated analogously and both are given in Tab. 1.1 and Tabs. B.1-B.3.

B.2 Piezomagnetism of a system with a cylindrical Fermi surface

Here we consider the cylindrical Fermi surface characterised by $\xi_k = \frac{\mathbf{k}_{2d}^2}{2m} - \mu$. The Fermi surface therefore has a different symmetry to the spherical case, in particular along the z direction. For this reason we consider a magnetic field aligned along x in order to create a soft direction along z. Keeping $\mathbf{H} = H\hat{e}_z$ produces the same results as for the spherical Fermi surface as the symmetries are identical in the $x-y$ plane. For the dispersion of the boson, velocity along the z-direction is assumed to be much smaller than the velocity along the xy-plane.

B.2.1 Landau damping

Proceeding as in the main text

$$\Delta D_i(q) \equiv D_i(\Omega,\mathbf{q}) - D_i(0,\mathbf{q}) = \frac{2}{v_\mathrm{F}}\int\frac{dk_{2d}^2}{(2\pi)^2}\int\frac{dk_z}{2\pi}h_i^2(k)\delta(k_{2d}-k_\mathrm{F})\frac{1}{1-i\frac{v_\mathrm{F}\mathbf{q}_{2d}\cdot\hat{k}_{2d}}{\Omega}}. \tag{B.1}$$

Using the explicit expression of $\mathbf{h}(q)$, we obtain

$$\begin{aligned}\Delta D_x(q) &= \frac{2}{v_\mathrm{F}}\int\frac{d^2k_{2d}}{(2\pi)^2}\int_{-\pi/a_z}^{\pi/a_z}\frac{dk_z}{2\pi}\Big(\cos^2 k_x a - \cos^2 k_y a\Big)^2\frac{\delta(k_{2d}-k_\mathrm{F})}{1-iv_\mathrm{F}\mathbf{q}_{2d}\cdot\hat{k}_{2d}/\Omega}\\ &\approx \frac{(k_\mathrm{F}a)^4 k_\mathrm{F}}{2\pi v_\mathrm{F}a_z}\left[(1+\cos 4\phi_q)\frac{|\Omega|}{v_\mathrm{F}|\mathbf{q}_{2d}|} - 4\cos 4\phi_q\frac{\Omega^2}{v_\mathrm{F}^2|\mathbf{q}_{2d}|^2}\right],\end{aligned} \tag{B.2}$$

D_{2h} (mmm) point group		
AM irrep	coupling to fermions	piezomagnetic coupling
A_{1g}^-	$g\phi k_y k_z \sigma_x$	$\lambda\phi\epsilon_{yz}H_x$
	$g'\phi k_x k_z \sigma_y$	$\lambda'\phi\epsilon_{xz}H_y$
	$g''\phi k_x k_y \sigma_z$	$\lambda''\phi\epsilon_{xy}H_z$
FM irrep		
B_{1g}^-	$g\phi\sigma_z$	$\lambda\phi\epsilon_{A_{1g}}H_z$
		$\lambda'\phi\epsilon_{xz}H_x$
		$\lambda''\phi\epsilon_{yz}H_y$
B_{2g}^-	$g\phi\sigma_y$	$\lambda\phi\epsilon_{A_{1g}}H_y$
		$\lambda'\phi\epsilon_{xy}H_x$
		$\lambda''\phi\epsilon_{yz}H_z$
B_{3g}^-	$g\phi\sigma_x$	$\lambda\phi\epsilon_{A_{1g}}H_x$
		$\lambda'\phi\epsilon_{xy}H_y$
		$\lambda''\phi\epsilon_{xz}H_z$

Table B.1: The coupling of altermagnetic (AM) and ferromagnetic (FM) order parameters ϕ to fermions and to simultaneous magnetic and strain fields (piezomagnetism) for the orthorhombic point group D_{2h} (mmm). The first column indicates the irrep of ϕ. g and λ are coupling constants, k_α is the momentum, σ_α are Pauli matrices, $\epsilon_{\alpha\beta}$ is the strain tensor, and H_α is the magnetic field. The possibility of having $g' \neq g$ and $\lambda' \neq \lambda$ reflects magnetic anisotropy. $\epsilon_{A_{1g}}$ are the trivially transforming strain components. The coupling to lattice fermions is deduced by replacing $k_\alpha k_\beta$ with $\sin k_\alpha \sin k_\beta$. In contrast to the tetragonal case (Table 2.2), now there is only one altermagnetic state which is a combination of a magnetic dipole with a charge quadrupole. All other representations correspond to ferromagnetic orders along the crystalline axes, but display the same piezomagnetic behavior for field directions orthogonal to the easy axis. (Table reprinted from Ref. [17])

D_{6h} $(6/mmm)$ point group		
AM irrep	coupling to fermions	piezomagnetic coupling
A_{1g}^-	$g\phi k_z\left(k_y\sigma_x - k_x\sigma_y\right)$	$\lambda\phi\left(\epsilon_{yz}H_x - \epsilon_{xz}H_y\right)$
B_{1g}^-	$g\phi\left(\left(k_x^2 - k_y^2\right)\sigma_x - 2k_xk_y\sigma_y\right)$	$\lambda\phi\left(\epsilon_{x^2-y^2}H_x - 2\epsilon_{xy}H_y\right)$
B_{2g}^-	$g\phi\left(2k_xk_y\sigma_x + \left(k_x^2 - k_y^2\right)\sigma_y\right)$	$\lambda\phi\left(2\epsilon_{xy}H_x + \epsilon_{x^2-y^2}H_y\right)$
E_{2g}^-	$gk_z\left(\phi_1\left(k_y\sigma_x + k_x\sigma_y\right) - \phi_2\left(k_x\sigma_x - k_y\sigma_y\right)\right)$ $g'\left(2\phi_1k_xk_y - \phi_2\left(k_x^2 - k_y^2\right)\right)\sigma_z$	$\lambda\left(\phi_1\left(\epsilon_{yz}H_x + \epsilon_{xz}H_y\right) - \phi_2\left(\epsilon_{xz}H_x - \epsilon_{yz}H_y\right)\right)$ $\lambda'\left(2\phi_1\epsilon_{xy} - \phi_2\epsilon_{x^2-y^2}\right)H_z$
FM irrep		
A_{2g}^-	$g\phi\sigma_z$	$\lambda\phi\epsilon_{A_{1g}}H_z$ $\lambda'\phi\left(\epsilon_{xz}H_x + \epsilon_{yz}H_y\right)$
E_{1g}^-	$g\left(\phi_1\sigma_x + \phi_2\sigma_y\right)$	$\lambda\epsilon_{A_{1g}}\left(\phi_1H_x + \phi_2H_y\right)$ $\lambda'\left(\phi_1\left(\epsilon_{x^2-y^2}H_x + 2\epsilon_{xy}H_y\right) + \phi_2\left(2\epsilon_{xy}H_x - \epsilon_{x^2-y^2}H_y\right)\right)$ $\lambda''\left(\phi_1\epsilon_{xz} + \phi_2\epsilon_{yz}\right)H_z$

Table B.2: The coupling of altermagnetic (AM) and ferromagnetic (FM) order parameters ϕ to fermions and to simultaneous magnetic and strain fields (piezomagnetism) for the hexagonal point group D_{6h} $(6/mmm)$. Note that the hexagonal a axis is parallel to the y axis [28, Table 10.1] so $x^3 - 3xy^2 \in B_{1u}$ and $3x^2y - y^3 \in B_{2u}$. The first column indicates the irrep of ϕ. g and λ are coupling constants, k_α is the momentum, σ_α are Pauli matrices, $\epsilon_{\alpha\beta}$ is the strain tensor, and H_α is the magnetic field. The possibility of having $g' \neq g$ and $\lambda' \neq \lambda$ reflects magnetic anisotropy. $\epsilon_{A_{1g}}$ are the trivially transforming strain components. (Table reprinted from Ref. [17])

where a and a_z are lattice constants and $\mathbf{q}_{2d} = |\mathbf{q}_{2d}|(\cos\phi_q\hat{x} + \sin\phi_q\hat{x})$.

Similarly,

$$\Delta D_y(q) \approx \frac{(k_\mathrm{F}a)^2k_\mathrm{F}}{4\pi v_\mathrm{F}a_z}\left[(1-\cos 2\phi_q)\frac{|\Omega|}{v_\mathrm{F}|\mathbf{q}_{2d}|} + 2\cos 2\phi_q\frac{\Omega^2}{v_\mathrm{F}^2|\mathbf{q}_{2d}|^2}\right], \tag{B.3}$$

$$\Delta D_z(q) \approx \frac{(k_\mathrm{F}a)^2k_\mathrm{F}}{4\pi v_\mathrm{F}a_z}\left[(1+\cos 2\phi_q)\frac{|\Omega|}{v_\mathrm{F}|\mathbf{q}_{2d}|} - 2\cos 2\phi_q\frac{\Omega^2}{v_\mathrm{F}^2|\mathbf{q}_{2d}|^2}\right]. \tag{B.4}$$

Note that the angle dependent terms of ΔD_y and ΔD_z have opposite signs and so they cancel each other.

Combining the above results, we can get

$$\Delta S_\phi^c \approx \int\frac{d^4q}{(2\pi)^4}\frac{1}{2}\phi(q)\left[\frac{g_1^2k_\mathrm{F}(k_\mathrm{F}a)^4}{\pi v_\mathrm{F}a_z}\left(\sin^2 2\theta_q\frac{|\Omega|}{v_\mathrm{F}|\mathbf{q}_{2d}|} + 2\cos 4\theta_q\frac{\Omega^2}{v_\mathrm{F}^2|\mathbf{q}_{2d}|^2}\right) + \frac{g_2^2(k_\mathrm{F}a)^2k_\mathrm{F}}{2\pi v_\mathrm{F}a_z}\frac{|\Omega|}{v_\mathrm{F}|\mathbf{q}_{2d}|}\right]\phi(-q), \tag{B.5}$$

where θ_q is the angle between $\mathbf{q}_{2d}$ and the unit vector $\hat{k}_1 = \frac{\hat{x}+\hat{y}}{2}$ and $\theta_q = \phi_q - \frac{\pi}{4}$.

O_h ($m{-}3m$) point group		
AM irrep	coupling to fermions	piezomagnetic coupling
A_{1g}^-	$g\phi\Big(k_yk_z(k_y^2-k_z^2)\sigma_x - k_xk_z(k_x^2-k_z^2)\sigma_y + k_xk_y(k_x^2-k_y^2)\sigma_z\Big)$	$\lambda\phi\left(\epsilon_{yz}\epsilon_{y^2-z^2}H_x - \epsilon_{xz}\epsilon_{x^2-y^2}H_y + \epsilon_{xy}\epsilon_{x^2-y^2}H_z\right)$
A_{2g}^-	$g\phi\left(k_yk_z\sigma_x + k_xk_z\sigma_y + k_xk_y\sigma_z\right)$	$\lambda\phi\left(\epsilon_{yz}H_x + \epsilon_{xz}H_y + \epsilon_{xy}H_z\right)$
E_g^-	$g\Big(\phi_1\sqrt{3}k_z\Big(k_y\sigma_x - k_x\sigma_y\Big) - \phi_2\left(k_yk_z\sigma_x + k_yk_z\sigma_y - 2k_xk_y\sigma_z\right)\Big)$	$\lambda\left(\phi_1\sqrt{3}\left(\epsilon_{yz}H_x - \epsilon_{xz}H_y\right) - \phi_2\left(\epsilon_{yz}H_x + \epsilon_{xz}H_y - 2\epsilon_{xy}H_z\right)\right)$
T_{2g}^-	$g\Big(\phi_1k_x\Big(k_y\sigma_y - k_z\sigma_z\Big) - \phi_2k_y(k_x\sigma_x - k_z\sigma_z) + \phi_3k_z\Big(k_x\sigma_x - k_y\sigma_y\Big)\Big)$ $g'\Big(\phi_1\left(k_y^2-k_z^2\right)\sigma_x - \phi_2\left(k_x^2-k_z^2\right)\sigma_y + \phi_3\left(k_x^2-k_y^2\right)\sigma_z\Big)$	$\lambda\left(\phi_1\left(\epsilon_{xy}H_y - \epsilon_{xz}H_z\right) - \phi_2\left(\epsilon_{xy}H_x - \epsilon_{yz}H_z\right) + \phi_3\left(\epsilon_{xz}H_x - \epsilon_{yz}H_y\right)\right)$ $\lambda'\left(\phi_1\epsilon_{y^2-z^2}H_x - \phi_2\epsilon_{x^2-z^2}H_y + \phi_3\epsilon_{x^2-y^2}H_z\right)$
FM irrep		
T_{1g}^-	$g\left(\phi_1\sigma_x + \phi_2\sigma_y + \phi_3\sigma_z\right)$	$\lambda\epsilon_{A_{1g}}\left(\phi_1H_x + \phi_2H_y + \phi_3H_z\right)$ $\lambda'\left(\phi_1\left(\epsilon_{xy}H_y + \epsilon_{xz}H_z\right) + \phi_2\left(\epsilon_{xy}H_x + \epsilon_{yz}H_z\right) + \phi_3\left(\epsilon_{xz}H_x + \epsilon_{yz}H_y\right)\right)$ $\lambda''\left(\phi_1\epsilon_{y^2+z^2-2x^2}H_x + \phi_2\epsilon_{x^2+z^2-2y^2}H_y + \phi_3\epsilon_{x^2+y^2-2z^2}H_z\right)$

Table B.3: The coupling of altermagnetic (AM) and ferromagnetic (FM) order parameters ϕ to fermions and to simultaneous magnetic and strain fields (piezomagnetism) for the cubic point group O_h ($m{-}3m$). The first column indicates the irrep of ϕ. g and λ are coupling constants, k_α is the momentum, σ_α are Pauli matrices, $\epsilon_{\alpha\beta}$ is the strain tensor, and H_α is the magnetic field. The possibility of having $g' \neq g$ and $\lambda' \neq \lambda$ reflects magnetic anisotropy. $\epsilon_{A_{1g}}$ are the trivially transforming strain components. The coupling to lattice fermions is deduced by replacing k_α with $\sin k_\alpha$. Notice how the coupling for the altermagnetic order of A_{1g}^-, which forms a dotricontapolar or 32-polar state, is possible only at high order in momentum and strains. (Table reprinted from Ref. [17])

B.2.2 Elastocaloric effect

We expand the mass near the new critical directions

$$\bar{m}^2(\mathbf{q},\mathbf{H}) \approx \begin{cases} \frac{\bar{q}_y^2+\bar{q}_z^2}{\bar{q}_x^2}, & (i)\ |q_x| \gg |q_y|, |q_z| \\ \frac{\bar{q}_x^2+\bar{q}_y^2}{\bar{q}_z^2}, & (ii)\ |q_z| \gg |q_x|, |q_y| \\ 1, & (iii)\ |q_y| \gg |q_x|, |q_z| \end{cases} \tag{B.6}$$

Using the spherical coordinates, setting the largest momentum to be $q\cos\theta$, we obtain following expressions for Eq. (2.102):

$$f^{(i)} \approx 2\int_0^\infty dx \int_0^\infty dq \int_0^{\theta_0}\int_0^{2\pi} d\phi \frac{\theta q^3\sqrt{1-\theta^2\cos^2\phi}x^2\mathrm{csch}^2(x/2)}{q^2[1-\theta^2\cos^2\phi]\Big(q^2[1-(1-c_z^2)\theta^2\cos^2\phi]+\theta^2\Big)^2+x^2\bar{T}^2}, \tag{B.7}$$

$$f^{(ii)} \approx 4\pi\int_0^\infty dx \int_0^{\theta_0} d\theta \int_0^\infty dq \frac{\theta^2 q^3 x^2\mathrm{csch}^2(x/2)}{q^2\theta^2\Big(q^2\theta^2+c_z^2q^2(1-\theta^2)+\theta^2\Big)^2+x^2\bar{T}^2}, \tag{B.8}$$

$$f^{(iii)} \approx 2\int_0^{2\pi} d\phi \int_0^{\theta_0} d\theta \int_0^\infty dq \int_0^\infty dx \frac{x^2q^3\theta\sqrt{1-\theta^2\cos^2\phi}\mathrm{csch}^2(x/2)}{q^2(1-\theta^2\cos^2\phi)(q^2[1-(1-c_z^2)\theta^2\cos^2\phi]+1)^2+x^2\bar{T}^2}. \tag{B.9}$$

At finite temperatures one finds,

$$f^{(ii)} \approx \bar{T}^{-2/3}. \tag{B.10}$$

To evaluate the $f^{(i)}$ and $f^{(iii)}$, we first use Taylor expansion with respect to $\theta^2\cos^2\phi$ and consider only zeroth order terms (Higher order terms give sub-leading contributions). Then,

$$f^{(i)} \approx 2\int_0^\infty dx \int_0^\infty dq \int_0^{\theta_0}\int_0^{2\pi} d\phi \frac{\theta q^3x^2\mathrm{csch}^2(x/2)}{q^2\Big(q^2+\theta^2\Big)^2+x^2\bar{T}^2}, \tag{B.11}$$

$$f^{(iii)} \approx 2\int_0^{2\pi} d\phi \int_0^{\theta_0} d\theta \int_0^\infty dx \int_0^\infty dq \frac{x^2q^3\theta\mathrm{csch}^2(x/2)}{q^2[q^2+1]^2+x^2\bar{T}^2}. \tag{B.12}$$

We can get following qualitative behaviour of the $f^{(i)}$ and $f^{(iii)}$:

$$f^{(i)} \approx \begin{cases} -\log\bar{T} & \bar{T}\ll 1, \\ \bar{T}^{-2/3} & \bar{T}\gg 1 \end{cases}, \quad f^{(iii)} \approx \begin{cases} \text{const}, & \bar{T}\ll 1. \\ \bar{T}^{-2/3}, & \bar{T}\gg 1 \end{cases} \tag{B.13}$$

Combining the contributions from (i), (ii) and (iii) gives the following elastocaloric change:

$$\eta \approx -144\pi b\Gamma_{*,0}T_*\frac{\Big(T/T_*\Big)^{1/3}}{\log\frac{T_0}{T}} \tag{B.14}$$

Such that the $\frac{T^{1/3}}{\log T}$ behaviour is evident not only at the high temperature regime but also at the low energy regime. This is a result of a soft mode along the broken symmetry found when one goes from a spherical to a cylindrical Fermi surface.

Bibliography

[1] V. Baltz, A Hoffmann, S Emori, D.-F. Shao, and T Jungwirth, "Emerging materials in antiferromagnetic spintronics," APL Materials **12** (2024) (cit. on pp. ix, 8, 10).

[2] L. Šmejkal, J. Sinova, and T. Jungwirth, "Emerging research landscape of altermagnetism," Phys. Rev. X **12**, 040501 (2022) (cit. on pp. ix, 5, 7–9, 78).

[3] A. Barman, G. Gubbiotti, S. Ladak, A. O. Adeyeye, M. Krawczyk, J. Gräfe, C. Adelmann, S. Cotofana, A. Naeemi, V. I. Vasyuchka, et al., "The 2021 magnonics roadmap," Journal of Physics: Condensed Matter **33**, 413001 (2021) (cit. on pp. ix, 8).

[4] W.-Y. He, D. Goldhaber-Gordon, and K. T. Law, "Giant orbital magnetoelectric effect and current-induced magnetization switching in twisted bilayer graphene," Nature communications **11**, 1650 (2020) (cit. on pp. ix, x, 13, 98, 107).

[5] C. G. Shull and J. S. Smart, "Detection of antiferromagnetism by neutron diffraction," Physical review **76**, 1256 (1949) (cit. on p. ix).

[6] I. I. Pomeranchuk, "On the stability of a fermi liquid," Sov. Phys. JETP **8**, 361 (1958) (cit. on pp. ix, 10).

[7] R. Qi, R. Shi, Y. Li, Y. Sun, M. Wu, N. Li, J. Du, K. Liu, C. Chen, J. Chen, et al., "Measuring phonon dispersion at an interface," Nature **599**, 399–403 (2021) (cit. on p. ix).

[8] A. Politano, A. R. Marino, D. Campi, D. Farias, R. Miranda, and G. Chiarello, "Elastic properties of a macroscopic graphene sample from phonon dispersion measurements," Carbon **50**, 4903–4910 (2012) (cit. on p. ix).

[9] M Schwoerer-Böhning, A. Macrander, and D. Arms, "Phonon dispersion of diamond measured by inelastic x-ray scattering," Phys. Rev. Lett. **80**, 5572 (1998) (cit. on p. ix).

[10] A. L. Sharpe, E. J. Fox, A. W. Barnard, J. Finney, K. Watanabe, T. Taniguchi, M. A. Kastner, and D. Goldhaber-Gordon, "Evidence of orbital ferromagnetism in twisted bilayer graphene aligned to hexagonal boron nitride," Nano Letters **21**, 4299–4304 (2021) (cit. on pp. x, xi, 5, 10, 11, 97, 98).

[11] Y.-H. Zhang, D. Mao, and T Senthil, "Twisted bilayer graphene aligned with hexagonal boron nitride: anomalous hall effect and a lattice model," Physical Review Research **1**, 033126 (2019) (cit. on pp. x, 11, 13).

[12] C. Tschirhart, M Serlin, H Polshyn, A Shragai, Z Xia, J Zhu, Y Zhang, K Watanabe, T Taniguchi, M. Huber, et al., "Imaging orbital ferromagnetism in a moiré chern insulator," Science **372**, 1323–1327 (2021) (cit. on pp. x, 11, 98).

[13] J. Liu, Z. Ma, J. Gao, and X. Dai, "Quantum valley hall effect, orbital magnetism, and anomalous hall effect in twisted multilayer graphene systems," Phys. Rev. X **9**, 031021 (2019) (cit. on pp. x, 11).

[14] A. E. Böhmer, J.-H. Chu, S. Lederer, and M. Yi, "Nematicity and nematic fluctuations in iron-based superconductors," Nature Physics **18**, 1412–1419 (2022) (cit. on p. x).

[15] R. Fernandes, A. Chubukov, and J Schmalian, "What drives nematic order in iron-based superconductors?" Nature Physics **10**, 97–104 (2014) (cit. on pp. x, 35, 76).

[16] I Paul and M Garst, "Lattice effects on nematic quantum criticality in metals," Phys. Rev. Lett. **118**, 227601 (2017) (cit. on pp. x, xi, 10, 14, 16, 17, 26, 30, 35–40, 44, 47–49, 51, 53, 55, 56, 59, 62, 65, 66, 73).

[17] C. R. Steward, G. Palle, M. Garst, J. Schmalian, and I. Jang, "Elastic quantum criticality in nematics and altermagnets via the elasto-caloric effect," arXiv preprint arXiv:2502.14033 (2025) (cit. on pp. xi, 3, 6, 7, 35, 37–39, 41, 50, 52, 57, 61, 63, 64, 67, 73, 118–120, 139).

[18] K. Takahashi, C. R. W. Steward, M. Ogata, R. M. Fernandes, and J. Schmalian, "Elasto-hall conductivity and the anomalous hall effect in altermagnets," Phys. Rev. B **111**, 184408 (2025) (cit. on pp. xi, 67, 69, 72, 73, 139).

[19] U. Karahasanovic and J. Schmalian, "Elastic coupling and spin-driven nematicity in iron-based superconductors," Phys. Rev. B **93**, 064520 (2016) (cit. on pp. xi, 2, 3, 30, 36, 40, 44–50, 81).

[20] C. R. Steward, R. M. Fernandes, and J. Schmalian, "Dynamic paramagnon-polarons in altermagnets," Phys. Rev. B **108**, 144418 (2023) (cit. on pp. xi, 6, 8, 32, 38, 49, 75, 77, 83–86, 92, 93, 102, 104, 107, 139).

[21] C. R. Steward, R. M. Fernandes, and J. Schmalian, "Dynamic coupling of magnetic collective modes and damped phasons in incommensurate twisted bilayer graphene," (In preparation) (2025) (cit. on pp. xi, 97, 103–107, 139).

[22] H. Ochoa and R. M. Fernandes, "Degradation of phonons in disordered moiré superlattices," Phys. Rev. Lett. **128**, 065901 (2022) (cit. on pp. xi, 4–6, 11, 98, 100, 110).

[23] A. L. Sharpe, E. J. Fox, A. W. Barnard, J. Finney, K. Watanabe, T. Taniguchi, M. Kastner, and D. Goldhaber-Gordon, "Emergent ferromagnetism near three-quarters filling in twisted bilayer graphene," Science **365**, 605–608 (2019) (cit. on pp. xi, 5, 10, 11, 97).

[24] J. Liu and X. Dai, "Theories for the correlated insulating states and quantum anomalous hall effect phenomena in twisted bilayer graphene," Physical Review B **103**, 035427 (2021) (cit. on pp. xi, 5, 10, 97).

[25] X. Bo, F. Li, X. Xu, X. Wan, and Y. Pu, "Calculated magnetic exchange interactions in the van der waals layered magnet CrSBr," New Journal of Physics **25**, 013026 (2023) (cit. on p. 1).

[26] X. Qing, H. Li, C. Zhong, P. Zhou, Z. Dong, and J. Liu, "Magnetism and spin exchange coupling in strained monolayer CrOCl," Physical Chemistry Chemical Physics **22**, 17255–17262 (2020) (cit. on p. 1).

[27] L. D. Landau, E. M. Lifšic, E. M. Lifshitz, A. M. Kosevich, and L. P. Pitaevskii, *Theory of elasticity: volume 7*, Vol. 7 (Elsevier, 1986) (cit. on pp. 2, 79).

[28] M. S. Dresselhaus, G. Dresselhaus, and A. Jorio, *Group theory: application to the physics of condensed matter* (Springer Science & Business Media, 2007) (cit. on pp. 2, 4, 6, 7, 29, 30, 119).

[29] H. Ochoa, "Moiré-pattern fluctuations and electron-phason coupling in twisted bilayer graphene," Phys. Rev. B **100**, 155426 (2019) (cit. on pp. 3, 4, 11, 13, 26, 98–100).

[30] E. Y. Andrei and A. H. MacDonald, "Graphene bilayers with a twist," Nature materials **19**, 1265–1275 (2020) (cit. on p. 3).

[31] R. Bistritzer and A. H. MacDonald, "Moiré bands in twisted double-layer graphene," Proceedings of the National Academy of Sciences **108**, 12233–12237 (2011) (cit. on pp. 3, 11, 97).

[32] D.-h. Ding, W. Yang, C. Hu, and R. Wang, "Generalized elasticity theory of quasicrystals," Phys. Rev. B **48**, 7003 (1993) (cit. on p. 4).

[33] D. Levine, T. Lubensky, S. Ostlund, S. Ramaswamy, P. J. Steinhardt, and J. Toner, "Elasticity and dislocations in pentagonal and icosahedral quasicrystals," Phys. Rev. Lett. **54**, 1520 (1985) (cit. on p. 4).

[34] P. De and R. A. Pelcovits, "Linear elasticity theory of pentagonal quasicrystals," Phys. Rev. B **35**, 8609 (1987) (cit. on p. 4).

[35] J. Gaa, G. Palle, R. M. Fernandes, and J. Schmalian, "Fracton-elasticity duality in twisted moiré superlattices," Physical Review B **104**, 064109 (2021) (cit. on p. 4).

[36] N. N. Nam and M. Koshino, "Lattice relaxation and energy band modulation in twisted bilayer graphene," Phys. Rev. B **96**, 075311 (2017) (cit. on p. 4).

[37] M Widom, "Discussion of phasons in quasicrystals and their dynamics," Philosophical Magazine **88**, 2339–2350 (2008) (cit. on p. 4).

[38] M. Landry et al., "Effective field theory for quasicrystals and phasons dynamics," SciPost Physics **9**, 062 (2020) (cit. on p. 4).

[39] Q. Gao and E. Khalaf, "Symmetry origin of lattice vibration modes in twisted multilayer graphene: phasons versus moiré phonons," Phys. Rev. B **106**, 075420 (2022) (cit. on p. 4).

[40] L. Šmejkal, R. González-Hernández, T. Jungwirth, and J. Sinova, "Crystal time-reversal symmetry breaking and spontaneous hall effect in collinear antiferromagnets," Science Advances **6**, eaaz8809 (2020) (cit. on p. 5).

[41] I. I. Mazin, K. Koepernik, M. D. Johannes, R. González-Hernández, and L. Šmejkal, "Prediction of unconventional magnetism in doped $FeSb_2$," Proceedings of the National Academy of Sciences **118**, e2108924118 (2021) (cit. on p. 5).

[42] I Turek, "Altermagnetism and magnetic groups with pseudoscalar electron spin," Phys. Rev. B **106**, 094432 (2022) (cit. on p. 5).

[43] A. Urru and N. A. Spaldin, "Magnetic octupole tensor decomposition and second-order magnetoelectric effect," Annals of Physics **447**, 168964 (2022) (cit. on p. 5).

[44] S. Bhowal and N. A. Spaldin, "Magnetic octupoles as the order parameter for unconventional antiferromagnetism," arXiv preprint arXiv:2212.03756 (2022) (cit. on pp. 5, 76, 80).

[45] I. Mazin, "Altermagnetism in MnTe: origin, predicted manifestations, and routes to detwinning," Phys. Rev. B **107**, L100418 (2023) (cit. on p. 5).

[46] Z. Feng, X. Zhou, L. Šmejkal, L. Wu, Z. Zhu, H. Guo, R. González-Hernández, X. Wang, H. Yan, P. Qin, et al., "An anomalous hall effect in altermagnetic ruthenium dioxide," Nature Electronics, 1–9 (2022) (cit. on p. 5).

[47] S. Voleti, D. D. Maharaj, B. D. Gaulin, G. Luke, and A. Paramekanti, "Multipolar magnetism in d-orbital systems: crystal field levels, octupolar order, and orbital loop currents," Phys. Rev. B **101**, 155118 (2020) (cit. on p. 5).

[48] D. F. Mosca, L. V. Pourovskii, and C. Franchini, "Modeling magnetic multipolar phases in density functional theory," Phys. Rev. B **106**, 035127 (2022) (cit. on p. 5).

[49] R. G. Betancourt, J Zubáč, R Gonzalez-Hernandez, K Geishendorf, Z Šobáň, G Springholz, K Olejník, L Šmejkal, J Sinova, T Jungwirth, et al., "Spontaneous anomalous hall effect arising from an unconventional compensated magnetic phase in a semiconductor," Phys. Rev. Lett. **130**, 036702 (2023) (cit. on p. 5).

[50] R Winkler and U Zülicke, "Theory of electric, magnetic, and toroidal polarizations in crystalline solids with applications to hexagonal lonsdaleite and cubic diamond," Phys. Rev. B **107**, 155201 (2023) (cit. on p. 5).

[51] L.-D. Yuan, Z. Wang, J.-W. Luo, and A. Zunger, "Prediction of low-z collinear and noncollinear antiferromagnetic compounds having momentum-dependent spin splitting even without spin-orbit coupling," Phys. Rev. Materials **5**, 014409 (2021) (cit. on p. 5).

[52] P. Liu, J. Li, J. Han, X. Wan, and Q. Liu, "Spin-group symmetry in magnetic materials with negligible spin-orbit coupling," Phys. Rev. X **12**, 021016 (2022) (cit. on pp. 5, 7).

[53] H Bai, Y. Zhang, Y. Zhou, P Chen, C. Wan, L Han, W. Zhu, S. Liang, Y. Su, X. Han, et al., "Efficient spin-to-charge conversion via altermagnetic spin splitting effect in antiferromagnet RuO2," Phys. Rev. Lett. **130**, 216701 (2023) (cit. on p. 5).

[54] L. Šmejkal, A. H. MacDonald, J. Sinova, S. Nakatsuji, and T. Jungwirth, "Anomalous hall antiferromagnets," Nature Reviews Materials **7**, 482–496 (2022) (cit. on p. 5).

[55] J. Yang, Z.-X. Liu, and C. Fang, "Symmetry invariants and classes of quasiparticles in magnetically ordered systems having weak spin-orbit coupling," Nature Communications **15**, 10203 (2024) (cit. on p. 5).

[56] Y. Jiang, Z. Song, T. Zhu, Z. Fang, H. Weng, Z.-X. Liu, J. Yang, and C. Fang, "Enumeration of spin-space groups: toward a complete description of symmetries of magnetic orders," Phys. Rev. X **14**, 031039 (2024) (cit. on p. 5).

[57] P. M. Chaikin, T. C. Lubensky, and T. A. Witten, *Principles of condensed matter physics*, Vol. 10 (Cambridge university press Cambridge, 1995) (cit. on pp. 6, 13–15, 19, 22, 36, 45, 89).

[58] R. M. Fernandes, V. S. de Carvalho, T. Birol, and R. G. Pereira, "Topological transition from nodal to nodeless zeeman splitting in altermagnets," Phys. Rev. B **109**, 024404 (2024) (cit. on pp. 6, 7, 10, 38, 40, 41, 70, 80).

[59] S. Hayami, Y. Yanagi, and H. Kusunose, "Bottom-up design of spin-split and reshaped electronic band structures in antiferromagnets without spin-orbit coupling: procedure on the basis of augmented multipoles," Phys. Rev. B **102**, 144441 (2020) (cit. on pp. 8, 78).

[60] L. Bai, W. Feng, S. Liu, L. Šmejkal, Y. Mokrousov, and Y. Yao, "Altermagnetism: exploring new frontiers in magnetism and spintronics," Advanced Functional Materials, 2409327 (2024) (cit. on pp. 8, 9).

[61] S. Das, D. Suri, and A. Soori, "Transport across junctions of altermagnets with normal metals and ferromagnets," Journal of Physics: Condensed Matter **35**, 435302 (2023) (cit. on pp. 8, 10).

[62] C. Sun and J. Linder, "Spin pumping from a ferromagnetic insulator into an altermagnet," Phys. Rev. B **108**, L140408 (2023) (cit. on pp. 8, 10).

[63] A. Corticelli, R. Moessner, and P. A. McClarty, "Spin-space groups and magnon band topology," Phys. Rev. B **105**, 064430 (2022) (cit. on p. 8).

[64] O Gomonay, V. Kravchuk, R Jaeschke-Ubiergo, K. Yershov, T Jungwirth, L Šmejkal, J. v. d. Brink, and J Sinova, "Structure, control, and dynamics of altermagnetic textures," npj Spintronics **2**, 35 (2024) (cit. on p. 8).

[65] I. I. Mazin, "Notes on altermagnetism and superconductivity," arXiv preprint arXiv:2203.05000, `https://doi.org/10.48550/arXiv.2203.05000` (2022) (cit. on p. 9).

[66] D. Zhu, Z.-Y. Zhuang, Z. Wu, and Z. Yan, "Topological superconductivity in two-dimensional altermagnetic metals," Phys. Rev. B **108**, 184505 (2023) (cit. on p. 9).

[67] M. Papaj, "Andreev reflection at the altermagnet-superconductor interface," Phys. Rev. B **108**, L060508 (2023) (cit. on p. 9).

[68] C. Sun, A. Brataas, and J. Linder, "Andreev reflection in altermagnets," Phys. Rev. B **108**, 054511 (2023) (cit. on p. 9).

[69] J. A. Ouassou, A. Brataas, and J. Linder, "Dc josephson effect in altermagnets," Phys. Rev. Lett. **131**, 076003 (2023) (cit. on p. 9).

[70] B. Lu, K. Maeda, H. Ito, K. Yada, and Y. Tanaka, "φ Josephson junction induced by altermagnetism," Phys. Rev. Lett. **133**, 226002 (2024) (cit. on p. 9).

[71] S.-B. Zhang, L.-H. Hu, and T. Neupert, "Finite-momentum cooper pairing in proximitized altermagnets," Nature Communications **15**, 1801 (2024) (cit. on p. 9).

[72] O. Fedchenko, J. Minár, A. Akashdeep, S. W. DSouza, D. Vasilyev, O. Tkach, L. Odenbreit, Q. Nguyen, D. Kutnyakhov, N. Wind, et al., "Observation of time-reversal symmetry breaking in the band structure of altermagnetic ruO_2," Science advances **10**, eadj4883 (2024) (cit. on p. 10).

[73] J. Song, S. H. Lee, S. Kang, D. Kim, J. H. Jeong, T. Oh, S. Lee, S. Lee, S. Lee, K.-H. Ahn, et al., "Spin-orbit coupling driven magnetic response in altermagnetic ruO_2," Small, 2407722 (2024) (cit. on p. 10).

[74] T Osumi, S Souma, T Aoyama, K Yamauchi, A Honma, K Nakayama, T Takahashi, K. Ohgushi, and T. Sato, "Observation of a giant band splitting in altermagnetic mnTe," Phys. Rev. B **109**, 115102 (2024) (cit. on p. 10).

[75] A Hariki, A Dal Din, O. Amin, T Yamaguchi, A Badura, D Kriegner, K. Edmonds, R. Campion, P Wadley, D Backes, et al., "X-ray magnetic circular dichroism in altermagnetic α-MnTe," Phys. Rev. Lett. **132**, 176701 (2024) (cit. on p. 10).

[76] S. Sorn and A. S. Patri, "Signatures of hidden octupolar order from nonlinear hall effects," Phys. Rev. B **110**, 125127 (2024) (cit. on pp. 10, 67).

[77] Z. Liu, Y. Shi, Q. Jiang, E. W. Rosenberg, J. M. DeStefano, J. Liu, C. Hu, Y. Zhao, Z. Wang, Y. Yao, et al., "Absence of E_{2g} nematic instability and dominant A_{1g} response in the kagome metal CsV_3Sb_5," Phys. Rev. X **14**, 031015 (2024) (cit. on pp. 10, 33, 110).

[78] M. S. Ikeda, T. Worasaran, E. W. Rosenberg, J. C. Palmstrom, S. A. Kivelson, and I. R. Fisher, "Elastocaloric signature of nematic fluctuations," Proceedings of the National Academy of Sciences **118**, e2105911118 (2021) (cit. on pp. 10, 33, 34, 110).

[79] E. S. Morell, J. Correa, P Vargas, M Pacheco, and Z Barticevic, "Flat bands in slightly twisted bilayer graphene: tight-binding calculations," Phys. Rev. B **82**, 121407 (2010) (cit. on pp. 11, 97).

[80] Y. Cao, V. Fatemi, S. Fang, K. Watanabe, T. Taniguchi, E. Kaxiras, and P. Jarillo-Herrero, "Unconventional superconductivity in magic-angle graphene superlattices," Nature **556**, 43–50 (2018) (cit. on p. 11).

[81] M. Yankowitz, S. Chen, H. Polshyn, Y. Zhang, K Watanabe, T Taniguchi, D. Graf, A. F. Young, and C. R. Dean, "Tuning superconductivity in twisted bilayer graphene," Science **363**, 1059–1064 (2019) (cit. on p. 11).

[82] Y. Cao, V. Fatemi, A. Demir, S. Fang, S. L. Tomarken, J. Y. Luo, J. D. Sanchez-Yamagishi, K. Watanabe, T. Taniguchi, E. Kaxiras, et al., "Correlated insulator behaviour at half-filling in magic-angle graphene superlattices," Nature **556**, 80–84 (2018) (cit. on p. 11).

[83] S. Bhowmik, B. Ghawri, N. Leconte, S. Appalakondaiah, M. Pandey, P. S. Mahapatra, D. Lee, K Watanabe, T Taniguchi, J. Jung, et al., "Broken-symmetry states at half-integer band fillings in twisted bilayer graphene," Nature Physics **18**, 639–643 (2022) (cit. on p. 11).

[84] M Serlin, C. Tschirhart, H Polshyn, Y Zhang, J Zhu, K Watanabe, T Taniguchi, L Balents, and A. Young, "Intrinsic quantized anomalous hall effect in a moiré heterostructure," Science **367**, 900–903 (2020) (cit. on pp. 11, 13, 97).

[85] J. Liu and X. Dai, "Orbital magnetic states in moiré graphene systems," Nature Reviews Physics **3**, 367–382 (2021) (cit. on pp. 11, 12, 98).

[86] K. v. Klitzing, G. Dorda, and M. Pepper, "New method for high-accuracy determination of the fine-structure constant based on quantized hall resistance," Phys. Rev. Lett. **45**, 494 (1980) (cit. on p. 12).

[87] D. Xiao, M.-C. Chang, and Q. Niu, "Berry phase effects on electronic properties," Reviews of modern physics **82**, 1959–2007 (2010) (cit. on p. 12).

[88] J. Ge, Y. Liu, J. Li, H. Li, T. Luo, Y. Wu, Y. Xu, and J. Wang, "High-chern-number and high-temperature quantum hall effect without landau levels," National science review **7**, 1280–1287 (2020) (cit. on p. 13).

[89] C.-Z. Chang, C.-X. Liu, and A. H. MacDonald, "Colloquium: quantum anomalous hall effect," Reviews of Modern Physics **95**, 011002 (2023) (cit. on p. 13).

[90] N. Bultinck, S. Chatterjee, and M. P. Zaletel, "Anomalous hall ferromagnetism in twisted bilayer graphene," arXiv, arXiv–1901 (2019) (cit. on p. 13).

[91] T. Cea, P. A. Pantaleón, and F. Guinea, "Band structure of twisted bilayer graphene on hexagonal boron nitride," Phys. Rev. B **102**, 155136 (2020) (cit. on p. 13).

[92] J. Shi, J. Zhu, and A. MacDonald, "Moiré commensurability and the quantum anomalous hall effect in twisted bilayer graphene on hexagonal boron nitride," Phys. Rev. B **103**, 075122 (2021) (cit. on p. 13).

[93] G. Giovannetti, P. A. Khomyakov, G. Brocks, P. J. Kelly, and J. Van Den Brink, "Substrate-induced band gap in graphene on hexagonal boron nitride: ab initio density functional calculations," Physical Review B **76**, 073103 (2007) (cit. on p. 13).

[94] P. San-Jose, A Gutiérrez-Rubio, M. Sturla, and F. Guinea, "Spontaneous strains and gap in graphene on boron nitride," Phys. Rev. B **90**, 075428 (2014) (cit. on p. 13).

[95] C. Liu, Y. Wang, M. Yang, J. Mao, H. Li, Y. Li, J. Li, H. Zhu, J. Wang, L. Li, et al., "Magnetic-field-induced robust zero hall plateau state in $MnBi_2Te_4$ chern insulator," Nature Communications **12**, 4647 (2021) (cit. on p. 13).

[96] S. Sachdev, "Quantum phase transitions," Encyclopedia of Mathematical Physics. USA (2004) (cit. on p. 13).

[97] S. Sachdev, "Quantum phase transitions," Physics world **12**, 33 (1999) (cit. on pp. 14, 76).

[98] T. Andrews, "Xviii. the bakerian lecture.on the continuity of the gaseous and liquid states of matter," Philosophical Transactions of the Royal Society of London, 575–590 (1869) (cit. on p. 14).

[99] T. Vojta, "Quantum phase transitions in electronic systems," Annalen der Physik **512**, 403–440 (2000) (cit. on pp. 14, 18).

[100] P. Curie, *Propriétés magnétiques des corps a diverses températures*, 4 (Gauthier-Villars et fils, 1895) (cit. on p. 14).

[101] H. v. Löhneysen, C Pfleiderer, T Pietrus, O Stockert, and B Will, "Pressure versus magnetic-field tuning of a magnetic quantum phase transition," Phys. Rev. B **63**, 134411 (2001) (cit. on p. 14).

[102] G. Gehring, "Pressure-induced quantum phase transitions," Europhysics Letters **82**, 60004 (2008) (cit. on p. 14).

[103] Z. Weng, M Smidman, L Jiao, X. Lu, and H. Yuan, "Multiple quantum phase transitions and superconductivity in ce-based heavy fermions," Reports on Progress in Physics **79**, 094503 (2016) (cit. on p. 14).

[104] E Helgren, L Zeng, K Burch, D Basov, and F Hellman, "Field-and concentration-tuned scaling of a quantum phase transition in a magnetically doped semiconductor," Phys. Rev. B **73**, 155201 (2006) (cit. on p. 14).

[105] M. Vojta, "Quantum phase transitions," Reports on Progress in Physics **66**, 2069 (2003) (cit. on pp. 14, 16–18, 76).

[106] E.-A. Kim, M. J. Lawler, P. Oreto, S. Sachdev, E. Fradkin, and S. A. Kivelson, "Theory of the nodal nematic quantum phase transition in superconductors," Phys. Rev. B **77**, 184514 (2008) (cit. on p. 14).

[107] Z. Zhou, D. Wang, Z. Y. Meng, Y. Wang, and C. Wu, "Mott insulating states and quantum phase transitions of correlated $SU(2N)$ dirac fermions," Phys. Rev. B **93**, 245157 (2016) (cit. on p. 14).

[108] J. Ostmeyer, E. Berkowitz, S. Krieg, T. A. Lähde, T. Luu, and C. Urbach, "Semimetal–mott insulator quantum phase transition of the hubbard model on the honeycomb lattice," Phys. Rev. B **102**, 245105 (2020) (cit. on p. 14).

[109] M. Bernaschi, I. González-Adalid Pemartín, V. Martín-Mayor, and G. Parisi, "The quantum transition of the two-dimensional ising spin glass," Nature **631**, 749–754 (2024) (cit. on p. 14).

[110] T. M. Nieuwenhuizen and F. Ritort, "Quantum phase transition in spin glasses with multi-spin interactions," Physica A: Statistical Mechanics and its Applications **250**, 8–45 (1998) (cit. on p. 14).

[111] Y. Wang, A. Abanov, B. L. Altshuler, E. A. Yuzbashyan, and A. V. Chubukov, "Superconductivity near a quantum-critical point: the special role of the first matsubara frequency," Phys. Rev. Lett. **117**, 157001 (2016) (cit. on p. 14).

[112] S. L. Sondhi, S. Girvin, J. Carini, and D. Shahar, "Continuous quantum phase transitions," Reviews of modern physics **69**, 315 (1997) (cit. on pp. 14, 15).

[113] T. H. Hsieh, "From d-dimensional quantum to d+ 1-dimensional classical systems," Student Review (2016) (cit. on p. 15).

[114] L. D. Landau et al., "On the theory of phase transitions," Zh. eksp. teor. Fiz **7**, 926 (1937) (cit. on p. 15).

[115] P. Wölfle, "Quasiparticles in condensed matter systems," Reports on Progress in Physics **81**, 032501 (2018) (cit. on pp. 16, 17).

[116] V. Oganesyan, S. A. Kivelson, and E. Fradkin, "Quantum theory of a nematic fermi fluid," Phys. Rev. B **64**, 195109 (2001) (cit. on pp. 17, 35).

[117] W. Metzner, D. Rohe, and S. Andergassen, "Soft fermi surfaces and breakdown of fermi-liquid behavior," Phys. Rev. Lett. **91**, 066402 (2003) (cit. on pp. 17, 35, 55).

[118] M. Garst and A. V. Chubukov, "Electron self-energy near a nematic quantum critical point," Phys. Rev. B **81**, 235105 (2010) (cit. on pp. 17, 55).

[119] H. v. Löhneysen, A. Rosch, M. Vojta, and P. Wölfle, "Fermi-liquid instabilities at magnetic quantum phase transitions," Rev. Mod. Phys. **79**, 1015–1075 (2007) (cit. on p. 17).

[120] L. P. Kadanoff, "Scaling laws for ising models near T_c," Physics Physique Fizika **2**, 263 (1966) (cit. on p. 17).

[121] A. Koberinski and D. Fraser, "Renormalization group methods and the epistemology of effective field theories," Studies in History and Philosophy of Science **98**, 1428 (2023) (cit. on p. 18).

[122] L. Bulaevskii, C. Batista, M. Mostovoy, and D. Khomskii, "Electronic orbital currents and polarization in mott insulators," Phys. Rev. B **78**, 024402 (2008) (cit. on p. 19).

[123] A. Altland and B. D. Simons, *Condensed matter field theory* (Cambridge university press, 2010) (cit. on pp. 19, 20).

[124] A. C. D'Auria, L De Cesare, and I Rabuffo, "Low-temperature quantum critical behaviour of systems with transverse ising-like intrinsic dynamics," Physica A: Statistical Mechanics and its Applications **327**, 442–460 (2003) (cit. on pp. 23, 90, 92, 106).

[125] J. Bardeen, L. N. Cooper, and J. R. Schrieffer, "Theory of superconductivity," Physical review **108**, 1175 (1957) (cit. on p. 25).

[126] M. L. Kulić, "Interplay of electron–phonon interaction and strong correlations: the possible way to high-temperature superconductivity," Physics Reports **338**, 1–264 (2000) (cit. on p. 25).

[127] A. Levchenko and J. Schmalian, "Transport properties of strongly coupled electron–phonon liquids," Annals of Physics **419**, 168218 (2020) (cit. on p. 25).

[128] Y. Quan, S. Yue, and B. Liao, "Impact of electron-phonon interaction on thermal transport: a review," Nanoscale and Microscale Thermophysical Engineering **25**, 73–90 (2021) (cit. on p. 25).

[129] M. Greiter, V. Schnells, and R. Thomale, "The 1d ising model and the topological phase of the kitaev chain," Annals of Physics **351**, 1026–1033 (2014) (cit. on p. 26).

[130] B. Flebus, K. Shen, T. Kikkawa, K.-i. Uchida, Z. Qiu, E. Saitoh, R. A. Duine, and G. E. Bauer, "Magnon-polaron transport in magnetic insulators," Phys. Rev. B **95**, 144420 (2017) (cit. on pp. 26, 76, 78, 83).

[131] H. T. Simensen, R. E. Troncoso, A. Kamra, and A. Brataas, "Magnon-polarons in cubic collinear antiferromagnets," Phys. Rev. B **99**, 064421 (2019) (cit. on pp. 26, 76, 78).

[132] G. Go, S. K. Kim, and K.-J. Lee, "Topological magnon-phonon hybrid excitations in two-dimensional ferromagnets with tunable chern numbers," Phys. Rev. Lett. **123**, 237207 (2019) (cit. on pp. 26, 76).

[133] S. Zhang, G. Go, K.-J. Lee, and S. K. Kim, "Su(3) topology of magnon-phonon hybridization in 2d antiferromagnets," Phys. Rev. Lett. **124**, 147204 (2020) (cit. on pp. 26, 76).

[134] T. Aoyama and K. Ohgushi, "Piezomagnetic properties in altermagnetic MnTe," arXiv preprint arXiv:2305.14786 (2023) (cit. on pp. 26, 38, 76).

[135] A. S. Patri, A. Sakai, S. Lee, A. Paramekanti, S. Nakatsuji, and Y. B. Kim, "Unveiling hidden multipolar orders with magnetostriction," Nature Communications **10**, 4092 (2019) (cit. on pp. 26, 38, 76).

[136] M. E. Sorensen and I. R. Fisher, "Proposal for methods to measure the octupole susceptibility in certain cubic pr compounds," Phys. Rev. B **103**, 155106 (2021) (cit. on pp. 26, 76).

[137] G. Palle, C. Hicks, R. Valentí, Z. Hu, Y.-S. Li, A. Rost, M. Nicklas, A. P. Mackenzie, and J. Schmalian, "Constraints on the superconducting state of Sr_2RuO_4 from elastocaloric measurements," Phys. Rev. B **108**, 094516 (2023) (cit. on p. 27).

[138] T Moriya, "Piezomagnetism in coF_2," Journal of Physics and Chemistry of Solids **11**, 73–77 (1959) (cit. on p. 31).

[139] J. M. Link, D. E. Sheehy, B. N. Narozhny, and J. Schmalian, "Elastic response of the electron fluid in intrinsic graphene: the collisionless regime," Phys. Rev. B **98**, 195103 (2018) (cit. on pp. 32, 33).

[140] P. Rao and B. Bradlyn, "Hall viscosity in quantum systems with discrete symmetry: point group and lattice anisotropy," Phys. Rev. X **10**, 021005 (2020) (cit. on pp. 32, 33, 76).

[141] J. Tušek, K. Engelbrecht, L. Mañosa, E. Vives, and N. Pryds, "Understanding the thermodynamic properties of the elastocaloric effect through experimentation and modelling," Shape Memory and Superelasticity **2**, 317–329 (2016) (cit. on p. 33).

[142] Y.-S. Li, M. Garst, J. Schmalian, S. Ghosh, N. Kikugawa, D. A. Sokolov, C. W. Hicks, F. Jerzembeck, M. S. Ikeda, Z. Hu, et al., "Elastocaloric determination of the phase diagram of Sr_2RuO_4," Nature **607**, 276–280 (2022) (cit. on p. 33).

[143] Y. Yao, R. Willa, T. Lacmann, S.-M. Souliou, M. Frachet, K. Willa, M. Merz, F. Weber, C. Meingast, R. Heid, et al., "An electronic nematic liquid in $baNi_2As_2$," Nature communications **13**, 4535 (2022) (cit. on p. 34).

[144] A. Othonos, "Probing ultrafast carrier and phonon dynamics in semiconductors," Journal of applied physics **83**, 1789–1830 (1998) (cit. on p. 34).

[145] H.-Y. Kee, E. H. Kim, and C.-H. Chung, "Signatures of an electronic nematic phase at the isotropic-nematic phase transition," Phys. Rev. B **68**, 245109 (2003) (cit. on p. 35).

[146] L. DellAnna and W. Metzner, "Electrical resistivity near pomeranchuk instability in two dimensions," Phys. Rev. Lett. **98**, 136402 (2007) (cit. on p. 35).

[147] M. Zacharias, P. Wölfle, and M. Garst, "Multiscale quantum criticality: pomeranchuk instability in isotropic metals," Phys. Rev. B **80**, 165116 (2009) (cit. on p. 35).

[148] E. Fradkin, S. A. Kivelson, M. J. Lawler, J. P. Eisenstein, and A. P. Mackenzie, "Nematic fermi fluids in condensed matter physics," Annu. Rev. Condens. Matter Phys. **1**, 153–178 (2010) (cit. on p. 35).

[149] M. A. Metlitski and S. Sachdev, "Quantum phase transitions of metals in two spatial dimensions. i. ising-nematic order," Phys. Rev. B **82**, 075127 (2010) (cit. on p. 35).

[150] L. Nie, G. Tarjus, and S. A. Kivelson, "Quenched disorder and vestigial nematicity in the pseudogap regime of the cuprates," Proceedings of the National Academy of Sciences **111**, 7980–7985 (2014) (cit. on p. 35).

[151] A. Klein, A. V. Chubukov, Y. Schattner, and E. Berg, "Normal state properties of quantum critical metals at finite temperature," Phys. Rev. X **10**, 031053 (2020) (cit. on p. 35).

[152] C. M. Varma, P. B. Littlewood, S. Schmitt-Rink, E. Abrahams, and A. E. Ruckenstein, "Phenomenology of the normal state of Cu-O high-temperature superconductors," Phys. Rev. Lett. **63**, 1996–1999 (1989) (cit. on p. 36).

[153] R. M. Fernandes, L. H. VanBebber, S. Bhattacharya, P. Chandra, V. Keppens, D. Mandrus, M. A. McGuire, B. C. Sales, A. S. Sefat, and J. Schmalian, "Effects of nematic fluctuations on the elastic properties of iron arsenide superconductors," Phys. Rev. Lett. **105**, 157003 (2010) (cit. on pp. 36, 42).

[154] A. Böhmer, P Burger, F Hardy, T Wolf, P Schweiss, R Fromknecht, M Reinecker, W Schranz, and C Meingast, "Nematic susceptibility of hole-doped and electron-doped $BaFe_2As_2$ iron-based superconductors from shear modulus measurements," Phys. Rev. Lett. **112**, 047001 (2014) (cit. on p. 36).

[155] T. Goto, R. Kurihara, K. Araki, K. Mitsumoto, M. Akatsu, Y. Nemoto, S. Tatematsu, and M. Sato, "Quadrupole effects of layered iron pnictide superconductor Ba $(Fe_{0.9}Co_{0.1}))2As_2$," Journal of the Physical Society of Japan **80**, 073702 (2011) (cit. on p. 36).

[156] A. Levanyuk and A. Sobyanin, "Second-order phase transitions without divergences in the second derivatives of the thermodynamic potential," ZhETF Pisma Redaktsiiu **11**, 540 (1970) (cit. on p. 36).

[157] R. A. Cowley, "Acoustic phonon instabilities and structural phase transitions," Phys. Rev. B **13**, 4877–4885 (1976) (cit. on pp. 36, 74).

[158] M. S. Ikeda, J. A. Straquadine, A. T. Hristov, T. Worasaran, J. C. Palmstrom, M. Sorensen, P. Walmsley, and I. R. Fisher, "AC Elastocaloric effect as a probe for thermodynamic signatures of continuous phase transitions," Review of Scientific Instruments **90**, 10.1063/1.5099924 (2019) (cit. on p. 37).

[159] H.-Y. Ma, M. Hu, N. Li, J. Liu, W. Yao, J.-F. Jia, and J. Liu, "Multifunctional antiferromagnetic materials with giant piezomagnetism and noncollinear spin current," Nature communications **12**, 2846 (2021) (cit. on pp. 38, 66, 93).

[160] P. A. McClarty and J. G. Rau, "Landau theory of altermagnetism," Phys. Rev. Lett. **132**, 176702 (2024) (cit. on p. 38).

[161] K. V. Yershov, V. P. Kravchuk, M. Daghofer, and J. van den Brink, "Fluctuation-induced piezomagnetism in local moment altermagnets," Phys. Rev. B **110**, 144421 (2024) (cit. on p. 38).

[162] M. Zacharias, I. Paul, and M. Garst, "Quantum critical elasticity," Phys. Rev. Lett. **115**, 025703 (2015) (cit. on pp. 38, 44, 47, 66).

[163] T. Aoyama and K. Ohgushi, "Piezomagnetic properties in altermagnetic mnte," Phys. Rev. Mat. **8**, L041402 (2024) (cit. on pp. 44, 65).

[164] S. Simayi, K. Sakano, H. Takezawa, M. Nakamura, Y. Nakanishi, K. Kihou, M. Nakajima, C.-H. Lee, A. Iyo, H. Eisaki, et al., "Strange inter-layer properties of ba$(Fe_{1-x}Co_x)2As_2$ appearing in ultrasonic measurements," Journal of the Physical Society of Japan **82**, 114604 (2013) (cit. on p. 47).

[165] R. Melcher, "Elastic properties of MnF_2," Phys. Rev. B **2**, 733 (1970) (cit. on p. 47).

[166] L. Zhu, M. Garst, A. Rosch, and Q. Si, "Universally diverging grüneisen parameter and the magnetocaloric effect close to quantum critical points," Phys. Rev. Lett. **91**, 066404 (2003) (cit. on pp. 60, 65).

[167] A. A. Abrikosov, L. P. Gorkov, and I. E. Dzyaloshinski, *Methods of quantum field theory in statistical physics* (Courier Corporation, 2012) (cit. on pp. 61, 62).

[168] F Schwabl, "Propagation of sound at continuous structural phase transitions," Journal of Statistical Physics **39**, 719–737 (1985) (cit. on p. 66).

[169] M. Shapiro, P. Hlobil, A. Hristov, A. V. Maharaj, and I. Fisher, "Symmetry constraints on the elastoresistivity tensor," Physical Review B **92**, 235147 (2015) (cit. on pp. 68, 80).

[170] M. E. Sorensen and I. R. Fisher, "Proposal for methods to measure the octupole susceptibility in certain cubic Pr compounds," Phys. Rev. B **103**, 155106 (2021) (cit. on p. 68).

[171] Y. Sun, S. E. Thompson, and T. Nishida, "Strain Effect in Semiconductors: Theory and Device Applications," Springer Science & Business Media (2009) (cit. on p. 68).

[172] H.-H. Kuo, M. C. Shapiro, S. C. Riggs, and I. R. Fisher, "Measurement of the elastoresistivity coefficients of the underdoped iron arsenide $Ba(Fe_{0.975}Co_{0.025})_2As_2$," Phys. Rev. B **88**, 085113 (2013) (cit. on p. 68).

[173] L. Nie, K. Sun, W. Ma, D. Song, L. Zheng, Z. Liang, P. Wu, F. Yu, J. Li, M. Shan, et al., "Charge-density-wave-driven electronic nematicity in a kagome superconductor," Nature **604**, 59–64 (2022) (cit. on p. 68).

[174] M Frachet, P Wiecki, T Lacmann, S. Souliou, K Willa, C Meingast, M Merz, A.-A. Haghighirad, M Le Tacon, and A. Böhmer, "Elastoresistivity in the incommensurate charge density wave phase of $BaNi_2(As_{1-x}P_x)_2$," npj Quantum Materials **7**, 115 (2022) (cit. on p. 68).

[175] A. G. Singh, M. D. Bachmann, J. J. Sanchez, A. Pandey, A. Kapitulnik, J. W. Kim, P. J. Ryan, S. A. Kivelson, and I. R. Fisher, "Emergent tetragonality in a fundamentally orthorhombic material," Science Advances **10**, eadk3321 (2024) (cit. on p. 68).

[176] H. Jahn, "Note on the bhagavantam–suranarayana method of enumerating the physical constants of crystals," Acta Crystallographica **2**, 30–33 (1949) (cit. on p. 71).

[177] H. Schiff, P. McClarty, J. G. Rau, and J. Romhanyi, "Collinear Altermagnets and their Landau Theories," arXiv:2412.18025 (2024) (cit. on p. 71).

[178] H. T. Stokes, D. M. Hatch, and B. J. Campbell, *ISOTROPY Software Suite, iso.byu.edu*, version 2.1.2, June 1, 2022 (cit. on p. 71).

[179] M. I. Aroyo, J. M. Perez-Mato, C. Capillas, E. Kroumova, S. Ivantchev, G. Madariaga, A. Kirov, and H. Wondratschek, "Bilbao Crystallographic Server: I. Databases and crystallographic computing programs," Zeitschrift für Kristallographie-Crystalline Materials **221**, 15–27 (2006) (cit. on p. 71).

[180] M. I. Aroyo, A. Kirov, C. Capillas, J. Perez-Mato, and H. Wondratschek, "Bilbao Crystallographic Server. II. Representations of crystallographic point groups and space groups," Acta Crystallographica Section A: Foundations of Crystallography **62**, 115–128 (2006) (cit. on p. 71).

[181] Y. Jiang, X. Zhang, H. Bai, Y. Tian, B. Zhang, W.-J. Gong, and X. Kong, "Strain-engineering spin-valley locking effect in altermagnetic monolayer with multipiezo properties," Applied Physics Letters **126** (2025) (cit. on p. 71).

[182] R. Caciuffo, P Santini, S Carretta, G Amoretti, A Hiess, N. Magnani, L.-P. Regnault, and G. Lander, "Multipolar, magnetic, and vibrational lattice dynamics in the low-temperature phase of uranium dioxide," Phys. Rev. B **84**, 104409 (2011) (cit. on p. 76).

[183] B. H. Rimmler, B. K. Hazra, B. Pal, K. Mohseni, J. M. Taylor, A. Bedoya-Pinto, H. Deniz, M. R. Tangi, I. Kostanovskiy, C. Luo, et al., "Atomic displacements enabling the observation of the anomalous hall effect in a non-collinear antiferromagnet," Advanced Materials, 2209616 (2023) (cit. on p. 76).

[184] T. Kikkawa, K. Shen, B. Flebus, R. A. Duine, K.-i. Uchida, Z. Qiu, G. E. Bauer, and E. Saitoh, "Magnon polarons in the spin seebeck effect," Phys. Rev.Lett. **117**, 207203 (2016) (cit. on p. 76).

[185] C. Fang, H. Yao, W.-F. Tsai, J. Hu, and S. A. Kivelson, "Theory of electron nematic order in LaFeAsO," Phys. Rev. B **77**, 224509 (2008) (cit. on p. 76).

[186] R. A. Borzi, S. A. Grigera, J Farrell, R. Perry, S. Lister, S. Lee, D. Tennant, Y. Maeno, and A. P. Mackenzie, "Formation of a nematic fluid at high fields in Sr3Ru2o7," Science **315**, 214–217 (2007) (cit. on p. 76).

[187] G. E. Volovik, "Superfluid properties of 3He-A," Soviet Physics Uspekhi **27**, 363 (1984) (cit. on p. 76).

[188] J. Avron, R. Seiler, and P. G. Zograf, "Viscosity of quantum hall fluids," Phys. Rev. Lett. **75**, 697 (1995) (cit. on p. 76).

[189] T. L. Hughes, R. G. Leigh, and E. Fradkin, "Torsional response and dissipationless viscosity in topological insulators," Phys. Rev. Lett. **107**, 075502 (2011) (cit. on p. 76).

[190] B. Bradlyn, M. Goldstein, and N Read, "Kubo formulas for viscosity: hall viscosity, ward identities, and the relation with conductivity," Phys. Rev. B **86**, 245309 (2012) (cit. on pp. 76, 79).

[191] F. Hong-Yi and Y. Peng, "One-and two-mode combination squeezing operator for two harmonic oscillators with coordinate-momentum coupling," Communications in Theoretical Physics **48**, 428 (2007) (cit. on pp. 76, 87, 88).

[192] R Bogdanovic and M. Gopinathan, "A canonical transformation of the hamiltonians quadratic in coordinate and momentum operators," Journal of Physics A: Mathematical and General **12**, 1457 (1979) (cit. on pp. 76, 87).

[193] S. M. Stishov, "Quantum phase transitions," Physics-Uspekhi **47**, 789 (2004) (cit. on p. 76).

[194] Y. Schattner, S. Lederer, S. A. Kivelson, and E. Berg, "Ising nematic quantum critical point in a metal: a monte carlo study," Phys. Rev. X **6**, 031028 (2016) (cit. on p. 76).

[195] S. Hayami, M. Yatsushiro, Y. Yanagi, and H. Kusunose, "Classification of atomic-scale multipoles under crystallographic point groups and application to linear response tensors," Phys. Rev. B **98**, 165110 (2018) (cit. on p. 78).

[196] L. Šmejkal, J. Sinova, and T. Jungwirth, "Beyond conventional ferromagnetism and antiferromagnetism: a phase with nonrelativistic spin and crystal rotation symmetry," Phys. Rev. X **12**, 031042 (2022) (cit. on pp. 78, 80, 93).

[197] J.-M. Lai, Y.-R. Xie, and J. Zhang, "Detection of electron-phonon coupling in two-dimensional materials by light scattering," Nano Research **14**, 1711–1733 (2021) (cit. on p. 79).

[198] S. Sugai, "Phonon raman scattering in $\left(La_{1-x}Sr_x\right)2CuO_4$ single crystals," Phys. Rev. B **39**, 4306 (1989) (cit. on p. 79).

[199] N Mironova-Ulmane, A Kuzmin, I Sildos, L Puust, and J Grabis, "Magnon and phonon excitations in nanosized nio," Latvian Journal of Physics and Technical Sciences **56**, 61–72 (2019) (cit. on p. 79).

[200] A. Abdalian, J Cibert, and P Moch, "Raman scattering in the one-dimensional ferromagnet $CsNiF_3$," Journal of Physics C: Solid State Physics **13**, 5587 (1980) (cit. on p. 79).

[201] S Kamba, V Goian, V Skoromets, J Hejtmánek, V Bovtun, M Kempa, F Borodavka, P Vaněk, A. Belik, J. Lee, et al., "Strong spin-phonon coupling in infrared and raman spectra of $SrMnO_3$," Phys. Rev. B **89**, 064308 (2014) (cit. on p. 79).

[202] T. Chatterji, M. Zbiri, and S. Rols, "Phonon–magnon coupling in CoF2 investigated by time-of-flight neutron spectroscopy," Solid state communications **174**, 55–62 (2013) (cit. on p. 79).

[203] H. F. Fong, B. Keimer, P. W. Anderson, D Reznik, F Doğan, and I. A. Aksay, "Phonon and magnetic neutron scattering at 41 meV in YB $a_2Cu_3O_7$," Phys. Rev. Lett **75**, 316 (1995) (cit. on p. 79).

[204] L Pintschovius, "Electron–phonon coupling effects explored by inelastic neutron scattering," physica status solidi (b) **242**, 30–50 (2005) (cit. on p. 79).

[205] W. Shaw and L. Muhlestein, "Investigation of the phonon dispersion relations of chromium by inelastic neutron scattering," Physical Review B **4**, 969 (1971) (cit. on p. 79).

[206] J. Kulda, D. Strauch, P. Pavone, and Y. Ishii, "Inelastic-neutron-scattering study of phonon eigenvectors and frequencies in Si," Physical Review B **50**, 13347 (1994) (cit. on p. 79).

[207] S. Apostolov, D. Pesin, and A Levchenko, "Magnetodrag in the hydrodynamic regime: effects of magnetoplasmon resonance and hall viscosity," Phys. Rev. B **100**, 115401 (2019) (cit. on p. 79).

[208] T. Scaffidi, N. Nandi, B. Schmidt, A. P. Mackenzie, and J. E. Moore, "Hydrodynamic electron flow and hall viscosity," Phys. Rev. Lett. **118**, 226601 (2017) (cit. on p. 79).

[209] J. Dziarmaga, "Dynamics of a quantum phase transition: exact solution of the quantum ising model," Phys. Rev. Lett. **95**, 245701 (2005) (cit. on p. 80).

[210] A. Pelissetto and E. Vicari, "Critical phenomena and renormalization-group theory," Physics Reports **368**, 549–727 (2002) (cit. on p. 88).

[211] J. Rudnick and D. R. Nelson, "Equations of state and renormalization-group recursion relations," Phys. Rev. B **13**, 2208 (1976) (cit. on p. 91).

[212] X. Chen, D. Wang, L. Li, and B. Sanyal, "Room temperature two-dimensional antiferromagnetic weyl semimetal cro with giant spin-splitting and spin-momentum locked transport," arXiv preprint arXiv:2104.07390 (2021) (cit. on p. 93).

[213] M. Masahito and I. Masatoshi, "G-type antiferromagnetism and orbital ordering due to the crystal field from the rare-earth ions induced by the $GdFeO_3$-type distorion in RTio3 where R= La, Pr, Nd and Sm," Journal of the Physical Society of Japan **73**, 1833–1850 (2004) (cit. on p. 95).

[214] M. Koshino and Y.-W. Son, "Moiré phonons in twisted bilayer graphene," Phys. Rev. B **100**, 075416 (2019) (cit. on p. 98).

[215] B. Lian, Z. Wang, and B. A. Bernevig, "Twisted bilayer graphene: a phonon-driven superconductor," Phys. Rev. Lett **122**, 257002 (2019) (cit. on p. 98).

[216] X. Lin, B.-B. Chen, W. Li, Z. Y. Meng, and T. Shi, "Exciton proliferation and fate of the topological mott insulator in a twisted bilayer graphene lattice model," Phys. Rev. Lett. **128**, 157201 (2022) (cit. on p. 99).

[217] R. M. Fernandes and J. W. Venderbos, "Nematicity with a twist: rotational symmetry breaking in a moiré superlattice," Science Advances **6**, eaba8834 (2020) (cit. on p. 100).

Publications

I was involved in the following publications during my PhD

- Ref.[20] C. R. Steward, R. M. Fernandes, and J. Schmalian, Dynamic paramagnon-polarons in altermagnets, Physical Review B 108, 144418 (2023).
- Ref. [17] C. R. Steward, G. Palle, M. Garst, J. Schmalian, and I. Jang, Elastic quantum criticality in nematics and altermagnets via the elasto-caloric effect, arXiv preprint arXiv:2502.14033 (2025).
- Ref. [18] K. Takahashi, C. R. W. Steward, M. Ogata, R. M. Fernandes, and J. Schmalian, Elasto-hall conductivity and the anomalous hall effect in altermagnets, Phys. Rev. B 111, 184408 (2025).

In addition to

- Ref.[21] Dynamic coupling of magnetic collective modes and damped phasons in incommensurate twisted bilayer graphene, (In preparation)

Acknowledgments

First and foremost I would like to thank my supervisor Jörg Schmalian, without his guidance, nothing contained within this thesis would have been achieved. Working under his supervision has allowed me to grow substantially as both a physicist and a person, it has been nothing short of an absolute pleasure to work in this research group. As well as my supervisor, I have also had the pleasure of collaborating with many great people and so with this in mind I would like to thank Rafael Fernandes, Iksu Jang, Markus Garst, Grgur Palle, Keigo Takahashi and Masao Ogata for their large contribution to the content of this thesis. I would also like to thank my second supervisor Igor Gornyi, whom I first contacted about the possibility of a position at the TKM.

The TKM provided the best working environment one could hope for and so I must thank my colleagues, in particular Veronika Stangier and Roland Willa, without whom I don't think I would have survived the first two years in Germany. I would also like to thank Elmer Doggen, Vannessa Gall, Paul Pöpperl, Adrian Reich, Jinhong Park, Jonas Gaa, Jonas Karcher, Tamaghna Hazra, Jose Este, Thibault Scoquart, Igor Poboiko, Hugo Perrin, Davide Valentinis, Sopheak Sorn, Daniel Schultz, Lindsay Orr, Risto Ojajärvi and Romy Morin for making this such a great place to work. Special thanks go to Sonja König who shields us everyday from all manner of bureaucratic pain and to Andreas Poenicke for his support on all technical matters.

I would also like to acknowledge the KSQM and in particular Yu Goldscheider whose support on matters inside and outside of academia is invaluable.

I am thankful to the DFG whose grant supported the work carried out during my PhD.

Finally I would like to acknowledge my parents, my brother and my late grandmother, all of whom have supported me throughout my PhD, as well as my girlfriend Juliette who always offered her support when work was not going as well as I'd hoped and I was being especially unbearable.